

INFORMATION TO USERS

This manuscript has been reproduced from the microfilm master. UMI films the text directly from the original or copy submitted. Thus, some thesis and dissertation copies are in typewriter face, while others may be from any type of computer printer.

The quality of this reproduction is dependent upon the quality of the copy submitted. Broken or indistinct print, colored or poor quality illustrations and photographs, print bleedthrough, substandard margins, and improper alignment can adversely affect reproduction.

In the unlikely event that the author did not send UMI a complete manuscript and there are missing pages, these will be noted. Also, if unauthorized copyright material had to be removed, a note will indicate the deletion.

Oversize materials (e.g., maps, drawings, charts) are reproduced by sectioning the original, beginning at the upper left-hand corner and continuing from left to right in equal sections with small overlaps. Each original is also photographed in one exposure and is included in reduced form at the back of the book.

Photographs included in the original manuscript have been reproduced xerographically in this copy. Higher quality 6" x 9" black and white photographic prints are available for any photographs or illustrations appearing in this copy for an additional charge. Contact UMI directly to order.

U·M·I

University Microfilms International
A Bell & Howell Information Company
300 North Zeeb Road, Ann Arbor, MI 48106-1346 USA
313/761-4700 800/521-0600

Order Number 9213156

**Hydrogeologic characterization of a multiple aquifer fractured
basalt system**

Li, Tong, Ph.D.

University of Idaho, 1991

U·M·I
300 N. Zeeb Rd.
Ann Arbor, MI 48106

**HYDROGEOLOGIC CHARACTERIZATION OF
A MULTIPLE AQUIFER FRACTURED BASALT SYSTEM**

A Dissertation

Presented in Partial Fulfillment of the Requirements for the

Degree of Doctor of Philosophy

with a

Major in Geology/Hydrogeology

in the

College of Graduate Studies

University of Idaho

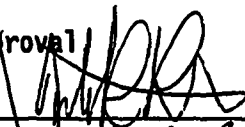
by

Tong Li

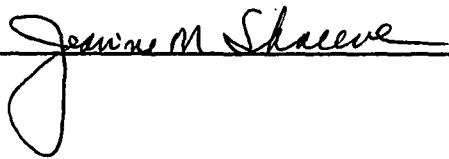
November, 1991

**AUTHORIZATION TO SUBMIT
DISSERTATION**

This dissertation of Tong Li, submitted for the degree of Doctor of Philosophy with a major in Geology/Hydrogeology and titled "Hydrogeologic Characterization of a Multiple Aquifer Fractured Basalt System," has been reviewed in final form, as indicated by the signatures and dates given below. Permission is now granted to submit final copies to the College of Graduate Studies for approval

Major Professor	<u></u>	Date <u>11/22/91</u>
Committee Members	<u></u>	Date <u>11/22/91</u>
	<u>Scott Kellogg</u>	Date <u>11/22/91</u>
	<u>George Blemsburg</u>	Date <u>11/22/91</u>
	<u>Stanley M. Miller</u>	Date <u>11-22-91</u>
Department Administrator	<u>Rolland R. Reid</u>	Date <u>12-02-91</u>
College Dean	<u>R. Santala</u>	Date <u>12-2-91</u>

College of Graduate Studies Final Approval and Acceptance:

 Date 12/3/91

ABSTRACT

Hydrogeological characterization of fractured basalt is important for water supplies and *in-situ* investigation and remediation of hazardous wastes in the Pacific Northwest. Numerous investigations and research conducted on the Columbia River Basalt in the last decade have focused on hydraulic and solute transport characteristics of the fractured basalt on a large scale. The objectives of this study are to develop a conceptual model(s) of a multiple aquifer fractured basalt system, evaluate the applicability of alternative analytical models to the system, and characterize the hydraulic behavior of fractured basalt on a small scale based upon a sequence of hydraulic tests.

Geological and stratigraphic data were collected via examination of basalt outcrops and logging of rock cuttings while nine wells were drilled in the Lolo Basalt of the Wanapum Formation. Borehole geophysical logging was conducted to identify the fracture patterns. Static water levels in nine basalt wells and nine shallow wells in the alluvium have been measured by hand using steel tapes on a daily basis for about three years. Two phases of multiple well hydraulic testing and nine single well slug tests were conducted during this study.

The intraflow structures of the Lolo Basalt primarily form the fracture system; two major fracture zones named as E and W with different static water levels and hydraulic behaviors are identified at the study site. A three aquifer system, formed by the two fracture zones and the alluvium, is conceptualized at the site. The less fractured flow interiors are recognized as aquitards; the upper aquitard separates the alluvial and E aquifers, the middle aquitard lies between the E and W aquifers, and the lower aquitard underlies the W aquifer.

The E aquifer behaves like an equivalent porous medium during the four multiple well aquifer tests conducted in the E aquifer wells. Alternative analytical approaches including Hantush, modified Hantush and Neuman and Witherspoon leaky aquifer models are applicable for the test data analysis. The Hantush model may be the optimum model because of the significant leakage from the alluvial aquifer. The W aquifer exhibits double-porosity behavior during the three multiple well aquifer tests. The Moench double-porosity with fracture skin model probably is the optimum approach with the modified Hantush as an alternative model to analyze the test data from the W aquifer. The hydraulic properties of both aquifers are estimated using the optimum and alternative analytical models.

Heterogeneities of the two fractured aquifers are illustrated by the slug test results. The early drawdown deviations of the multiple well test data from the type curves of analytical models are identified. The drawdown deviations are discussed based on the characteristics of fractured rock.

ACKNOWLEDGMENTS

I would like to express great appreciation and gratitude to Dr. Dale Ralston, my major professor, for his advice and encouragement during all phases of my degree program as well as the guidance and comments on this study. I am sincerely grateful for the discussions and reviews of this dissertation by members of my committee: Dr. Roy Mink, Dr. George Bloomsburg, Dr. Stanley Miller and Dr. Scott Kellogg.

I wish to acknowledge Tom Brooks and all the hydrogeology students in the University of Idaho for their participation and assistance in the well construction and aquifer hydraulic testing. My appreciation also goes to Tom Weber, Dr. Kent Keller and Washington State University students for their efforts to conduct borehole geophysical logging and to construct the shallow wells. Special appreciation is extended to Dr. Scott Kellogg for his counsel and advice in computer drawing and writing programs.

I would especially like to thank my wife, Minna for her patience, understanding and dedicated support during these years. Special thanks are extended to my daughter, Xiaochang, for the time that belongs to her and the many lonely evenings and weekends she spent.

This study has been supported by the grants from the U.S. Environmental Protection Agency (R-816136-01-0), the U.S. Geological Survey (14-08-0001-G1559), and Pullman-Moscow Water Resources Committee.

To my father and mother, and my motherland

TABLE OF CONTENTS

ABSTRACT.....	iii
ACKNOWLEDGMENTS.....	v
DEDICATION.....	vi
LIST OF TABLES.....	x
LIST OF FIGURES.....	xiii
CHAPTER I INTRODUCTION.....	1
Statement of the Problem.....	1
Purpose and Objectives.....	2
Methodology.....	5
Research Site Development.....	6
CHAPTER II GEOLOGICAL SETTINGS.....	12
Regional Geology.....	12
Lithology and Stratigraphy.....	12
Structure.....	15
Geology of the Research Site.....	17
Stratigraphy.....	17
Intraflow Structures of Lolo Flow.....	19
Analysis of Well Geological and Geophysical Logs.....	24
Well Geological Logs.....	24
Borehole Geophysical Logs.....	25
Geological Cross Sections.....	30
Summary.....	35
CHAPTER III GROUND WATER HYDROLOGY.....	39
Ground Water Hydrographs.....	39
Ground Water Level Contours.....	50
Ground Water Recharge and Discharge.....	53
Recharge and Discharge of the Shallow Alluvial Aquifer.....	53
Recharge and Discharge of the E Fracture Zone.....	55
Recharge and Discharge of the W Fracture Zone.....	55
Interrelationship between Paradise Creek and the Aquifers.....	56
Microbial Ecology of the Fracture Systems.....	57
Hydrogeological Conceptual Model.....	57
The Shallow Alluvial Aquifer.....	58
The E Fractured Basalt Aquifer.....	58
The W Fractured Basalt Aquifer.....	59
The Aquitards.....	60
CHAPTER IV DISCUSSION OF THE CONCEPTUAL AND ANALYTICAL MODELS OF FRACTURED ROCK.....	61
Basic Concepts and Definitions.....	61

Analytical Approaches to Ground Water Flow in Fractured Rock.....	64
Discrete Fracture Models.....	64
Single Fracture in Homogeneous Matrix Models.....	66
Gringarten's Models.....	67
Linear Flow (one-dimensional flow) Models.....	69
Double-porosity Analytical Models.....	71
Pseudo-steady State Block-to-fissure Flow Models.....	72
Transient Block-to-fissure Flow Models.....	75
Double-porosity with Fracture Skin Model.....	76
Double-porosity Slug Test Model.....	84
Slope (Pressure Derivative) Analysis Approach.....	86
Equivalent Porous Medium Models.....	88
Homogeneous Isotropic Models.....	89
Homogeneous Anisotropic Models.....	91
Evaluation of Applicability of Analytical models.....	97
 CHAPTER V HYDRAULIC TESTING--SCOPE AND METHODOLOGY.....	 100
Testing Equipment.....	100
Slug Testing.....	101
Multiple Well Aquifer Testing.....	102
Phase One Testing.....	102
Phase Two Testing.....	104
Water Level Measurements--Quality Assurance.....	106
 CHAPTER VI AQUIFER TEST DATA ANALYSIS AND ANALYTICAL MODEL EVALUATION.....	 111
Aquifer Test Data Analysis.....	111
Multiple Well Aquifer Test 9-22-89.....	111
Multiple Well Aquifer Test 4-4-90.....	115
Multiple Well Aquifer Test 4-11-90.....	118
Multiple Well Aquifer Test 6-3-90.....	121
Multiple Well Aquifer Test 8-14-90.....	124
Multiple Well Aquifer Test 8-17-90.....	127
Multiple Well Aquifer Test 3-8-91.....	131
Slug Tests.....	133
Summary.....	134
Applicability of Alternative Analytical Models for Multiple Well Aquifer Tests.....	134
Selection of Analytical Models.....	135
Analytical Model Evaluation.....	137
Theis Model.....	137
Hantush Leaky Aquifer Model (r/B solution).....	138
Modified Hantush Leaky Aquifer Model.....	140
Neuman and Witherspoon Leaky Aquifer Model.....	141
Moench Double-porosity with Fracture Skin Model.....	145
Applicability of Alternative Analytical Models for Slug Tests.....	146
 CHAPTER VII ANALYTICAL MODEL APPLICATION AND AQUIFER PARAMETER ESTIMATION.....	 147
Deviations of Drawdown Data of Multiple Well Aquifer Tests.....	147

Conceptual Models for Drawdown Deviations.....	147
Analysis of Log-log Plots of Drawdown vs. t/r^2	150
Graphical Curve Matching and Parameter Estimation for Multiple	
Well Aquifer Test Data.....	154
The E Fractured Aquifer.....	155
Aquifer Test 9-22-89.....	155
Aquifer Test 4-4-90.....	163
Aquifer Test 4-11-90.....	169
Aquifer Test 6-3-90.....	171
Summary.....	179
The W Fractured Aquifer.....	181
Aquifer Test 8-14-90.....	181
Aquifer Test 8-17-90.....	195
Aquifer Test 3-8-91.....	199
Summary.....	208
Graphical Curve Matching and Parameter Estimation for Slug	
Test Data.....	211
CHAPTER VIII DISCUSSION OF THE TEST RESULTS AND SUMMARY OF THE	
FINDINGS.....	215
Discussion of the Aquifer Test Results.....	215
Aquifer Transmissivity.....	215
Aquifer Storativity.....	221
Lumped Aquitard Parameter $K'Ss'$	222
Summary of the Findings.....	224
Geology, Stratigraphy and Basalt Intraflow Structures.....	224
Ground Water Hydrology and Conceptual Model.....	225
Hydraulic Behavior of the Fractured Aquifer System.....	227
CHAPTER IX CONCLUSIONS AND RECOMMENDATIONS.....	230
Conclusions.....	230
Recommendations.....	232
REFERENCES.....	234
APPENDIX A WELL CONSTRUCTION AND GEOLOGICAL LOGS AT UIGRS.....	242
APPENDIX B AQUIFER HYDRAULIC TEST DATA.....	257
APPENDIX C STATIC WATER LEVEL DATA AT UIGRS.....	293

LIST OF TABLES

TABLES	PAGE
1-1 Well Construction Information at the UIGRS.....	8
2-1 Generalized Stratigraphic Section of the Pullman-Moscow Basin.....	13
3-1 Ground Water Level and Well Yield Capacity Data at the UIGRS.....	40
5-1 Summary of Phase One Multiple Well Aquifer Testing Results.....	103
6-1 Summary of Configurations of Phase Two Multiple Well Aquifer Testing.....	112
6-2 Observation Well Responses of Aquifer Test 9-22-89.....	114
6-3 Observation Well Responses of Aquifer Test 4-4-90.....	116
6-4 Observation Well Responses of Aquifer Test 4-11-90.....	119
6-5 Observation Well Responses of Aquifer Test 6-3-90.....	121
6-6 Observation Well Responses of Aquifer Test 8-14-90.....	125
6-7 Observation Well Responses of Aquifer Test 8-17-90.....	128
6-8 Observation Well Responses of Aquifer Test 3-8-91.....	133
7-1 Calculated Aquifer Parameters from Well T16D Data, Aquifer Test 9-22-89.....	158
7-2 Calculated Aquifer Parameters from Well S12D1 Data, Aquifer Test 9-22-89.....	160
7-3 Calculated Aquifer Parameters from Well V16D Data, Aquifer Test 9-22-89.....	162
7-4 Calculated Aquifer Parameters from Well Q17D Data, Aquifer Test 4-4-90.....	165
7-5 Calculated Aquifer Parameters from Well V16D Data, Aquifer Test 4-4-90.....	167
7-6 Calculated Aquifer Parameters from Well S12D1 Data, Aquifer Test 4-4-90.....	169
7-7 Calculated Aquifer Parameters from Wells T16D and V16D data, Aquifer Test 4-11-90.....	171
7-8 Calculated Aquifer Parameters from Well T16D Data, Aquifer Test 6-3-90.....	173

7-9 Calculated Aquifer Parameters from Well Q17D Data, Aquifer Test 6-3-90.....	175
7-10 Calculated Aquifer Parameters from Wells S12D1 and Q16D Data, Aquifer Test 6-3-90.....	178
7-11 Comparison and Summary of the Parameters Estimated from the E Aquifer Tests.....	180
7-12 Estimated Aquifer Parameters by Theis and Modified Hantush Models with Well D19D Data, Aquifer Test 8-14-90.....	185
7-13 Estimated Aquifer Parameters by Moench Model with Application of Well D19D Data of Aquifer Test 8-14-90.....	186
7-14 Estimated Aquifer Parameters by Theis and Modified Hantush Models with Well U3D Data, Aquifer Test 8-14-90.....	189
7-15 Estimated Aquifer Parameters by Moench Model with Application of Well U3D Data of Aquifer Test 8-14-90.....	190
7-16 Estimated Aquifer Parameters by Theis and Modified Hantush Models with Well S12D2 Data, Aquifer Test 8-14-90.....	194
7-17 Estimated Aquifer Parameters by Moench Model with Application of Well S12D2 Data of Aquifer Test 8-14-90.....	194
7-18 Estimated Aquifer Parameters by Theis and Modified Hantush Models with Wells J16D Data, Aquifer Test 8-17-90.....	198
7-19 Estimated Aquifer Parameters by Moench Model with Application of Well J16D Data, Aquifer Test 8-17-90.....	198
7-20 Estimated Aquifer Parameters by Theis and Modified Hantush Models with Well D19D Data, Aquifer Test 3-8-91.....	203
7-21 Estimated Aquifer Parameters by Theis and Modified Hantush Models with Wells J16D and S12D2 Data, Aquifer Test 3-8-91.....	205
7-22 Estimated Aquifer Parameters by Moench Model with Application of the Data from All Wells during Aquifer Test 3-8-91.....	208
7-23 Comparison and Summary of the Parameters Estimated from the W Aquifer Tests.....	209
7-24 Estimated Aquifer Parameters by Cooper Model with Slug Test Data..	214
8-1 Estimated Transmissivity Values for Different Observation Wells....	216
8-2 Estimated Storativity Values for Different Observation Wells.....	221
8-3 Estimated Lumped Aquitard Parameter $K'Ss'$ Values for Different Observation Wells.....	223

B-1 Aquifer Test 9-22-89 Data.....	258
B-2 Aquifer Test 4-4-90 Data.....	263
B-3 Aquifer Test 4-11-90 Data.....	268
B-4 Aquifer Test 6-3-90 Data.....	270
B-5 Aquifer Test 8-14-90 Data.....	276
B-6 Aquifer Test 8-17-90 Data.....	281
B-7 Aquifer Test 3-8-91 Data.....	285
B-8 Slug Test Data.....	290
C-1 Static Water Level of Five Deep Wells.....	294
C-2 Static Water Level of Three Shallow Wells and Wells S12D1 and S12D2.....	299
C-3 Static Water Level of Three Deep Wells Q17D, U3D and J16D, Shallow Well T8S and Paradise Creek.....	304
C-4 Static Water Level of Five Shallow Wells.....	306

LIST OF FIGURES

FIGURES	PAGE
1-1 Site plan view map, University of Idaho Groundwater Research Site (UIGRS).....	3
1-2 Grid map and nomenclature of wells at UIGRS.....	11
2-1 Basalt chemistry, percentage of TiO_2 and P_2O_5 of Wanapum and Grande Ronde Formations (after Wood, 1987).....	16
2-2 Thickness of Wanapum Basalt at vicinity of the UIGRS.....	18
2-3 Typical intraflow structures in the basalt flow (after DOE, 1981)..	20
2-4 Basalt intraflow structure types (after Long, 1978).....	21
2-5 Intraflow structures in Lolo flow, Pullman-Moscow highway, three miles west of the UIGRS.....	23
2-6 Correlation of geology and borehole geophysical logs of well Q16D..	28
2-7 Correlation of geology and borehole geophysical logs of well U3D...	29
2-8 Locations of the geological cross-sections.....	31
2-9 Cross-section A-A' with caliper logs along north side of the UIGRS.....	32
2-10 Cross-section B-B' along southeast side of the UIGRS.....	34
2-11 Cross-section C-C' from north to south at the UIGRS.....	36
3-1 Ground water hydrographs of deep basalt wells (1988-1991).....	42
3-2 Water level hydrographs of shallow wells and Paradise Creek.....	44
3-3 Water level hydrographs of Paradise Creek and some wells in the E fracture zone.....	46
3-4 Annual (1990-1991) ground water hydrographs of deep basalt wells...	47
3-5 Annual (1990-1991) water level hydrographs of shallow wells and Paradise Creek.....	48
3-6 Comparison of water level hydrographs of Paradise Creek, shallow alluvial aquifer, and E fractured aquifer.....	49
3-7 Ground water contour map of fractured basalt aquifers on October 2, 1990.....	51

3-8	Ground water contour map of fractured basalt aquifers on January 15, 1991.....	52
3-9	Water table contour map of shallow alluvial aquifer (October 2, 1990).....	54
4-1	Type curves for selective values of parameters of double-porosity with fracture skin model (after Moench, 1984).....	83
4-2	Comparison between pressure curve and pressure-derivative curve with different hydraulic conditions (after Beauheim, 1988).....	87
4-3	Type curve for point injection/observation solution of cross-hole method (after Hsieh and Neuman, 1985).....	95
5-1	Comparison of pressure transducer and hand measurements in arithmetic coordinates during aquifer test 8-14-90.....	108
5-2	Comparison of pressure transducer and hand measurements as log-log plots during aquifer test 8-14-90.....	109
6-1	Log-log plots of drawdown vs. time for all the wells during aquifer test 9-22-89 and well locations.....	113
6-2	Log-log plots of drawdown vs. time for all the wells during aquifer test 4-4-90 and well locations.....	117
6-3	Log-log plots of drawdown vs. time for observation wells V16D and T16D during aquifer test 4-11-90 and well locations.....	120
6-4	Log-log plots of drawdown vs. time for observation wells during aquifer test 6-3-90 and well locations.....	122
6-5	Log-log plots of drawdown vs. time for all the wells during aquifer test 8-14-90 and well locations.....	126
6-6	Log-log plots of drawdown vs. time for all the wells during aquifer test 8-17-90 and well locations.....	130
6-7	Log-log plots of drawdown vs. time for all the wells during aquifer test 3-8-91 and well locations.....	132
6-8	Type curve comparison of Hantush r/B solution with Neuman and Witherspoon solution (after Neuman and Witherspoon, 1969b).....	144
7-1	Log-log drawdown versus t/r^2 of the observation wells during the aquifer tests conducted in the E aquifer.....	151
7-2	Log-log drawdown versus t/r^2 of the observation wells during the aquifer tests conducted in the W aquifer.....	153
7-3	Graphical curve matching of observation well T16D data with alternative analytical models during test 9-22-89.....	156

7-4 Graphical curve matching of observation well S12D1 data with alternative analytical models during test 9-22-89.....	159
7-5 Graphical curve matching of observation well V16D data with alternative analytical models during test 9-22-89.....	161
7-6 Graphical curve matching of observation well Q17D data with alternative analytical models during test 4-4-90.....	164
7-7 Graphical curve matching of observation well V16D data with alternative analytical models during test 4-4-90.....	166
7-8 Graphical curve matching of observation well S12D1 data with the Theis and modified Hantush models during test 4-4-90.....	168
7-9 Graphical curve matching of observation well T16D data with the Theis and Hantush models during test 4-11-90.....	170
7-10 Graphical curve matching of observation well V16D data with the Theis and Hantush models during test 4-11-90.....	170
7-11 Graphical curve matching of observation well T16D data with alternative analytical models during test 6-3-90.....	172
7-12 Graphical curve matching of observation well Q17D data with alternative analytical models during test 6-3-90.....	174
7-13 Graphical curve matching of observation well S12D1 data with alternative analytical models during test 6-3-90.....	176
7-14 Graphical curve matching of observation well Q16D data with alternative analytical models during test 6-3-90.....	177
7-15 Graphical curve matching of observation well D19D data with the Theis and modified Hantush models during test 8-14-90.....	182
7-16 Graphical curve matching of observation well D19D data with the Moench model during test 8-14-90.....	183
7-17 Graphical curve matching of observation well U3D data with alternative analytical models during test 8-14-90.....	187
7-18 Graphical curve matching of observation well U3D data with the Moench model during test 8-14-90.....	188
7-19 Graphical curve matching of observation well S12D2 data with alternative analytical models during test 8-14-90.....	192
7-20 Graphical curve matching of observation well S12D2 data with the Moench model during test 8-14-90.....	193
7-21. Graphical curve matching of observation well J16D data with the Theis and modified Hantush models during test 8-17-90.....	196

7-22 Graphical curve matching of observation well J16D data with the Moench model during test 8-17-90.....	197
7-23 Graphical curve matching of observation well S12D2 data with alternative analytical models during test 8-17-90.....	200
7-24 Graphical curve matching of observation well U3D data with alternative analytical models during test 8-17-90.....	201
7-25 Graphical curve matching of pumping well U3D data with the Jacob straight line and Moench models during test 3-8-91.....	202
7-26 Graphical curve matching of observation well D19D data with the Theis and Moench models during test 3-8-91.....	202
7-27 Graphical curve matching of observation well D19D data with the modified Hantush model during test 3-8-91.....	204
7-28 Graphical curve matching of observation well J16D data with alternative analytical models during test 3-8-91.....	206
7-29 Graphical curve matching of observation well S12D2 data with alternative analytical models during test 3-8-91.....	207
7-30 Graphical curve matching of single well slug tests conducted in the E fractured aquifer.....	212
7-31 Graphical curve matching of single well slug tests conducted in the W fractured aquifer.....	213
8-1 The transmissivity values (ft ² /day) at the different well locations in the UIGRS.....	218
8-2 Directional T values (ft ² /day) from well S12D1 to different pumping wells during the multiple well aquifer tests.....	220
8-3 Directional T values (ft ² /day) from different observation wells to the pumping well during aquifer test 4-4-90.....	220
A-1 Construction and geology logs of well V16D.....	243
A-2 Construction and geology logs of well Q17D.....	244
A-3 Construction and geology logs of well D19D.....	245
A-4 Construction and geology logs of wells S12D1 and S12D2.....	246
A-5 Construction and geology logs of well T16D.....	247
A-6 Construction and geology logs of wells Q16D and Q16S.....	248
A-7 Construction and geology logs of wells U3D and U3S.....	249

A-8 Construction and geology logs of wells J16D and J16S..... 250
A-9 Construction and geology logs of well P17S..... 251
A-10 Construction and geology logs of well V16S..... 252
A-11 Construction and geology logs of well N18S..... 253
A-12 Construction and geology logs of well T8S..... 254
A-13 Construction and geology logs of well H12S..... 255
A-14 Construction and geology logs of well J17S..... 256

CHAPTER I

Introduction

Statement of the Problem

Effective programs aimed at water supply and waste disposal in the Pacific Northwest require an understanding of the occurrence and movement of ground water and solute transport characteristics in basalt. The aquifers of the Columbia River Basalt Group in Washington, Oregon and northern Idaho as well as the Snake River Basalt in southern Idaho have been exploited as principal sources of water for agricultural, domestic and municipal use. At the same time, a number of land disposal sites including many municipal landfills and several hazardous and low-level radioactive waste disposal facilities have been located overlying these basalt groups. At many of these sites, the primary concern is the transport of contaminants by ground water movement through underlying basalt aquifers.

Numerous investigations and large-scale research projects, particularly at the Hanford site in southeastern Washington and the Idaho National Engineering Laboratory (INEL) in southeastern Idaho, have increased understanding of basalt geology and hydrogeology. The concept that ground water movement through basalt at large scale occurs primarily along the highly fractured contact zones between individual basalt flows is widely accepted. The studies on basalt hydrology (for estimation of aquifer parameters, large scale ground water modeling, and solute transport testing), are typically based on the assumption that basalt can be considered as a porous medium.

The research results from Hanford, INEL and other sites illustrate

that very little is known about hydrogeological characteristics and hydraulic behavior of the fractured basalt aquifers on a small scale, particularly within a basalt lava flow (DOE, 1981; Levenue and Domenico, 1986; Kunke1 *et al.*, 1988). These fractured basalt aquifers commonly have limited lateral continuities with very complex fracture patterns. They are generally highly heterogeneous and anisotropic, which makes their characterization difficult.

A basalt aquifer research facility within the Wanapum basalt of the Yakima Subgroup of the Columbia River Basalt Group has been developed at the University of Idaho (Figure 1-1). The facility is officially named the University of Idaho Groundwater Research Site (UIGRS). A number of research projects have been conducted at UIGRS to understand site geology and hydrogeology, ground water and surface water relationships, and hydraulic behavior of the fractured basalt aquifers. Research focused on solute transport characteristics, microbial bioindicators and ecology in saturated/unsaturated ground water environments, and *in situ* studies of biological degradation of toxic chemicals also have been started. The present study is a fundamental portion of the entire multi-discipline research program, with a focus on hydrogeology and hydraulic characteristics of the fractured basalt aquifers.

Purpose and Objectives

The purpose of this study is to increase the understanding of basalt hydrogeology and hydraulic behavior of fractured basalt aquifers. The general objective is to develop the conceptual model(s) of ground water flow in fractured basalt aquifers at UIGRS, evaluate the applicability of

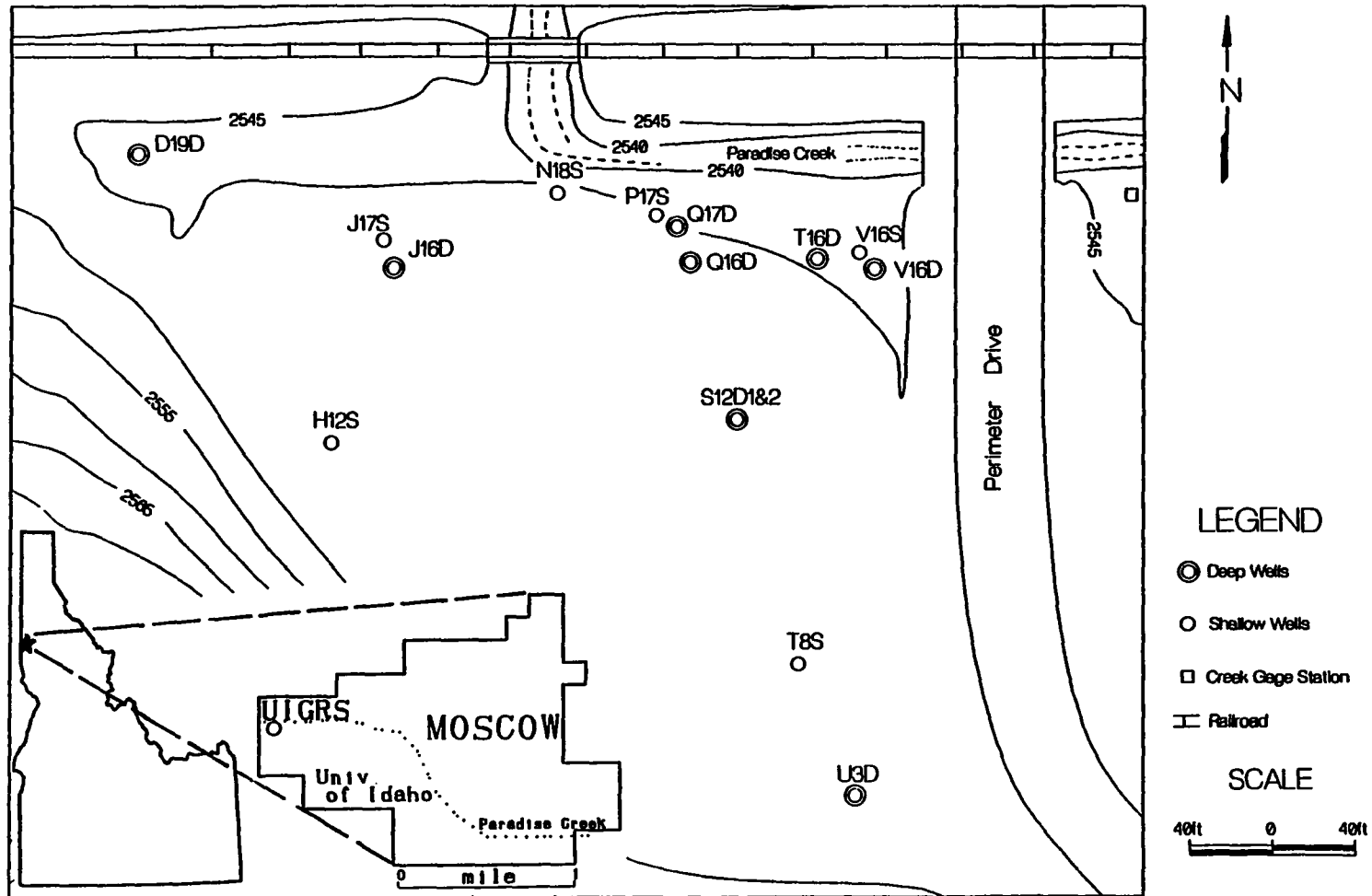


Figure 1-1. Site plan view map, University of Idaho Groundwater Research Site (UIGRS)

alternative analytical approaches for aquifer test analysis, and characterize the aquifer hydraulic properties by analyzing data from a sequence of hydraulic tests with applicable models. The specific objectives are to:

- 1) Develop the University of Idaho Groundwater Research Site within the Wanapum Basalt near Moscow campus.
- 2) Analyze geological and stratigraphic data, as well as drilling and borehole geophysical logs, to understand the site stratigraphy and basalt fracture patterns.
- 3) Collect and analyze static ground water levels and Paradise Creek discharge and flow elevation data to understand recharge and discharge patterns and the interrelationships between ground water and surface water.
- 4) Develop and evaluate hydrogeological conceptual model(s) of the fractured basalt aquifer system at the site.
- 5) Review and discuss conceptual and analytical hydraulic models that have been developed for porous media and fractured rock systems, and evaluate the applicability of these analytical approaches to the fractured aquifers at UIGRS.
- 6) Conduct a sequence of single well slug tests and multiple well aquifer tests.
- 7) Analyze the test data using applicable analytical models to characterize hydraulic properties of the fractured basalt aquifers.
- 8) Compare and discuss the analysis results with different test data using alternative models, and analyze the aquifer heterogeneity and anisotropy.
- 9) Summarize the findings and present recommendations for future

studies.

Methodology

Geological and stratigraphic data were collected via three ways during this study: 1) logging of rock cuttings while wells were drilled at the site, 2) examination of the basalt outcrops at rock crusher sites along the Pullman-Moscow highway west of the UIGRS, and 3) borehole geophysical logging of wells. Basalt fractures were identified through changes in the drilling penetration rate, the size of the rock cuttings and the water yield capacity. Borehole geophysical logging was conducted using a logging rig owned and operated by Washington State University. Both digitized data and chart plots of nine types of logs were collected for a total of eight deep wells. Fracture patterns of the basalt flow at the UIGRS were recognized through correlation among the well logs as well as the rock outcrops.

Static ground water level data have been collected by hand measurements using a steel tape on a daily basis since December 28, 1987. Water levels were measured from the tops of the well casings, which had been surveyed for the elevation above mean sea level (AMSL). Water level and discharge flow data for Paradise Creek were collected from the USGS gaging station and corrected for the stream head drop from the station to the UIGRS.

Methodology of data collection of the hydraulic testing is presented hereafter in Chapter V. The hydraulic test data were analyzed with the assistance of an IBM 386 computer using the aquifer test software package AQTESOLV.

Research Site Development

The UIGRS is located at the western edge of the University of Idaho campus in section 12, T39N. R6W. on Moscow West, Idaho-Washington (Figure 1-1). The site was selected based on a geological and geophysical reconnaissance survey of available sites on the western portion of the campus. The site is relatively flat with a moderate hill standing at its southwestern edge. The northern boundary is formed by Paradise Creek and Burlington Northern Railroad, and Perimeter Drive is its eastern boundary (Figure 1-1).

Paradise Creek is one of the primary streams in the Pullman-Moscow Basin. Originating from Moscow Mountain, Paradise Creek is a tributary to the South Fork of the Palouse River. Drainage area of the creek is 17.7 square miles. Average discharge of the creek, based on a twelve-year record, is 6.72 cfs (191 l³/s) and 4870 acre-ft/yr. Maximum discharge during the period of record is 543 cfs (15166 l³/s), which occurred on January 8, 1990. The minimum daily flow was on November 29, 1987 with a discharge of 0.04 cfs (1.1 l³/s) (Harenberg *et al.*, 1990; 1991). Peak discharge generally occurs when snow melts in the spring. The creek hydrologic data are collected via the U.S. Geological Survey gaging station located approximately 100 feet (30 meters) east of Perimeter Drive, northeast of the UIGRS.

The study site has been under development since December, 1987. Eight deep wells have been drilled within the Wanapum basalt and completed at different depth and fracture zones. Nine shallow wells have been constructed in upper alluvial sediments since April, 1988 (Figure 1-1).

Phase I of the site development started with five deep wells drilled in the Wanapum basalt. Five shallow wells were drilled during Phase II from April 1988 to April 1990. Phase III of site development was completed in June 1990, when three new deep wells and four shallow wells were added to the research facility. A summary of well construction information is presented in Table 1-1.

All deep wells were drilled using an air rotary rig and completed with a combination of steel and plastic casing. Six-inch or eight-inch steel surface casing was installed to about 20 feet through the upper sediments. Most of the deep wells were completed with four-inch PVC casing perforated or screened at selected fracture intervals.

Deep wells S12D1 and S12D2 were completed with 1.25-inch PVC casing in the same borehole. Two fracture intervals at depths of 65 to 75 feet (20 to 23 meters) and 120 to 130 feet (37 to 40 meters) from the ground surface were identified through geological and borehole geophysical logging. Well S12D1 was completed in the lower fracture interval, and well S12D2 was perforated opposite the upper fracture zone. The smaller diameter plastic casing was used to allow installation of the double casing, sand packs and effective seals.

Four shallow wells N18S, T8S, H12S and J17S were drilled with the Washington State University hollow-stem auger. These wells were completed with two-inch PVC casing and screened over one to three feet in the shallow alluvial sand and gravel layer. Shallow wells V16S and P17S were drilled with a hand auger to the sand and gravel layer. One-inch PVC casing with the open bottom covered by fiberglass screen was installed in these wells.

Table 1-1. Well Construction Information at the UIGRS

	WELL NO.	GROUND ELEV. (AMSL) (ft)	TOTAL DEPTH (ft)	BOREHOLE DIAMETER (in)	SURFACE CASING		PVC LINER		PERFORATION (PVC)	PERF. INTERVAL (ft)	SANDPACK INTERVAL (ft)	SEALING
					DEP.(ft)	DIA.(in)	DEP.(ft)	DIA.(in)				
I	V16D	2543.46	70	6	20	6	70	4	40-slot Screen	65-67.5	63-70	C+B*
	Q17D	2544.98	100	6	30	6	81	4	Hacksaw Slots	76-79	73-81	C+B
	T16D	2543.61	80	6	22	6	70	4	Hacksaw Slots	65-69	59-70	C+B
	D19D	2542.74	140	6	20	6	140	4	40-slot Screen	137-139	133-140	C+B
	S12D1	2545.95	146	6	23	6	127	1.25	Hacksaw Slots	119-126	117-129	B**
	S12D2						75	1.25	Hacksaw Slots	65-74	64-75	B
II	V16S	2543.05	10	3	2	4	10	1	Open Bottom	10	9-10	B
	P17S	2544.70	10	3	2	4	10	1	Open Bottom	10	9-10	B
	H18S	2544.02	17	6	3	4	16	2	20-slot Screen	13-16	12-17	B
	T8S	2546.50	15	6	4	6	15	2	20-slot Screen	13-15	12-15	B
	H12S	2546.65	17	6	4	6	16	2	20-slot Screen	13-16	12-16	B
III	Q16D	2545.10	80	8	20	8	73	4	40-slot Screen	70-72.5	69-73	B
	Q16S						27	1.25	Hacksaw Slots	26-27	25-27.5	B
	U3D	2547.65	83	8	18	8	83	4	40-slot Screen	81-83	79-83	B
	U3S						34	1.25	Hacksaw Slots	33-34	32-35	B
	J16D	2545.60	68	8	18	8	68	4	40-slot Screen	65-67.5	63-68	B
	J16S						20	1.25	Hacksaw Slots	19-20	18-21	B
	J17S	2545.50	16	6	5	6	16	2	20-slot Screen	14-16	12-16	B

* C+B -- Cement and Bentonite Mixture

** B -- Bentonite Pellets or Plugs

Shallow wells Q16S, U3S and J16S were completed together with three deep wells Q16D, U3D and J16D in the same borehole at different depths. More than one fracture interval was identified in each borehole; the deep wells generally were completed in the lower and more productive fracture zones. Three shallow wells were completed with 1.25-inch PVC casing and perforated in the uppermost broken or fractured basalt zones. The installation of double casing in these boreholes could be accomplished because of their larger diameter (eight inches).

Sand packs were installed in all wells in the perforation or screen intervals. Generally, the bottom of the sand pack is 0.5 to one foot below the screen interval and the top of the pack is 0.5 to one foot above the perforation in each well. Schedule 8-12 and 10-20 Colorado silica sand was used for the sand packs.

Wells V16D, Q17D, D19D, and T16D were sealed with a mixture of cement and powdered high yield bentonite. Bentonite pellets or medium to large bentonite Enviro-plugs (chips) were used for the seals of the remaining wells. The wells are all sealed from the top of the sand packs to the ground surface. Concrete bases were built around well protective casings on the ground surface for all the wells at the UIGRS.

The test well locations were selected to meet the requirements of geostatistical analysis, hydraulic tests and solute transport tests. Distances between any two deep wells range from 20 feet (6 meters) to approximately 500 feet (152 meters).

The nomenclature of the wells was based upon the spatial location of the well. A 20 feet by 20 feet (6 meters by 6 meters) grid net was constructed at UIGRS, numbered A to bb from west to east and 1 to 21 from south to north. The wells fall into different grids because the minimum

spacing of wells is 20 feet (6 meters). The well is named by the numbers of the particular grid. The letter D or S following the grid number represents a deep or shallow well. If two deep or shallow wells are constructed in the same grid area, the number one or two is added on the well name. The grid map of UIGRS and well nomenclature are illustrated in Figure 1-2.

The construction data and geological logs of all the wells at UIGRS are presented in Figures A-1 to A-14 in Appendix A.

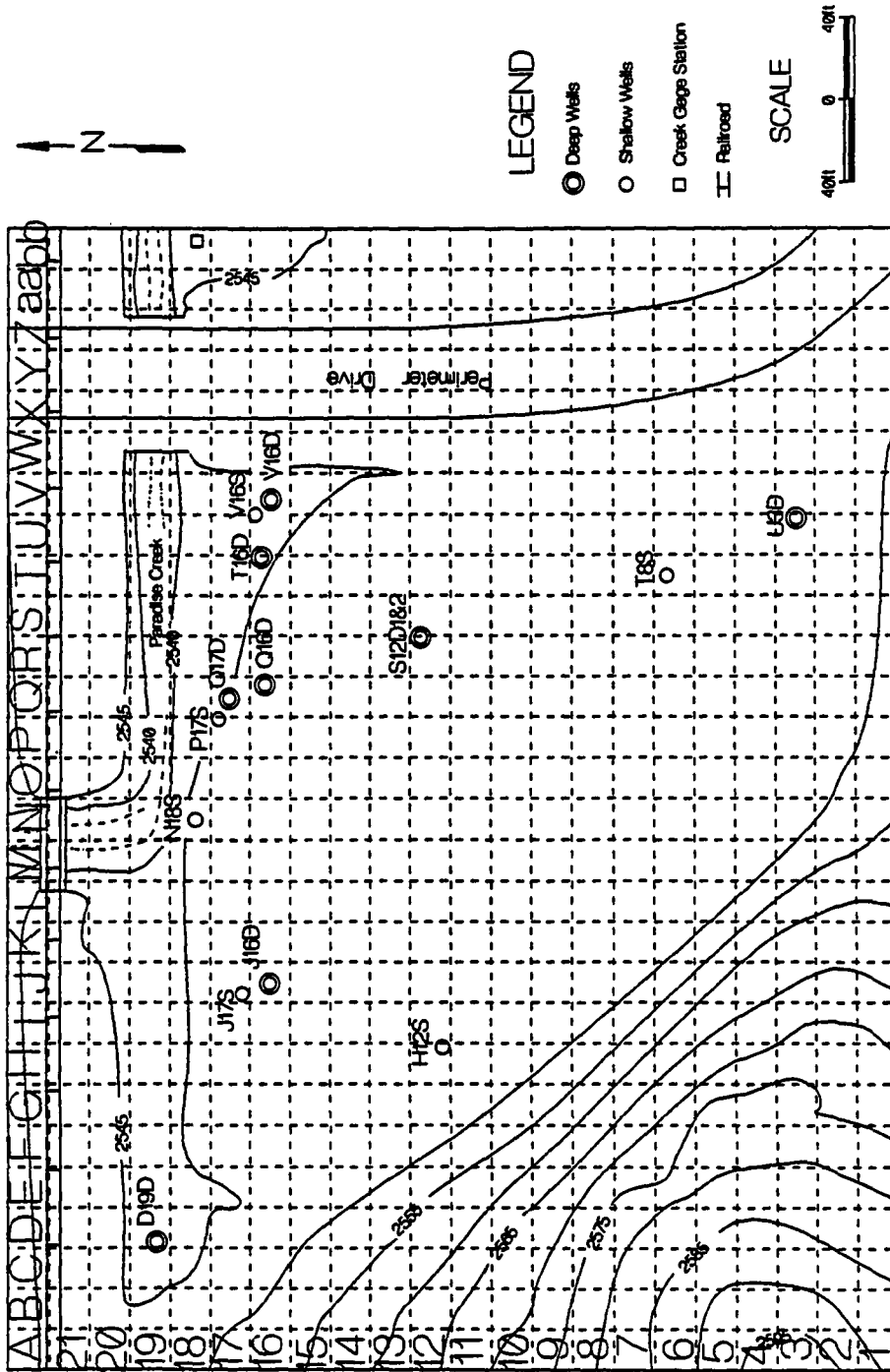


Figure 1-2. Grid map and nomenclature of wells at UIGRS

CHAPTER II

Geological Settings

Regional Geology

Lithology and Stratigraphy

The Pullman-Moscow Basin is located at the eastern edge of the Columbia Plateau within the Palouse Region. The basin base consists of pre-Tertiary crystalline rocks overlain by the Yakima Subgroup of Columbia River Basalt with an irregular buried contact surface (Klein *et al.*, 1987). Most of the basin is covered by Pleistocene loess which is named the Palouse Formation (Hooper and Webster, 1982). A generalized stratigraphic section of the formations and basalt flows is presented in Table 2-1.

Cretaceous intrusions and Cambrian orthoquartzite form the basement of the Pullman-Moscow Basin. The rocks are exposed on the ground surface only around the edges of the basin to the northeast and southeast of Moscow as well as northwest of Pullman. Two varieties of coarse-grained intrusives are found in the area: quartz-rich tonalite and quartz-free hornblende monzodiorite. Cambrian orthoquartzite outcrops are found to the southeast of Moscow over the top of Paradise Ridge, and at Kamiak Butte located at the northwest of Pullman (Hooper and Webster, 1982).

Miocene basalt interbedded with sediments overlies the crystalline rocks. The basalt formations were formed when large volumes of lava erupted from fissures located near Pullman and elsewhere in southeastern Washington and northeastern Oregon over millions of years during Miocene time (Swanson *et al.*, 1977; 1980). Individual basalt flows range in thickness from a few feet to over several hundred feet. The thickness of

Table 2-1. Generalized Stratigraphic Section of the Pullman-Moscow Basin*

PERIOD	EPOCH	GROUP	SUBGROUP	FORMATION	K-Ar AGE (m-year)	MEMBER	STRATIGRAPHY	THICKNESS
Quaternary	Pleistocene /Holocene	Surficial Deposits				Stream Valley Sediments	Alluvium	1-10 ft (0-3 m)
	Pleistocene			Palouse			Loess	0-250 ft (0-76 m)
Tertiary	Miocene	Columbia River Basalt Group	Yakima Basalt Subgroup	Wanapum Basalt	13.6-14.5	Priest Rapids	Lolo Flow w/ Rosalia Basalt	0-250 ft (0-76 m)
				Ellensburg Interbeds		Vantage	Siltstone, Claystone Tuffaceous rocks	0-500 ft (0-152 m)
				Grande Ronde Basalt	14.5-16.5		Many Basalt Flows	0-3500 ft (0-1067 m)
Cretaceous					66-144		Granitic Intrusives	
Cambrian					505-570		Orthoquartzite	

* Data from Hooper and Webster (1982); Tolan *et al.* (1989); and Wood (1987).

most flows in the region is about 50 to 100 feet (15-30 meters) (Wood, 1987). The total number of the basalt flows in the Pullman-Moscow Basin is not known but the thickness of the sequence is estimated at over 3,000 feet (914 meters) in the west portion of the Basin. Total thickness of the basalt flows overlying the basin basement is about 1400 feet (427 meters) under the UIGRS (Ralston, personal communication, 1991).

The Palouse Formation that covers the entire Basin consists of loess with quartz and feldspar composition. The loess was derived from central Washington and Oregon throughout Pleistocene and Recent epochs. The Formation forms modified dune topography overlying the basalt surface and flanks of steptoes. Thickness of the loess varies from zero to several hundred feet. Recent alluvial deposits, found along ancient and current stream channels, are composed of loess, silt and clay, as well as sand and gravel formed from basalt, quartz and granitoid rocks (Hooper and Webster, 1982).

The basalt flows in the Pullman-Moscow Basin are classified into Wanapum and Grande Ronde Formations of the Yakima Basalt Subgroup of the Columbia River Basalt Group (Swanson *et al.*, 1979, 1980). The Wanapum basalt that forms the uppermost section of the basalt sequence is stratigraphically separated from the Grande Ronde basalt by a sedimentary interbed, the Vantage Member of Miocene Ellensburg Formation. Most flows of Wanapum basalt are absent; the Priest Rapids member is the only unit found in the basin. The thickness of the Priest Rapids basalt ranges from zero to 250 feet (76 meters) (Hooper and Webster, 1982).

The Wanapum basalt is distinct geochemically from the Grande Ronde basalt as it contains higher concentrations of phosphorus and titanium than the Grande Ronde Formation (Wright *et al.*, 1973; Hearn *et al.*, 1984; Wood,

1987). The percentage relationship of TiO_2 and P_2O_5 concentrations in the different formations is shown in Figure 2-1.

The Grande Ronde basalt consists of many flows and interbedded sediments in the Basin area. The thickness of an individual Grande Ronde basalt flow averages 40 to 80 feet (12 to 24 meters) although flows over 200 feet (61 meters) in thickness have been observed (Lum *et al.*, 1990). Total thickness of the Grande Ronde Formation ranges from zero to over 2500 feet (762 meters), with increasing thickness from east to west. The thickness of the Grande Ronde basalt is approximately 1300 feet (396 meters) under the UIGRS.

The Vantage Member of claystone and shale is widely found in the Pullman-Moscow Basin. More sediments occur above and below the Vantage Member near the east margin of the basin. Thickness of the Vantage Member ranges only 5-10 feet (1.5-3 meters) in the basin but the sedimentary interbeds are over 200 feet (61 meters) in total thickness in the Moscow area (Ralston, 1991). Laterally, the interbeds generally tend to become thinner in thickness and finer in grain size to the west of the basin though the spatial distribution of the interbeds has not been mapped adequately (Lum *et al.*, 1990; Ralston, personal communication, 1991).

Structure

Very little structural deformation of basalt has been detected in the Pullman-Moscow Basin. The basalt formations generally dip a few degrees to the northwest. Some subsidence appears to have occurred in the vicinity of Pullman. The results from previous investigations do not reveal any structural features other than the regional dip and local subsidence (Brown, 1976; Barker, 1979; Hooper and Camp, 1981; Lum *et al.*, 1990).

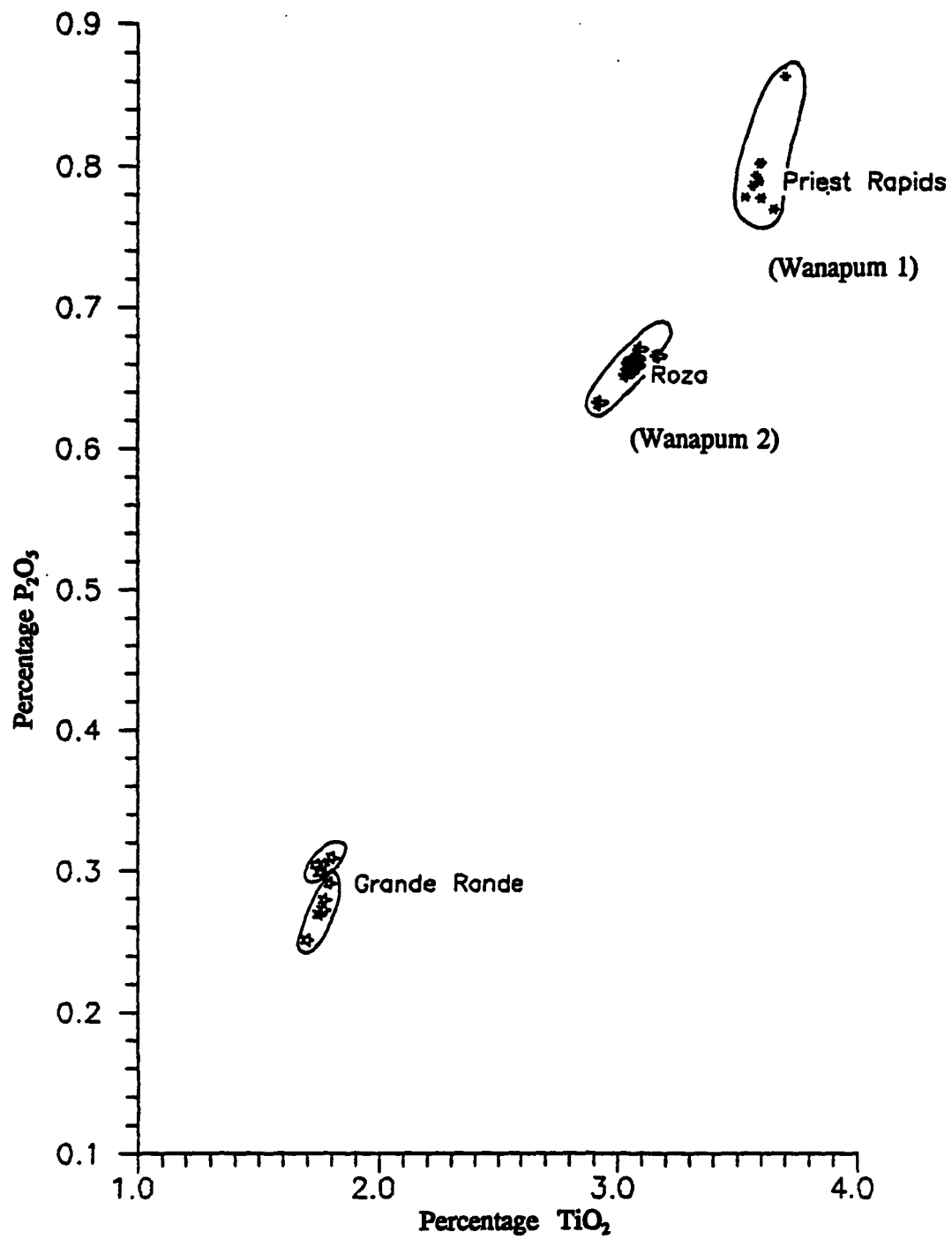


Figure 2-1. Basalt chemistry, percentage of TiO_2 and P_2O_5 of Wanapum and Grande Ronde Formations (after Wood, 1987)

Geology of the Research Site

Stratigraphy

The Priest Rapids Member is the only unit of the Wanapum basalt occurring in the Pullman-Moscow Basin according to Hooper and Webster (1982), Tolan et al., (1989) and Bush (personal communication, 1990). Two chemical types of basalt, Lolo and Rosalia, are found in the Palouse area. Small patches of Rosalia basalt lie both above and below the main flow of the Lolo basalt that underlies the whole basin floor (Hooper and Webster, 1982).

The Wanapum Formation occurs in the interval from 15 feet (4.5 meters) to about 200 feet (61 meters) below ground surface at the UIGRS. The Wanapum basalt flow is overlain by Palouse loess and alluvial sediments. The basalt outcrops are found along the Pullman-Moscow highway, west of the study site.

The Palouse Formation appears to increase in thickness toward the east and the southeast of the UIGRS. The thickness of the Palouse Formation and the Wanapum Basalt at the vicinity of the UIGRS is shown in Figure 2-2.

The field investigation, borehole geological and geophysical logging, and regional stratigraphic data analysis show that only the Lolo basalt flow of the Priest Rapids Member of the Wanapum Formation occurs at the UIGRS. The Lolo basalt flow surface capped by the alluvium and loess soil appears to be near the flow top based on the examination of the flow outcrops to the west of the site (Ralston, personal communication, 1991; Bush, personal communication, 1990). The fine-grained sediments have not been explored, but they are expected at depths of 180 to 200 feet (55 to 61

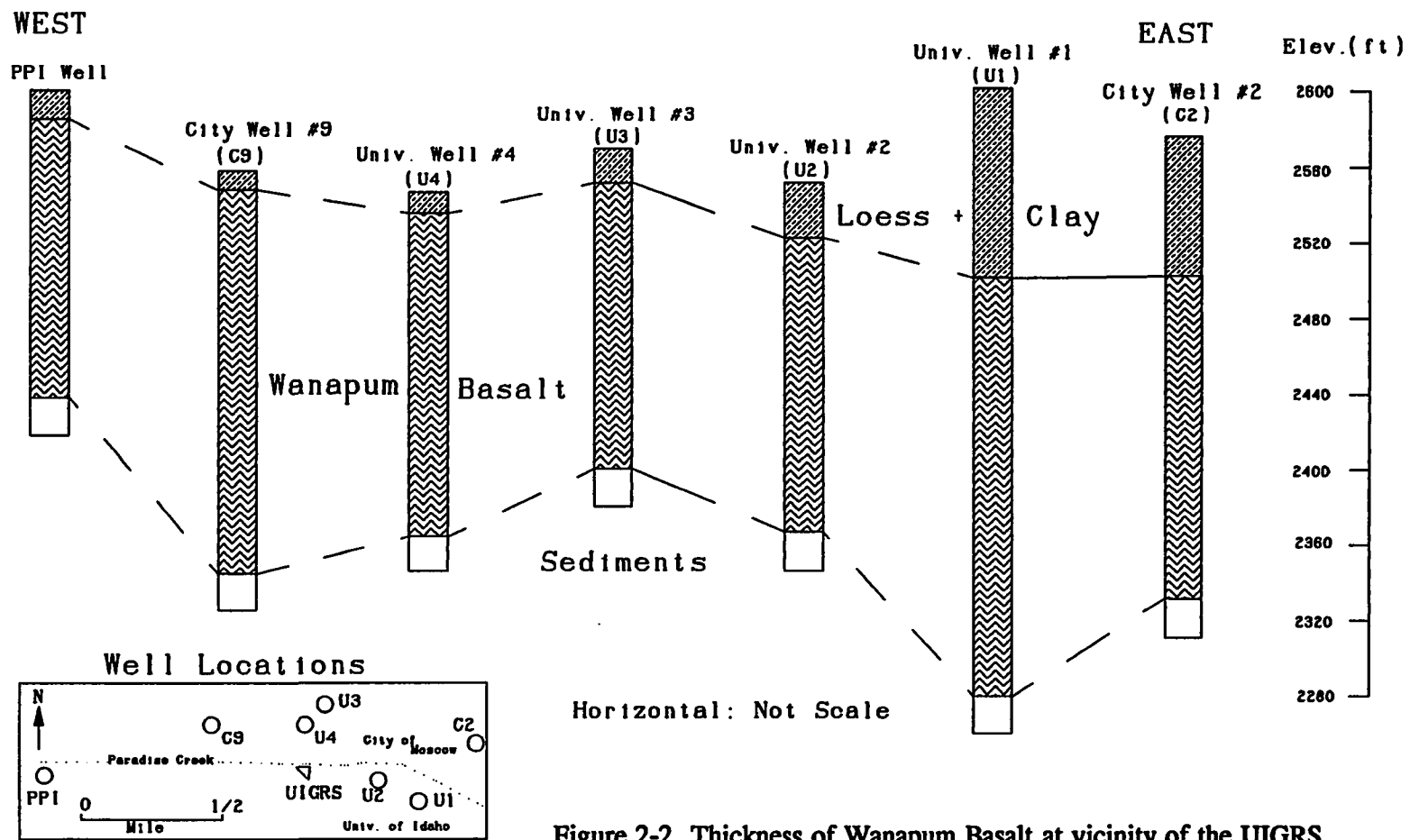


Figure 2-2. Thickness of Wanapum Basalt at vicinity of the UIGRS

meters).

Intraflow Structures of the Lolo Flow

The basalt internal structures, which developed during the emplacement and subsequent cooling of the lava, are termed intraflow structures. They are generally identified by the abundance and geometry of the fractures. Figure 2-3 shows typical intraflow structures that may be present within a flow in the Columbia River Basalt Group.

The intraflow structural features may vary greatly both stratigraphically and from site to site. Some structures may be absent entirely in one flow or occur repeatedly within another flow. The intraflow structure patterns have been classified by Long (1978) into three general types (Figure 2-4). These types are best thought of as end members with nearly continuous gradations between the types.

Type I flows lack a distinct entablature and have a poorly developed vesicular flow top. They are relatively thin with thicknesses of 30 to 100 feet (10 to 30 meters). Type II flows are very thick with columnar tiers of alternating entablature and colonnade in the lower section of the flow and hackly entablature on the upper section. An oxidized flow top with large frothy blocks is common, and vesicles are abundant in the upper third of the flow. There are commonly several horizontal or nearly horizontal breaks between the entablature and colonnade. Type III flows lack flow tops and vesicular zones and generally are moderately to very thick. The colonnade of the flow is well developed in the lower section. The entablature is a complex pattern of smaller radiating columns. A sharp break that extends in nearly horizontal directions often is found between entablature and colonnade (DOE, 1981).

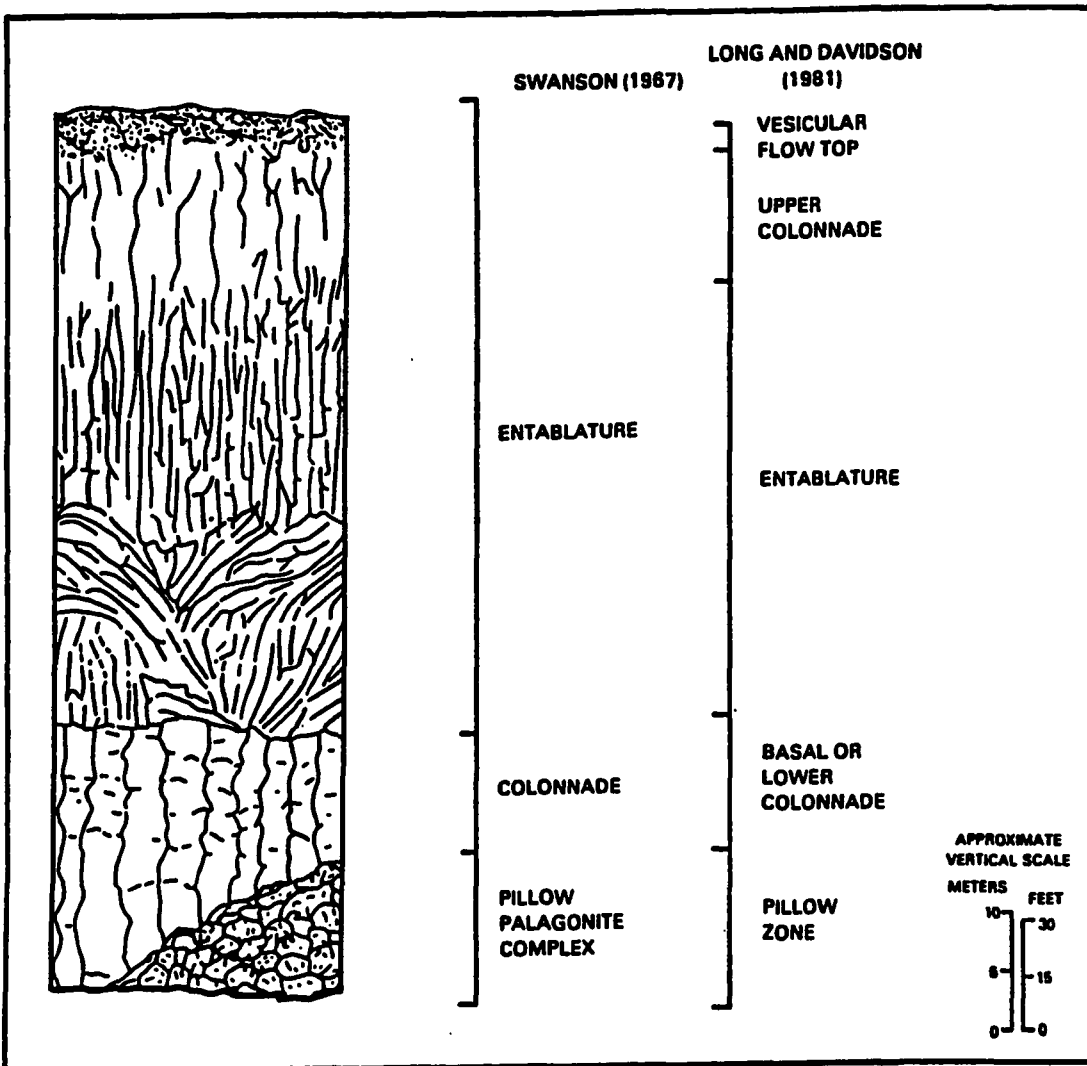


Figure 2-3. Typical intraflow structures in the basalt flow

(after DOE, 1981)

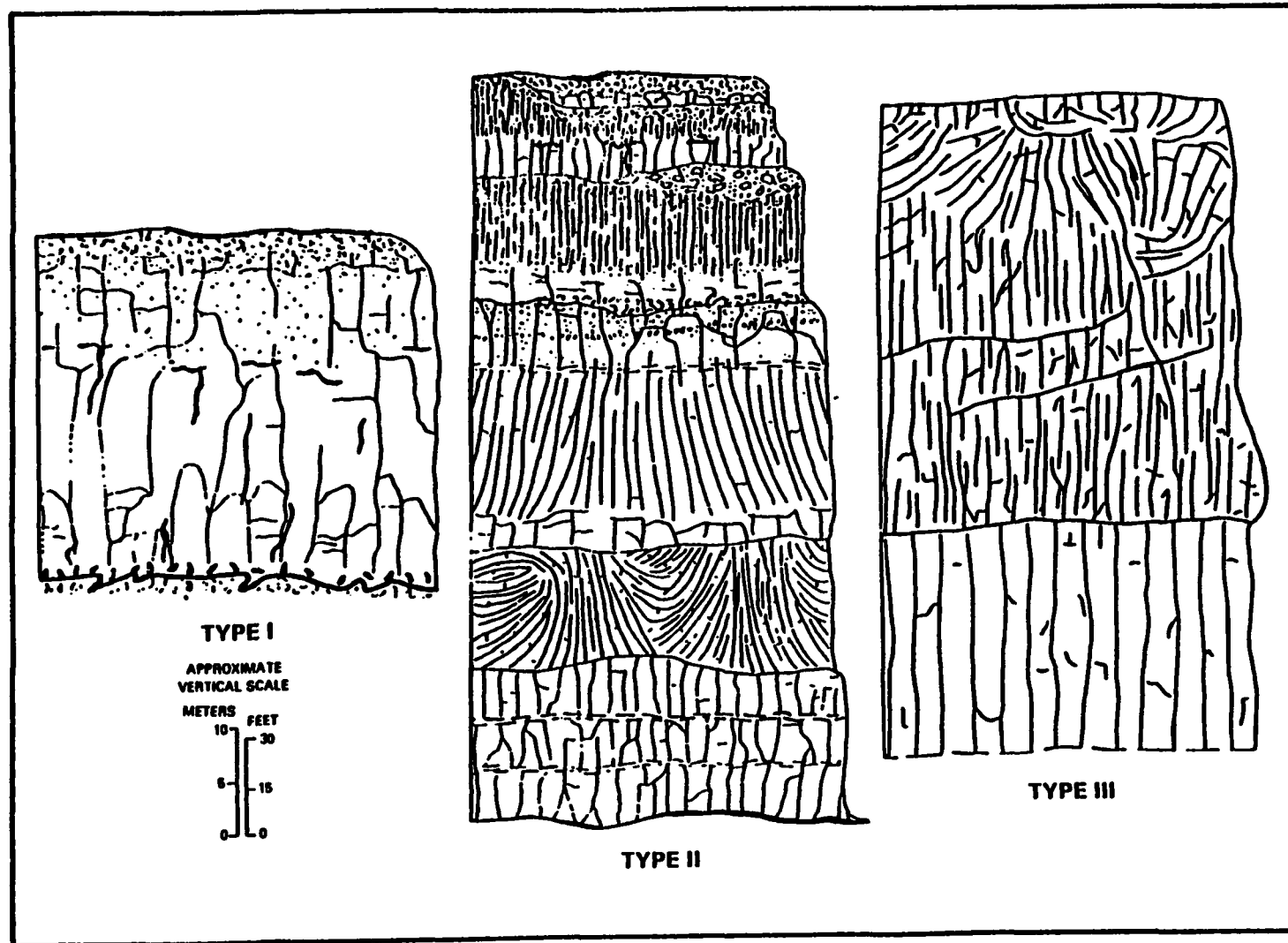


Figure 2-4. Basalt intraflow structure types (after Long, 1978)

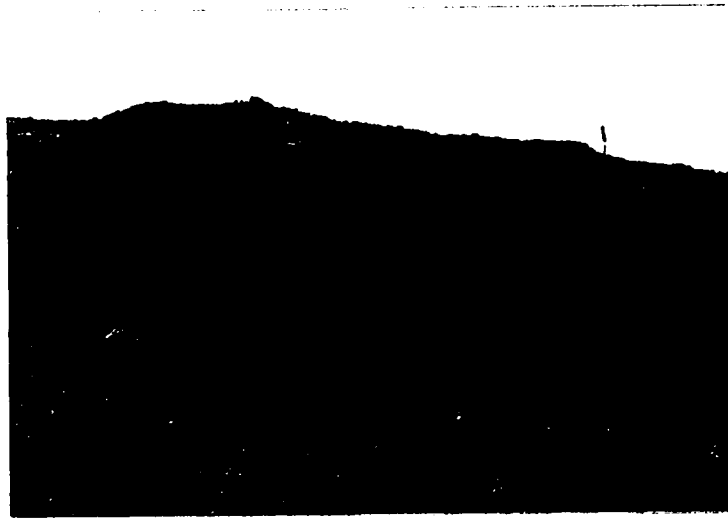
Intraflow structures of the Lolo flow at the research site can be well observed from the outcrops at rock crusher sites along the Pullman-Moscow highway. Both type II and Type III have been observed in the area and some intermediate gradation types also exist. Figure 2-5 shows an example of intraflow structure patterns of the Lolo flow exposed at the crusher sites.

The Lolo flow generally is very thick (120-200 feet, 35-60 meters), exhibiting an oxidized flow top with large frothy blocks and nearly horizontal platy fractures in the uppermost portion of the flow. The columnar tiers of alternating entablature and colonnade occur in the middle portion of the flow, which grade upward into hackly entablature. The lower portion of the flow generally is composed of colonnade columns with a width of several feet.

Sharp breaks commonly separate the intraflow structures and extend in a nearly horizontal direction or dip at an angle of less than 30 degrees. Vesicular zones commonly are observed just below the horizontal breaks in the upper portion of the flow. Some columnar fractures are well developed and clearly cut through the entire portion of entablature or colonnade. These fractures commonly are formed by aggregates of many small vertical or nearly vertical joints rather than a large single fracture (Bush, personal communication, 1990).

The relationships between the vertical fractures and horizontal breaks (intraflow structure contact zones) are very complex. They may cross each other, forming a fracture net or be terminated by each other, showing a Z pattern. No displacement was observed along any of these fractures or breaks.

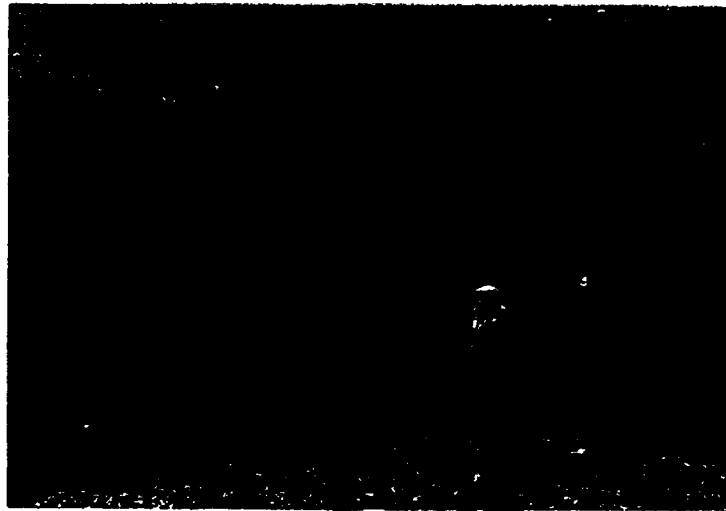
Lateral variation of the intraflow structures is very significant.



A. Flow top



B. Vesicular zone near horizontal break in the flow interior



C. Entablature and colonnade (middle portion of the flow)



D. Entablature and colonnade (lower portion of the flow)

Figure 2-5. Intraflow structures in Lolo flow, Pullman-Moscow highway, three miles west of the UIGRS

Most structures do not extend over distances more than a few hundred feet. However, similar patterns have repeatedly been observed from site to site over a great distance. Thicknesses of the flow top, entablature and colonnade may also change dramatically over short distances. All the lateral variations of the intraflow structures reflect the complex cooling conditions and emplacement environment of the basalt lava at the edge of the Columbia River Basalt Plateau (Bush, personal communication, 1990).

Analysis of Well Geological and Geophysical Logs

Well Geological Logs

Geological logs of the wells provide the primary basis for description of the hydrogeology of the UIGRS. The logs are presented in Figures A-1 to A-14 of Appendix A. The Pleistocene sediments, as the first stratigraphic unit, are penetrated by all of the deep and shallow wells. There are basically two layers of sediments at the study site: black loess soil and silty clay graded to silt at the top, and yellow and black sand and gravel lying below. The average thickness of the top fine-grain sediments is approximately 10 feet (3 meters); the coarse layer averages 2 to 10 feet (0.6-3 meters) in thickness.

Lateral distribution of the coarse sand and gravel layer appears to be related to the ancient channels of Paradise Creek. The layer tends to become finer in grain size and thinner in thickness toward the south and southwest from the present creek channel. The sand and gravel layer is absent at the west edge of the site at well D19D.

A broken or highly fractured basalt zone underlies the Pleistocene sediments (Figures A-1 to A-14). The broken basalt is composed of

vesicular basalt rubble based on an examination of the rock cuttings. The broken basalt zone is believed to be part of the flow top. This conclusion is supported by outcrop observations one mile west of the site and a stratigraphic correlation. The thickness of this zone ranges from 6 to 16 feet (1.8 to 4.8 meters).

The bottom of the Lolo basalt flow is expected at depths of 160 to 200 feet (48 to 60 meters) at the UIGRS. The deep wells penetrate the upper and middle portions of the flow. None of the wells fully penetrate the Lolo flow. The flow interior consists of dark gray to black, medium to very dense basalt with fracture zones. Most of the fracture zones could be observed only through change of the drilling penetration rate and the size of rock cuttings. There is generally no change in basalt lithology across the fracture zones. These zones are very likely the horizontal or nearly horizontal breaks between the intraflow structures.

The major fracture zones are generally water productive. Thickness of the fracture zones ranges from 0.5 to 5 feet (0.1 to 1.5 meters) with significant lateral variation in both thickness and depth.

Borehole Geophysical Logs

Borehole geophysical logging was conducted on eight deep wells at the UIGRS. A logging rig owned by Washington State University was used for the study. Nine borehole logs were obtained in each of the wells: spontaneous potential/resistivity log, natural gamma log, neutron-gamma log, gamma-gamma log, neutron-epithermal log, flow meter log, fluid temperature log, fluid resistivity log, and caliper log.

Flow meter logs show that there is no measurable vertical flow in any of the wells. Some of the flow meter logs were disturbed at certain points

due to the propeller being restricted by solids in the wells.

Fluid temperature logs show that an increase of water temperature corresponding to the geothermal gradient was observed at depths below 70 feet (21 meters). The water temperature near the water table is obviously affected by the atmospheric temperature.

The flow meter and fluid temperature logs are of limited value for identification of water productive fracture zones because of two reasons: 1) the wells are relatively shallow so that the water temperature anomalies caused by variations in atmospheric temperature is dominant, and 2) most of the minor intraflow fractures are not open enough to allow significant ground water to enter or leave the borehole. The water flow velocity within the borehole may be too small to be detected in the flow meter logs.

The most useful geophysical logs for identifying the intraflow fractures in the basalt are the caliper, gamma-gamma and neutron-neutron logs. Gamma-gamma logging is based on the principle that the attenuation of gamma radiation as it passes through the borehole and surrounding rocks is proportional to the bulk density of those rocks. This log generally is used for determining the bulk density of the formation. In this study, the gamma ray count rate is inversely proportional to the bulk density of surrounding basalt because the probe detects only radiation resulting from the logging process.

Neutron logging is utilized to detect the porosity of the saturated rock, based on the principle that neutron interactions are related to the quantity of hydrogen present as water. Low neutron counts generally indicate high saturated porosity in the saturated zone and high moisture content in the unsaturated zone.

Caliper logging is used to detect borehole diameter variation.

Abrupt increases of borehole diameter represent rock lithology changes or fracture zones in the borehole.

Example correlations between the geology and geophysical logs at wells Q16D and U3D are shown in Figures 2-6 and 2-7. The borehole geophysical logs are plotted with digitized data records, whereas the geology log is based on the drilling records. The logs have shown high agreement with each other for identifying the fractured basalt zones.

Broken and fractured basalt zones are clearly seen in the caliper logs as larger bore hole diameter. The major fractures with low bulk density and high saturated porosity also are seen in the gamma-gamma and neutron-neutron logs.

The gamma-gamma and neutron-neutron logs are affected by the borehole diameter changes. Keys (1989) suggests that when sharp peaks on a caliper log, which indicate borehole rugosity, match sharp negative deflections on a gamma-gamma log, the gamma-gamma deflections are most likely the result of borehole diameter changes. The neutron log also is influenced by the variation of borehole diameter but to a lesser degree than the gamma-gamma log (Keys, 1986; 1989).

Some of the small, sharp deflections on the gamma-gamma logs, as shown in Figure 2-6 and Figure 2-7, are possibly the results of the borehole diameter changes rather than the variation of the basalt bulk density. In fact, many minor fractures in the Lolo flow may or may not change the rock bulk density; possibly, the equipment is not sensitive enough to detect the minor changes.

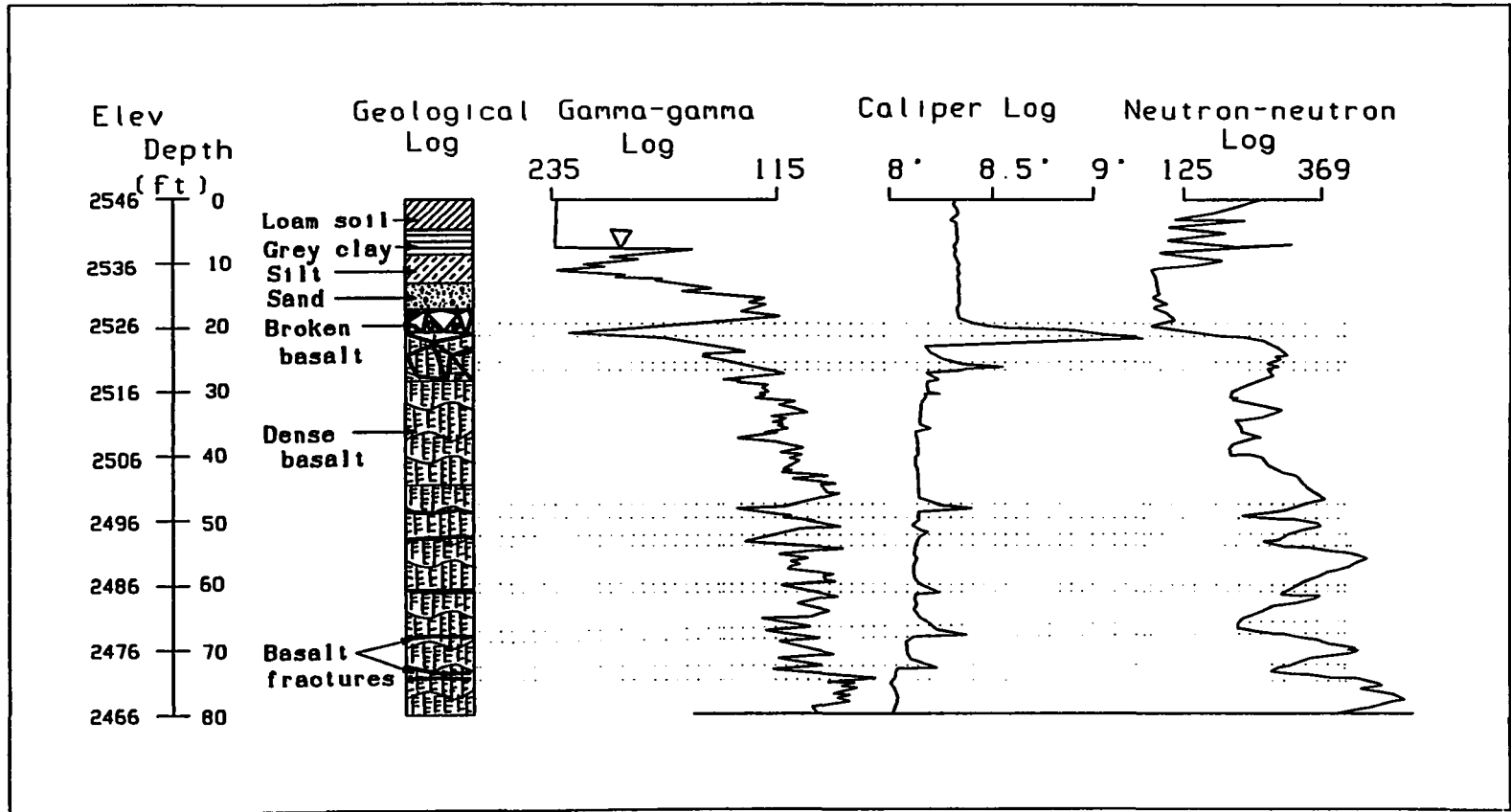


Figure 2-6. Correlation of geology and borehole geophysical logs of well Q16D

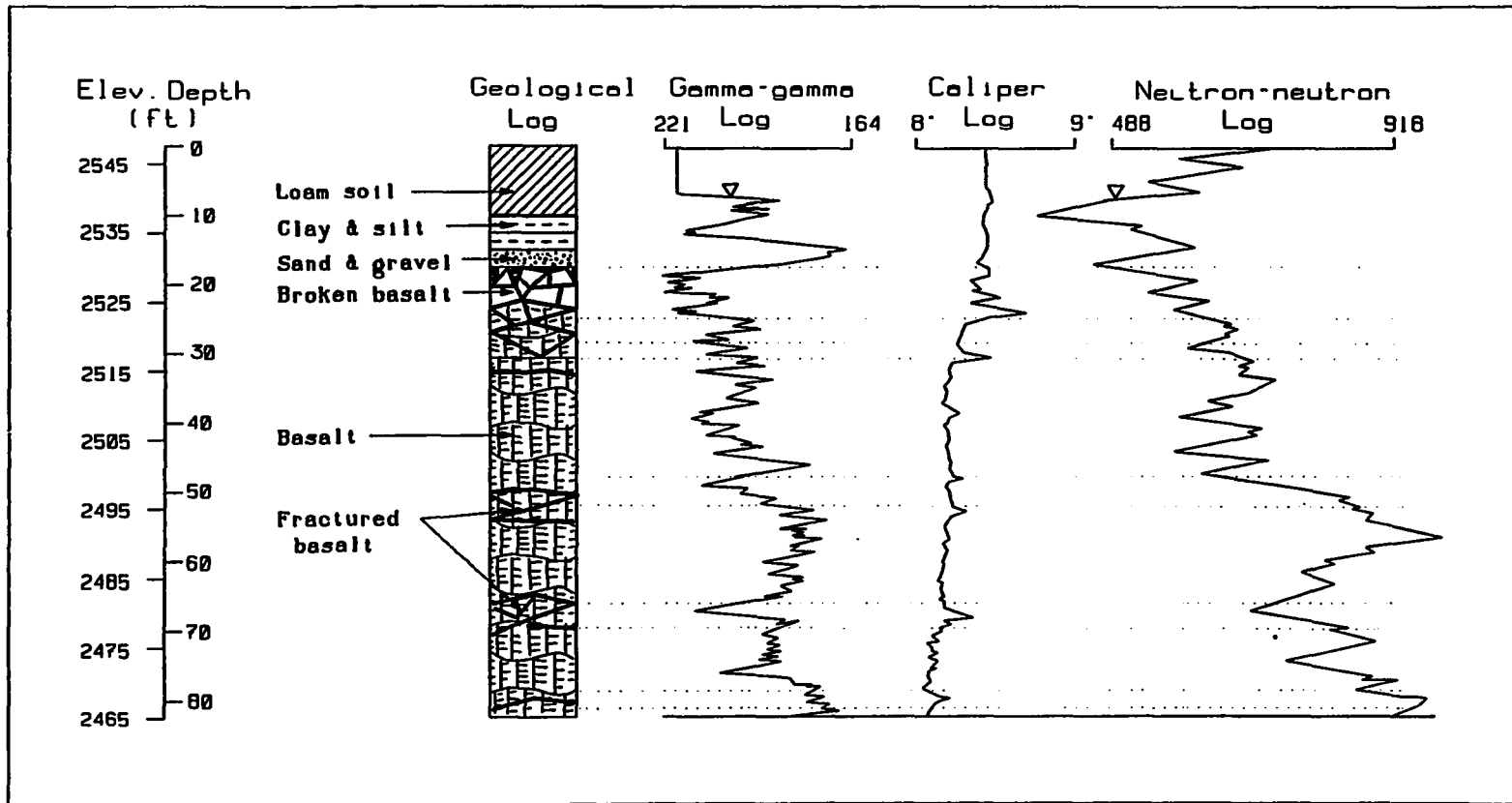


Figure 2-7. Correlation of geology and borehole geophysical logs of well U3D

Geological Cross Sections

Three geological cross sections are presented in this section. The locations of these cross sections are shown on Figure 2-8. The caliper logs are used to construct the cross sections to demonstrate the fracture patterns at the UIGRS.

The cross section A-A' along the northern boundary of the UIGRS is shown in Figure 2-9. A major fracture zone with thickness of 1 to 3 feet (0.3 to 1 meter) is present at depths of 60 to 75 feet (18 to 22 meters) in the northeastern portion of the site (Figure 2-8). This zone is very likely a nearly horizontal break that divides the entablature and colonnade of the Lolo flow. The fracture zone dips slightly toward the west or southwest. The thickness of the fracture zone and the openness and density of the fractures are believed to decrease from the northeast to the southwest. The fracture zone is completely absent at the south and west portions of the site.

The entablature portion of the basalt flow above the major fracture zone in the eastern portion of the UIGRS is generally less dense and more fractured than the entablature in the western portion of the site. Three or four nearly horizontal minor fracture zones occur at the interval of 30 to 60 feet (10 to 20 meters) from ground surface. No significant ground water flow was observed from these minor fracture zones when the wells were drilled.

Major fractures in the west portion of the study site were observed at depths of 70 and 140 feet (21 and 42 meters) in two wells J16D and D19D. The fractures explored at different depths are considered as a single zone because of their direct hydraulic connection as demonstrated during the aquifer tests. Two hypotheses are proposed to explain the hydraulic

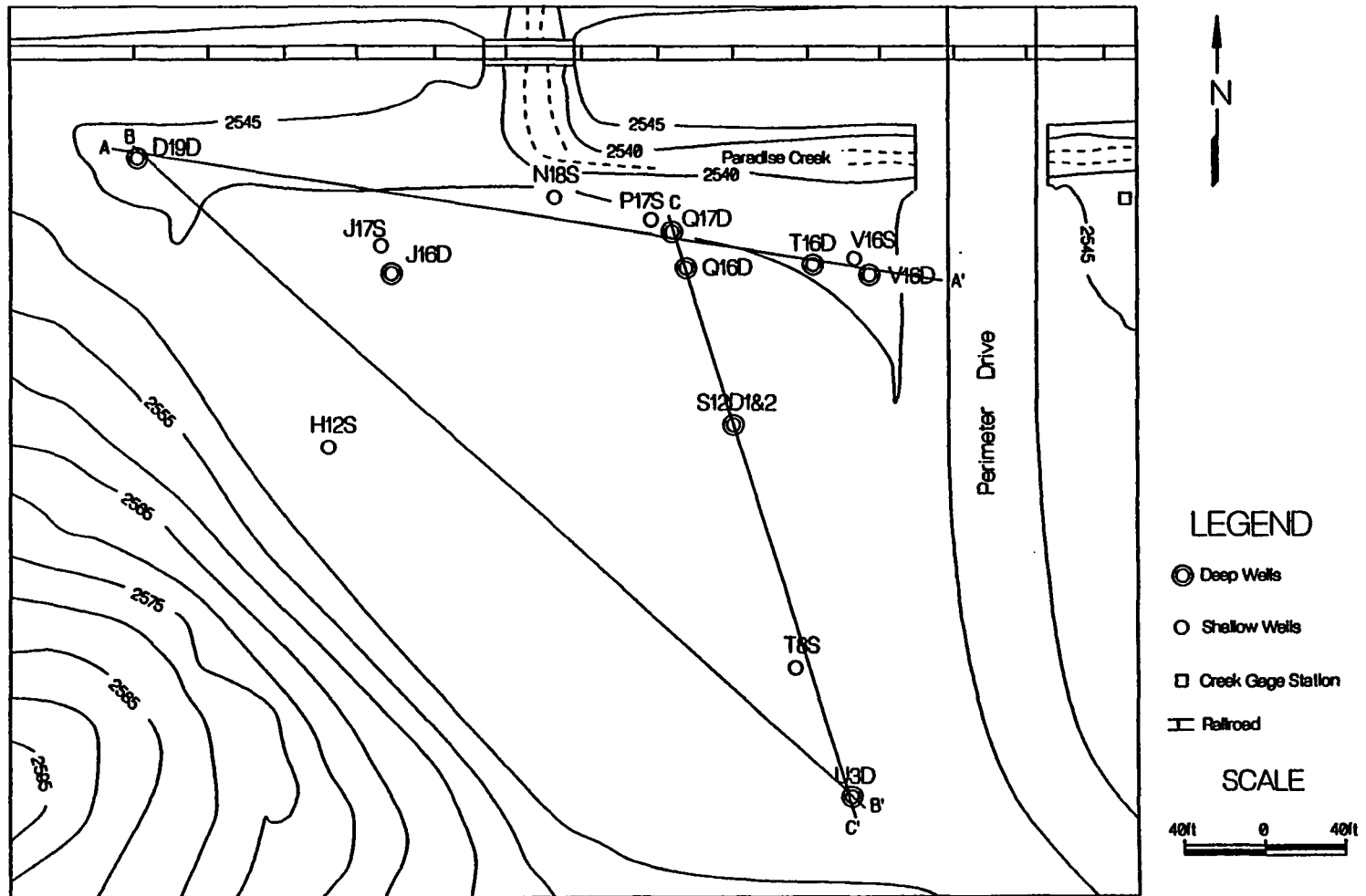


Figure 2-8. Locations of the geological cross-sections.

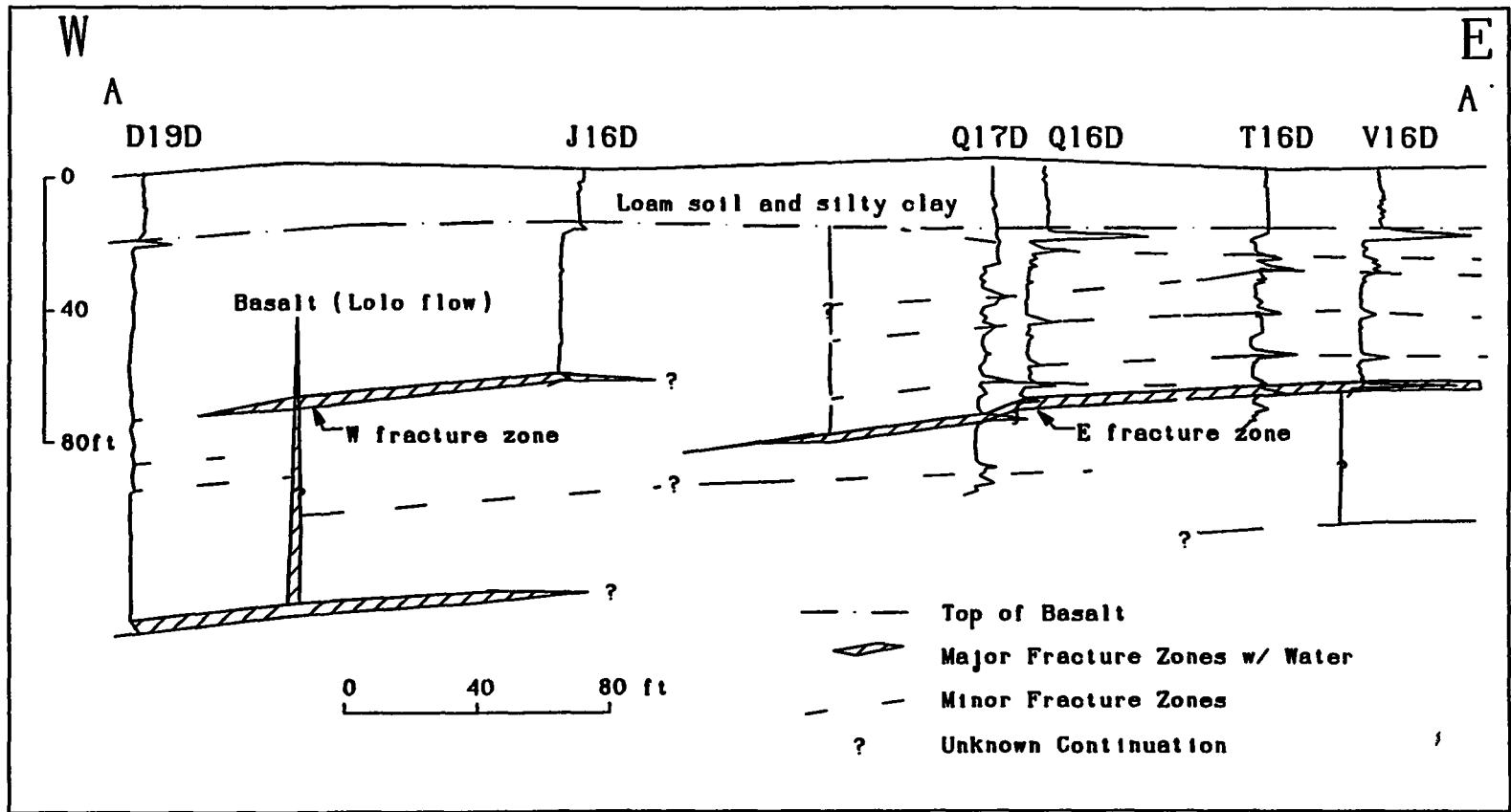


Figure 2-9. Cross-section A-A' with caliper logs along the north side of the UIGRS

interconnection of these fracture zones: 1) the zone is in "Z" shape with vertical fractures connecting two horizontal or nearly horizontal breaks, or 2) a single zone dips toward the west at a large angle. The Z shape is more likely the actual fracture pattern based on the observation of the outcrops near the site. This interpretation is shown on Figure 2-9.

Lateral variation of the fracture zone in the west of the site is significant; the thickness and fracture openness of this zone decrease from west to east. The zone was observed in lower sections of wells Q17D and Q16D in the northern central part of the site but is less productive than the west portion of the same fracture zone. The zone occurs at a depth of 80 feet (24 meters) in the southeast portion of the site.

The significant difference in basalt lithology across the UIGRS is that the Lolo flow appears to be much denser and less fractured in the western part of the site. There are hardly any fracture zones to a depth of about 140 feet (42 meters) in well D19D. The type III structure (Figure 2-4) model is most appropriate in the western portion of the UIGRS.

The major fracture zone occurring in the eastern portion of the UIGRS is named E fracture zone, and the Z-shape fracture zone in the west is called W fracture zone for this study. The two fracture zones are identifiable from water level data, results of aquifer tests, and microbial ecology data. The nine deep wells are all completed in one of the two zones.

Cross section B-B' shows the subsurface geology from northwest to southeast along the hillside edge of the UIGRS (Figures 2-8 and 2-10). The W fracture zone was penetrated at a depth about 80 feet (24 meters) in the southeast portion of the site at well U3D. Several minor fractures were observed above the W zone, and well U3S was completed in the upper one at a

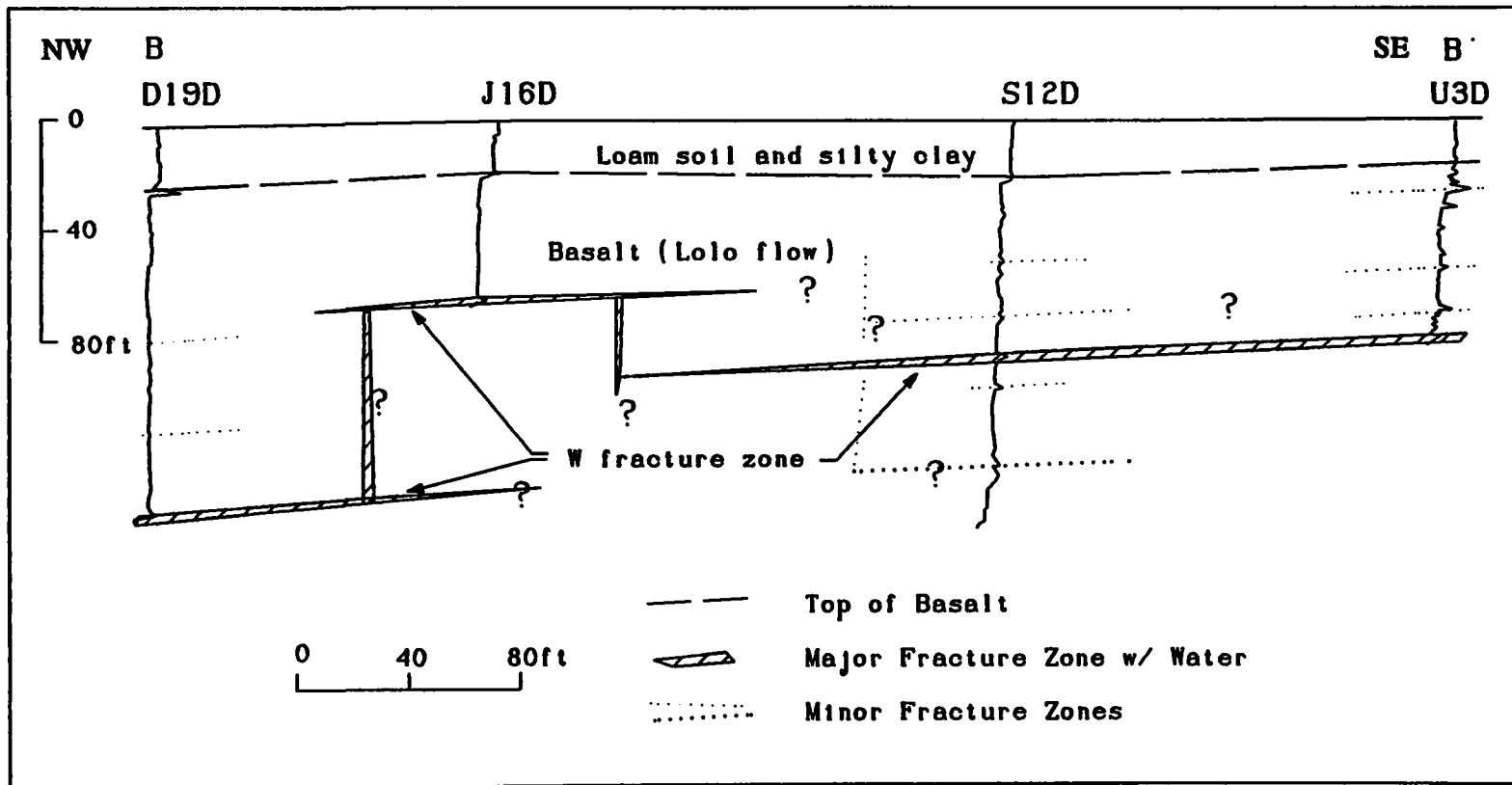


Figure 2-10. Cross-section B-B' along southeast side of the UIGRS

depth of 33 to 35 feet (10 to 11 meters). The W fracture zone was observed in well S12D at a similar depth of 75 to 80 feet (22.5 to 24 meters) in the central part of the UIGRS.

Cross section C-C' from north to south across the central part of the UIGRS is presented in Figure 2-11. The W fracture zone is shown in all four wells at depths of 75 to 90 feet (23 to 27 meters). The E fracture zone is observed 10 to 15 feet (3 to 4.5 meters) above the W zone at wells Q17D and Q16D in the northern portion of the site.

The lateral extension of the E fracture zone to the south illustrates the complexity of the fracture patterns at the UIGRS. A minor fracture zone at depths of 120 to 130 feet (46 to 49 meters) in well S12D is hydraulically connected with the E zone (Figure 2-11) at the central portion of the site. This minor fracture zone is deeper than the W fracture zone but isolated from it. The connection between the minor fracture and the E fracture may be through vertical columnar fractures in an area where the W fracture is absent.

The lateral extension of the minor fractures is generally limited. However, the minor fractures are not hydraulically isolated because of the vertical columnar structures through the entire basalt flow.

Summary

The geology of UIGRS can be summarized as follows:

- 1) The UIGRS is located at the west edge of the University of Idaho campus within the eastern portion of the Pullman-Moscow Basin, in which the Palouse Formation, and the Wanapum and Grande Ronde basalt of the Yakima Subgroup of Columbia River Basalt Group overlie a

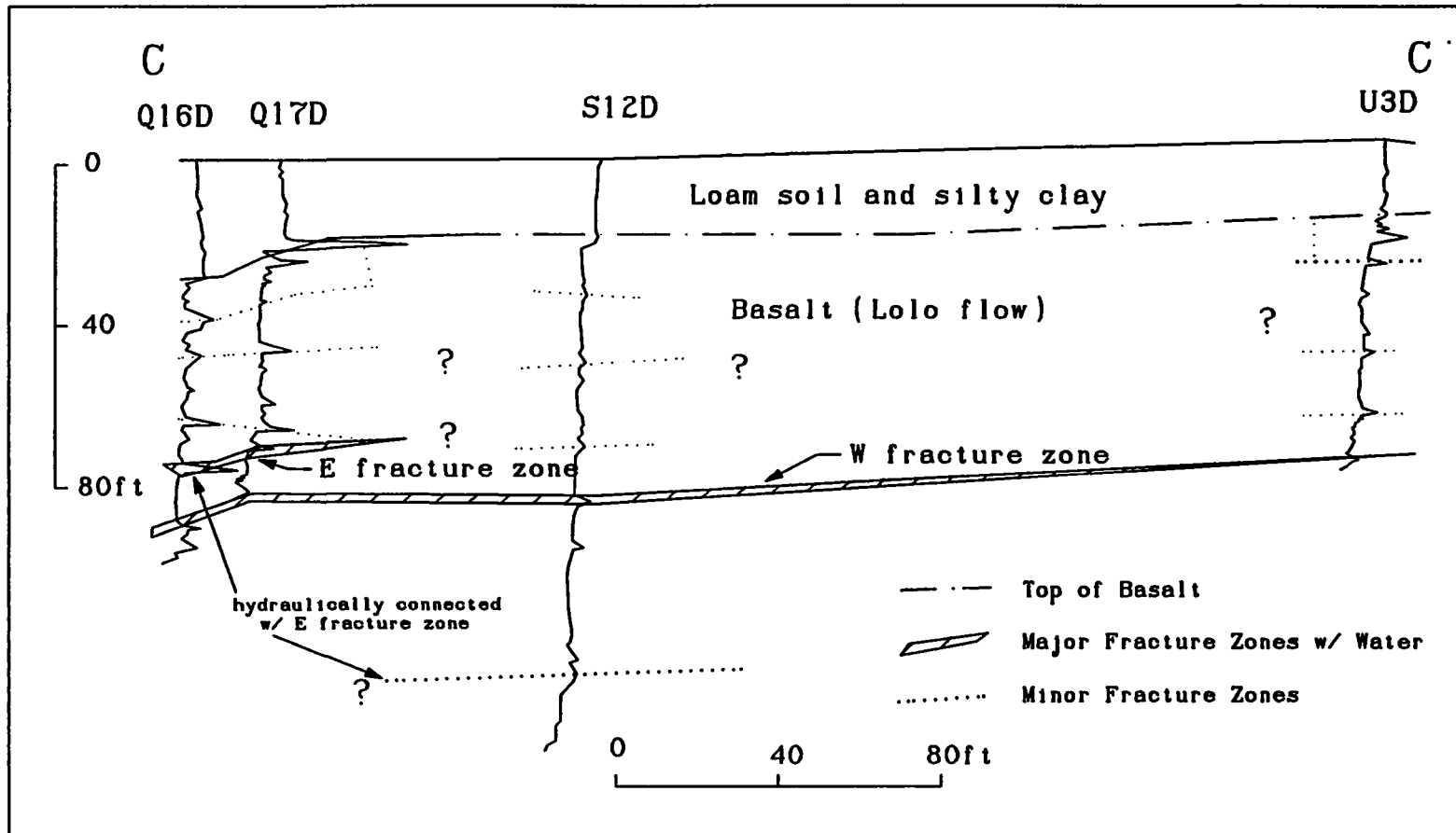


Figure 2-11. Cross-section C-C' from north to south at the UIGRS

granitic basement.

- 2) The upper portion of the Palouse Formation consists of black loess soil, clay and silt that form the first layer of the stratigraphic section. Thickness of this unit ranges from 9 to 12 feet (2.7 to 3.6 meters).
- 3) A layer of alluvial sand and gravel is the second stratigraphic unit at the site. The thickness of the layer and the grain size of the sediments have great lateral variation. The unit is very likely associated with the ancient Paradise Creek channel. The layer averages 2 to 10 feet (0.6 to 3 meters) in thickness at the north side of the site.
- 4) The basalt assigned to the Lolo flow of the Priest Rapids basalt of the Wanapum Formation forms the third and major stratigraphic unit of the site. Wells have been drilled into the upper portion of the Lolo flow that sits on top of the Vantage Formation. Wells are completed from 15 feet to 146 feet (4.5 to 44 meters) from ground surface. The bottom of the Lolo flow is expected at depths of approximately 180 to 200 feet (55 to 61 meters).
- 5) The intraflow structures of the basalt are dominant features in terms of fracture patterns intercepted by the wells. No flow contact zone was explored at the site, because there is only a single Lolo flow at a depth of up to 200 feet (61 meters).
- 6) Three types of fractured basalt are identified at the site. The broken basalt at depths of 15 to 30 feet (4.5 to 9 meters) is a partially eroded flow top. Two major fracture zones identified as E and W fracture zones occur at depths of 63 to 75 feet (19 to 23 meters) in the east portion of the site and at depths of 70 to 140

feet (21 to 42 meters) in the western portion of the site, respectively. Several minor fractures occur at depths of 30 to 60 feet (9 to 18 meters) in the eastern and southern portions of the site.

- 7) The lateral extension of the major fracture zones is limited in terms of fracture density and openness. Both E and W zones become minor fractures at a distance of a few hundred feet. The E fracture zone dips slightly (less than ten degrees) to the west and extends from the northeast to the middle portion of the site. The W fracture zone is found in a larger area of the west and south portions of the site. It is probably in a "Z" shape that is formed by the major horizontal fractures at different depths with connection by the columnar fractures.

CHAPTER III

Ground Water Hydrology

Hydrographs and contour maps of water levels from deep wells completed in the two basalt fracture zones and from shallow wells in the alluvium are presented in this chapter. Ground water recharge and discharge, and the interrelationship between Paradise Creek and subsurface aquifers are analyzed. A hydrogeological conceptual model is proposed based on the geology and hydrogeology studies.

Ground Water Hydrographs

Static ground water levels at the UIGRS have been monitored on a daily basis since December 28, 1987, when five deep basalt wells were drilled (development Phase I). Additional shallow and deep wells were added to the monitoring program in the research facility as they were drilled. Water levels were measured by hand with a steel tape. The early water level hydrographs were presented by Ralston and Li (1989). A datum marker was set on top of the steel protective casing or the PVC well casing for each well. The marker locations and elevations for all wells at the UIGRS are presented in Table 3-1.

Annual water level fluctuations in the wells range approximately from one to four feet. High water levels occur in the spring and low levels occur in the fall. The daily water levels in the deep basalt wells respond to barometric pressure changes and precipitation events. Generalized hydrological data of the wells also are presented in Table 3-1.

Table 3-1. Ground Water Level and Well Yield Capacity Data at the UIGRS

WELL NO.	WATER LEVEL ELEV.(AMSL) (ft)		MAX. WELL YIELD (gpm)	SPEC. WELL YIELD (gpm/ft)	DATUM MARKER FOR WATER LEVEL MEASUREMENT	DATUM ELEV. (ft)
	ANNUAL HIGH	ANNUAL LOW				
V16D	2540.7	2537.0	40-50	3.25	Top of 6" Casing	2544.41
Q17D	2540.3	2536.6	7-10	0.25	Top of 6" Casing	2545.95
T16D	2540.4	2536.7	7-10	0.3-0.4	Top of 6" Casing	2545.24
D19D	2519.8	2518.9	30-50	0.2-0.3	Top of 6" Casing	2543.76
S12D1	2540.4	2535.4	<1	Data not available	Top of 6" Casing	2546.93
S12D2	2520.3	2519.3	<1		Top of 8" Casing	2546.96
Q16D	2540.6	2536.8	2-3(?)			
Q16S	2540.5	2536.6	<1(?)			
U3D	2521(?)	2519.3	1-2(?)			
U3S	2544.1	2541.2	1-2(?)	0.4-0.5	Top of 8" Casing	2548.62
J16D	2521(?)	2519.3	40-60		Top of 8" Casing	2546.68
J16S	2540.5	2536.4	<1	Data not available	Top of 1" Casing	2546.27
P17S	2540.0	2536.3	<.5			
V16S	2541.0	2536.7	<.5			
N18S	2539.7	2536.2	<1			
H12S	2540.5	2537.3	<.2			
T8S	2541.0	2537.5	<.2			
J17S	2540.1	2536.2	<1			
				Top of 2" Casing	2546.64	

The water level hydrographs of all the deep basalt wells over a three-year period are shown in Figure 3-1. The hydrographs may be divided into two groups based on water level elevations. The first group includes wells V16D, Q17D, T16D, Q16D and S12D1 completed in the E fracture zone; the second group wells are D19D, J16D, U3D and S12D2 completed in the W fracture zone. The static water levels in the E fracture group wells average 2537 feet (773 meters) AMSL, whereas the W fracture group wells in the W fracture zone have water levels 10 to 20 feet (4.5 to 6 meters) lower. Wells within a particular group also have nearly identical fluctuation patterns.

Characteristics of the well hydrographs of the E fracture zone are summarized as follows: 1) the annual high water level occurs during the period of spring snow melt; 2) the annual low water level occurs in the fall following the dry summer; 3) the water levels respond to precipitation events rather closely, generally within 6 to 12 hours; and 4) the annual amplitude of water level fluctuations averages 3 to 4 feet (1 meter).

The general hydrographic features of the wells in the W fracture zone are: 1) the annual fluctuation of static water level is much less than that of the E fracture zone, averaging less than one foot (0.3 meters); 2) the annual low water level occurs at the end of the dry season, generally at the beginning of winter; 3) the water levels respond only to large precipitation events with a delay of several days to a few weeks; and 4) the daily water level change is mainly due to barometric pressure variations.

There was a remarkable water level rise in well Q17D and a water level drop in well D19D on Oct 22, 1988. This was caused by the completion of well Q17D in the E fracture zone and elimination of the interconnection

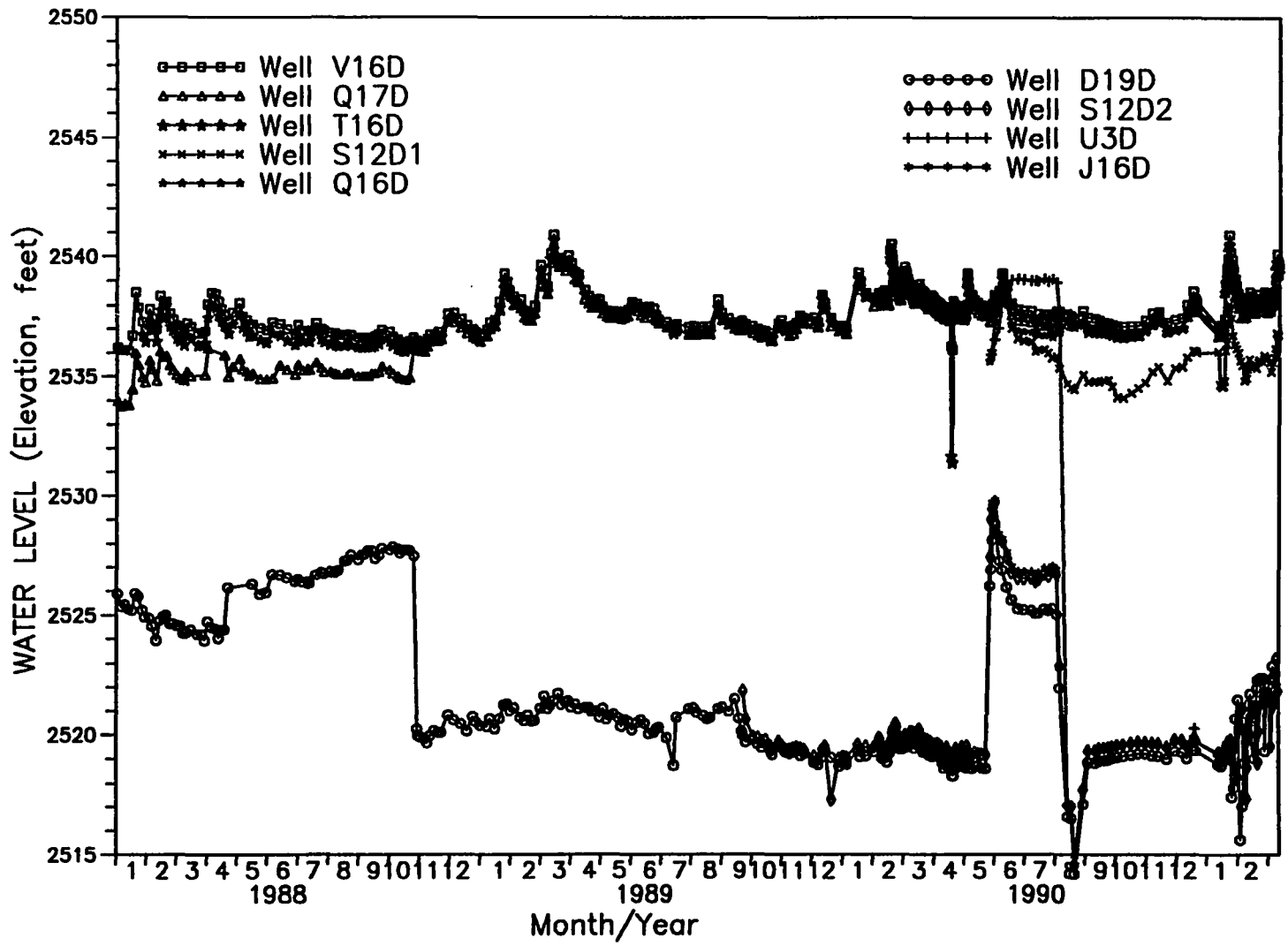


Figure 3-1. Ground water hydrographs of deep basalt wells (1988-1991)

of the two zones through the borehole. A mixed water level consisting of two fracture zones was observed again in the W fracture wells from June to August, 1990, when wells Q16D and U3D were drilled but not completed in one fracture zone. Completion of the new wells brought the water level in the W fracture zone back to its normal elevation. The water level in the E fracture zone was not affected significantly because flow lost from the E zone probably is very low.

The water level in well U3D prior to completion in the W fracture zone was high during the summer of 1990 (Figure 3-1). This is caused by the higher water level elevation in the upper portion of the basalt flow in the south portion of the UIGRS. The water level in well U3S, completed at 34 feet from ground surface (Figure A-7), is about 3 feet higher than that of the E fracture group and the shallow alluvium group wells. This higher water level in the upper portion of the flow has been observed only in well U3S. The reason for such behavior is currently unknown, but it certainly indicates complex fracture patterns in the upper portion of the Lolo flow.

A sharp water level drop at the E fracture zone in April, 1990, resulted from a 45-hour aquifer test. The water level disturbance in the W fracture zone in late February and early March, 1991 probably was caused by the drilling and pumping of the Aquaculture Lab water supply well located about 400 feet (122 meters) southwest of the UIGRS.

Hydrographs of the shallow wells and Paradise Creek are presented in Figure 3-2. The annual water table fluctuation is about 5 feet (1.5 meters). High level is in the spring and low level occurs at the end of summer. The water levels from the shallow wells and the creek correspond closely with each other. Their fluctuation patterns are similar to that of the E fracture group wells, responding closely to precipitation events.

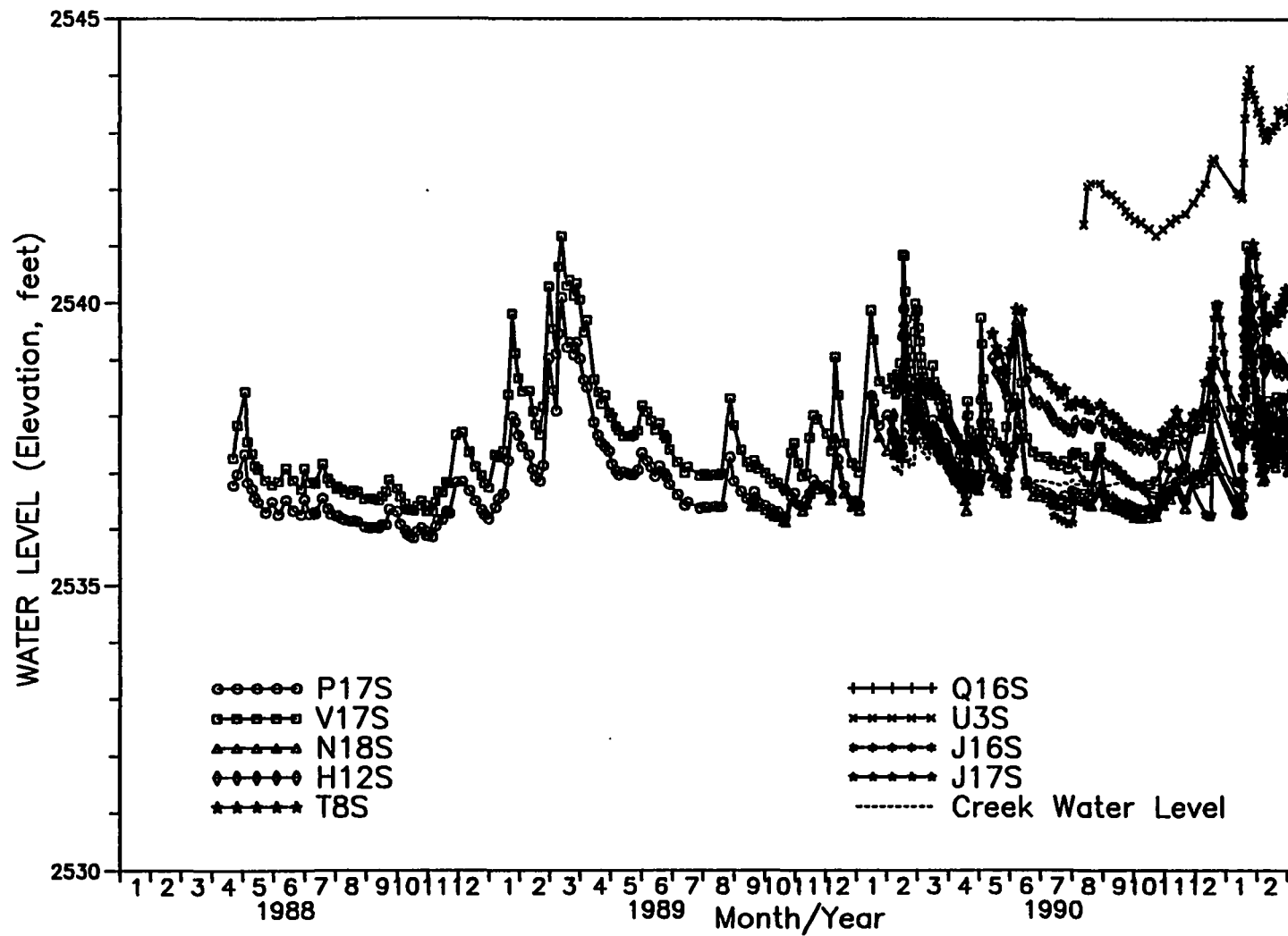


Figure 3-2. Water level hydrographs of shallow wells and Paradise Creek

The Paradise Creek water level was lower than the water levels in most of the shallow wells, as shown in Figure 3-2. The creek water level was measured from the USGS gaging station, which is approximately 100 feet (30 meters) upstream from the UIGRS. According to Patrick (1990), the creek water level drops more than one foot crossing the Perimeter Drive culvert. The section of the creek directly to the north of the site averages 1.5 feet (0.45 meters) lower than the water level at the gaging station (Patrick, 1990). Therefore, the creek water level at the site is considered lower than the water level of the shallow alluvial aquifer during the entire observation period.

The ground water hydrographs of the E fracture group wells and the creek hydrographs are shown in a larger scale in Figure 3-3. The water level in the E fracture zone was higher than the creek level during most of 1990. The water level fluctuation of the E fracture zone corresponds closely with the creek fluctuation during the spring recharge period.

Water level hydrographs of the deep basalt aquifers and the shallow wells for the period of February 1990 to February of 1991 are presented in Figures 3-4 and 3-5. More detail with respect to the group characteristics of different basalt fracture zones and the relationship between the ground water and Paradise Creek is illustrated in these hydrographs.

Comparison of the hydrographs of the E fracture zone of basalt, shallow alluvial aquifer, and Paradise Creek is presented in Figure 3-6. The hydrographs demonstrate that: 1) the E fracture zone, shallow aquifer, and Paradise Creek have very similar water level fluctuation patterns; 2) there is an upward hydraulic gradient from the E fracture to the shallow aquifer at the northeastern portion of the site during most of the year; 3) the downward hydraulic gradient occurs during the major recharge events

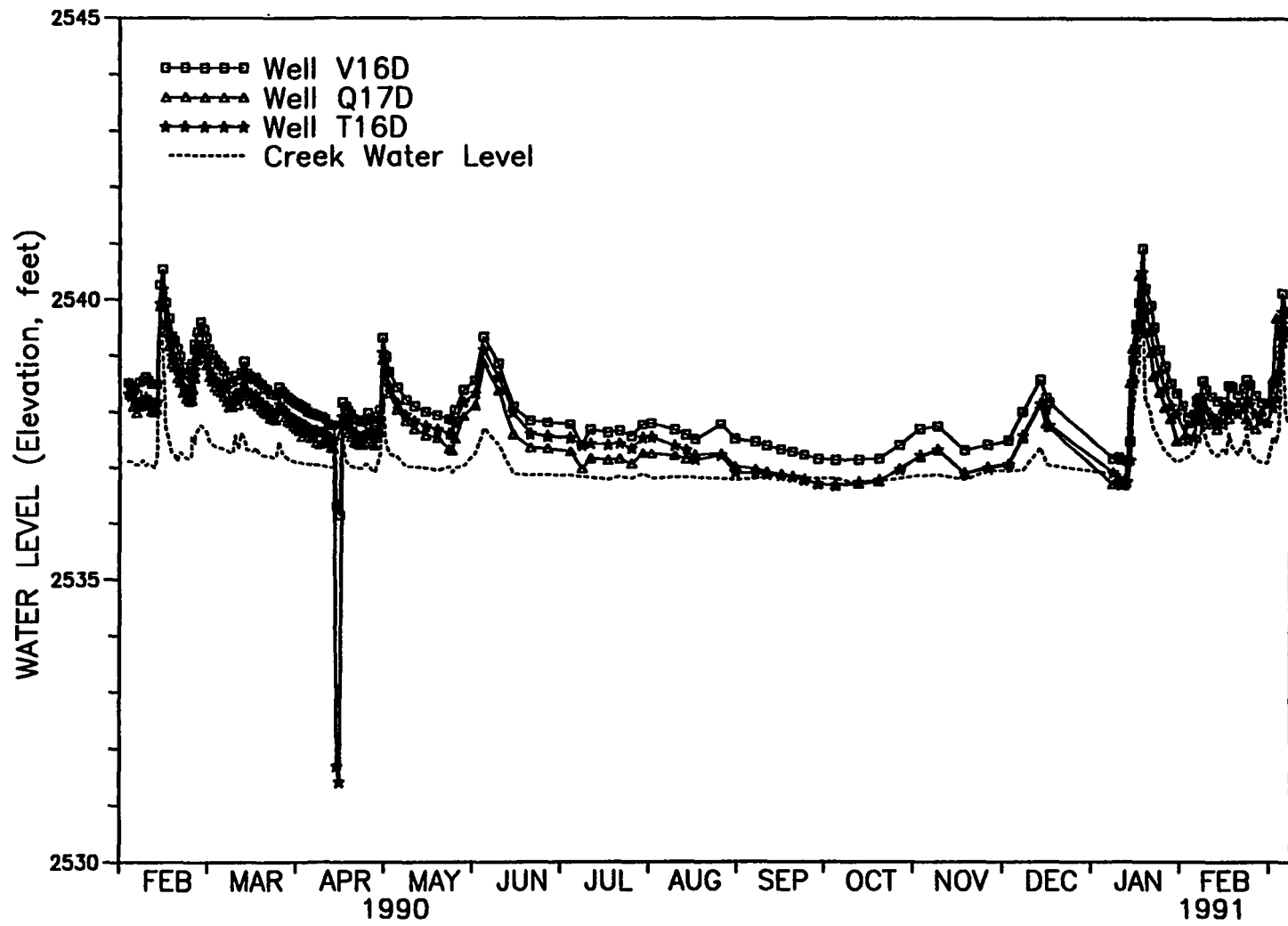


Figure 3-3. Water level hydrographs of Paradise Creek and some wells in the E fracture zone

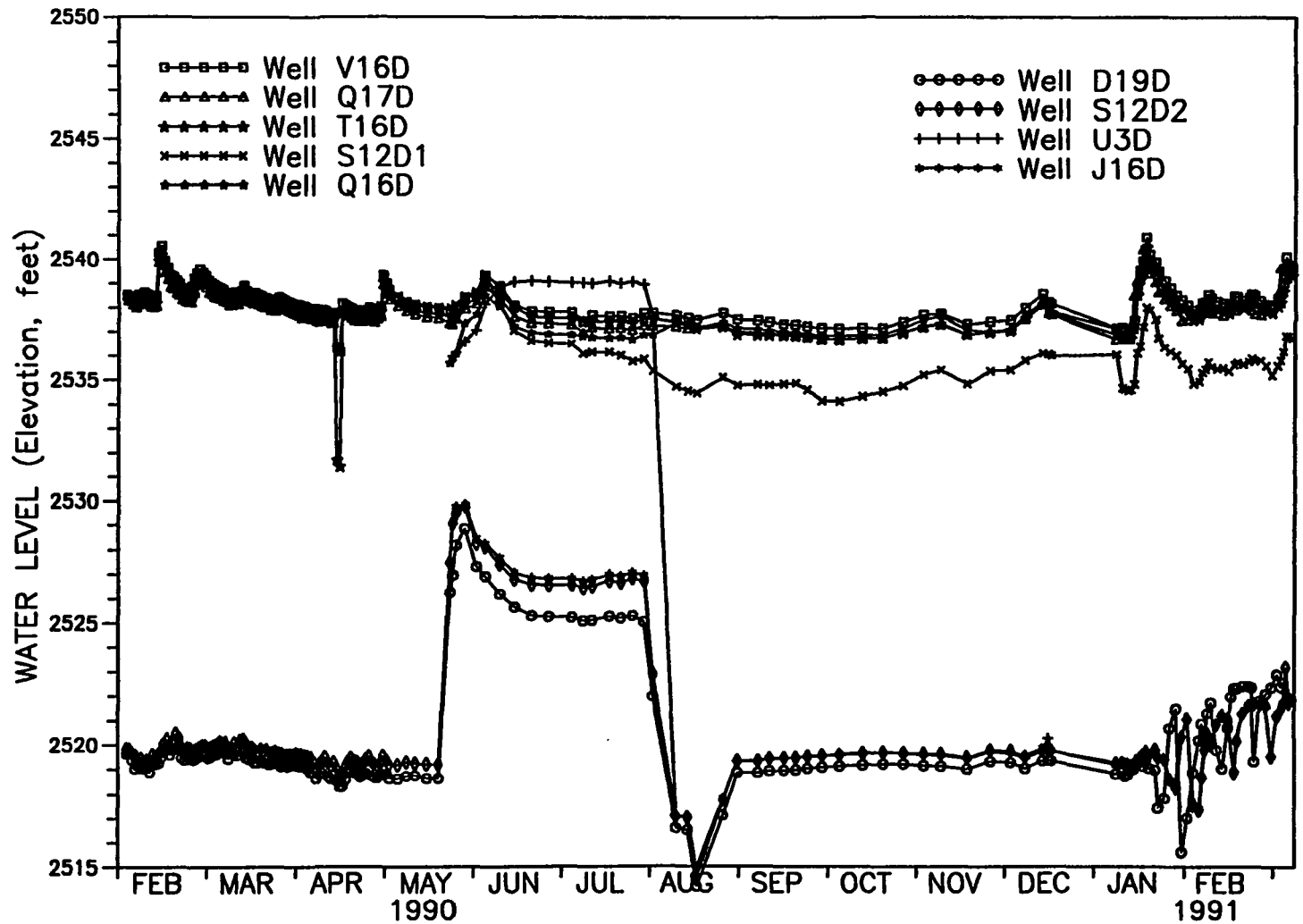


Figure 3-4. Annual (1990-1991) ground water hydrographs of deep basalt wells

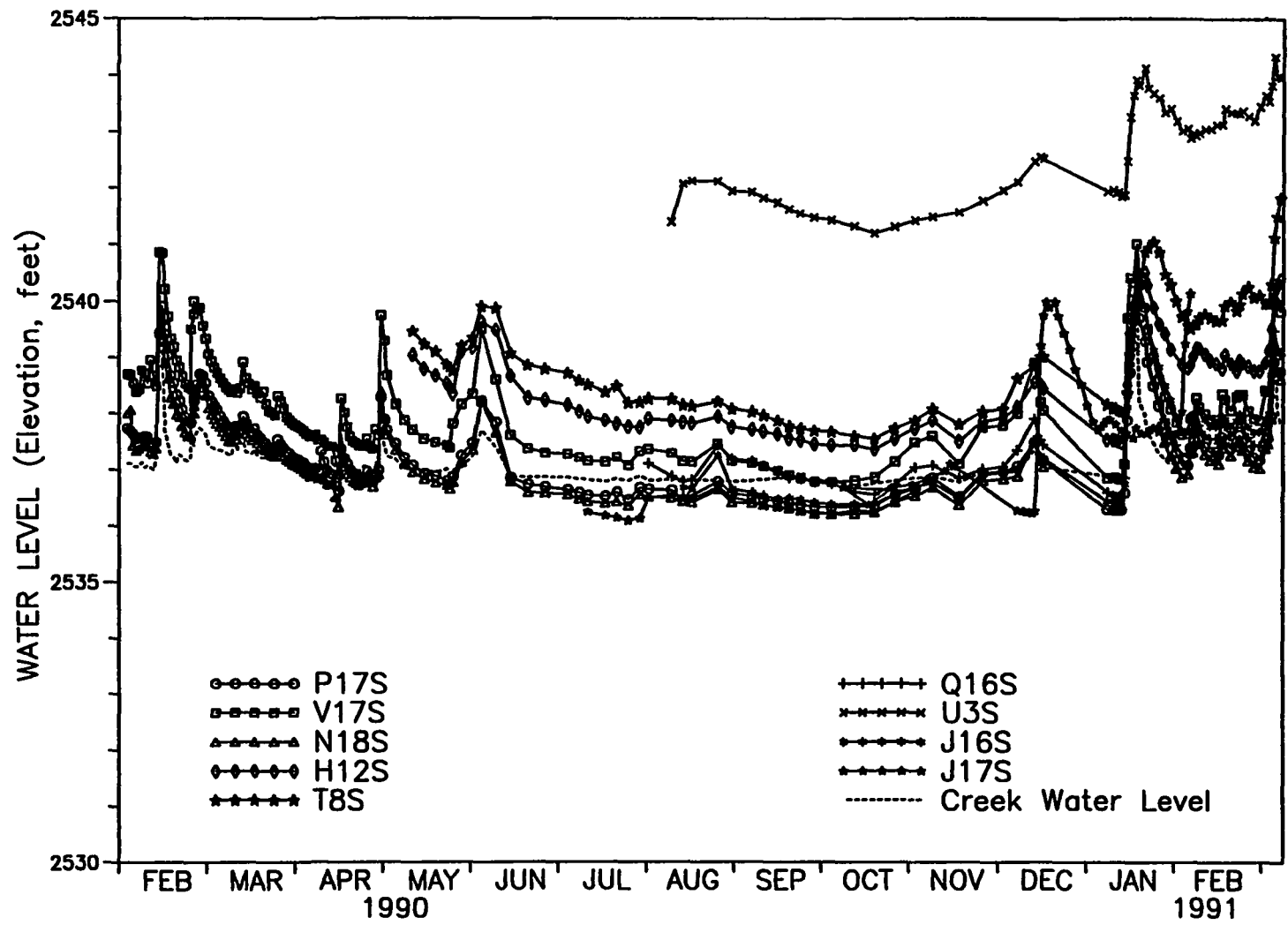


Figure 3-5. Annual (1990-1991) water level hydrographs of shallow wells and Paradise Creek

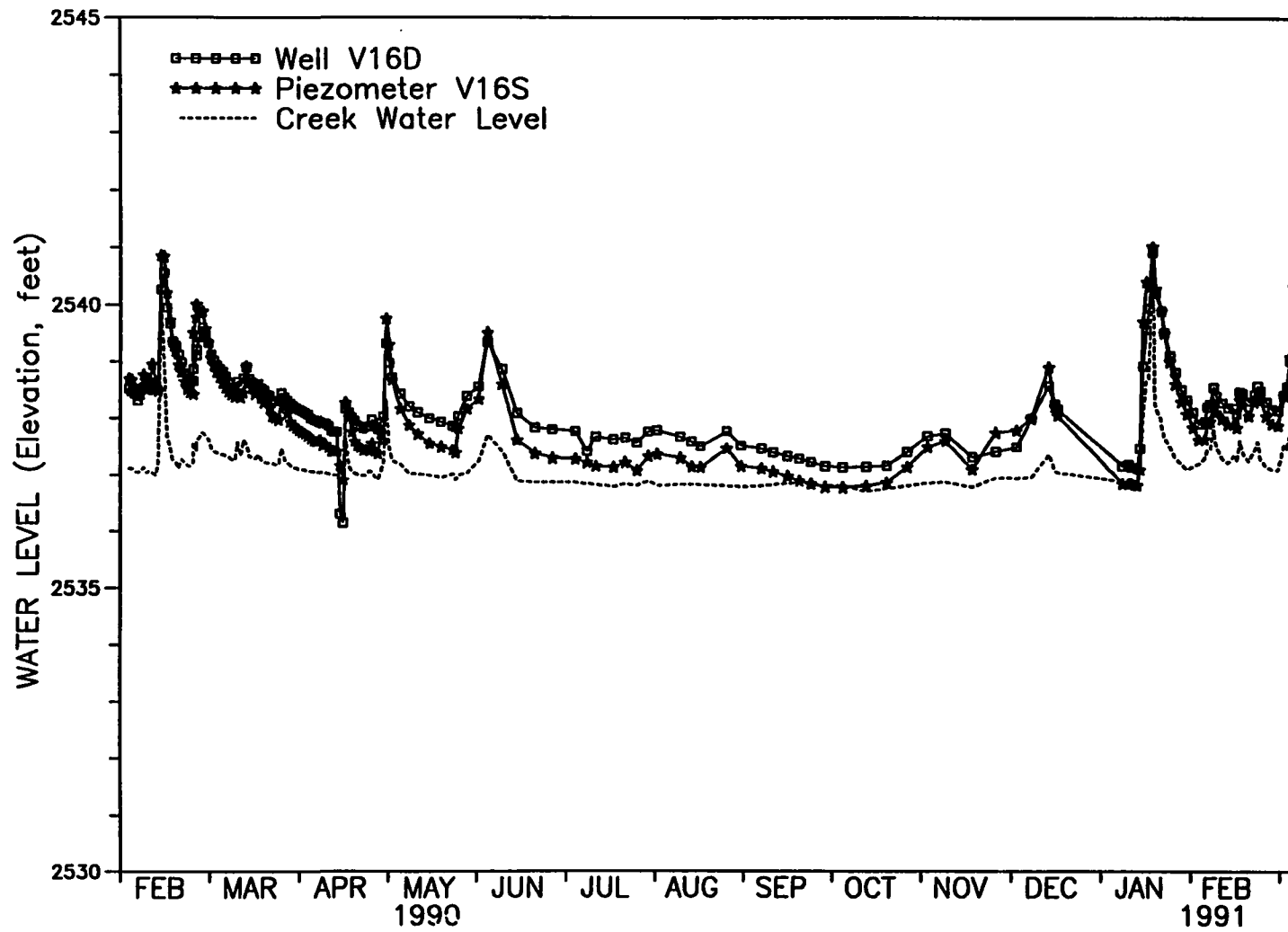


Figure 3-6. Comparison of water level hydrographs of Paradise Creek, shallow alluvial aquifer, and E fractured aquifer

of snow melt in the spring and extensive rainfalls in other seasons; 4) the peak flow of the creek matches the high water levels in both shallow and basalt aquifers; 5) the ground water levels in the E fracture and shallow aquifer have longer recession periods after a high flow event than does the creek; and 6) the E fracture zone and shallow alluvial aquifers appear to discharge to Paradise Creek at the UIGRS during most of the year.

Ground Water Level Contours

Water level contour maps of the basalt aquifers are presented in Figures 3-7 and 3-8 for low and high water level periods. Figure 3-7 shows the dry season water level contours of both E and W fracture zones on October 2, 1990. Figure 3-8 presents the basalt aquifer's high water level contours on January 15, 1991 in the recharge period. The contour interval is 0.2 feet (6 cm) for all the maps.

The basalt aquifer contour maps show that ground water flow directions and gradients are different for the E and W fracture zones. The magnitude of the gradient is generally smaller in the W fracture zone than that in the E fracture zone. The gradient direction in the W fracture zone is consistent with the regional ground water flow to the southwest (Lum *et al.*, 1990). The gradient in the E fracture zone is to the north and northeast toward Paradise Creek. The directions and magnitude of water level gradients in both fracture zones do not seem to be affected by low or high flow conditions and are fairly constant during the entire year.

The water level gradient to the north-northeast in the E fracture zone probably results from the area topography and locations of local recharge and discharge areas. Based upon analysis of the hydrographs, the

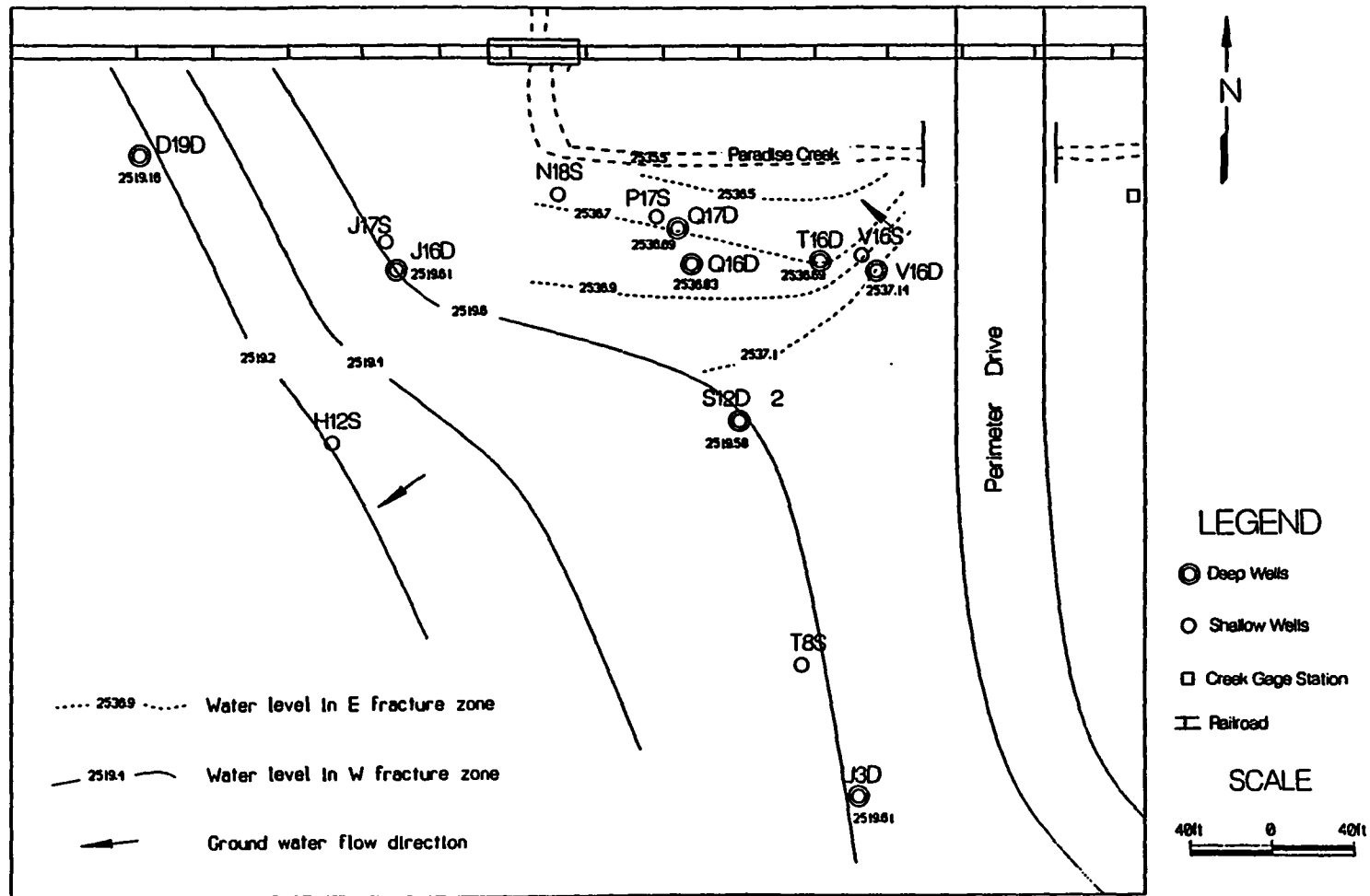


Figure 3-7. Ground water contour map of fractured basalt aquifers on October 2, 1990

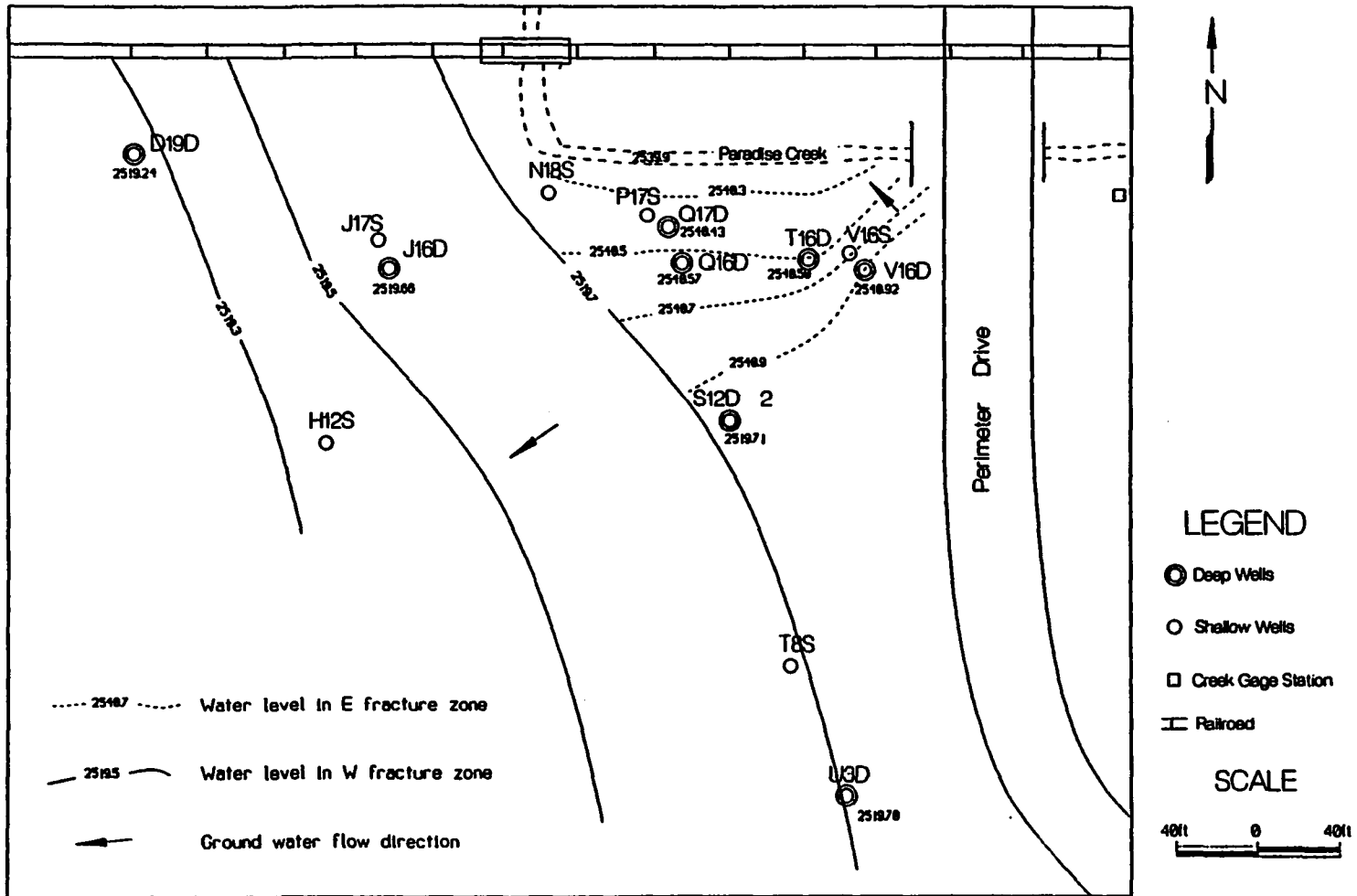


Figure 3-8. Ground water contour map of fractured basalt aquifers on January 15, 1991

section of Paradise Creek just north of the UIGRS is a local discharge channel for the shallow aquifer and the E fracture zone. The stream discharge area is probably the reason for the northerly hydraulic gradient in the E fracture zone.

A dry season, water table contour map of the shallow alluvial aquifer is presented in Figure 3-9. The ground water flow direction in the shallow aquifer is from south to north, consistent with the topography of the site. The higher gradient occurring in the western portion of the site probably is due to the topographic rise to the southwest.

The water table gradient may be affected by infiltration from the ground surface. Ponding is often formed at the low elevation along the eastern border of the site and the southwestern hillside after snow melt or extensive rainfall.

Ground Water Recharge and Discharge

Ground water recharge and discharge are analyzed based on water level hydrographs and contour maps. Hydraulic interrelationships of the shallow alluvial aquifer, fractured basalt aquifer, and Paradise Creek are described in this section.

Recharge and Discharge of the Shallow Alluvial Aquifer

The alluvial (sand and gravel) aquifer is the uppermost saturated water-bearing zone in the UIGRS. The aquifer is covered by loam soil and silty clay in variable thickness. Recharge to the shallow aquifer is mainly from the infiltration of precipitation and snow melt through the soil profile.

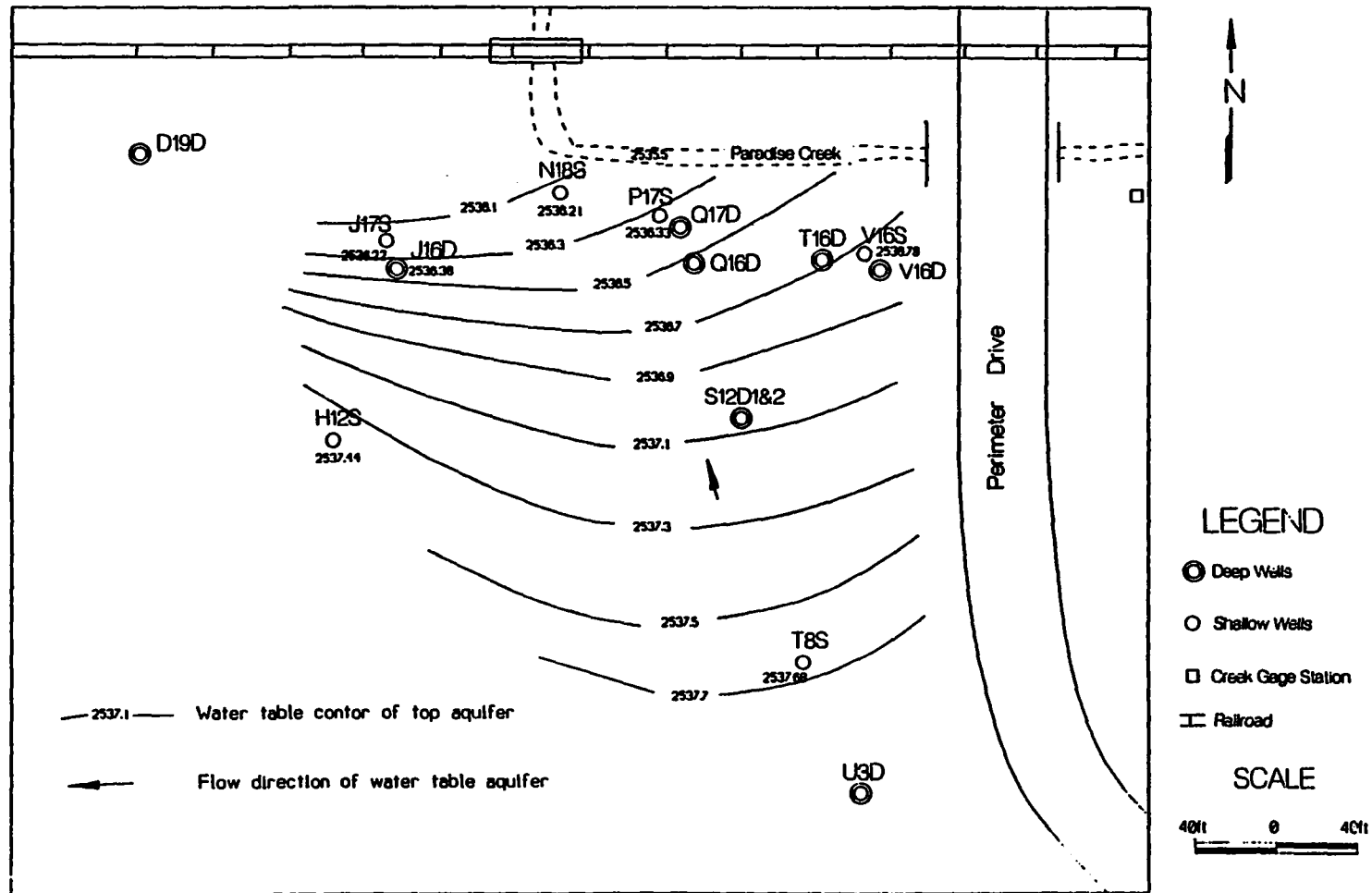


Figure 3-9. Water table contour map of shallow alluvial aquifer (October 2, 1990)

Discharge of the shallow alluvial aquifer occurs in two ways: 1) laterally towards the north to Paradise Creek, and 2) vertically down to the basalt aquifers. Ground water discharge is not visible along the creek channel.

Recharge and Discharge of the E Fracture Zone

The E fracture zone in the UIGRS is closely related to the shallow alluvial aquifer and to Paradise Creek. Recharge to the E fracture zone also is primarily from the vertical infiltration from the alluvial aquifer through the intervening basalt. The quantity of recharge is controlled by the vertical hydraulic conductivity of the basalt.

The discharge of the E fracture zone appears to occur in two directions: 1) downward flow through vertical fractures to the deeper fractured zones, and 2) upward flow through the shallow alluvial aquifer to Paradise Creek. The downward flow in the basalt most likely is controlled by the characteristics of the columnar fractures in the colonnade portion of the Lolo flow. The direction of vertical hydraulic gradient between the shallow alluvial aquifer and the E fracture zone changes during the year. Downward flow is dominant after snow melt in the spring and extensive rainfall in the other seasons. Upward flow occurs during the remainder of the year. The upward vertical gradient generally is less in magnitude than the downward gradient.

Recharge and Discharge of the W Fracture Zone

The W fracture zone is closely associated with the aquifer formed at the base of the Lolo flow. This conclusion is supported by the following observations: 1) flow direction of the W fracture zone is consistent with

the regional flow and may be controlled by areas of the greater vertical hydraulic conductivity in the lower section of the Lolo flow; 2) the ground water hydrographs of the W fractures do not show a close relationship with precipitation events and creek runoff; 3) ground water level fluctuations are small, related more to barometric pressure changes rather than rainfall and snow melting; and 4) water levels of the W fracture zone response to pumping of the Aquaculture Lab well that obtains water from the aquifer at base of the Lolo flow.

The discharge of the W fracture zone at the UIGRS occurs laterally as ground water flow to the southwest. The downward flow to deeper aquifers probably occurs but has not been documented.

Interrelationship between Paradise Creek and the Aquifers

Based upon the previous analysis, the interrelationship between stream flow and ground water is summarized as follows:

- 1) There are two ground water flow systems within the Lolo flow of Wanapum basalt to a depth of 150 feet (45 meters) at the UIGRS. The E fracture zone is very closely related to the surface runoff and W fracture zone has limited connection with the stream.
- 2) Paradise Creek behaves as a discharge area for ground water in the alluvial aquifer and the E fracture zone during most of the year.
- 3) The shallow alluvial aquifer is recharged from the infiltration of snow melt and rainfall through the soil profile. The discharge is lateral to the creek or downward to the E fracture zone.
- 4) The recharge-discharge relation of stream flow and ground water is reversed during the spring stream peak flow period. The E fracture zone probably gains recharge from the stream flow.

- 5) Pumping in the E fracture zone could obtain considerable recharge from creek flow if the water level in the E zone is lowered below the stream level. However, the increase of recharge from the stream caused by pumping in the W fracture zone probably would be small.

Microbial Ecology of the Fracture Systems

Recent *in situ* microbial ecology research conducted at the UIGRS has provided more evidence to support the hypothesis of two separate fracture flow systems: 1) the geochemistry of ground water in the W fracture zone is significantly different from that in the E fracture zone; 2) the bacteria population composition in ground water varies considerably from the E fracture zone to the W fracture zone; and 3) the number of bacteria in the E fracture zone is over two magnitudes higher than that in the W fracture zone (Kellogg and Zheng, personal communication, 1990).

The composition of the bacteria population in ground water generally is related to the geochemical and biochemical environments of the recharge area and geochemical conditions of the aquifer. Also, the bacteria population in a ground water flow system should be reduced as the travel time and distance increase from its recharge area when no contamination occurs. Consequently, we can tentatively conclude that water from the W fracture zone has a greater lag time from surface recharge than that from the E fracture zone.

Hydrogeological Conceptual Model

The previous discussions on the site geology and hydrogeology illustrate the complexity of the basalt fracture patterns and hydrologic

behavior of the Lolo flow of the Wanapum Formation at the UIGRS. The hydrogeological conceptual model proposed here is based on the analysis of available geological, borehole geophysical and hydrological data.

The conceptual model considers three aquifers in the UIGRS: 1) the upper or shallow alluvial aquifer; 2) the E fractured basalt aquifer or the E fracture zone; and 3) the W fractured basalt aquifer or W fracture zone. Three aquitards, named upper, middle, and lower according to their stratigraphic positions, also are identified at the site.

The Shallow Alluvial Aquifer

The shallow aquifer, which is composed of alluvial sand and gravel as well as basalt rubble and broken basalt, is unconfined. The bottom of the aquifer is at a depth of 20 to 30 feet (6 to 9 meters) below ground surface. Total saturated thickness averages 5 to 10 feet (1.5 to 3 meters) and generally decreases from north to south or from northeast to southwest.

Hydraulic characteristics of the shallow alluvial aquifer are determined by the coarseness of sand and gravel and the thickness of the alluvium. The aquifer is generally heterogenous. The maximum yield capacity of the aquifer is estimated at one to two gallons per minute (gpm).

The E Fractured Basalt Aquifer

The E fractured basalt aquifer occurs in the northeast portion of the UIGRS. The aquifer is nearly horizontally distributed and probably extends to the north and the east outside of the study site. The fractured basalt aquifer was observed at depths of 65 to 75 feet (20 to 23 meters) with a thickness of 1 to 3 feet (0.3 to 0.9 meters).

The major fracture that forms the E basalt aquifer is likely a nearly horizontal break that separates the entablature and colonnade of the Lolo basalt flow. A dense set of horizontal joints and an internal vesicular zone associated with the major break form the aquifer. The orientations of the small joints within the break zone are so random that any meaningful orientation can be defined only in terms of the overall fracture zone.

The E fractured aquifer is highly heterogeneous and anisotropic. Yield capacity of the E fractured basalt aquifer ranges from 7 to 50 gpm with higher values trending toward the east and northeast. The specific yield of the aquifer averages 0.3 to 3.3 gpm per foot.

The W Fractured Basalt Aquifer

The W fractured aquifer occurs in the western and southern portion of the UIGRS and very likely extends to the southwest and the west beyond the site. It is at a depth of 70 to 85 feet (21 to 26 meters) in most areas of the site, but appears at a greater depth of 135 feet (41 meters) to the west. The W basalt aquifer is most likely formed by two horizontal fracture zones that are connected through the columnar fractures (Figure 2-9). Thickness of the W basalt aquifer is 0.5 to 1 foot (0.1 to 0.3 meters).

The W basalt aquifer probably consists of several large horizontal intraflow breaks with joints or fissures and smaller associated vesicular zones. The horizontal intraflow breaks have great lateral variation in openness and thickness. The W aquifer is also heterogeneous and anisotropic.

The W fractured basalt aquifer has a maximum yield capacity up to 60 gpm with much greater drawdown than that in the E aquifer. The aquifer

yield capacity decreases significantly to the central and southern parts of the site. The specific yield of the W aquifer is less than 0.5 gallon per minute per foot at the highest yield location.

The Aquitards

The basalt blocks separating the aquifers consist of rock with many minor intraflow fractures. These blocks have significant water storage in comparison with the fractured aquifers. The blocks generally have weak hydraulic connection with the aquifers through vertical joints. Leakage from and through these blocks has been observed during aquifer tests conducted at the UIGRS. Ground water flow is believed to be primarily vertical in the aquitard blocks.

The upper aquitard is formed by the basalt block underlying the shallow alluvial aquifer. The aquitard is believed to be an entablature section of the Lolo flow; consisting of several minor horizontal fractures and vertical joints within a total thickness of approximately 40 feet (12 meters). The upper aquitard is mainly observed at the east portion of the site and plays an important part in the hydraulic connection between the shallow aquifer and the E basalt aquifer.

The middle aquitard is located between the E and W fractured aquifers, which is possibly a section of colonnade of the Lolo basalt flow. The leaky connection between the two aquifers is through the middle aquitard. However, the leakage appears not to be as significant in the lower aquitard as in the upper aquitard.

The lower aquitard is believed to exist underneath the W aquifer. This aquitard was not investigated in this study.

CHAPTER IV
Discussion of the Conceptual and Analytical
Models of the Fractured Rock

Ground water flow through fractured rocks has been an important subject in hydrogeology for many years. Two of the major issues in fractured rock hydrology are: 1) whether or not the fractured rocks behave like porous media given large representative elemental volumes; and 2) how to evaluate quantitatively the hydraulic characteristics of ground water flow in the fractured rocks. These two topics have been discussed by many hydrogeologists since the early 1950s. The purpose of this chapter is to review some of the definitions, conceptual and analytical models in fractured rock hydrology, and to discuss the concepts and theories in comparison with the fractured basalt conceptual model at the UIGRS.

Basic Concepts and Definitions

In studying the physical properties of fractured rocks, Pirson (1953) classifies the porosity of water bearing formations into three major types: 1) intergranular, consisting of the void spaces between mineral grains of the rock; 2) vesicular, resulting from physical or chemical weathering; and 3) fracture, consisting of openings such as faults, fissures and joints. Freeze and Cherry (1979) provide a similar classification and recognize the soil or rock matrix porosity as primary or original porosity and others as secondary or induced porosity. The concept of double-porosity in fractured rock systems has been a subject of many studies in the past two decades (Barenblatt et al. 1960; Warren and Root, 1963; Gale, 1982; Gringarten,

1982, 1984; Streltsova, 1983; Moench, 1984).

The basic concepts that have been widely accepted for the fractured rock are as follows: 1) primary porosity is high but the hydraulic conductivity provided by these features is low; and 2) secondary porosity is low but these features are highly permeable (Streltsova, 1976a). Consequently the hydraulic conductivity of a block of fractured rock is determined by the secondary features and storativity is due to the primary porosity (Beauheim, 1988).

Streltsova (1976a) classifies fractured media into four groups: 1) a fractured medium, in which the conducting properties are associated mainly with the fracture permeability whereas the storage properties are related to the primary porosity; 2) a purely fractured medium, which consists entirely of the continuous fracture porosity; 3) a double-porosity medium, in which the hydraulic properties are controlled by the fracture and the block porosities at the same order of magnitude; and 4) a heterogeneous medium, in which the fractures are filled with materials such as silty clays that have lower permeability than that of the porous blocks.

There is some confusion with Streltsova's definition (1976a). First, the fractured medium basically is in the same category of the double-porosity medium defined by others (Barenblatt *et al*, 1960; Warren and Root, 1963). Second, the purely fractured medium may still show the double-porosity behavior with the major fractures (fault zone or large fractures) as secondary features and numerous joints and minor fissures as the block matrix porosity. Third, her double-porosity medium should behave like a porous medium if the hydraulic properties are controlled by both fracture and block porosities at the same order of magnitude. Fourth, by her definition, the heterogeneous medium with filled fractures should be

considered as a heterogeneous porous medium rather than a fractured one.

In summary, the fractured rocks can be classified into three types of ground water flow media. The first is discrete fractures (conduits) in which the hydraulic properties are controlled by secondary fracturing features such as continuity, density, geometry (shape, orientation, aperture and scale), and interconnectedness. The primary porosity of this type of fracture medium is negligible. Double-porosity medium is the second in which primary porosity occurs in the rock block matrix and fractures or fracture zones form the secondary porosity. The primary porosity is comprised of either intergranular pores or randomly distributed smaller fissures and joints. The third is equivalent porous medium, in which the fractures are so frequent that the rock system behaves as porous medium. In this case the porosities of fractures and block matrix are at the same magnitude.

Three types of fractured media are not clearly divided. The determination of the hydraulic behavior of many fractured rocks depends largely on the testing scale. The fractured basalts of the Columbia River Basalt Group in the Pacific Northwest commonly have been considered as porous media because the lava flow contact zones are tested on a large scale. The basalt probably behaves as discrete conduits or a double-porosity medium when testing is on a small scale, for example, when a flow interior is being tested. Practically speaking, many different types of fractured rocks show a response of discrete conduits in a small scale test but behave as a double-porosity medium or even an equivalent porous medium when the testing scale increases to large scale (Long *et al.*, 1982; Long and Witherspoon, 1985; Beauheim, 1988).

The concept of representative elementary volume (REV) has been used

to define continuum and homogeneity of a fracture medium (Long *et al.*, 1982). The REV is defined as a volume at which the aquifer properties (or parameter of interest) first cease to vary with increases in volume considered. An REV may or may not exist in a given fractured rock or may be larger than the testing volume; in this case, the fractured rock must be treated as a discontinuous medium. A fractured rock can be considered as a continuum and equivalent porous medium or double-porosity medium only if the REV exists and is smaller than the testing volume.

Two types of double-porosity media have been recognized based on the characteristics of the block matrix of the fractured rock. The rock matrix may be porous, such as sandstone or vesicular basalt, or non-porous but has numerous joints or small fissures. The latter situation is more common in crystalline rocks. The overall porosity of the fissured block matrix generally is larger but hydraulic conducting properties are smaller than that of the fractures. The difference of the hydraulic properties between the fractures and fissured block matrix can range widely.

Analytical Approaches to Ground Water Flow in Fractured Rock

Discrete Fracture Models

The discrete fracture analytical models that have been developed are based upon simplification of fracture systems because of mathematical limitations. The models generally require the detailed knowledge of fracture geometry and continuity (Snow, 1968).

Many researchers have characterized and simulated the flow through discrete fractures by a system of pipes or by horizontal or vertical

plates. The cubic law is representative of these models; the discrete flow system is described by orthogonal plates with parameters such as aperture size and friction coefficient. The fractures generally are assumed to be infinite in lateral extent and the influence of rock stress conditions is often considered. Ground water flow is either laminar or turbulent based on the Reynolds number. In most subsurface environments, laminar flow exists and Darcy's law is valid.

The emphasis of the research in discrete systems has been with laboratory experiments. Type curve solutions are not available to the discrete fracture models because the aquifer can not be treated as a continuum.

Snow (1969) develops solutions for anisotropic hydraulic conductivity tensors of fracture media based on the fracture aperture and spacing as well as the relationship between the driving force and flow in idealized fractured media (three dimensional anisotropic Darcy's law). The basic findings of his work include:

- 1) A medium (nonconducting solid) cut by parallel fractures has infinite anisotropy. The hydraulic conductivity parallel to the conduits is proportional to the average of the apertures and inversely to the average spacing between the conduits.
- 2) If there is flow on each of two or more intersecting parallel plate openings, there is an unique hydraulic gradient generally not lying on either plane: the projections of the gradient on the planes cause the flow.
- 3) In cases of double-porosity, the hydraulic conductivity tensor of jointed granular porous media may be obtained by superposition of contributions due to fractures and the permeable matrix.

- 4) The hydraulic conductivity of dispersed or multiple sets of plane conduits is a symmetric second rank tensor; the contributing term from each individual conduit is weighted inversely to the absolute value of the cosine of its inclination from the average direction.
- 5) For any arbitrary system of plane conduits, the principal axes of the hydraulic conductivity tensor can be estimated from inspection of a stereo-net plot of normals but can not be specified unless apertures are measured. Fracture media with three equal orthogonal sets are statistically isotropic.
- 6) Variations in hydraulic conductivity measures, such as in drill holes, are consequences of sampling heterogeneity; each test reflects the properties of a few intersected joint conductors in the large population contained in a formation.

The major problem with applying Snow's solutions is that hydraulic conductivity tensor analysis depends on the complete knowledge of fracture geometry. Also, storage properties of the fractured aquifer can not be determined by his model.

Single Fracture in Homogeneous Matrix Models

The single fracture models presented in this section could actually be included into the double-porosity models because the fracture-matrix relationship is considered in the models. On the other hand, the single fracture models could be considered as porous medium models with special inner boundary conditions and flow patterns. The models are grouped and described here to emphasize the "single fracture" pattern.

Gringarten's Models

Analytical solutions have been developed to describe the pressure behavior of a well that intersects a single horizontal fracture (Gringarten and Ramey, 1974) or a single vertical fracture (Gringarten *et al.*, 1974).

The basic assumptions of these models are:

- 1) A single plane vertical or horizontal fracture with finite extent and much higher hydraulic conductivity is located in a radially infinite homogeneous porous medium.
- 2) A single plane fracture with an infinitely small aperture is intersected by pumping well in the middle of total fracture length.
- 3) A pumping well is located along the vertical fracture or the horizontal fracture planes (vertical or horizontal wells).
- 4) Observation wells are located along the fracture planes or along a plane that is perpendicular to and equally divides the vertical or horizontal fractures.
- 5) Either the hydraulic head along the fracture is uniform (fracture with infinite hydraulic conductivity or no flow through the fracture) or water enters the fracture at a constant rate per unit area (fracture with uniform flux).
- 6) The aquifer is bounded by both upper and lower impermeable boundaries, and the vertical fracture penetrates the entire aquifer thickness.
- 7) The well fully penetrates the aquifer and is pumped at a constant rate.

The solutions developed by Gringarten *et al.*, (1974) and Gringarten and Ramey (1974) are expressed by three dimensionless parameters s_D , t_D ,

and r_D . These parameters are defined as follows:

$$s_D = \frac{4\pi s \sqrt{T_f T_m}}{Q} ; \quad t_D = \frac{T_f t}{S x_f^2} ; \quad \text{and} \quad r_D = \frac{y}{x_f} \sqrt{\frac{T_f}{T_m}} \quad (1)$$

where

Q = discharge rate of pumping well

s = drawdown in pumping well or observation wells

T_f and T_m = transmissivity of fracture and matrix

S = storativity (of matrix)

t = time since pumping started

x_f = half of total fracture length

y = distance from observation well to fracture where the well is not along the fracture planes

The type curves of dimensionless drawdown vs. dimensionless time in log-log plots for pumping well and observation well solutions are available in Gringarten and Witherspoon (1972), Gringarten and Ramey (1974), and Sauveplane (1981).

One unique and interesting character of the log-log type curves is that the pumping well solution of both vertical and horizontal fracture models is a straight line with a slope of 0.5 at the early time. An observation well that intersects the pumped vertical fracture also shows the initial half-unit slope response. This characteristic straight line response disappears where the observation well is at a distance from the vertical fracture; the slope of the initial drawdown generally increases with the distance the observation well is from the vertical fracture. The observation well solution of single vertical or horizontal fractures becomes identical to the Theis solution when $r_D > 5$.

Gringarten's single fracture models provide a way to check whether the pumping and observation wells intersect a large single fracture, and whether the fracture trend is essentially horizontal or vertical. In the cases that Gringarten's assumptions are met, the hydraulic properties of the aquifer can be estimated. The solutions of Gringarten's models are modified by Gringarten and Witherspoon (1972) to account for a homogeneous anisotropic matrix.

Linear Flow (one-dimensional flow) Models

Jenkins and Prentice (1982) and Sen (1986a) study ground water flow toward a single vertical fracture with a very large permeability under linear (non-radial) flow conditions. The linear flow condition is obtained when the length of the vertical fracture is infinite or very large. The linear flow models are described by a one-dimensional flow equation with initial conditions and boundary conditions. Assumptions of the linear flow models are similar to those of Gringarten (1982) except: 1) the flow is assumed to be laminar with a linear flow pattern from the homogeneous isotropic aquifer toward the fracture, and 2) the water level in the fracture at any time during the pumping is assumed to be constant along the entire length of the fracture.

The solutions of a linear flow model by Sen (1986a) are expressed by a fracture well function $W(u)$ and dimensionless time u . The type curves of $W(u)$ vs. u on a log-log plot generated from the equations by Sen are somewhat similar to the type curves of the modified Hantush leaky aquifer model. The type curves tend to be straight lines with a half unit slope on a log-log plot at large values of time. Aquifer transmissivity and storativity can be estimated by type curve matching if the length of the

vertical fracture is known.

Type curves for a recovery test solution are also presented by Sen (1986a). The recovery type curves show that for a short aquifer test, the drawdown in an observation well continues to increase for a while even after the pumping stopped, and then decreases asymptotically to zero after a very long time.

The solutions of the linear flow model by Jenkins and Prentice (1982) reveal a linear relationship of pressure drawdown with respect to the square root of time, indicating a half unit slope on the log-log plot of drawdown vs. time. Two basic results can be obtained from Jenkins and Prentice's solutions: 1) the ratio of transmissivity to storativity (hydraulic diffusivity) can be determined if the direction of the vertical fracture is known; and 2) direction of the vertical fracture can be determined if at least two observation wells are on the same side of the fracture.

An error is evident in the derivation of the recovery solution by Sen (1986a). The definition of the minimum dimensionless time factor u_r appears to be wrong. A correct definition should be $u_r = x^2 S / 4T_r$, in order to make the derivation of the solution be consistent with the other definitions and the application of the solution be valid. Jenkins and Prentice's study (1982), according to Sen (1986a, page 72), also "suffered from some errors in the derivation of basic equations and in interpretations".

The common feature of single fracture models is the half unit slope of drawdown response on a log-log plot. Gringarten's vertical and horizontal fracture models show straight lines with a slope of 0.5 at early

time on the log-log drawdown responses of the pumping well or observation wells intersecting the fracture. Sen's vertical fracture models with linear flow pattern demonstrate that the slope of 0.5 is observed at the late portion of type curves on a log-log plot. The linear flow solution of the vertical fracture model developed by Jenkins and Prentice illustrate a completely straight line with the slope of 0.5 on a log-log plot of drawdown vs. time. The half unit slope appears to indicate a linear flow pattern from matrix to fracture in the single fracture models.

Double-porosity Analytical Models

Generally, all the double-porosity models are based on the continua assumption; that is, ground water flow can be defined as a continuous function throughout the entire fractured medium (both fracture network and matrix blocks). The further assumption of uniform fracture distribution idealizes the double-porosity medium to be two homogeneous continua overlapped together, each of them having different hydraulic conductivity and porosity. Most double-porosity models only consider flow in the fracture continuum, with flow contribution of the matrix block through fracture-block interfaces.

The specific assumptions made for mathematical development of the double-porosity models are as follows:

- 1) The aquifer is infinite in radial extent with homogeneous matrix block and uniform fracture distribution.
- 2) The aquifer is confined and bounded by upper and lower impermeable boundaries.
- 3) Initial hydraulic head is uniform throughout the aquifer.
- 4) Flow in fractures is laminar, and Darcy's law is valid.

- 5) Water is extracted at a constant rate through a pumping well that fully penetrates the aquifer thickness.
- 6) The fracture network has high hydraulic conductivity and low porosity, whereas the matrix block has low hydraulic conductivity and high porosity.
- 7) Flow to the pumping well is only through fractures because of the low hydraulic conductivity of matrix blocks.

Three representative double-porosity models are presented in this section. These models have been widely used in the last three decades for characterizing fractured aquifer systems.

Pseudo-steady State Block-to-fissure Flow Models

The representative studies of the pseudo-steady state double porosity models have been accomplished by Barenblatt *et al.* (1960) and Warren and Root (1963). Barenblatt's model considers an elementary volume of the aquifer that comprises a large number of irregular sized blocks bounded by randomly distributed and arbitrarily oriented fractures. The elementary volume is large in comparison with the average size of the blocks but remains small as compared to the total volume of the aquifer. Flow from blocks to fractures is assumed to be steady state. The blocks are considered to be isotropic and homogeneous, and the compressibility of fractures is assumed to be negligible (no storage in the fractures).

Warren and Root's model (1963) is a modification of the model of Barenblatt *et al.* (1960) to consider the compressibility of the fractures. The problem is solved for an idealized fracture network consisting of orthogonal, uniform and continuous sets of fractures. Because each

fracture is parallel to one of the principal axes of hydraulic conductivity, the overall system is thus treated as a homogeneous anisotropic medium (Sauveplane, 1981).

The pseudo-steady state models are solved using Laplace and Hankel transforms. The solutions by Warren and Root (1963) can be described as

$$\overline{s_D} = \frac{2}{p} K_0(r_D \sqrt{p + q_D}) \quad (2)$$

where s_D is the dimensionless drawdown; the overline represents the parameters in Laplace space; p is the Laplace transform variable with respect to dimensionless time; K_0 is the modified Bessel function of the second kind of zero order; and r_D is dimensionless distance. q_D is dimensionless flow from block to fissure in Laplace space, which is defined as

$$\overline{q_D} = \frac{p}{1/\sigma + p/\lambda} \quad (3)$$

where two dimensionless parameters, σ and λ , are introduced to specify characteristics of the double-porosity system. They are defined as

$$\sigma = \frac{S'_s}{S_s} \quad (4)$$

$$\lambda = \alpha (K'/K) r_w^2 \quad (5)$$

where S_s and S'_s are the specific storages of the fissure system and matrix blocks; and K and K' are the hydraulic conductivities of the fissures and the blocks, respectively. Parameter α is related to the geometry of

fissured rock and has a dimension of inverse area, and r_w is the well bore radius of the pumping well. Dimensionless drawdown and dimensionless distance are defined as

$$s_D = \frac{4\pi KH}{Q} (h_i - h) \quad (6)$$

$$r_D = r / r_w \quad (7)$$

where H is the aquifer thickness; and Q is the constant pumping rate. h_i and h are the initial water head and the transient water head in the fissures. Dimensionless time is inversely related to the Laplace transform variable p and defined as

$$t_D = \frac{Kt}{S_D r_w^2} \quad (8)$$

The type curves of dimensionless drawdown vs. dimensionless time on log-log plot can be generated from the solution; the hydraulic properties of the fissures and matrix blocks can be computed through the type curve matching technique. Because the double-porosity model is based on two overlapping continua (fissures and blocks), the above analytical solution reduces to the Theis solution when dimensionless flow q_D is zero. In this case, the matrix block is neglected.

A similar solution was given by Kazemi *et al.* (1969), which is an extension for interference tests (multiple well tests) of the Warren and Root model.

Transient Block-to-fissure Flow Models

The fissure-block geometry must be specified in order to account for transient flow from blocks to fissures. Two types of idealized block geometry are presented by deSwaan (1976): 1) slab-shaped blocks with parallel horizontal fractures, and 2) sphere-shaped blocks with cross fractures. Other geometries, such as cylinders, also have been used to idealize the fracture network (Moench, 1984).

The transient block-to-fissure flow model was first proposed by Kazemi (1969). In addition to the assumptions of the Warren and Root model, Kazemi assumes that: 1) the fissured rock mass could be idealized as parallel alternating layers (slabs) of blocks and fissures where the thickness of the blocks and aperture of the fissures represent the average fracture spacing and apertures; and 2) flow from blocks to fissures is time dependent (transient) and occurs in both radial and vertical directions. The Kazemi transient model is solved by application of a finite difference approach.

Boulton and Streltsova (1977; 1978), and Najurieta (1980) solve the transient block-to-fissure flow model analytically by assuming that only vertical flow occurs in the blocks. The Laplace transform solution for dimensionless drawdown in the fissures under transient block-to-fissure flow condition is the same as equation (2), where the dimensionless flow is defined as, for the slab-shaped blocks

$$\overline{q}_D = \gamma^2 m \tanh(m) \quad (9)$$

Two dimensionless parameters m and γ are used to specify the system, which are defined as

$$m = \frac{\sqrt{\sigma p}}{\gamma} \quad (10)$$

$$\gamma = \frac{r_w}{b'} \sqrt{\frac{K'}{K}} \quad (11)$$

where σ is defined as equation (4) and b' is the average half thickness of the slab. For the sphere-shaped blocks, the dimensionless flow is

$$\overline{q_D} = 3 \gamma^2 [m \coth(m) - 1] \quad (12)$$

where m and γ are the same as equation (10) and (11); b' represents the average radius of the sphere-shaped blocks.

The derivation of analytical solutions and type curves for selected values of the parameters are presented by Boulton and Streltsova (1977). The type curve matching approach can be applied for interpretation of aquifer test data from fractured rock systems.

Double-porosity with Fracture Skin Model

Moench (1984) modifies the double-porosity model by proposing a thin layer of low-permeability material (fracture skin) that may be present at fissure-block interfaces to impede flow from blocks to fissures. The fracture skin possibly is a mineralized film that is the result of mineral deposition or alternation. Moench's model is based on the assumptions of transient block-to-fissure flow; two analytical solutions for slab-shaped and sphere-shaped blocks are derived using the Laplace transform. The additional assumptions of Moench's model are that: 1) the fracture skin is very thin but has finite thickness with negligible storage capacity, and 2) the flow from block to fissure is perpendicular to the interface.

Moench's model is described by two governing partial differential

equations defined using dimensionless parameters. For the fissure system, the governing equation is defined as

$$\frac{\partial^2 s_D}{\partial r_D^2} + \frac{1}{r_D} \frac{\partial s_D}{\partial r_D} = \frac{\partial s_D}{\partial t_D} + q_D' \quad r_D \geq 1 \quad (13)$$

where the source term for transient block-to-fissure flow is

$$q_D' = \gamma^2 \left(\frac{\partial s_D'}{\partial z_D} \right)_{z_D=1} \quad (14)$$

The initial condition is

$$s_D = 0 \quad r_D \geq 1 \quad (15)$$

The outer boundary condition is

$$s_D = 0, \quad r_D = \infty \quad (16)$$

and the inner boundary condition is

$$W_D \frac{\partial s_{wD}}{\partial t_D} - \frac{\partial s_D}{\partial r_D} = 2, \quad r_D = 1 \quad (17)$$

where

$$s_{wD} = s_D - S_w \frac{\partial s_D}{\partial r_D} \quad r_D = 1 \quad (18)$$

For the block system the governing equation becomes

$$\frac{\partial^2 s_D'}{\partial z_D^2} = \frac{\sigma}{\gamma^2} \frac{\partial s_D'}{\partial t_D}, \quad 0 \leq z_D \leq 1 \quad (19)$$

The initial condition is

$$s_D' = 0, \quad 0 \leq z_D \leq 1 \quad (20)$$

The boundary conditions are

$$\begin{aligned} \partial s_D' / \partial z_D &= 0, & z_D &= 0 \\ s_D' &= s_D - S_F \frac{\partial s_D'}{\partial z_D}, & z_D &= 1 \end{aligned} \quad (21)$$

where

s_D = dimensionless drawdown in fissures, defined by equation (6)

r_D = dimensionless distance, defined by equation (7)

t_D = dimensionless time, defined by equation (8)

σ = ratio of specific storage, defined by equation (4)

γ = dimensionless grouping of fracture system parameters, defined by equation (11).

s_D' = dimensionless drawdown in matrix blocks, defined as

$$s_D' = \frac{4\pi KH}{Q} (h_i - h)' \quad (22)$$

s_{wD} = dimensionless drawdown in the pumping well, defined as

$$s_{wD} = \frac{4\pi KH}{Q} (h_i - h_w) \quad (23)$$

z_D = dimensionless vertical coordinate, defined as

$$z_D = z/b' \quad (24)$$

S_F = dimensionless fracture skin, defined as

$$S_F = \frac{K' b_s}{K_s b'} \quad (25)$$

W_D = dimensionless well bore storage, defined as

$$W_D = \frac{r_c^2}{2r_w^2 S_s H} \quad (26)$$

H = aquifer thickness (L)

Q = is constant pumping discharge (L^3T^{-1})

h_i = initial hydraulic head (L)

h_w = hydraulic head in pumping well (L)

h' = hydraulic head in matrix blocks (L)

b' = half of average thickness of the slab-shaped blocks or average radius of the sphere-shaped blocks (L)

b_s = average thickness of fracture skin (L)

z = generalized vertical coordinate, representing the distance measured from the center of a slab-shaped block to the fissure (L)

K' = hydraulic conductivity of block system (LT^{-1})

K = hydraulic conductivity of fissure system (LT^{-1})

K_s = hydraulic conductivity of fracture skin (LT^{-1})

r = radial distance measured from center of pumped well (L)

r_c = internal radius of pumped well casing (L)

r_w = effective radius of pumped well bore (L)

S_s = specific storage of fissure system (L^{-1})

S_s' = specific storages of block system (L^{-1})

D = (as a subscript) dimensionless parameter

Analytical solutions of equations (13)-(21) can be derived by the Laplace transforms (Moench, 1984). The solutions of fissure flow in

Laplace space can be described as, for the pumping well

$$\overline{s_w} = \frac{2 [K_0(x) + x S_w K_1(x)]}{p \{ p W_D [K_0(x) + x S_w K_1(x)] + x K_1(x) \}} \quad (27)$$

for the observation well

$$\overline{s_D} = \frac{2 K_0(r_D x)}{p \{ p W_D [K_0(x) + x S_w K_1(x)] + x K_1(x) \}} \quad (28)$$

where

$$x = \sqrt{p + \overline{q_D}} \quad (29)$$

for slab-shaped blocks

$$\overline{q_D} = \frac{\gamma^2 m \tanh(m)}{1 + S_p m \tanh(m)} \quad (30)$$

and for sphere-shaped blocks

$$\overline{q_D} = \frac{3\gamma^2 [m \coth(m) - 1]}{1 + S_p [m \coth(m) - 1]} \quad (31)$$

where

p = Laplace transform variable which is inversely related to the dimensionless time

K_0 = modified Bessel function of second kind of zero order

K_1 = modified Bessel function of second kind of first order

m = dimensionless grouping of parameters, defined by equation (9).

The solutions of block flow equations that are described in (19)-(21) are as follows, for slab-shaped blocks

$$\overline{s_D'} = \frac{\overline{s_D}}{[1 + S_F m \tanh(m)]} \frac{\cosh(z_D m)}{\cosh(m)} \quad (32)$$

and for sphere-shaped blocks

$$\overline{s_D'} = \frac{\overline{s_D}}{\rho_D \{1 + S_F [m \coth(m) - 1]\}} \frac{\sinh(\rho_D m)}{\sinh(m)} \quad (33)$$

where

ρ_D = dimensionless distance defined as distance measured from center of a sphere-shaped block divided by the average radius of the sphere blocks.

The Laplace transform solutions for the cases of pseudo-steady state block-to-fissure flow from slab-shaped and sphere-shaped blocks with fracture skin are also presented by Moench (1984). Based on Moench (1984), the transient block-to-fissure flow solutions could be reduced to the pseudo-steady state solutions at large values of time while S_F is large. The long time criterion set by Moench is $m^2 \leq 0.1$ or in real space

$$t \geq 10 \frac{(b')^2}{K'/S_s'} \quad (34)$$

Moench's transient flow with fracture skin solutions becomes the same as pseudo-steady state flow with fracture skin solutions when the S_F is large and block diffusivity (K'/S_s') is large and/or block size is small. Therefore the double-porosity with fracture skin model gives a theoretical relationship between pseudo-steady state and transient block-to-fissure flow models (Moench, 1984).

The physical explanation of this theoretical relationship is obvious. From the definition of equation (25), sufficiently large S_F means low fracture skin hydraulic conductivity or large ratio of hydraulic conductivities of the block and the fracture skin (K'/K_s). Most of the hydraulic head loss from the blocks to the fissures occurs across the fracture skin. Consequently, the gradient of water head within the blocks remains small, and flow from blocks to fissures can be assumed as steady state.

The Moench solutions (30) and (31) reduce to Boulton and Streltsova double-porosity transient flow solutions of (9) and (12) when S_F is zero. The fracture skin no longer exists in this extreme situation.

Many groups of type curves of dimensionless drawdown vs. dimensionless time can be generated from equations (27) and (28), based on the selective parameters r_D , γ , σ , S_F , and S_w . From equations (4), (7), (11) and (25), these parameters are directly related to the geometry of the fracture system, hydraulic conductivities and specific storages of the fissures and block matrix, as well as the wellbore skin (Ramey, 1982) and fracture skin characteristics.

Type curves for selective values of S_F , $r_D=1$, $\sigma=100$, $\gamma=.01$ and $S_w=0$ are shown in Figure 4-1. The type curves show that the hydraulic response of the model is very similar to that of Neuman delayed yield solution for an unconfined aquifer when S_F is large enough (Neuman, 1972; 1973).

The early hydraulic response of the Moench solution follows a Theis type curve that corresponds to the hydraulic properties of the fissure system. A transition section at smaller drawdown increasing rate than Theis curve occurs due to water derived from the block matrix after the

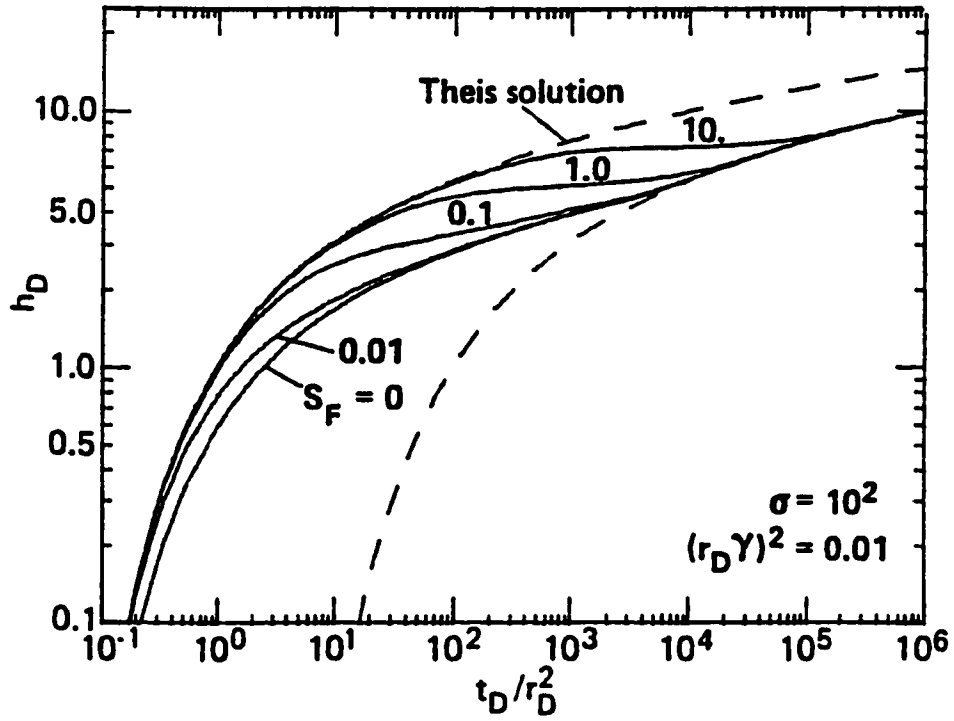


Figure 4-1. Type curves for selective values of parameters of double-porosity with fracture skin model (after Moench, 1984)

initial period. The later response follows a new Theis type curve that probably corresponds to the average hydraulic properties of the entire fractured aquifer (fissures and block matrix).

The early hydraulic responses of the Moench model are very similar in shape to that of the modified Hantush leaky aquifer model (Hantush, 1960) when S_F is less than 0.1. Water derived from the block matrix in the double-porosity models is the same as leakage derived from storage of the confining layers in a multiple layer leaky aquifer system (Williams, 1985).

A weakness of Moench's solutions is that the model is described using more parameters than other double-porosity models. The determination of these parameters needs more detailed information on hydrostratigraphy and fracture geometry. The fractured aquifer system may be simulated by the model with many combinations of the parameter values to fit the observational data; remarkably different estimations of the aquifer properties can be obtained.

Double-porosity Slug Test Model

Barker and Black (1983) propose an analytical model for slug tests in fissured aquifers, based upon the same conceptual models as that by deSwaan (1976) and Boulton and Streltsova (1977). The test technology and design are adopted from Cooper *et al.* (1967).

An analytical solution is derived through Laplace transforms (Barker and Black, 1983). However, the solution does not appear to be practically applicable because: 1) the solution is described by three dimensionless parameters α , β and γ in addition to the dimensionless time t_D , which requires more detailed data on geology such as fracture size, numbering and

geometry; 2) a tremendously large number of type curves is required in order to cover the full range of feasible combinations of α , β and γ ; and 3) many of these combinations will produce almost identical type curves, that will result in a fundamental problem of solution uniqueness (Barker and Black, 1983).

An important finding of Barker and Black's work is derived from a comparison between the results of the double-porosity slug test model and a homogeneous and isotropic slug test model (Cooper et al, 1967). After an error analysis using the least squares technique, Barker and Black (1983) concluded that if the homogeneous model is applied in fractured aquifers: 1) the derived transmissivity value will only be slightly overestimated by a factor less than three, 2) the storage coefficient will underestimate total aquifer storage coefficient by a factor possibly as great as 10^6 , and 3) the fissure storage coefficient may be either underestimated or overestimated.

Actually, the aquifer storage coefficient can not be estimated accurately by any slug test model due to intrinsic problems of the method. The type curves of the slug test solution for homogeneous and isotropic porous medium are very similar and basically parallel to each other. The estimated storage coefficient could vary in a range as large as 10^3 to 10^4 based on the different type curve matching. Problems for applying the homogeneous slug test models to estimate the aquifer storage coefficient always exist regardless of fractured or porous aquifers.

Slope (Pressure Derivative) Analysis Approach

Slope analysis or pressure derivative data analysis on a hydraulic test has been discussed in the petroleum literature in recent years (Gringarten, 1984; Beauheim, 1988;). Slope analysis is basically a qualitative approach that is used to identify efficiently the different hydraulic responses due to the characteristics of an aquifer system through a pressure or drawdown derivative curve compared with the drawdown curve.

Gringarten (1984) proposes a drawdown derivative curve as a log-log plot of the derivative of dimensionless drawdown with respect to the natural log of dimensionless time t_D as a function of t_D . In other words, Gringarten's drawdown derivative curve is a log-log plot of the product of time and drawdown derivative as a function of time. Such a plot is characterized by a horizontal straight line for homogeneous flow solution (Theis solution) in the later stage of a hydraulic test.

The drawdown and drawdown-derivative curves generally are plotted in the same time coordinate on a log-log scale for purposes of comparison. An example of pressure(drawdown) curves and pressure(drawdown)-derivative curves with different hydraulic conditions is presented in Figure 4-2. The horizontal coordinate (x axis) is log values of dimensionless time group that is defined by dimensionless time divided by dimensionless wellbore storage constant (t_D/C_D); the vertical coordinate (y axis) represents log values of dimensionless pressure(drawdown) and product of pressure-derivative and dimensionless time group.

Figure 4-2 shows that the pressure(drawdown)-derivative curve is particularly useful for recognizing qualitatively the different shapes of transition segment of the pressure or drawdown responses in fractured

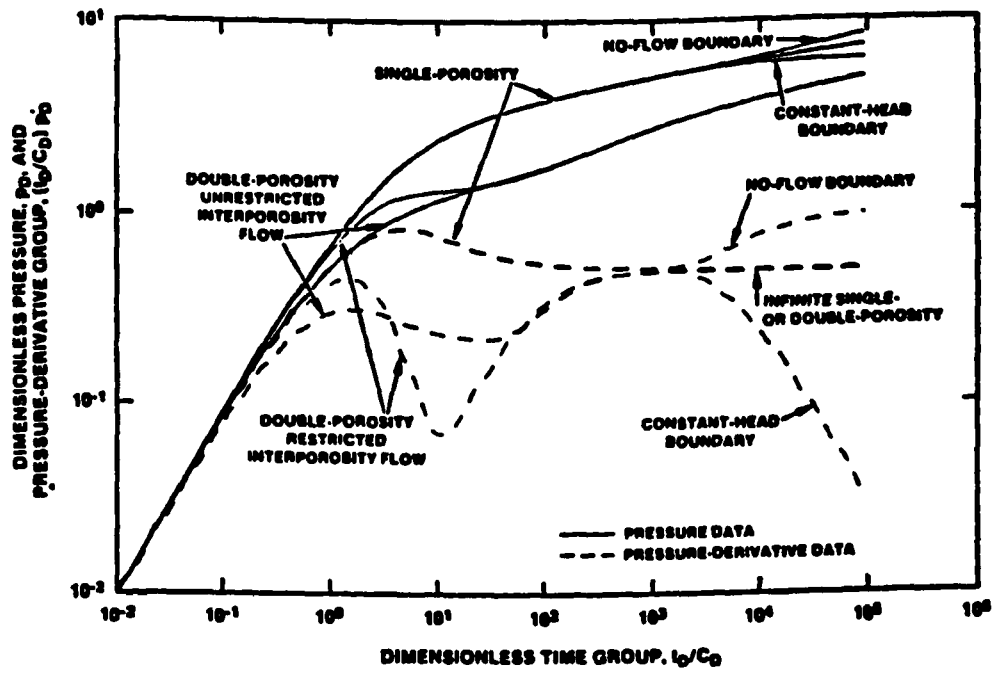


Figure 4-2. Comparison between pressure curve and pressure-derivative curve with different hydraulic conditions (after Beauheim, 1988)

rocks. The slope or derivative curve of the double-porosity flow exhibits a characteristic hump below the curve of the single porosity flow. The hump is greater for the double-porosity with fracture skin model (restricted interporosity flow) than that of the ordinary double-porosity model. The distinction between the different types of flow behavior is more clearly illustrated by the slope or derivative curves.

As shown in Figure 4-2, the slope or derivative curve is also useful for identifying the boundary conditions. The drawdown-derivative curve of ground water flow in a laterally infinite single or double-porosity aquifer shows a horizontal line in the later stage of the hydraulic test. The deviations of the slope or derivative curve caused by constant head and no-flow boundaries are more recognizable than that of the pressure(drawdown) curve.

Equivalent Porous Medium Models

Many analytical ground water flow models developed for porous media have been applied successfully in aquifer test analysis in fractured rock systems (Lee, 1982; Prudic, 1982; Kruseman and de Ridder, 1983; Uhl and Joshi, 1986). Porous medium models have been applied to analyze ground water flow behavior in fractured rocks though disagreement about the applicability of the models has always existed. Long *et al.* (1982, page 647) suggest that two criteria have to be met for applying the porous medium models in a fractured rock: 1) there is an insignificant change in the value of the equivalent permeability with a small addition or subtraction to the test volume, and 2) an equivalent permeability tensor exists which predicts the correct flux when the direction of a constant gradient is changed.

Further research on the fracture geometry and testing size by Long *et al.* (1982; 1985) demonstrates that fracture systems behave more like homogeneous porous media when 1) fracture density is increased, 2) apertures are constant rather than distributed, 3) orientations are distributed rather than constant, and 4) large sample sizes are tested. Porous medium analytical models are applicable when these standards are satisfied.

Homogeneous Isotropic Models

The assumptions and analytical solution for flow in the homogeneous and isotropic porous media are presented by Theis (1935). Many modifications have been developed to account for different boundary conditions (Papadopoulos and Cooper, 1967), leakage from upper or lower confining layers (Hantush and Jacob, 1955; Hantush, 1960; Neuman and Witherspoon, 1969a; 1969b; 1972; Javandel and Witherspoon, 1969; 1983), unconfined conditions (Boulton, 1970; Boulton and Pintin, 1971; Neuman, 1972; 1973) and partially penetrated pumping and observation wells (Hantush, 1962a, 1962b; Weeks, 1969; Neuman, 1974).

Cooper *et al.* (1967) presents an analytical model to describe water level change in a well of finite diameter after a known volume of water (slug) is "instantaneously" injected to or withdrawn from the well. The model has been known as the slug-test model and is widely used in practice to determine hydraulic properties of the aquifer in the vicinity of the well. A modified slug-test model for unconfined aquifers with completely or partially penetrating wells is presented by Bouwer and Rice (1976). Some theoretical problems of the model and field test technical problems such as initial turbulence are discussed by Pandit and Miner (1986) and

Kabala *et al.* (1985).

Analytical models for leaky multiple aquifer system developed by Hantush (1960), Papadopoulos (1966), Neuman and Witherspoon (1969a; 1972), and Streltsova, (1976b) have a similarity with the double-porosity model. The fissures and matrix blocks act similar to the pumped aquifer and aquitards of the leaky aquifer system. One difference between the two types of models is that fissures and blocks are overlapped together in the double-porosity model and leaky aquitards are parallel to the pumped aquifer.

Sen (1986b) presented a slope-matching method to interpret aquifer test data quantitatively based on the Theis model and Hantush leaky aquifer model (leaky without storage). The basic steps of the method are: 1) to calculate the type curve slopes of $\log W(u)$ with respect to $\log u$ and list the results as type curve slope table; 2) to calculate the drawdown data slope between two successive data points after the second data point on the log-log coordinates; 3) to identify the values of well function $W(u)$ and dimensionless variable u from the type curve slope table corresponding to the slope at this data point; 4) to compute the local hydraulic properties for that particular data point based on the analytical model solutions; 5) to repeat the steps (2), (3) and (4) with the next drawdown record (data point) to obtain sequence estimations of the aquifer hydraulic property, and 6) to apply statistical analysis to the results in terms of frequency functions and confidence limits with the assumption that the Gaussian distribution is valid for the parameter estimates.

Sen's method is completely based on the Theis and Hantush leaky aquifer assumptions. The method provides an approach for analyzing aquifer test data if the Theis and leaky assumptions are satisfied. However, Sen's

slope-matching method does not consider any variation of the hydrogeologic conditions. Application of the method without a complete knowledge of the aquifer system could result in great error.

Homogeneous Anisotropic Models

Fractured rocks generally behave more like anisotropic media rather than isotropic media. This anisotropic behavior is commonly due to stratification and directional tectonic fracturing.

Hydraulic conducting properties of anisotropic fractured rocks are generally described by a second-rank symmetric positive-definite tensor. Hantush (1966a; 1966b), Hantush and Thomas (1966), and Neuman *et al.* (1984) have developed analytical models to determine the two-dimensional transmissivity tensor under the condition of horizontal flow. Weeks (1969) proposes a model with assumptions of a partially penetrating pumping well and nearby piezometers or partially penetrating observation wells to determine the ratio of horizontal to vertical hydraulic conductivity of confined aquifers. Also a model that is applied in anisotropic unconfined aquifers to obtain the vertical and horizontal hydraulic conductivities was developed by Neuman (1975).

Way and McKee (1982) present an analytical model of three dimensional flow in homogeneous, anisotropic and leaky aquifers to determine the directional hydraulic conductivity. The model is applied in fractured rock case studies to evaluate hydraulic properties of an aquifer and to estimate statistical distribution of the fractures. The model is developed based on the following assumptions:

- 1) Darcy's law is valid.
- 2) aquifer is homogeneous with infinite lateral extent.

- 3) aquifer is bounded by an upper or lower aquitard within which the storage can be considered as negligible.
- 4) hydraulic head in the unpumped aquifer remains constant during the test.
- 5) aquifer and aquitard are horizontally distributed with constant thickness.
- 6) initial water level is constant.
- 7) water is extracted at constant rate from the pumping well that partially penetrates the aquifer thickness with a known screen completion height from both the top and bottom of the aquifer.
- 8) a minimum of three observation wells located within a distance of 1.5 times the aquifer thickness at three different directions to the pumping well is required. All of them are partially penetrating wells with known screen completion.

The analytical solutions and type curves generated from the solutions are presented by Way and McKee (1982). Through the type curve matching technique, the horizontal and vertical hydraulic conductivities K_x , K_y , and K_z , storativity S and leaky factor r/B of the aquifer can be estimated.

Hsieh and Neuman (1985) propose a field testing method, known as a cross-hole test, and corresponding analytical models to determine the 3-D hydraulic conductivity tensor and the specific storage of an anisotropic porous or fractured medium. The cross-hole test method is conducted by injecting water into (or pumping from) a rock interval isolated through packers in a borehole and observing the water head variations within isolated intervals in other boreholes. The method is particularly designed

for a medium in which the principal directions of anisotropy are initially unknown.

The cross-hole test requires a minimum of six observation intervals that are located in a 3-D pattern around the injecting interval; more intervals are preferable. The boreholes can be vertical, inclined, or in any direction, as long as the observation intervals are in the appropriate 3-D pattern. A constant flow injection (or pumping) rate and a constant initial head throughout the testing volume are assumed by the method. The double-porosity feature of the fractured rocks is not considered. The method considers that there are no upper or lower impermeable boundaries and the effects of planar constant-head and no-flow boundaries in any direction can be analyzed by image theory.

Four solutions with different mathematical treatments with respect to the injection/observation intervals are derived by Hsieh and Neuman (1985). The basic and simplest solution considers the point injection/observation in which the injection/observation intervals must be short compared to the distances between them. The solutions for line injection/point observation, point injection/line observation, and line injection/line observation are basically integrations of the point injection solution and/or averages of the point observation solution. Thus, more parameters related to the length of the injection/observation intervals are utilized and the solutions are more complicated for the later cases. The steady state solutions and effects of a planar boundary are also presented by Hsieh and Neuman (1985).

The simplest point injection/observation solution of Hsieh's model is preferable for purpose of an application. The solution for hydraulic head response to the injection at a constant rate in the rock mass sufficiently

far from boundaries can be described graphically by a single type curve (Figure 4-3). The solution is described analytically by dimensionless parameters as follows:

$$s_D = \operatorname{erfc}\left(\frac{1}{\sqrt{4 t_D}}\right) \quad (35)$$

where $\operatorname{erfc}(\)$ is the complementary error function, s_D is the dimensionless head increase (or drawdown), which is defined as

$$s_D = \frac{4 \pi s \sqrt{G_{xx}}}{Q} \quad (36)$$

and t_D is the dimensionless time

$$t_D = \frac{D t}{S_s G_{xx}} \quad (37)$$

Where

Q = constant injection (discharge) rate ($L^3 T^{-1}$)

s = hydraulic head increase (drawdown) in the observation intervals (L)

S_s = specific storage of the aquifer (L^{-1})

t = time since injection (pumping) started (T)

D = determinant of hydraulic conductivity matrix (second order tensor) K , defined as

$$D = K_{11}K_{22}K_{33} + 2K_{12}K_{23}K_{13} - K_{11}K_{23}^2 - K_{22}K_{13}^2 - K_{33}K_{12}^2 \quad (38)$$

G_{xx} = quadratic form, defined as

$$G_{xx} = \mathbf{x}^T \mathbf{A} \mathbf{x} = x_i x_j A_{ij} \quad (39)$$

K_{ij} ($i, j = 1, 2, 3$) = the coefficient in i^{th} row and j^{th} column of hydraulic conductivity matrix (tensor) K

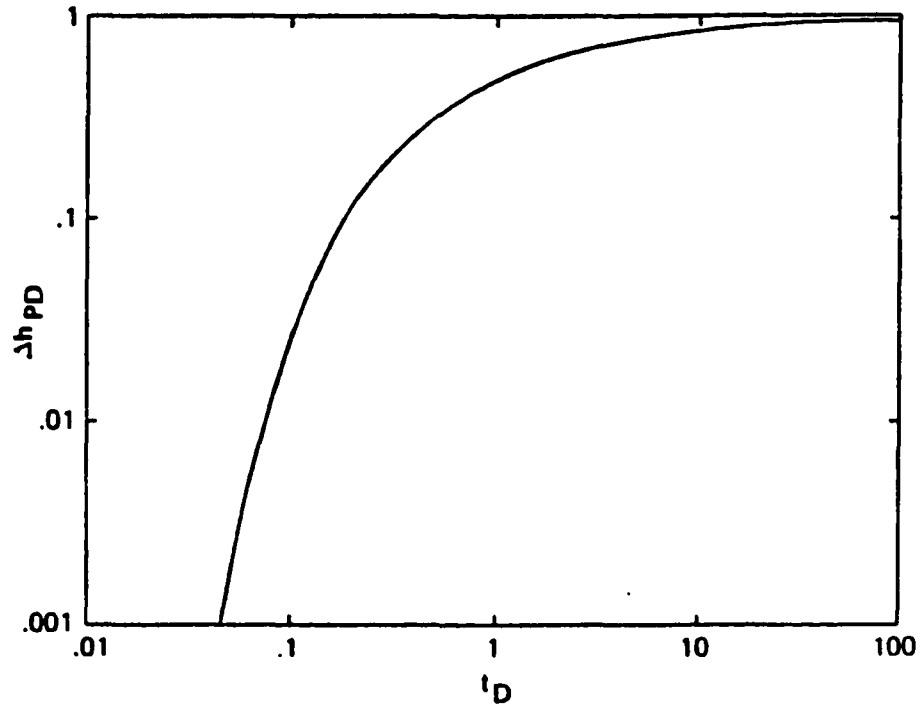


Figure 4-3. Type curve for point injection/observation solution of cross-hole method (after Hsieh and Neuman, 1985)

\mathbf{x} = vector of observation (from injection point)

\mathbf{A} = adjoint matrix of \mathbf{K}

i, j = index of the coefficient of a matrix or vector

bold letter = a vector or matrix

\mathbf{T} = (as superscript) matrix or vector transpose.

Hsieh et al. (1985) present the same solution in terms of directional hydraulic conductivity $K_d(\mathbf{n})$, which is defined as a ratio of magnitude of directional specific discharge \mathbf{q} to the component of hydraulic gradient $-\nabla h$ in the same direction of \mathbf{n} ,

$$K_d(\mathbf{n}) = -\frac{|\mathbf{q}|}{\mathbf{n}^T \nabla h} \quad (40)$$

Combined with Darcy's law,

$$\mathbf{q} = -\mathbf{K} \nabla h \quad (41)$$

the directional hydraulic conductivity in the direction of \mathbf{n} can be expressed as

$$K_d(\mathbf{n}) = \frac{1}{\mathbf{n}^T \mathbf{K}^{-1} \mathbf{n}} \quad (42)$$

If we assume \mathbf{e} to be the unit vector pointing from the injection point to the observation point, and r to be the distance between these points, with the matrix calculation, the G_{xx} can be written as

$$G_{xx} = r^2 (\mathbf{e}^T \mathbf{A} \mathbf{e}) = \frac{r^2 D}{K_d(\mathbf{e})} \quad (43)$$

Thus the solution of Hsieh's model described in equations (35), (36) and (37) for point injection and observation intervals can be described as

$$s_D = \frac{4\pi r s}{Q} \sqrt{\frac{D}{K_d(\theta)}} \quad (44)$$

and

$$t_D = \frac{K_d(\theta) t}{r^2 S_s} \quad (45)$$

The solutions other than the point injection/observation can be described graphically by a group of type curves that are defined by additional spatial parameters α and β . The type curves for selected values of the parameters are illustrated by Hsieh and Neuman (1985). A case study of the model application with point injection and observation intervals in fractured granitic rocks are presented by Hsieh et al. (1985).

Evaluation of Applicability of the Analytical Models

The purpose of this section is to discuss briefly the general procedures of evaluation or selection of alternative analytical models that might be applied to a particular hydrogeological environment. The applicability of the alternative analytical models to characterize the basalt aquifers in the UIGRS is presented in succeeding chapters.

Williams (1985) points out that one must conceptualize the hydrogeological environment in some manner prior to deciding which theoretical analysis is appropriate to the particular hydrogeological conditions with which one must deal at a specific site. This step is important because the same observational data could be simulated by

alternative models. An aquifer test analysis could result in significant error if the hydrogeological environment is not described by proper conceptual models. One of the theoretical disadvantages of characterizing a ground water flow system by aquifer tests is that there is no unique solution for given observational data (Williams, 1985; Freeze and Cherry, 1979).

A five-step procedure for selection of an appropriate analytical model after formulation of conceptual models is proposed by Levens (1990, page 27): 1) identify alternative analytical models corresponding to alternative conceptual models, 2) evaluate the validity of the assumptions of each alternative analytical model, 3) evaluate the correspondence between hydraulic test data and theoretical type curves, 4) evaluate the applicability of alternative analytical models using different plots, and 5) estimate hydraulic coefficients if feasible.

The hydraulic behavior of a complex naturally fractured rock generally is scale-dependent. Therefore the testing scale effects that relate to the testing well setting and testing duration should be considered in detail in the evaluation procedures. Different alternative analytical models may be applicable at different testing scales.

Beauheim (1988) presents an analysis of scale effects on well testing in fractured media. Two kinds of scale are proposed by Beauheim: the scale of testing and scale of observation. The testing scale relates to the magnitude and duration of hydraulic stress imposed and determines what components of an aquifer such as individual fractures or the entire fracture system respond to an observable degree. The scale of observation refers to the distance from the pumping well where the responses can be observed during the test. Generally, the observation scale is dependent on

the testing magnitude and duration.

Small-scale tests are often referred to drillstem or slug tests. These are sensitive only to the fractures in direct connection with the wellbore. The boundary effect, leakage condition, and pressure equilibration between the fissures and matrix blocks generally are not observable in small scale tests.

Short-term, single-well and multiple-well tests stress a larger volume of the aquifer than slug tests. Double-porosity responses, leaky effects and boundary conditions are commonly observed in the pumping well and nearby observation wells. A long-term, multiple-well test with distant observation wells generally reveals a single-porosity behavior, which is related to the overall average hydraulic properties of the entire heterogeneous aquifer system at a large scale. The long-term test data in the fractured rocks may well be analyzed by the homogeneous analytical models of porous media. Short or long terms are relative concepts that depend on the testing stress (volume) and the aquifer condition.

The hydraulic behavior of the fractured rocks observed in one testing scale will not necessarily be the same as observed on a different scale. Thus, the analytical models applied to the same fractured aquifer may be changed according to the testing scale. Consequently, the hydraulic properties estimated from different scale tests may not be consistent. This may be equally true for porous media because there is no absolutely homogeneous system in any geological formation. The change of testing scale, which directly relates to the testing volume, may result in different average hydraulic properties over that volume.

CHAPTER V

Hydraulic Testing -- Scope and Methodology

Extensive hydraulic testing has been conducted at the UIGRS in order to characterize the hydraulic behavior of fractured basalt aquifers. Both slug tests and multiple well aquifer tests were performed in this study. The design and implementation of these tests are described in this chapter. The testing equipment, data collection method, testing scope, and procedures are presented.

Testing Equipment

Slug tests in four-inch wells were performed by dropping a "slug" into the wells and pulling the "slug" out after the water level reached steady state. The "slug" is a piece of 3-inch diameter PVC pipe of 6 foot length filled with sand and sealed at both ends. Water injection slug tests were conducted in wells with small diameters (wells S12D1 and S12D2).

The multiple-well aquifer tests were conducted using a 1.5 HP Berkeley submersible pump that was connected to a 1.25 inch steel discharge pipe. The pump has a maximum discharge capacity of approximately 38 gpm and a maximum head lift of over 200 feet (61 meters). A power winch was used to install and remove the pump. The pump generally was submerged 30 to 40 feet below the static water level for the tests. The pump discharge was channeled through a four-inch PVC surface discharge pipe into Paradise Creek during the tests.

Pump discharge was regulated by 1.5 inch diameter constant-flow valves, which are accurate as long as a proper pressure range is

maintained. Constant flow valves of 6, 12, and 28 gpm were used in the tests. The proper inlet pressure range of these valves is 7 to 110 psi. A 1.5 inch gate valve was used to regulate pressure in a range of 40 to 50 psi during the tests. Very low discharge rates were controlled by two ball valves with a pressure gauge in between. The first ball valve performed as a pressure regulator to keep constant inlet pressure for the second ball valve that was used for flow control. A fairly constant flow rate of 0.5 gpm was maintained using this discharge control device for several tests.

Drawdown responses were measured in two ways: 1) steel or electrical tapes operated by hydrology graduate students, and 2) Druck 830 series (0-20 psi) pressure transducers with output regulated and recorded by Campbell Scientific Model 21X dataloggers.

The power supply to the pump was provided by several different portable generators. The generators provided the minimum rated output of 3500 W recommended to operate the 1.5 HP submersible pump.

Slug Testing

Slug tests were conducted in all the deep basalt wells for two general objectives: 1) evaluating the applicability of the homogeneous and isotropic slug test model in the fractured basalt aquifer, and 2) estimating the transmissivity in the vicinity of each well.

The slug test water level data were collected using a datalogger and pressure transducers. When one test was conducted in a testing well, the water levels in nearby wells also were monitored through additional transducers. No responses were observed from nearby wells during any of the slug tests.

Multiple Well Aquifer Testing

Multiple well aquifer tests were designed to utilize each of the four-inch-diameter wells as a pumping well and the rest of the wells as observation wells. The objectives of the tests were: 1) to evaluate the intraflow structure continuity of the Wanapum Basalt, 2) to evaluate the applicability of alternative analytical models, 3) to characterize the hydraulic properties of the fractured basalt aquifers using applicable analytical models, and 4) to characterize the heterogeneity of the basalt system through extensive hydraulic testing.

Phase One Testing

The multiple well testing was completed in two phases. The first phase was a reconnaissance level testing. Four aquifer tests were conducted with wells V16D, Q17D, T16D and D19D as alternative pumping wells. There were only five deep basalt wells at the time of testing and all of them were open bore through the entire basalt section.

The phase one testing had several objectives: 1) to identify major fractures and fractured aquifers at the UIGRS; 2) to recognize the hydraulic continuity and interrelationships of the major fracture zones in the basalt and shallow alluvial aquifers, as well as Paradise Creek and the aquifers; and 3) to provide information for proper completion of the testing wells. The information gained from phase one testing is summarized in Table 5-1.

Aquifer tests 4-15-88, 7-7-89 and 7-9-89 were similar in terms of deep and shallow observation well responses and recovery time. The three pumping wells (Q17D, V16D and T16D) all intercept the E fractured aquifer

Table 5-1. Summary of Phase One Multiple Well Aquifer Testing Results

Test No. (date)	Pumping Well	Pumping Rate (gpm)	Test Duration (min)	Pumping Well Drawdown (ft)	Shallow Well Responses	Recovery Time* (min)	OBSERVATION WELL RESPONSES			
							Well No.	Radius (ft)	Response Time**(min)	Final drawdown(ft)
4-15-88	Q17D	6.5	280	26	P17S and V16S (all available shallow wells)	<720	V16D	100	<1	0.65
							T16D	70	<1	2.6
							S12D***	100	4	2.1
							D19D	275	15	2.7
7-5-89	D19D	9	1230	34.1	NONE	>4320	V16D	375	>400	0.08
							Q17D	275	>400	0.13
							T16D	345	300	0.38
							S12D	325	50	8.4
7-7-89	V16D	38	1135	11.7	P17S and V16S (all available shallow wells)	<720	T16D	30	0.3	7.1
							Q17D	100	0.3	5.7
							S12D	100	4	2.0
							D19D	375	on recovery	on recovery
7-9-89	T16D	6	1379	13.7	P17S and V16S (all available shallow wells)	<720	V16D	30	0.4	0.8
							Q17D	70	0.2	2.8
							S12D	89	20	0.3
							D19D	345	no response	no response

- * Time until pumping well fully recovered since pump off.
- ** Time until having a measurable drawdown from pumping begins.
- *** Well S12D had not been completed as S12D1 and S12D2 at the time.

at depths of 63 to 75 feet (19 to 23 meters). The drawdown responses among the three wells generally were observed in less than a minute. Water level recovery in the pumping well was fast compared to test 7-5-89. The shallow piezometers installed in the shallow alluvial aquifer all responded in less than 30 minutes. The primary difference among these three tests was the specific capacity of the pumping well. Well V16D had the highest specific yield; the value decreased to the west from well V16D to well Q17D.

Aquifer test 7-5-89 had completely different observation well responses. The pumping well D19D intercepts only the W fractured aquifer. Pumping this well created no drawdown in the shallow alluvial aquifer. Drawdown was observed in the other deep wells with a long time delay.

Phase Two Testing

The second phase of multiple well aquifer testing was conducted after each of the wells was completed in a selected fracture zone. A sequence of seven aquifer tests was performed from September 1989 to March, 1991. Six wells were tested during this phase of testing; three wells (V16D, Q17D and T16D) were completed in the E fractured aquifer and the other three (wells D19D, J16D and U3D) were screened in the W fractured aquifer. The interconnection of the two aquifers through the wells S12D, Q17D, Q16D and U3D was eliminated after the well completion. The well construction and completion information is presented in Table 1-1 and Appendix A.

Data collected from the phase two testing are presented and analyzed in the following chapters. The testing was designed to stress one fractured aquifer in each test and to monitor the hydraulic responses in both fractured aquifers and the shallow alluvial aquifer. The pumping rate and duration of the tests were determined based on the results of the first

phase of testing.

Aquifer test 9-22-89 was conducted on September 22, 1989 with the participation of students in the Geology 410 class from the University of Idaho and Washington State University. Well Q17D was pumped for 1440 minutes at a constant discharge of 6 gpm, regulated by a constant flow valve. Five deep wells, V16D, T16D, S12D1, S12D2 and D19D as well as three shallow wells V16S, P17S and N18S, were monitored as observation wells. A maximum drawdown of 24.6 feet was observed in the pumping well.

Aquifer test 4-4-90 was conducted on April 4, 1990 with pumping well T16D. Students from the University of Idaho Hydrology 568 class were involved in monitoring observation well responses. The pumping duration was 303 minutes and the discharge was 6 gpm. Observation wells V16D, Q17D, S12D1, S12D2, V16S, P17S and N18S were monitored for drawdown responses. Well D19D had no response until the very end of the test. The test was terminated a little earlier than originally planned (480 minutes) due to failure of the generator.

Aquifer test 4-11-90 was conducted with the same pumping well and the same pumping rate used for test 9-22-89. The test was designed originally for a two-well tracer test. Both well hydraulic data and water chemistry data were collected in selected wells during the test. Two wells V16D and T16D were observed for drawdown responses. The test was performed over an extended period of 2910 minutes.

Aquifer test 6-3-90 was conducted on June 3, 1990 with the assistance of UI geology field camp students. The pumping well V16D was completed in the E fractured aquifer and had the highest yield capacity at the UIGRS. The discharge rate of the test (28 gpm) was controlled using a constant flow valve. The pumping duration was 428 minutes and water levels were

monitored in the pumping well and all the remaining wells at the UIGRS.

Three new deep wells and two shallow wells were drilled before the test 6-3-90. The hydraulic connection between the E and W fracture zones through the new well bores was observed during the period between drilling and well completion.

Aquifer tests 8-14-90 and 8-17-90 were conducted on August 14 and 17, 1990 with the help of UI hydrogeology graduate students. Well J16D was the pumping well in test 8-14-90; the discharge rate was 15 gpm. Well D19D was pumped in test 8-17-90 with a pumping rate of 12 gpm. Both pumping wells were completed in the W fractured aquifer.

The test 8-14-90 continued for 373 minutes, whereas the duration of test 8-17-90 was 607 minutes. Both tests were stopped because the maximum drawdown reached the pump installation depth. Water levels in the pumping wells were nearly stabilized at the end of both tests, but drawdowns in the observation wells were far from stabilized. Water levels in the shallow wells did not respond during either of the aquifer tests.

Aquifer test 3-8-91 was conducted on March 8, 1991 with assistance from UI Hydrology 568 students. Well U3D was selected as the pumping well with an average pumping rate of only 0.5 gpm. The test was stopped after 181 minutes because drawdown in the pumping well reached the pump installation limit. Water level responses were measured in the W fractured aquifer but not in the E fractured aquifer or the shallow alluvial aquifer.

Water Level Measurements--Quality Assurance

In most of the multiple well aquifer tests, water levels in the pumping well and observation wells were measured in two ways: 1) pressure

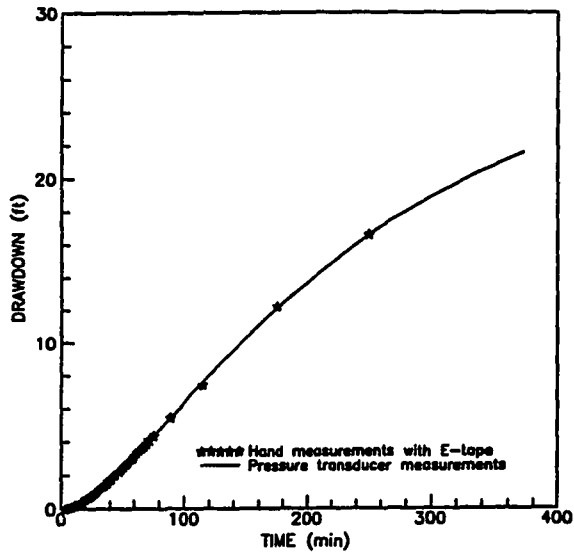
transducers connected to data loggers, and 2) electrical or steel tapes. The precision of the transducer measurements recorded by the Campbell Scientific Model 21X datalogger depends on the pressure range of the transducers and the working conditions of the instruments. Hand measurements with electrical or steel tapes were collected whenever human resources were available, for quality assurance and quality control purposes to validate the data logger record.

Comparisons between the pressure transducer and hand measurements in aquifer test 8-14-90 are presented in Figures 5-1 and 5-2 as examples. Figure 5-1 shows arithmetic plots of the pressure transducer and hand measurements. The same data are plotted on the log-log coordinates on Figure 5-2.

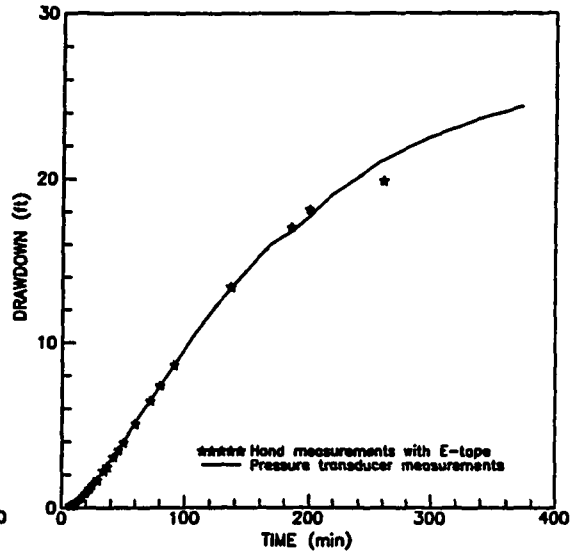
Figure 5-1 shows that the absolute error of a transducer measurement can be as great as one foot in the later stage of the test; the relative error is generally less than 10%. The measurement error of the transducer is more significant when the drawdown response is small in the observation well S12D1. Generally, the relative error of the transducer measurements is greater at the early stage of test than in the later time. This error at the early time of the test is not clearly illustrated in Figure 5-1 because of the scale on the drawdown axis.

The early time deviation of transducer measurements is clearly shown on the log-log plots in Figure 5-2. The large absolute error of transducer measurements at the later stage of the test disappears in the log-log plots.

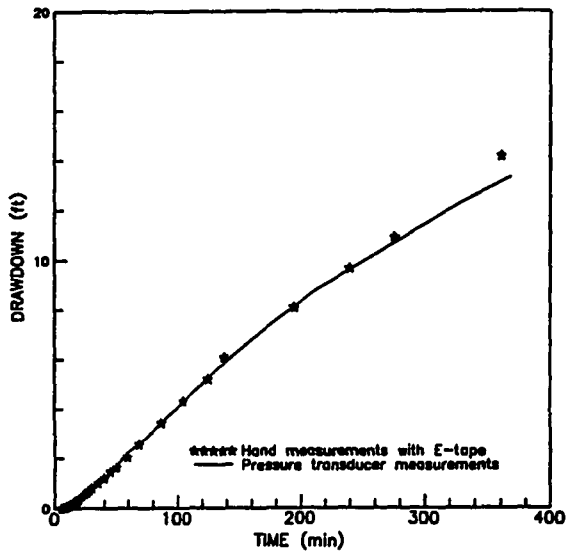
The utilization of pressure transducers to collect aquifer test or water level data should be carefully performed. A hand measurement check is always recommended whenever personnel are available. In order to



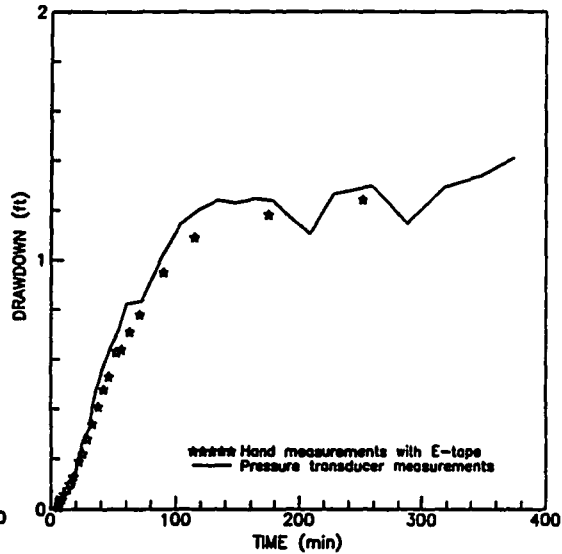
COMPARISON OF TRANSDUCER AND HAND MEASUREMENTS ON ARITHMETIC COORDINATES (equifer test 8-14-90 OW: S12D2)



COMPARISON OF TRANSDUCER AND HAND MEASUREMENTS ON ARITHMETIC COORDINATES (equifer test 8-14-90 OW: U3D)

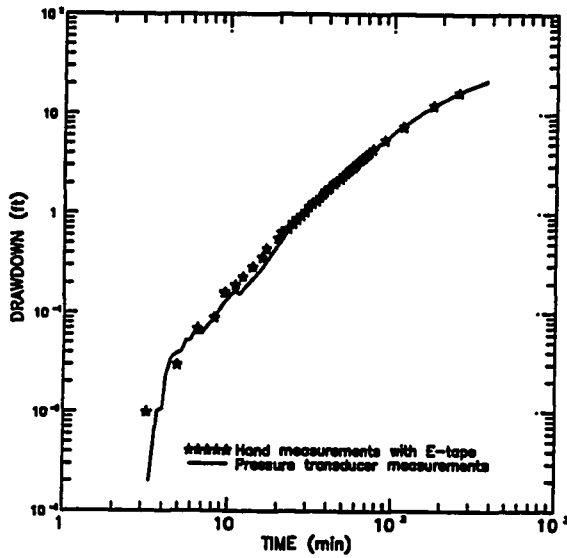


COMPARISON OF TRANSDUCER AND HAND MEASUREMENTS ON ARITHMETIC COORDINATES (pumping test 8-14-90 OW: D19D)

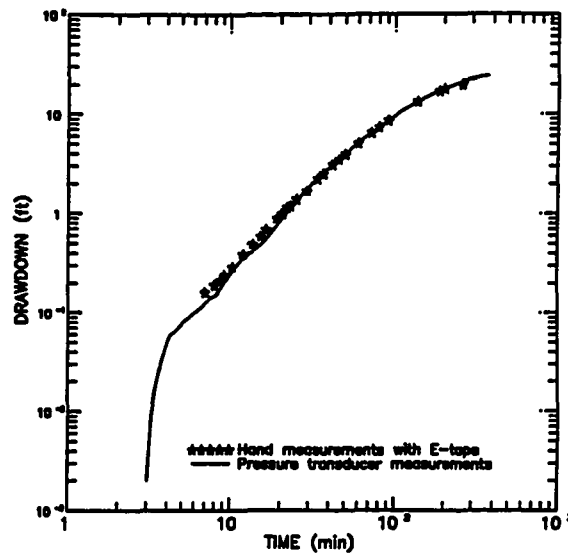


COMPARISON OF TRANSDUCER AND HAND MEASUREMENTS ON ARITHMETIC COORDINATES (aquifer test 8-14-90 OW: S12D1)

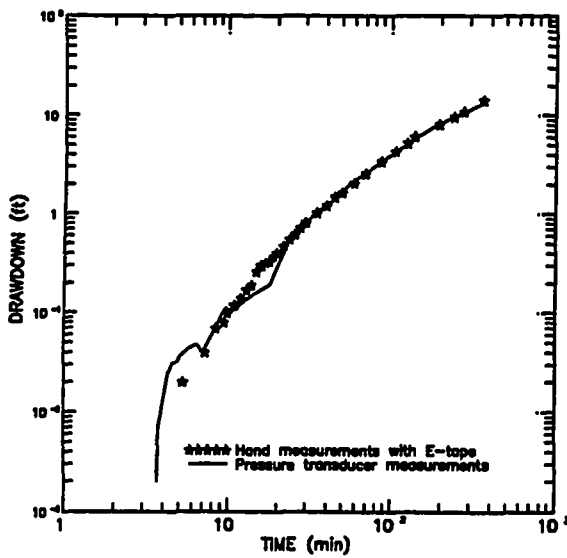
Figure 5-1. Comparison of pressure transducer and hand measurements in arithmetic coordinates during Aquifer test 8-14-90



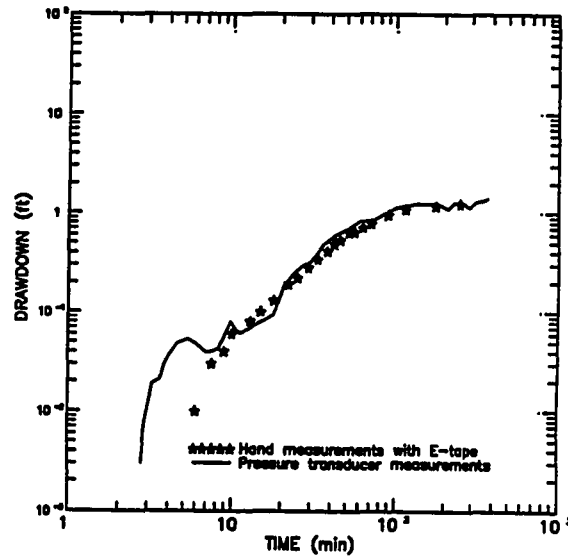
COMPARISON OF DRAWDOWN DATA COLLECTED BY TRANSDUCER AND HAND MEASUREMENT (pumping test 8-14-90 OW: S12D2)



COMPARISON OF DRAWDOWN DATA COLLECTED BY TRANSDUCER AND HAND MEASUREMENT (pumping test 8-14-90 OW: U3D)



COMPARISON OF DRAWDOWN DATA COLLECTED BY TRANSDUCER AND HAND MEASUREMENT (pumping test 8-14-90 OW: D19D)



COMPARISON OF DRAWDOWN DATA COLLECTED BY TRANSDUCER AND HAND MEASUREMENT (pumping test 8-14-90 OW: S12D1)

Figure 5-2. Comparison of pressure transducer and hand measurements as log-log plots during Aquifer test 8-14-90

minimize measurement error, a transducer with the proper pressure range should be selected for a specific purpose. Transducers with a 20 psi pressure range could be used for data collection in wells S12D2 and U3D during test 8-14-90 because total drawdowns in these wells were over 20 feet (6 meters). The same transducer may not be used in a observation well with a total drawdown of a few tenths of a foot. Figure 5-2 shows that the relative error is the greatest for the data collected from well S12D1, which had the smallest total drawdown among the four selected wells during test 8-14-90.

Hand measurement data were collected during most of the multiple well aquifer tests in phase two testing. The aquifer test analysis in succeeding chapters utilizes hand measurement data whenever these data are available. Analysis of tests 4-11-90 and 8-14-90 is based on transducer data, because only transducer measurements were collected during the tests.

CHAPTER VI
Aquifer Test Data Analysis and Analytical Model
Evaluation

The purpose of this chapter is to present the analysis of the hydraulic testing data and evaluation of the applicability of alternative analytical models. Data collected from seven multiple well aquifer tests of the phase two testing and slug tests are analyzed. Alternative analytical approaches applied are the Theis (1935), Hantush and Jacob (1955), modified Hantush (1960), Neuman and Witherspoon (1969a; 1972), Moench (1984), and Cooper *et al.* (1967).

Aquifer Test Data Analysis

A summary of configurations of seven multiple well aquifer tests of phase two testing is presented in Table 6-1. Four aquifer tests were conducted in the E fractured aquifer; the remaining three tests were in the W fractured aquifer. All the deep and shallow wells that had been constructed at the time of each test were monitored for drawdown response during the tests except for test 4-11-90.

Multiple Well Aquifer Test 9-22-89

The observed drawdowns within the pumping well Q17D and all the observation wells during aquifer test 9-22-89 are plotted versus time on a log-log scale as shown in Figure 6-1. The observation wells can be classified into three groups based on drawdown response characteristics as shown in Table 6-2: 1) group one wells V16D, T16D and S12D2 completed in

Table 6-1. Summary of Configurations of Phase Two Multiple Well Aquifer Testing

TEST No. (date)	PUMPING WELL	SCREEN DEPTH (ft)	FRACT. AQUIFER*	PUMPING RATE (gpm)	PUMPING WELL DRAWDOWN (ft)	DURATION (min)	OBSERVATION WELLS**	
							deep wells	shallow wells
9-22-89	Q17D	76-79	E	6	24.6	1440	V16D, T16D, D19D, S12D1, S12D2	V16S, P17S, N18S
4-4-90	T16D	65-69	E	6	27.9	303	V16D, Q17D, D19D, S12D1, S12D2	V16S, P17S, N18S
4-11-90	Q17D	76-79	E	6	24	2910	V16D, T16D	none
6-3-90	V16D	65-67.5	E	28	>15	428	T16D, Q17D, Q16D, U3D, D19D, J16D, S12D1, S12D2	V16S, P17S, N18S, T8S, H12S
8-14-90	J16D	65-67.5	W	15	29	373	D19D, U3D, S12D2, V16D, Q17D, T16D, Q16D, S12D1	no response on any wells
8-17-90	D19D	137-139	W	12	47	607	J16D, U3D, S12D2, V16D, Q17D, T16D, Q16D, S12D1	
3-8-91	U3D	81-83	W	0.5	43	181	J16D, D19D, S12D2 (no response on other wells)	

* E = E fractured aquifer; W = W fractured aquifer

** wells for which drawdown was measured during the tests.

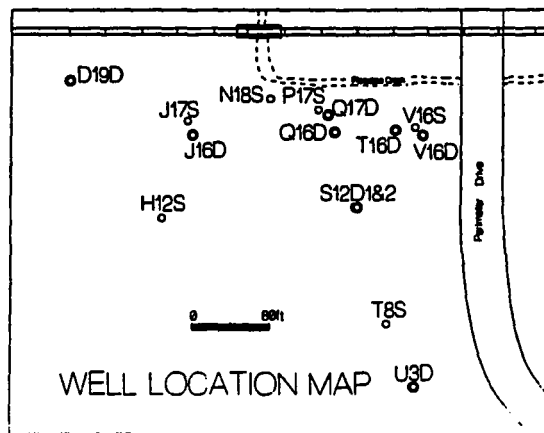
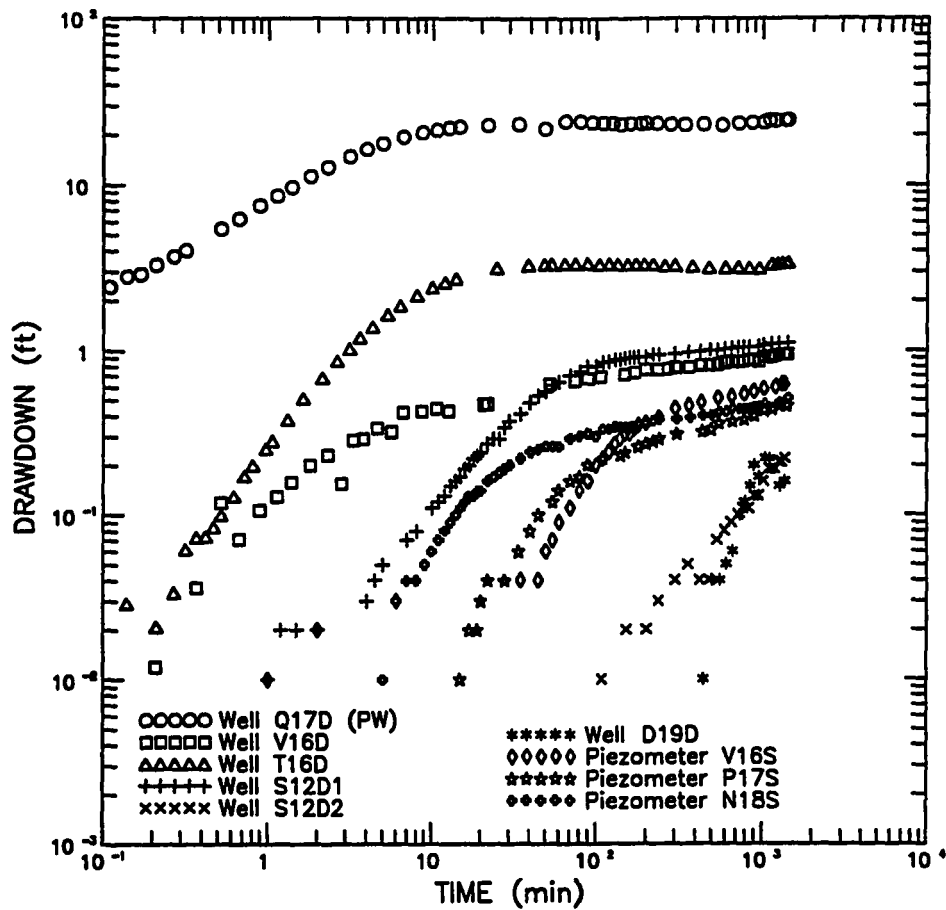


Figure 6-1. Log-log plots of drawdown vs. time for all the wells during aquifer test 9-22-89 and well locations

the E fracture had rapid response to the pumping and the largest final drawdown; 2) group two wells S12D2 and D19D in the W fracture had delayed response and the smallest final drawdown; and 3) group three shallow alluvial aquifer piezometers V16S, P17S and N18S had intermediate response time and intermediate final drawdown.

Table 6-2. Observation Well Responses of Aquifer Test 9-22-89

Aquifer	E Fracture Zone			W Fracture Zone		Shallow Alluvial Aquifer		
	V16D	T16D	S12D1	S12D2	D19D	V16S	P17S	N18S
Observation Well	V16D	T16D	S12D1	S12D2	D19D	V16S	P17S	N18S
Radius (ft)	100	70	100	100	275	90	12	62
Response Time(min)*	0.21	0.02	1	109	445	1	15	5
Final Drawdown(ft)	0.94	3.4	1.1	0.22	0.16	0.62	0.46	0.51

* Time until having a measurable drawdown (0.01 ft) from beginning of the test

Pumping discharge (Q) of test 9-22-89 was regulated by a 6 gpm constant discharge control valve. The Q value was held constantly throughout the test. Well Q16D in the E fracture and wells U3D and J16D in the W fracture were not yet constructed at the time of test 9-22-89.

The first group of wells was completed in the E fractured aquifer as was the pumping well. The log-log plot of drawdown in the pumping well Q17D shows a nearly straight line feature with a slope greater than 0.5 at the early stage of the test. The drawdown tends to stabilize after 10 minutes into the test with the plot following a nearly horizontal line (Figure 6-1). However, the drawdown plot of the pumping well may be affected considerably by the well loss. The slope of the log-log plot at the early time probably is not meaningful because the slope varies with different values of well loss.

The characteristics of drawdown responses in observation wells V16D, T16D and S12D1 are: 1) early responses follow a curve with a smaller slope than the Theis type curve; and 2) increases of drawdown in the wells appear to slow down and water levels tend to stabilize after the early part of the test (Figure 6-1). The drawdown responses in pumping well Q17D and observation wells V16D, T16D, and S12D1 show that: 1) the test is conducted in a confined aquifer; and 2) leakage from the aquitards occurs at early portion of the test and leakage occurs from the unpumped aquifer later in the test.

The leakage effect can be observed from responses of the wells completed in the shallow alluvial aquifer. The shallow wells had much quicker and greater responses than the wells in the W aquifer, indicating that the leakage from the shallow alluvial aquifer through the upper aquitard to the E fracture is significant. Water levels in the pumped E aquifer appear to stabilize about the same time when drawdown in the shallow aquifer starts. Wells D19D and S12D2, completed in the W fracture zones, show slower responses and smaller total drawdown than the shallow aquifer during the test. The drawdown versus time plots of the shallow wells and wells D19D and S12D2 are similar to the response of an unpumped aquifer in a multi-aquifer system (Neuman and Witherspoon, 1969b).

Multiple Well Aquifer Test 4-4-90

Aquifer test 4-4-90 also was conducted in the E fractured aquifer with pumping well T16D. The test duration was 303 minutes and discharge rate was constantly 6 gpm. All of the wells were measured for drawdown responses (Table 6-1).

The test data for the pumping well and all the observation wells are

presented as log-log drawdown versus time plots in Figure 6-2. The general water level responses are very similar to that observed in aquifer test 9-22-89, particularly for wells in the pumped aquifer (the E fracture zone). A summary of observation well responses is presented in Table 6-3. Again, the plot of drawdown data of the pumping well (T16D) may not be used for test analysis because of the well loss.

Table 6-3. Observation Well Responses of Aquifer Test 4-4-90

Aquifer	E Fracture Zone			Shallow Alluvial Aquifer			W Fracture Zone	
Observation Well	V16D	Q17D	S12D1	V16S	P17S	N18S	S12D2	D19D
Radius (ft)	30	70	89	20	80	130	89	345
Response Time (min)	0.02	0.02	0.5	22	17	3	84	NR*
Final Drawdown (ft)	1.64	4.55	1.74	0.33	0.2	0.24	0.18	NR

* NR = No responses were observed in the well

The drawdown responses in observation wells V16D, Q17D and S12D1 show a nearly straight line with a slope close to one. The water levels in the pumped aquifer (E fracture), as seen in pumping well and observation wells V16D and Q17D, tend to stabilize after 10 minutes into the test. The late drawdown responses of these wells indicate a confined aquifer condition with leakage from unpumped aquifers or possible recharge boundaries (Figure 6-2).

The early log-log drawdown plots of the observation wells completed in the pumped aquifer (V16D, Q17D and S12D1) show smaller slopes than that of Theis type curve, which probably indicates the effects of leakage from aquitards at the early stage of the test. The drawdown of wells V16D and Q17D stabilized concurrently with measured water level responses in the

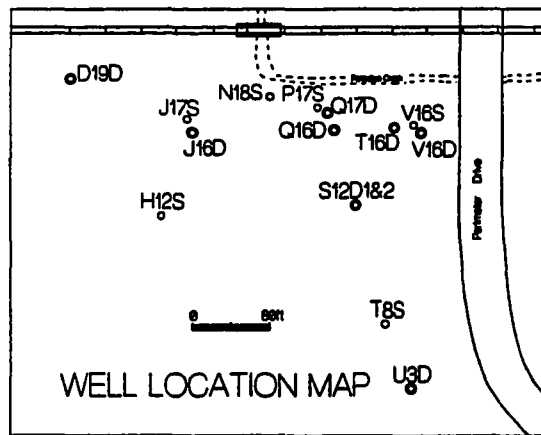
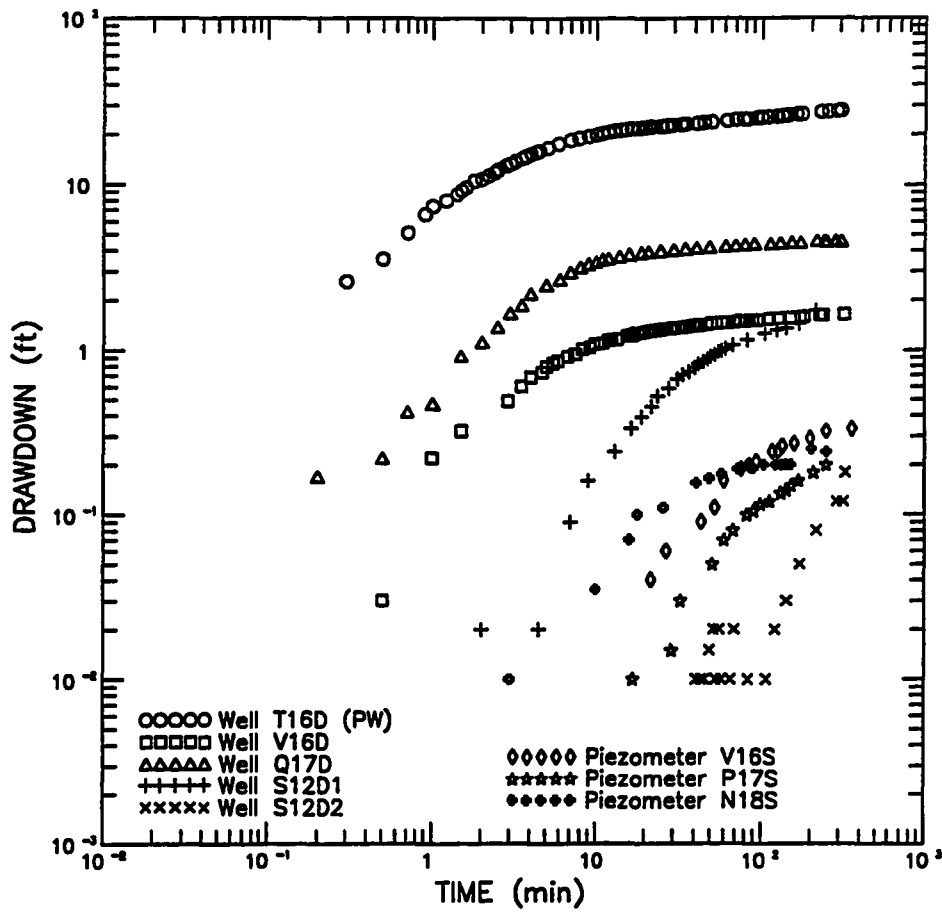


Figure 6-2. Log-log plots of drawdown vs. time for all the wells during aquifer test 4-4-90 and well locations

shallow aquifer. The results of this test clearly show that leakage occurs from the unpumped alluvial aquifer to the E fracture zone.

A slight drawdown response of the W fracture zone was observed only at well S12D2, that is 89 feet (27 meters) away from the pumping well. Well D19D at a distance of 345 feet (105 meters) from the pumping well had no response during the test. However, a measured drawdown response was observed in D19D during test 9-22-89 that also was conducted in the E aquifer with the same discharge rate. The possible reasons for different responses in well D19D during the two tests are that: 1) duration of test 4-4-90 is only 303 minutes, which was too short to obtain a measured drawdown in D19D; measured drawdown was not observed in D19D until 445 minutes into the test 9-22-89, and 2) distance from well D19D to the pumping well is 70 feet farther during test 4-4-90 compared to test 9-22-89.

Multiple Well Aquifer Test 4-11-90

Aquifer test 4-11-90 is a repeat of test 9-22-89 with an extended duration of 2910 minutes. Only two observation wells (V16D and T16D) completed in the pumped aquifer (E fracture zone) were monitored during the test because the test was designed originally for a two-well tracer test. Pumping discharge of the test was 6 gpm. Drawdown responses on two observation wells were collected only through pressure transducers and data logger (Table 6-1). Drawdown data in the pumping well (Q17D) were not collected because of a failure to install the transducer and lack of personnel.

Drawdown responses of two observation wells are presented in Table 6-4. The complete data records of drawdown vs. time are plotted on a log-log

scale in Figure 6-3.

Table 6-4. Observation Well Responses of Aquifer Test 4-11-90

Aquifer	E Fracture Zone		Shallow Alluvial Aquifer	W Fracture Zone
Observation Well	V16D	T16D	None of the shallow wells were monitored during the test	None of the wells completed in W fracture zone were monitored during the test
Radius (ft)	100	70		
Response Time (min)	1	1		
Final Drawdown (ft)	1.60	5.95		

The observed drawdown responses after the early time from test 4-11-90 are similar to that from test 9-22-89. However, the data from test 4-11-90 show significantly greater early slopes on log-log plots than the data from tests 9-22-89 and 4-4-90 (Figure 6-3). Because the data of test 4-11-90 were collected by pressure transducers, the early data may have considerable measurement error. Therefore, the early data from test 4-11-90 are not used for the aquifer test analysis.

Significant leakage effects on drawdown responses of the two observation wells occurred early in the test period (Figure 6-3). Slight decrease of drawdown was observed in both observation wells during the late stages of the test. There are two possible reasons for these drawdown disturbances: 1) high flow in Paradise Creek occurred late in the test because of heavy rainfall; higher stream flow may have decreased the final drawdown in both observation wells, and 2) pressure transducer measurement errors. The aquifer test analysis is not affected by drawdown disturbances late in test 4-11-90 because the error is relatively small compared with the final drawdown in the observation wells.

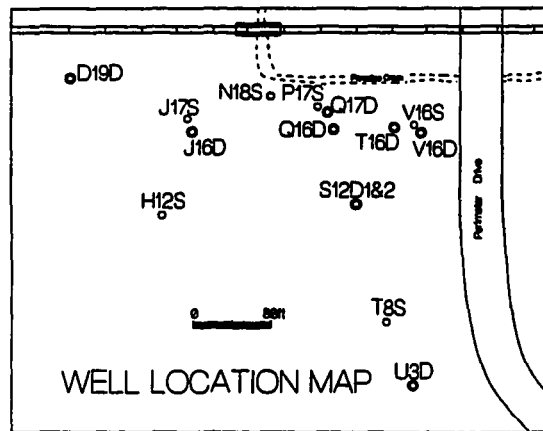
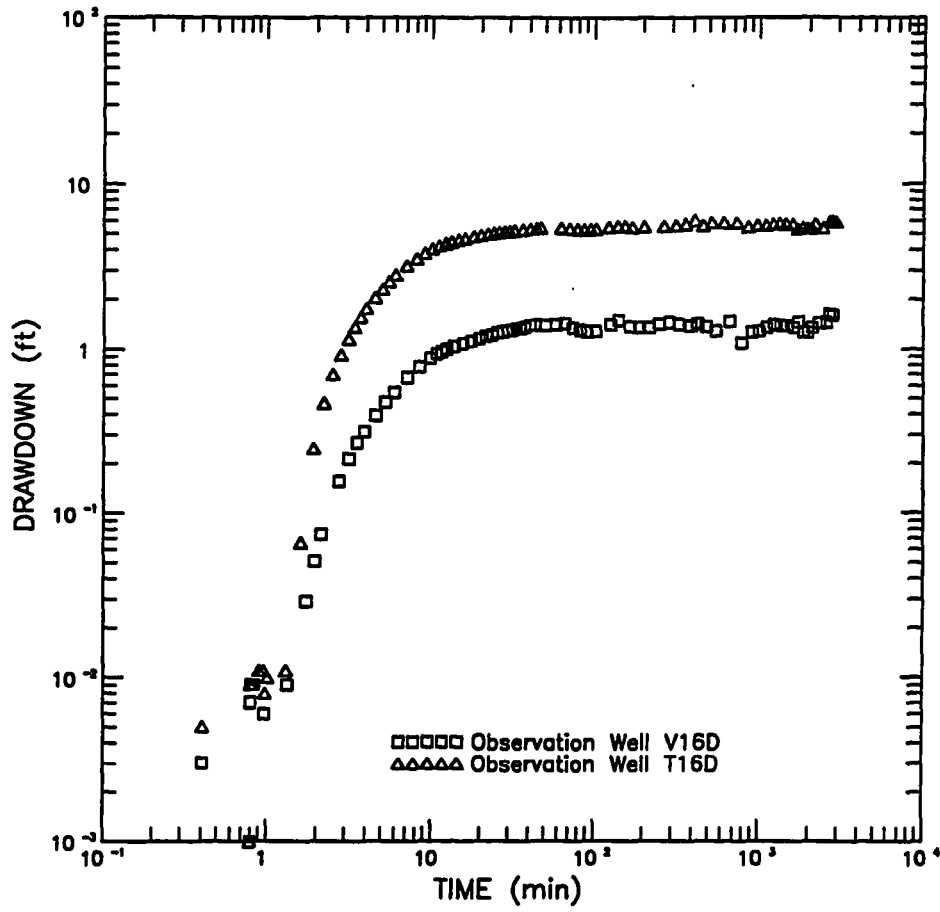


Figure 6-3. Log-log plots of drawdown vs. time for observation wells V16D and T16D during aquifer test 4-11-90 and well locations

Multiple Well Aquifer Test 6-3-90

Well V16D in the E fracture zone was pumped for 428 minutes during aquifer test 6-3-90. The discharge rate of the test was constantly 38 gpm (Table 6-1). Drawdown was measured in all of the observation wells. These data are summarized in Table 6-5.

Table 6-5. Observation Well Responses of Aquifer Test 6-3-90

Aquifer	E Fracture Zone			W Fracture Zone		Shallow Alluvial Aquifer					Open Borehole		
	T16D	Q17D	S12D1	D19D	S12D2	V16S	P17S	N18S	T8S	H12S	Q16D	J16D	U3D
Radius (ft)	30	100	100	375	100	10	110	160	220	280	92	235	260
Response Time (min)	<.1	<.3	<2	5	<18	<25	1	<2	29	21	.3	<32	99
Final Drawdown (ft)	13.5	8.4	16.3	.33	.48	1.45	0.57	0.65	0.12	.21	2.7	0.5	0.1

The log-log drawdown plots of all the basalt wells and two representative shallow wells are presented in Figure 6-4. The pumping well data are missing because of data logger problems; all observation well data are hand measurements.

The wells in the pumped E aquifer (T16D, Q17D and S12D1) responded quickly to the pumping of V16D. Drawdown at the end of the test ranged from 8.4 to 16.3 feet. Several common characteristics may be seen in the log-log drawdown plots of these wells (Figure 6-4): 1) a nearly straight line with an approximate unit slope at the early stage of the test ($t < 10$ minutes), 2) an intermediate portion of the plot that may be matched with the Theis type curve, and 3) the nearly zero slope of log drawdown vs. log time at the later times.

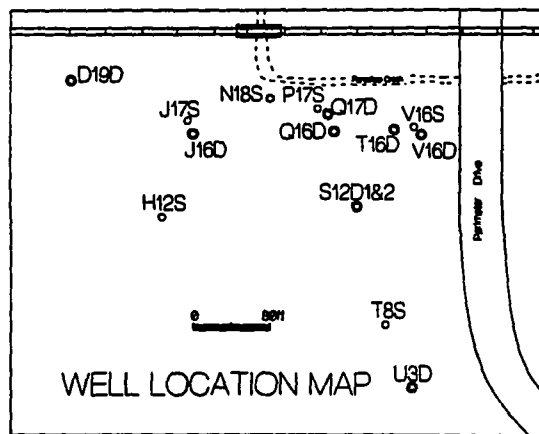
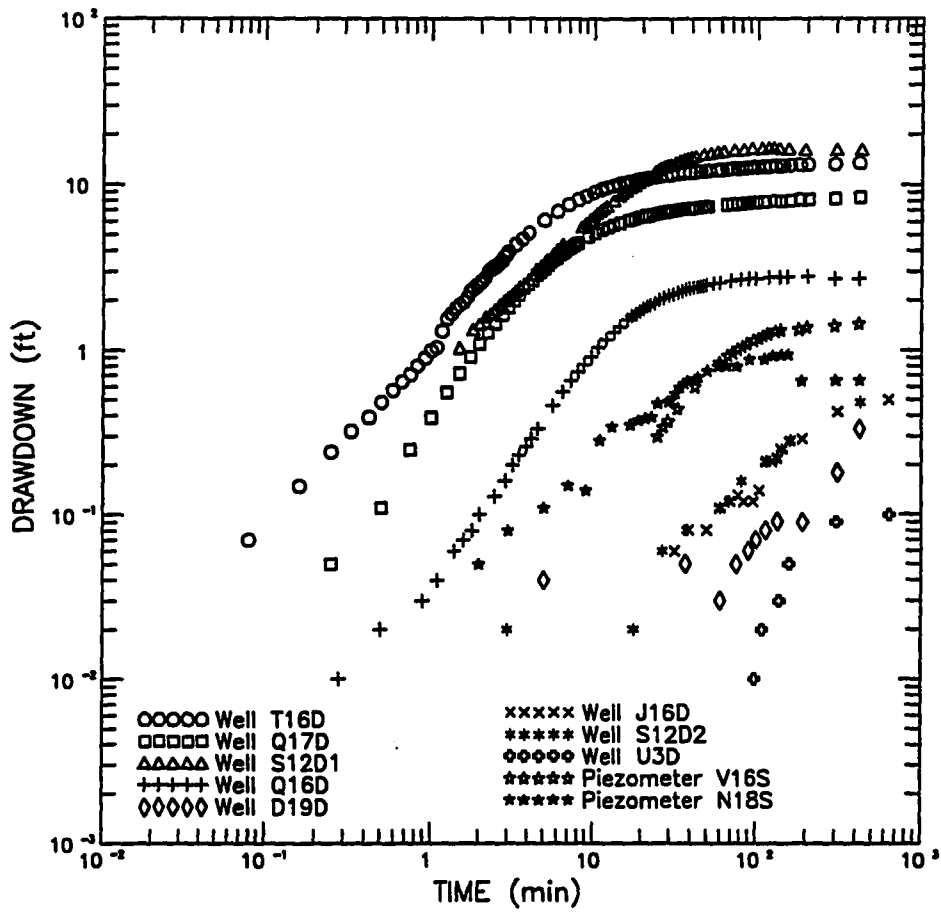


Figure 6-4. Log-log plots of drawdown vs. time for observation wells during aquifer test 6-3-90 and well locations

The early responses of the wells in the pumped aquifer probably were affected by leakage from aquitards. The leakage from the unpumped alluvial aquifer obviously controls the late drawdown features. The late drawdown data also may have been affected by possible recharge boundaries. However, no geological structures have been identified near the UIGRS. The channel of Paradise Creek only cuts through the shallow alluvial aquifer and thus can not be considered as a lateral boundary of the fractured basalt aquifer.

The shallow wells in the shallow alluvial aquifer had delayed drawdown, similar to the previous tests. The decrease in drawdown in well N18S was very likely caused by the infiltration from rainfall that occurred during the test (Figure 6-4).

Three new deep wells (Q16D, U3D and J16D) were drilled just before the test 6-3-90 was conducted. Water levels in these wells were monitored during the test (Figure 6-4). However, data interpretation is difficult because the wells were not cased or completed opposite any particular fractured aquifer at the time of the test.

The observed data from well Q16D represent the combined response of the pumped aquifer (E fracture) and the unpumped W fracture because the open bore of Q16D intercepts both fractures. The log drawdown vs. log time plot of well Q16D has an identical pattern to that of the other observation wells completed in the pumped aquifer but has a much smaller magnitude of drawdown (Figure 6-4).

Well J16D intercepts only the W fracture because the E fracture does not extend to the southwestern portion of the UIGRS. The shallow alluvial aquifer is sealed by surface protective casing with bentonite grouting to a depth of 20 feet (6 meters). Therefore, drawdown response of well J16D is

basically identical to that of wells completed in the W fracture zone (D19D and S12D2) though J16D was not cased in the basalt at the time of the test. The static water level data before the aquifer test also show that wells J16D, D19D and S12D2 belong to the same group; water levels of these wells are at a very similar elevations and are considerably different from those of the wells completed in the E fracture and other new well bores.

The drawdown observed in well U3D is a combined response of the W fracture and fractures in the upper portion of the Lolo flow. The lag time of delayed drawdown in U3D is greater and the final drawdown is smaller than that in the W fracture probably because of the leakage from the upper fractures through the well bore.

Multiple Well Aquifer Test 8-14-90

Aquifer test 8-14-90 was conducted after new wells Q16D, J16D and U3D were completed with PVC casing and screened opposite only one of the fractured aquifers. Well Q16D was perforated at the E fracture zone, whereas the wells J16D and U3D were screened at the W fracture zone (Appendix A).

All the wells were monitored for drawdown responses when well J16D in W aquifer was pumped for 373 minutes during test 8-14-90. Discharge rate of the test is 15 gpm. The test was stopped when drawdown in the pumping well reached a maximum value of 29 feet (8.8 meters) near the pump installation depth (Table 6-1).

A summary of observation responses is tabulated in Table 6-6. Drawdown in the observation wells completed in the pumped aquifer (W fracture) ranged from 14.2 to 24.4 feet at the end of the test, considerably greater than that in the wells of the unpumped E fracture.

Unlike previous tests, there is no significant difference of response (lag) time to the pumping of J16D between the two groups of wells. The observation wells in the pumped aquifer (D19D, U3D and S12D2) had a measured drawdown almost at the same time into the test. Distances from the pumping well to these wells did not affect either the lag time of response or final drawdown. Interestingly enough, well U3D which is farthest from the pumping well had the greatest final drawdown (24.4 ft) during the test.

Table 6-6. Observation Well Responses of Aquifer Test 8-14-90

Aquifer	W Fracture Zone			E Fracture Zone					Shallow Aquifer
Obs. Well	D19D	U3D	S12D2	V16D	Q17D	T16D	Q16D	S12D1	All Wells
Radius (ft)	144	303	181	235	142	210	150	181	NO RESPONSE
Response Time(min)	3.7	3	3.4	30	5	<24	3	6	
Final Drawdown(ft)	14.2	24.4	16.6	0.12	0.26	0.6	0.27	1.4	

Drawdown of the wells completed in the unpumped E fracture (V16D, Q17D, T16D, Q16D and S12D1) ranged from 0.1 to 1.4 feet at the end of the test. These wells probably responded to the pumping of J16D because of leakage through the lower aquitard. Well S12D1 had a considerably greater final drawdown than the remainder of wells in the E fracture, that probably indicates more significant leakage occurring near S12D1.

The log drawdowns vs. log time of all the wells during test 8-14-90 are graphed in Figure 6-5. The pumping well (J16D) drawdown data are presented in the graph for purpose of comparison. The log-log drawdown plot of the pumping well can not be analyzed because of significant well

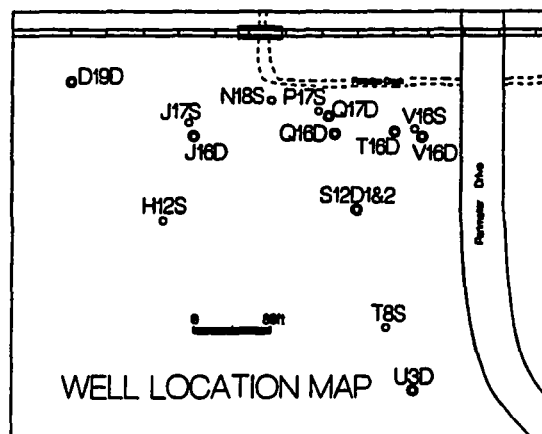
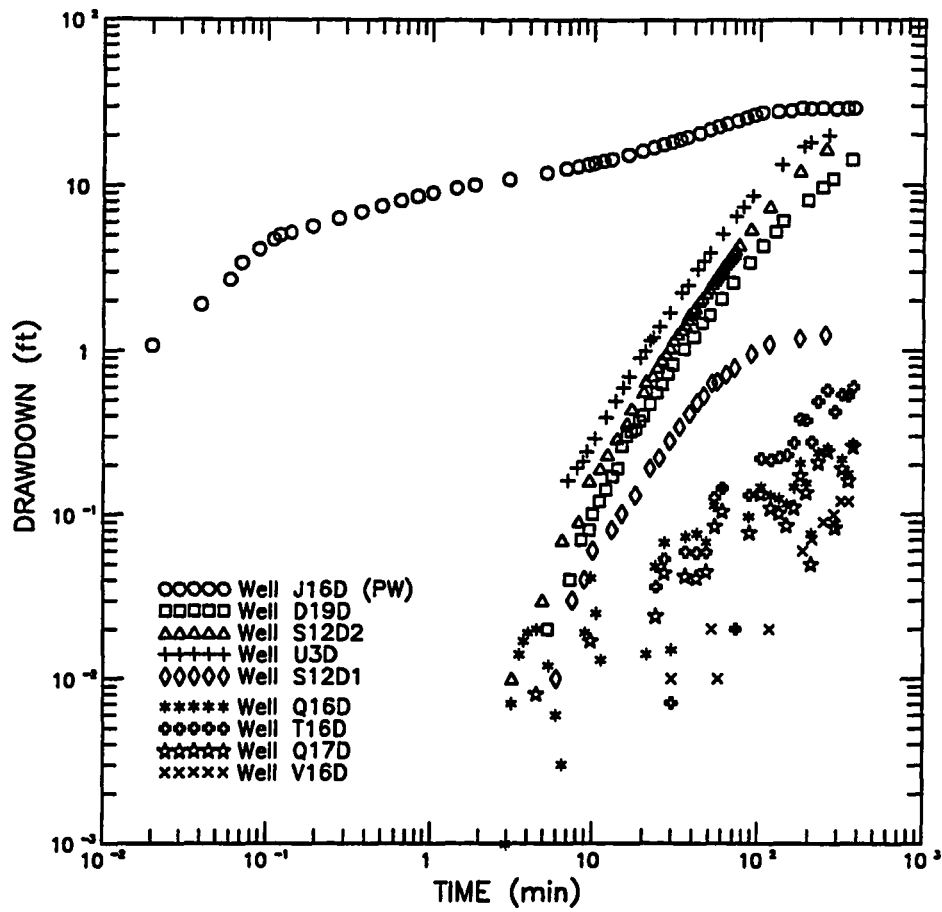


Figure 6-5. Log-log plots of drawdown vs. time for all the wells during aquifer test 8-14-90 and well locations

loss.

The three observation wells (D19D, U3D and S12D2) in the pumped aquifer (W fracture) have a very similar drawdown response pattern that is significantly different than that of the pumping well (Figure 6-5). The common features of the drawdown responses for these wells are: 1) responses to the pumping of J16D have approximately the same time lag even though the distances of these wells to the pumping well are remarkably different, 2) the plot of log drawdown vs. log time form a nearly straight line with a slope greater than one during most of the test, and 3) the drawdown continuously increases at the later times of the test; the increasing rate may be a little smaller than that in the early stages, but is far from stabilized.

Drawdown was observed in wells completed in the E fracture (V16D, T16D, Q17D, and Q16D). Among these wells, only Q16D shows a continuously increasing drawdown response. The factors that caused changes in drawdown several times in the remainder of the wells during the test are unknown (Figure 6-5).

The shallow wells constructed in the shallow alluvial aquifer did not respond at all during the aquifer test. This indicates a lack of direct hydraulic connection between the W fracture and the shallow alluvial aquifer. The leaky connection between the two fracture zones had been observed, but it was considerably less significant than the leakage from the upper aquifer to the E fracture zone.

Multiple Well Aquifer Test 8-17-90

Aquifer test 8-17-90 was conducted with pumping of well D19D in the W fractured aquifer. Discharge rate of the test was 12 gpm with a pumping

duration of 607 minutes. All the wells were measured for drawdown responses. The test was stopped when a maximum drawdown (pump installation depth) in the pumping well was reached (Table 6-1).

The observation wells were monitored only with pressure transducers during test 8-17-90 because of lack of personnel. As discussed in chapter V, the early data record may have a great relative error because of the transducer measurements, and may not be used in the aquifer test analysis. The measurement error occurs also in the late data record but may or may not affect the data analysis based upon the magnitude of drawdown in the wells.

Observation wells (J16D, U3D and S12D) completed in the pumped aquifer (W fracture) had a large final drawdown ranging from 14.2 to 17.2 feet (Table 6-7). These wells responded to the pumping of well D19D in less than one minute; responses were considerably quicker than that of test 8-14-90. However, the lag time may not be accurate because of the transducer measurement error.

Table 6-7. Observation Well Responses of Aquifer Test 8-17-90

Aquifer	W Fracture Zone			E Fracture Zone					Shallow Aquifer
Obs. Well	J16D	U3D	S12D2	V16D	Q17D	T16D	Q16D	S12D1	All Wells
Radius (ft)	144	441	325	375	275	345	280	325	NO RESPONSE
Response Time(min)	<0.6	<0.6	<0.6	NR*	Drawdown is too small to be measured precisely by pressure transducers			2	
Final Drawdown(ft)	17.2	15.4	14.2					1.2	

* NR = No response during the test

Most of the wells completed in the unpumped E fracture zone (Q17D, T16D and Q16D) had drawdown responses less than 0.1 feet; thus, the data record probably is meaningless because of the great relative error caused by the transducers. Drawdown measured in S12D1 at the end of the test was 1.2 feet; this value is similar in magnitude to that in the previous test 8-14-90. No drawdown was measured in well V16D.

The log-log drawdown data plots of test 8-17-90 are presented in Figure 6-6. The plot of log drawdown vs. log time of observation well J16D in the pumped aquifer shows a straight line pattern with nearly a unit slope. Drawdown in three observation wells completed in the pumped W aquifer (J16D, U3D and S12D2) was far from stable though a decrease in the slope of the drawdown curve was observed at the end of the test (Figure 6-6).

The drawdown data from observation wells U3D and S12D2 had an odd fluctuation pattern. The observed drawdown increased, then decreased rapidly after 10 minutes into the test and finally increased again. Similar fluctuation patterns were observed in the E aquifer wells but not at pumping well D19D and well J16D completed in the W aquifer (Figure 6-6). This strange disturbance of drawdown might be caused by several possible factors: 1) pressure transducer irregularities, 2) changes in data logger working conditions, and 3) unknown intrinsic complexity of the fractured basalt system. The first reason is unlikely; it is unlikely that six of eight transducers connected with two data loggers would fail at the same time and show the same record disturbance at approximately the same time. The second factor is possible; variations of temperature and humidity in the field might have affected electronic signal transference in certain channels of the data logger. The third possibility needs to be proven

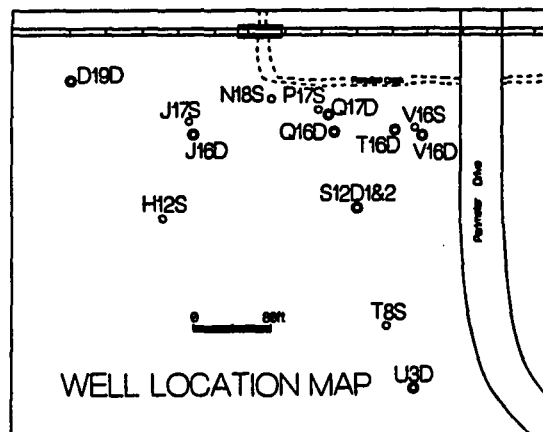
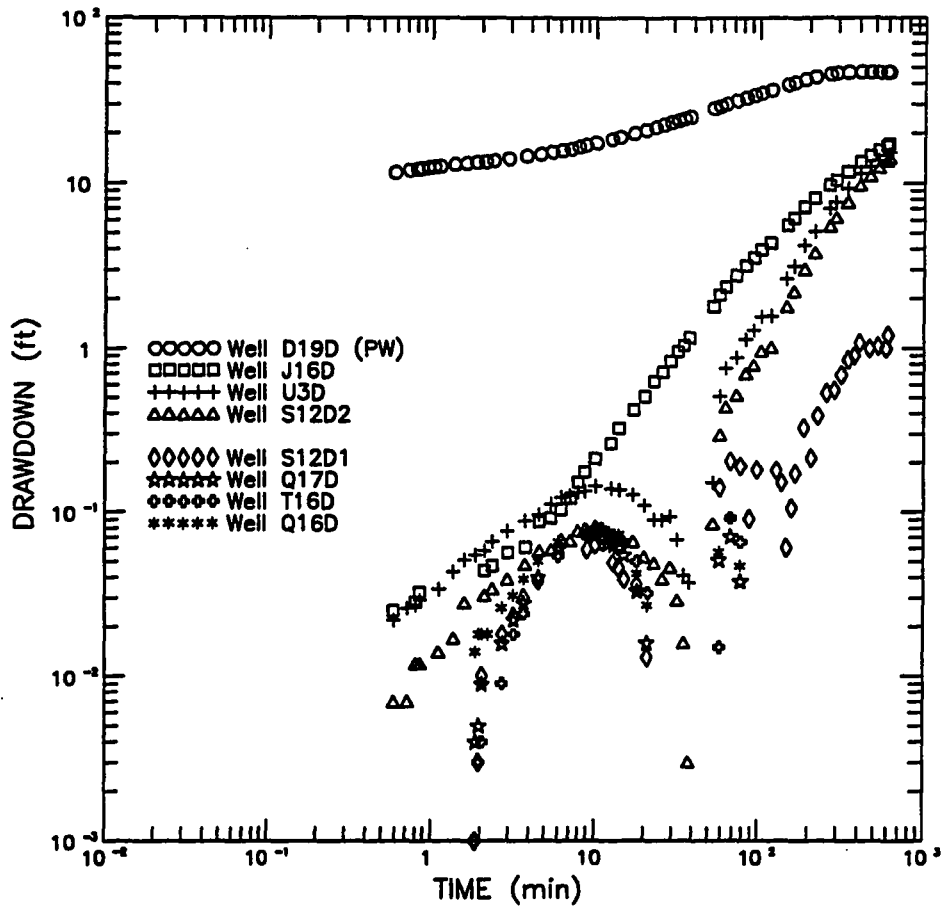


Figure 6-6. Log-log plots of drawdown vs. time for all the wells during aquifer test 8-17-90 and well locations

through more information and detailed study.

The responses of the unpumped E fracture wells (T16D, Q17D, Q16D and S12D1) again indicate that leakage exists between the two major fractured aquifers. Well V16D did not respond during the test 8-17-90 because of the great distance to the pumping well. The shallow wells in the upper alluvial aquifer did not respond during the entire test period.

Multiple Well Aquifer Test 3-8-91

Aquifer test 3-8-91 is special because it was conducted by pumping a low-yield well at 0.5 gpm. The test lasted only 181 minutes because drawdown exceeded the available drawdown at the pumping well. Only three observation wells constructed in the pumping aquifer (W fracture) responded during the test.

A summary of the observation data is presented in Table 6-8. Drawdown of the three observation wells (J16D, D19D and S12D2) completed in the pumped aquifer (W fracture) ranged from 0.4 to 1.2 feet. Significant differences of response lag time for the three wells relative to their respective distances to the pumping well U3D were observed during the test. As with the previous tests conducted in the W aquifer (8-14-90 and 8-17-90), the response lag time of these wells is not related to the distance to the pumping well. However, there is a direct relation between lag time and final drawdown in the observation wells; larger final drawdown occurred in wells with earlier responses.

The observation well data are graphed as log-log plots in Figure 6-7. The log drawdown responses of three observation wells (J16D, D19D and S12D2) show a nearly straight line pattern which is very similar to that of the tests 8-14-90 and 8-17-90. The straight line slopes of different

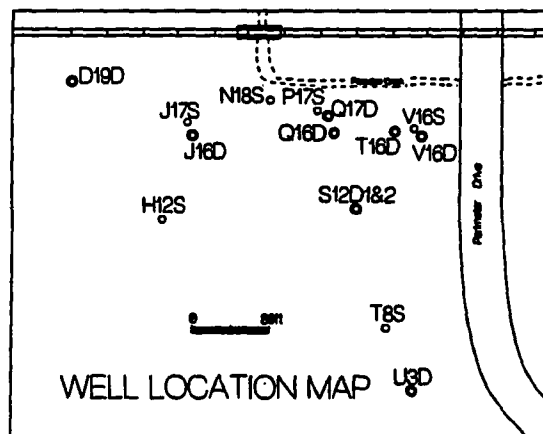
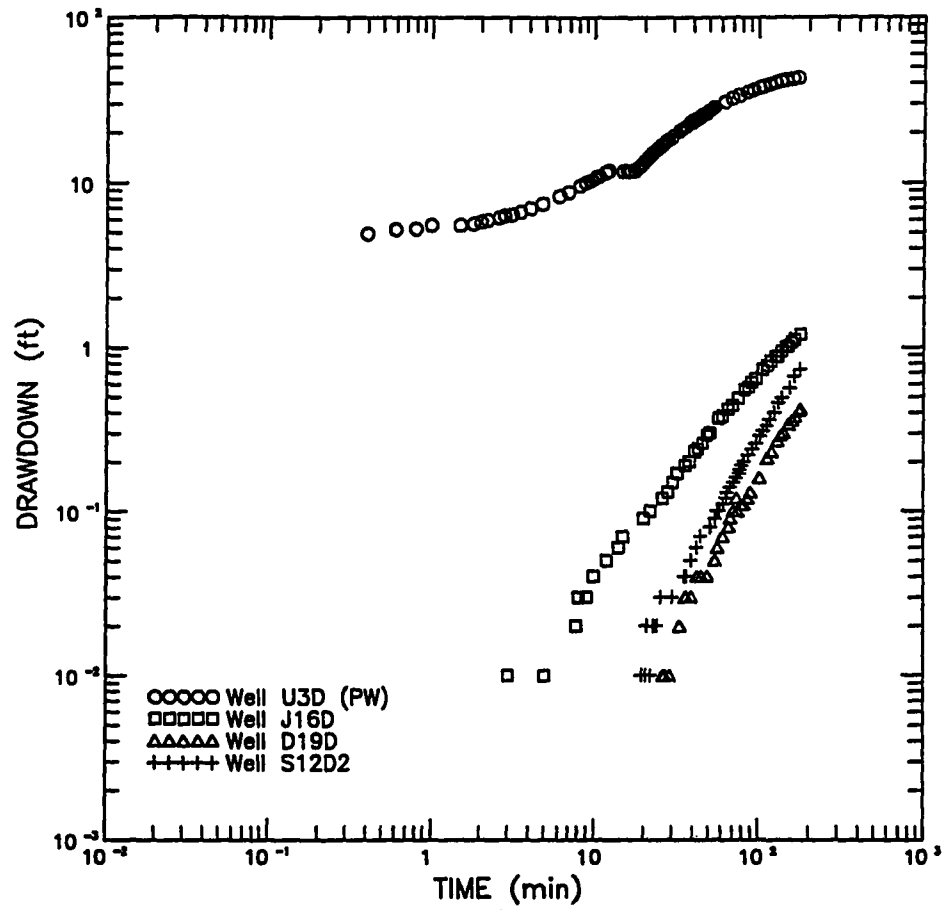


Figure 6-7. Log-log plots of drawdown vs. time for all the wells during aquifer test 3-8-91 and well locations

observation wells are close but not exactly the same; all slopes are greater than one (Figure 6-7).

Table 6-8. Observation Well Responses of Aquifer Test 3-8-91

Aquifer	W Fracture Zone			E Fracture Zone					Shallow Aquifer
Obs. Well	J16D	D19D	S12D2	V16D	Q17D	T16D	Q16D	S12D1	All Wells
Radius (ft)	303	441	155	260	255	262	235	155	NO RESPONSE
Response Time(min)	3	26	19.5	NO RESPONSE					
Final Drawdown(ft)	1.2	0.42	0.73						

Water levels in the shallow alluvial aquifer did not respond during test 3-8-90. Wells completed in the E fracture zone had shown slight drawdown by the end of the test. These drawdown data are not presented in Table 6-8 because static water level fluctuations in the E aquifer wells caused by barometric pressure change and rainfall infiltration could be greater than the drawdown responses due to pumping during the test.

Slug Tests

Slug tests were conducted in each of the nine deep wells at the UIGRS. The tests were performed to estimate the hydraulic conducting properties of the fractured aquifer in the immediate vicinity of each of the wells. The slug test data are presented in Appendix B (Table B-8). A complete analysis of the data is presented in the following chapter.

Summary

- 1) The second phase multiple well aquifer tests conducted in the UIGRS can be classified into two groups according to the pumped aquifer. Tests 9-22-89, 4-4-90, 4-11-90 and 6-3-90 were conducted by pumping from the E fractured basalt aquifer. Tests 8-14-90, 8-17-90 and 3-8-91 were conducted using pumping wells completed in the W aquifer.
- 2) Observation wells constructed in the pumped aquifer had drawdown responses that can be utilized for aquifer hydraulic characterization. The wells installed in the unpumped fractured basalt aquifer generally responded with certain time delays and had small final drawdowns. The drawdown in the unpumped aquifer shows a hydraulic connection between the two fractured basalt aquifers.
- 3) The shallow alluvial aquifer only responded to pumping from the E aquifer. The shallow alluvial aquifer is hydraulically interconnected to the E aquifer.

Applicability of Alternative Analytical Models for Multiple Well Aquifer Tests

The purpose of this section is to select appropriate alternative analytical models and evaluate the applicability of these models to analyze the data from phase two multiple well aquifer tests in the UIGRS. Selection of the analytical models is based on the hydrogeological model proposed in chapter III. The selected alternative models are evaluated based on: 1) validity of the assumptions of each model, and 2) similarity between hydraulic test data and theoretical type curves.

Selection of Analytical Models

As discussed in chapter III, the conceptual model of the aquifer system in the Wanapum basalt at the UIGRS is described as follows: 1) the system is fractured rather than porous, 2) the system includes two major aquifers (E and W fracture zones) and at least two aquitards, 3) the E fractured aquifer has direct hydraulic connection with an overlying porous aquifer, and 4) a limited hydraulic interconnection exists between the two fractured aquifers.

One essential question is whether or not the fractured aquifers at the UIGRS behave like porous media. According to Long *et al.* (1982), fracture systems behave more like porous media when larger sample sizes with proper fracture geometry (high fracture density, constant apertures and distributed orientations) are tested. Also, drawdown response patterns predicted by porous media analytical models should be observed if the fracture systems can be considered as porous media. Therefore, three criteria are used to determine behavior of the fractured aquifers at the UIGRS: 1) the geometry of the fracture system (density, apertures and orientations), 2) the test size or scale in comparison with the REV of the fractured aquifer, and 3) patterns of drawdown responses observed during the aquifer tests.

The geometry of the fracture system at the UIGRS is not completely known. However, highly developed intraflow structures were observed from outcrops of the Lolo basalt flow west of the UIGRS. The fracture density in these structural features is believed to be high. Many of the drawdown responses observed during the second phase hydraulic testing, especially data from the tests conducted in the E aquifer, show drawdown patterns similar to porous media models after very short time periods. Generally,

analytical models for porous media are believed to be applicable to analyze data from multiple well aquifer tests at the UIGRS, particularly from the E fracture zone.

Many analytical models applied in fractured media are discussed in chapter IV. Among these models, the double-porosity models probably are applicable at the UIGRS. The major fracture zones that form the two fractured aquifers (E and W) consist of fractures, fine joints and fissures. The fractures are believed to provide secondary porosity, and the joints and fissures form primary porosity within the aquifers. Single fracture models including linear flow models were not selected to analyze the test data at the UIGRS because: 1) basic assumptions such as single plane fracture, infinite hydraulic conductivity in the fracture, and impermeable upper and lower boundaries are not applicable; 2) pumping wells are not constructed along the fracture plane; 3) the fracture length and pumping well locations related to the fracture length are unknown; and 4) the unique drawdown response with a pumping well in a single fracture yielding a straight line with half unit slope on log-log plot, was not observed at the early or late times during any of the tests.

The Moench double-porosity with fracture skin model (Moench, 1984) is applied to analyze the test data in the following chapter. The Moench model was selected based on two reasons: 1) the model is representative for most double-porosity models; it can simulate either transient or pseudo-steady state flow by adjusting the value of fracture skin S_F and can be reduced to the general double-porosity models by allowing $S_F = 0$, and 2) the model is more widely applied than the other double-porosity models; type curves and computer programs for solutions are available as commercial

software.

Several porous medium analytical models were chosen for data analysis of the phase two multiple well hydraulic tests conducted at the UIGRS. The leaky aquifer models by Hantush and Jacob (1955), modified Hantush (1960), and Neuman and Witherspoon (1969a; 1972) are likely to be applicable based on the conceptual model and analysis of drawdown responses. The Theis (1935) model probably is not applicable to a multiple aquifer system such as found at the UIGRS. However, the Theis curve match is presented for purposes of comparison.

Analytical Model Evaluation

Many of the analytical models are valid tools for aquifer test analysis; however, interpretation of the test results must consider the extent to which underlying assumptions are violated. All of the assumptions for each analytical model are not completely satisfied at the UIGRS because of the complexity of the aquifer system.

Theis Model

The Theis model is evaluated because this model is the basis of many analytical porous medium models. The Theis model is applied widely for analysis of aquifer tests in both porous and fractured aquifer systems even though the underlying assumptions are not fully met. The purposes of the Theis model application usually are: 1) to identify aquifer hydrogeological conditions such as leakage, double-porosity, delayed yield and boundaries based on the data deviation from the type curve, and 2) to estimate aquifer parameters if Theis assumptions are applicable.

Hantush Leaky Aquifer Model (r/B solution)

The Hantush leaky aquifer model (leaky without storage model) is an analytical solution for transient ground water flow to a pumping well for a leaky aquifer system where the aquitard does not yield water from storage, and all leakage comes from the non-pumped aquifer (Hantush and Jacob, 1955). The model is described by the Hantush well function $W(u, r/B)$ and dimensionless leaky parameter r/B . Solutions are tabulated and graphed as type curves that have been used widely to characterize leaky aquifer systems.

The two basic assumptions of the model, in addition to the Theis assumptions, are: 1) leakage is proportional to the water head drop across the aquitard and 2) the hydraulic head in the unpumped aquifer remains constant. The first assumption requires that no water is yielded from storage in the aquitard; therefore the specific storage of the aquitard is assumed to be zero. The second assumption requires that the storativity of the unpumped aquifer is infinite.

These two assumptions generally are not fully satisfied for the aquifer system at the UIGRS. Water yielded from aquitards to the E and W fractured aquifers may be significant, especially in the early stages of the aquifer tests. Also, the hydraulic heads of the unpumped aquifers (primarily the shallow alluvial aquifer) did not remain constant throughout the tests.

Neuman and Witherspoon (1969b) evaluate the applicability of two essential assumptions by Hantush and Jacob (1955). According to Neuman and Witherspoon (1969b, page 822), for a multiple leaky aquifer system, most of the early leakage is derived from the aquitard. As time increases, more and more leakage is contributed by the unpumped aquifer, and the relative

amount of water that comes from storage in the aquitard diminishes. By the time drawdowns become constant, all of the leakage is supplied by the unpumped aquifer. The aquitard merely acts as a conduit for flow from the unpumped aquifer to the pumped aquifer. At large times, the storage capacity of the aquitard has no influence on the behavior of the system; therefore, the Hantush leaky aquifer solution (Hantush and Jacob, 1955) is applicable.

The leakage to the E fractured aquifer mainly occurs in two ways when an E aquifer well is tested: 1) from storage in the aquitards, and 2) from leakage from the unpumped shallow alluvial aquifer through the upper aquitard and, to lesser extent, from the W fractured aquifer. The first portion of the leakage (from storage in the aquitards) occurs during the early time of the test; the second portion is significant at the late time. Drawdown responses in the pumping well and the observation wells completed in the E aquifer appear to stabilize within 30 minutes during all tests conducted in the E aquifer. According to the above conclusions by Neuman and Witherspoon (1969b), the violation of the assumption of no storage in the aquitards will not affect the analysis of late time data from the tests conducted in the E aquifer.

The assumption of no drawdown in the unpumped aquifer is not valid during any time of any aquifer testing at the UIGRS. However, the violation of this assumption may not be significant for tests conducted in the E fractured aquifer. Drawdown measured in the unpumped alluvial aquifer generally is small (< 1 foot in most tests); the resultant change in vertical hydraulic gradient is insignificant.

In summary, the Hantush leaky aquifer model (r/B solution, Hantush and Jacob, 1955) may be applicable to data (late time) analysis of aquifer

tests conducted in the E fractured aquifer at the UIGRS. The early data of the tests conducted in the E aquifer and the aquifer tests conducted in the W aquifer can not be analyzed by the Hantush leaky aquifer model.

Modified Hantush Leaky Aquifer Model

Hantush (1960) modified his leaky aquifer solution by considering storage from aquitards. The solution, known as the leaky with storage model, has two forms that are used for small and large values of time respectively. The small time solution (β solution), described by the modified Hantush well function $H(u, \beta)$ and dimensionless parameter β , is evaluated in this section.

The modified Hantush model (β solution) is developed based on the assumption that unpumped aquifers have no impact on the solution (infinitely thick aquitards). This assumption is applicable at small values of time in most confined aquifer systems. Neuman and Witherspoon (1969b, page 823) state that the water level behavior in the pumped aquifer and aquitard is not affected by conditions in the unpumped aquifer as long as the small time criterion is satisfied.

Hantush (1960) suggests that his small value of time solution is valid when values of time are smaller than both values of $b'S'/10K'$ and $b''S''/10K''$; where b' , S' , and K' are thickness, storativity and vertical hydraulic conductivity of the overlying aquitard, b'' , S'' , and K'' are the same parameters of the underlying aquitard. Neuman and Witherspoon (1969b) indicate that the solution is good over a broader time span than that stated by Hantush. They state that Hantush's time criterion for validity of the small time solution is conservative.

In general, the modified Hantush leaky aquifer model (β solution) is

applicable to analysis of the early data (small value of time) from the aquifer tests conducted in both E and W aquifers at the UIGRS. The model may not be applied for analysis of the late data from tests conducted in the E aquifer because significant leakage occurs from the unpumped alluvial aquifer. The leakage derived from the aquitards to the W aquifer is more significant relative to leakage from the unpumped aquifer (E fracture) because the W aquifer has no direct hydraulic connection with the alluvial aquifer. Therefore, the modified Hantush solution is applicable to longer time periods for analysis of aquifer tests conducted in the W aquifer.

Neuman and Witherspoon Leaky Aquifer Model

Neuman and Witherspoon (1969a) developed an analytical solution for transient ground water flow to wells in a two-aquifer leaky system where both storage in the aquitard(s) and drawdown in the unpumped aquifer are considered. The two basic assumptions of Hantush's leaky aquifer model are eliminated in the Neuman and Witherspoon model. Thus, the model is applicable over a wider range of hydrogeological conditions.

Neuman and Witherspoon's solution is expressed in terms of five dimensionless parameters (β_{11} , β_{21} , r/B_{11} , r/B_{21} , and t_{D1}) that describe the aquitard properties with reference to proportions of the pumped and unpumped aquifers. This solution has not been applied widely because of the difficulty in attaining a solution with five dimensionless parameters.

The Neuman and Witherspoon leaky aquifer solution is more applicable to the analysis of aquifer tests from the UIGRS than either the Hantush or modified Hantush leaky aquifer models in term of validity of the assumptions. However, application of Neuman and Witherspoon's model is not practical because of the large number of dimensionless parameters. Curve

matching software has not been developed for the Neuman and Witherspoon method.

Neuman and Witherspoon (1969b) evaluate the applicability of the modified Hantush model (β solution) by comparison to their leaky aquifer model (Neuman and Witherspoon, 1969a). They conclude that the results from the two solutions are identical at small time values ($t < b'S'/10K'$ or $t < b'S''/10K''$). The physical explanation of this conclusion is obvious; at the early test time, leakage derived from an unpumped aquifer is negligible. The aquitard therefore can be considered to have an infinite thickness.

The modified Hantush leaky aquifer model is applicable as long as leakage is derived primarily from storage in the aquitard. When the vertical hydraulic conductivity of the aquitard is low and aquitard thickness and storativity are relatively high, the model can be applied for relatively large time intervals. For the aquifer tests conducted in the W fractured aquifer at the UIGRS, leakage from the unpumped aquifer is insignificant because there is no drawdown in the alluvial aquifer and only small drawdown in the E zone. Aquitards and aquifers underlying the W fracture are unknown. However, leakage from the underlying aquifers and aquitards is believed to be small because of the large drawdown measured in the W aquifer during the tests. The modified Hantush model should be applicable for the analysis of all data collected during these tests. The same results are expected if Neuman and Witherspoon's model is applied.

Drawdown data from the aquifer tests conducted in the E fractured aquifer at the UIGRS show a strong influence of leakage from the unpumped aquifer at late time. The modified Hantush model obviously is not applicable to the test data analysis for the late time period. The Hantush

leaky without storage model (r/B solution) may be applicable for this aquifer condition but error is induced by ignoring water derived from storage in the aquitard.

Neuman and Witherspoon (1969b) indicate that the error due to ignoring aquitard storage is negligible if the value of the parameter β is small ($\beta \leq 0.01$) as the error increases with increasing of the β value. The error caused by application of the Hantush r/B solution becomes significant at $\beta=1$. A comparison of type curves between the Hantush and Neuman and Witherspoon's leaky aquifer solutions when $\beta=1$ is presented in Figure 6-8.

The error induced by the Hantush r/B solution can be estimated from the deviation of the two sets of type curves shown in Figure 6-8. When the leakage effect from the unpumped aquifer is significant (say, $r/B > 0.4$), the deviation of the two sets of type curves mainly occurs in the horizontal direction. The error in estimated parameters is mainly an over-estimation of aquifer storativity; aquifer transmissivity and r/B values are not affected significantly. When the leakage portion derived from the unpumped aquifer is small so the r/B value is small ($r/B < .1$), the deviation of the two sets of type curves occurs primarily in the vertical direction. Aquifer transmissivity is over-estimated by matching data to type curves of the Hantush r/B solution, whereas parameter r/B is underestimated when the upward deviation of the data from type curves occurs.

In summary, the Hantush and modified Hantush leaky aquifer models (r/B and β solutions) may be applied with care to the aquifer system at the UIGRS. The data from the aquifer tests conducted in the W aquifer and the early data from the tests conducted in the E aquifer can be analyzed by the modified Hantush solution; the results should be consistent with that by

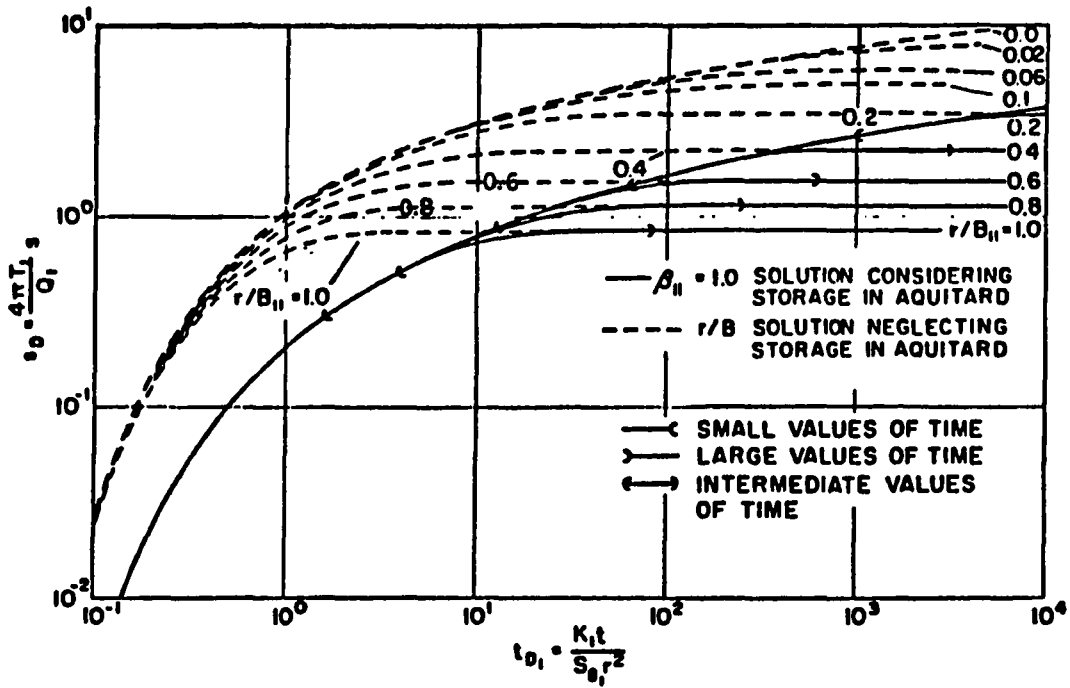


Figure 6-8. Type curve comparison of Hantush r/B solution with Neuman and Witherspoon solution (after Neuman and Witherspoon, 1969b)

the Neuman and Witherspoon solution. The Hantush leaky aquifer model (r/B solution) may be applicable to analysis of the late data from aquifer tests conducted in the E aquifer but errors on estimated T and S of the E aquifer are expected. The values of aquifer T and S may be over-estimated by the r/B solution.

Aquitard parameters estimated by the Hantush and modified Hantush models are lumped parameters of overlying and underlying aquitards. The product of hydraulic conductivity and specific storage ($K'Ss'$) of the aquitards at the UIGRS may be calculated by the modified Hantush model.

Moench Double-porosity with Fracture Skin Model

The double-porosity with fracture skin model is described by six parameters: hydraulic conductivity (K) and specific storage (Ss) of fractures, hydraulic conductivity (K') and specific storage (Ss') of the matrix rock, fracture skin (S_F), and well bore skin (S_w). The fracture skin is assumed to have a hydraulic conductivity that is less than that of the matrix rock which impedes the interchange of flow between the fractures and blocks. The well bore skin is assumed to be less permeable than the fractures and to restrict flow from fractures to the pumping well. The double-porosity with fracture skin model becomes a normal double-porosity model when fracture skin and well bore skin parameters are equal to zero.

The double-porosity with fracture skin model is applicable at the UIGRS according to the proposed hydrogeological conceptual model. The primary porosity occurs in the basalt blocks in the form of many randomly distributed joints. The major fractures in the E and W aquifer form secondary porosity media. The core samples collected at the UIGRS show that mineral crystalline deposits do occur in some of the fractures; these

deposits could behave as a fracture skin between the fractures and matrix rock.

Applicability of Alternative Analytical Models for Slug Tests

The analytical models for slug test analysis are discussed briefly in chapter IV. Three representative slug test models are: 1) Cooper model for a homogeneous confined aquifer (Cooper *et al.*, 1967), 2) Bouwer and Rice model for a homogeneous unconfined aquifer (Bouwer and Rice, 1976) and 3) double-porosity model for a fissured aquifer (Barker and Black, 1983). The Bouwer and Rice model is not applicable at the UIGRS because of the confined conditions of the fractured aquifers. As discussed in the previous chapter, application of the double-porosity slug test model is not practical because of the large number of dimensionless parameters.

The Cooper homogeneous slug test model is described by a relationship between the ratio of H/H_0 (hydraulic head at time t and initial hydraulic head due to slug injection or extraction) and the dimensionless parameters α and β . A group of type curves can be obtained from the model solution. The graphical curve matching of test data with the type curves provides an estimation of the aquifer hydraulic properties.

The Cooper model can be applied to analyze the slug test data from the UIGRS with several limitations. First, the model may be used only to estimate transmissivity of the aquifers because of the great error in estimating aquifer storativity via the model. Second, the estimated transmissivity probably represents that of the fractures immediately surrounding the wellbore.

CHAPTER VII
Analytical Model Application and Aquifer
Parameter Estimation

The application of alternative analytical models to data from seven multiple well aquifer tests and slug tests at the UIGRS and the associated parameter estimation of the fractured basalt aquifer system are presented in this chapter. A computer software package AQTESOLV was used to perform the type curve match and the aquifer parameter estimation.

AQTESOLV is a group of computer programs published by Geraghty & Miller, Inc. for quantitative analysis of aquifer test data with alternative analytical models (Duffield and Rumbaugh, 1989). The programs allow the users to match manually the type curves on the computer screen by vision or by statistical estimation methods. The graphical curve-matching technique basically is used to analyze the test data from the UIGRS with the assistance of statistical estimation by the programs.

Deviations of Drawdown Data of Multiple Well Aquifer Tests

The purpose of this section is to establish the criteria to accomplish the "best fit" of the graphical curve matches for the alternative analytical models.

Conceptual Models for Drawdown Deviations

Drawdown responses for a multiple well aquifer test conducted in a perfectly homogeneous and isotropic aquifer in which all these assumptions are valid should have the following characteristics: 1) plots of log

drawdown vs. log time of the observation wells should match the Theis type curve perfectly, and 2) drawdown data from different observation wells with different distances to the pumping well should form a single line on log-log plots of drawdown vs. t/r^2 . Perfectly homogeneous and isotropic aquifers do not exist in either porous media or fractured rocks. Plots of observed drawdown data during an aquifer test commonly deviate from the type curve because of aquifer heterogeneity.

Reasons for observed drawdown deviations from the Theis type curve may be obtained via analysis of hydraulic behavior of fractured aquifers. At the very earliest time in the test, the observed drawdown mainly is controlled by hydraulic properties of the larger fractures (secondary porosity). As the test continues, the blocks of less-fractured rock contribute to the hydraulic properties of the fractured aquifer. The transmissivity of the fractured aquifer is controlled primarily by the larger fractures and is not affected significantly by transmissive characteristics of the matrix blocks. The storativity of the aquifer, on the other hand, is controlled predominantly by the primary porosity of small joints and fractures in the matrix blocks; the S value should be small at the start of a test and then increase markedly (Gringarten, 1984; Ralston, personal communication, 1991; and Streltsova, 1976a).

Therefore, the drawdown responses of a hydraulic test conducted in a fractured aquifer are somewhat similar to the delayed yield response in the unconfined aquifer (Neuman, 1974; and Ralston, personal communication, 1991). The early drawdown reflects a large ratio of T/S that mainly represents the hydraulic properties of the fractures. As the test continues, the T/S ratio increases with increasing S ; as the matrix rock is now involved. The drawdown therefore deviates from the early curve. The

drawdown follows a new type curve when the S value reaches a maximum value and then stays constant.

Two differences between the fractured aquifer response and Neuman delayed yield response are: 1) the transition period during which S changes from a minimum value to a maximum value may be significantly shorter in the fractured aquifer than that in the unconfined aquifer, and 2) the early portion of the drawdown curve before the transition period may not be shown clearly in the fractured aquifer; the first type curve before the transition may not be matched because of change of the S value (Ralston, personal communication, 1991).

The observed drawdown at a specific time in an observation well located within the pumping influence distance generally is a weighted average of aquifer properties (T and S) over the testing volume. For a confined aquifer and a fully penetrating pumping well, the testing volume may be defined as the volume of cylinder with the pumping well as the axis of the cylinder, the pumping influence distance as the radius and aquifer thickness as the height. The testing volume increases with time and reaches its maximum value at the end of the test. The average aquifer properties may vary significantly as the testing volume increases, particularly at the early times. When the testing volume is larger than the representative elementary volume (REV) of an aquifer with no boundaries, average values of aquifer properties should become constant; and homogeneous analytical models are applicable (Long *et al.*, 1982).

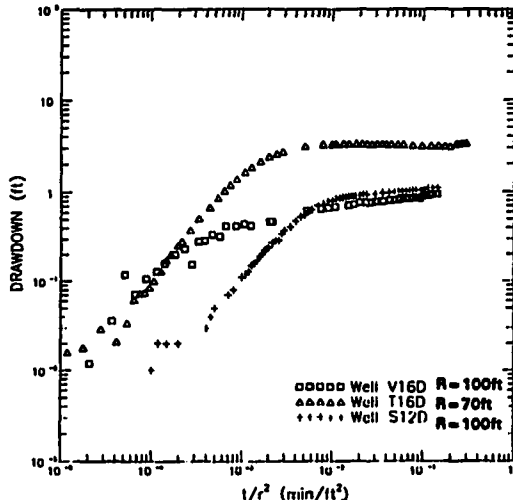
The boundary conditions of an aquifer represent large scale heterogeneities within the aquifer system (Ralston, personal communication, 1991). The observed drawdown response during an aquifer test conducted in an aquifer with boundaries is a function of the aquifer properties and the

boundary conditions. Generally, large scale aquifer heterogeneities caused by boundaries only impact test data during the late time when the testing volume is large enough to reach the boundaries. However, the aquifer test analysis becomes very complex if the boundaries are intercepted before the testing volume reaches the REV.

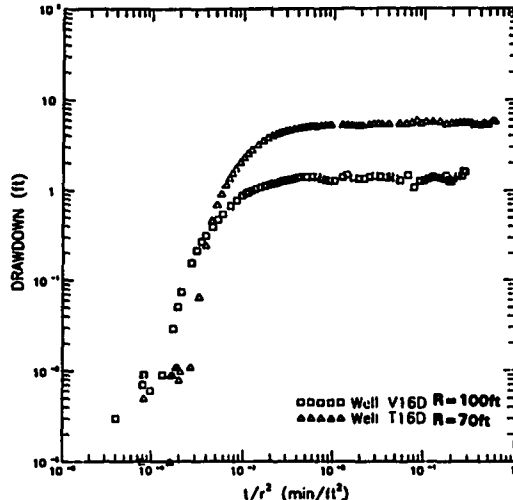
The REV of an aquifer in porous media generally is very small, and early drawdown deviation may never be observed during an aquifer test. The early drawdown deviation is more significant for an aquifer test conducted in fractured rock because of two reasons: 1) the REV of a fractured aquifer usually is larger, and 2) a fractured aquifer often exhibits a double-porosity behavior (Long et al., 1982; Streltsova, 1988). As is discussed above, drawdown deviations similar to the delayed yield response are commonly observed in the fractured aquifer.

Analysis of Log-log Plots of Drawdown vs. t/r^2

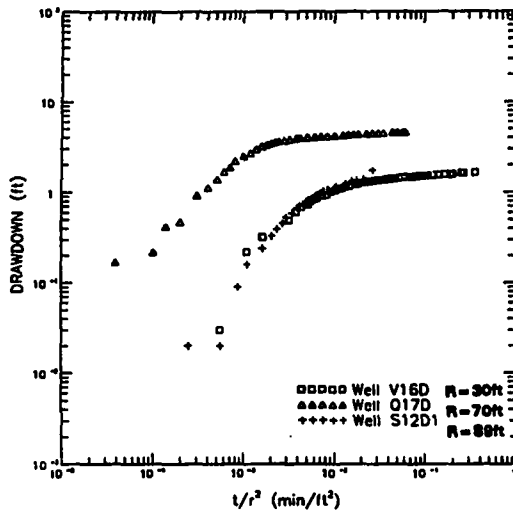
The plots of log drawdown vs. $\log t/r^2$ of the observation wells during the four aquifer tests conducted in the E fractured aquifer at the UIGRS are presented in Figure 7-1. The drawdown responses in unpumped aquifers are not presented in the graphs. Several common characteristics are observed from these plots: 1) the plots of different observation wells in each test do not coincide with each other; probably because of a leakage effects and aquifer heterogeneity, 2) early time data do not have curvature similar to the Theis type curve; probably showing drawdown deviations of fractured aquifer from the Theis solution, and 3) a strong impact of leakage derived from unpumped aquifers is shown on the late drawdown responses in all the wells.



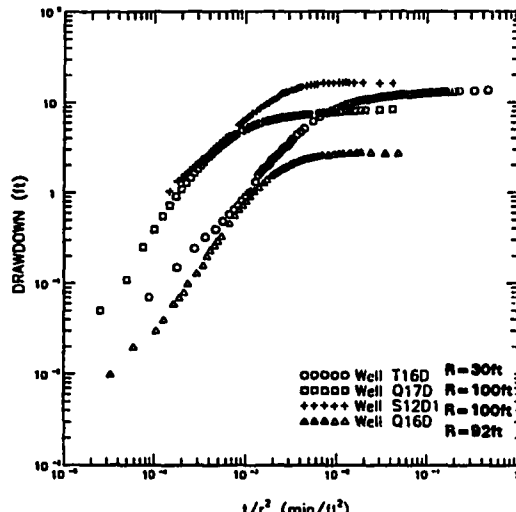
Log-log plot of drawdown vs. t/r^2 for observation wells V16D, T16D and S12D1 during pumping test 9-22-89



Log-log plot of drawdown vs. t/r^2 for observation wells V16D and T16D during pumping test 4-11-90



Log-log plot of drawdown vs. t/r^2 for observation wells V16D, Q17D and S12D1 during pumping test 4-4-90



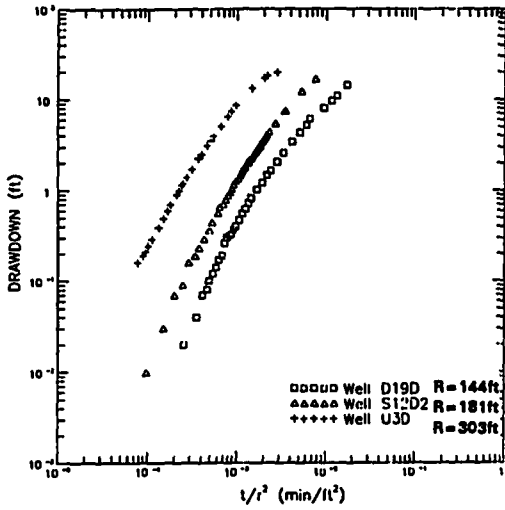
Log-log plot of drawdown vs. t/r^2 for observation wells T16D, Q17D, Q16D and S12D1 during pumping test 6-3-90

Figure 7-1. Log-log drawdown versus t/r^2 of the observation wells during the aquifer tests conducted in the E aquifer

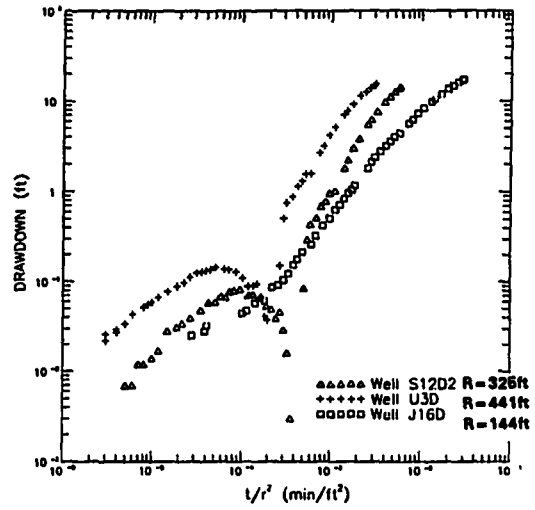
The criteria of data analysis from the aquifer tests conducted in the E aquifer should be: 1) the very early data are not used for graphical curve-matching and statistical estimation of aquifer parameters because of significant effects of small scale aquifer heterogeneities, 2) analytical models for homogeneous porous media are applicable after the very early stage of the tests, 3) the Theis type curve may be matched only by the intermediate portion of the data because of a leakage impact from both aquitards and unpumped aquifers on the late time data, and 4) the late portion of the test data may be matched only by the Hantush leaky aquifer model (r/B solution).

The graphs of log drawdown vs. $\log t/r^2$ of the three aquifer tests conducted in the W fractured aquifer are presented in Figure 7-2. The drawdown responses observed in these tests are significantly different from those of the tests conducted in the E aquifer (Figure 7-1). The general features of the plots shown in Figure 7-2 may be summarized as: 1) small scale aquifer heterogeneities and leakage impacts are significant so that plots of the different observation wells during each aquifer test do not form a single line, 2) log drawdowns vs. $\log t/r^2$ of the observation wells do not show the curvature similar to the Theis type curve; probably exhibiting the double-porosity behavior of the aquifer, and 3) effects of leakage derived from aquitards on the early data are evident on the graphs, but impacts of leakage derived from unpumped aquifers on the late data are not observed.

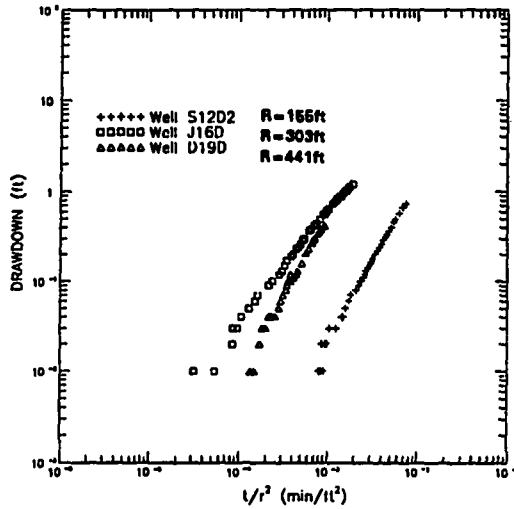
The different responses between the aquifer tests conducted in the E and W aquifers probably indicate different hydrogeological conditions of the two fracture zones. The W fractured aquifer behaves more like a



Log-log plot of drawdown vs t/r^2 for observation wells D19D U3D and S12D2 during pumping test 8-14-90



Log-log plot of drawdown vs t/r^2 for observation wells J16D U3D and S12D2 during pumping test 8-17-90



Log-log plot of drawdown vs t/r^2 for observation wells J16D, D19D and S12D2 during pumping test 3-8-91

Figure 7-2. Log-log drawdown versus t/r^2 of the observation wells during the aquifer tests conducted in the W aquifer

fractured medium rather than an equivalent porous medium; the REV of the W aquifer may be much larger than that of the E aquifer. Responses similar to leaky aquifer with storage in the aquitard may occur in the W fracture zone. However, other equivalent porous medium models such as the Theis and Hantush r/B solutions are not applicable. Typical responses of the Theis or Hantush models may be observed only after a longer period than the tests were conducted.

The criteria of data analysis with the tests conducted in the W aquifers at the UIGRS should be: 1) the very early data may not be useful because of aquifer heterogeneity, 2) analytical models for fractured rock such as the double-porosity models may be applicable, and 3) the modified Hantush model may also be applicable if one excludes the very early stages of the tests to estimate the average parameter values over the entire fracture zone.

Graphical Curve Matching and Parameter Estimation for Multiple Well Aquifer Test Data

Graphical curve matching of multiple well aquifer test data from the UIGRS is presented in this section. The hydraulic parameters of the E and W fractured aquifers and aquitards are estimated from the "best match" of test data to alternative type curves of the applicable analytical models based on the discussion presented above. Leakage from overlying and underlying aquitards can not be identified individually. Thus, the estimated aquitard parameters represent lumped values of both aquitards rather than the values for a specific aquitard.

The E Fractured Aquifer

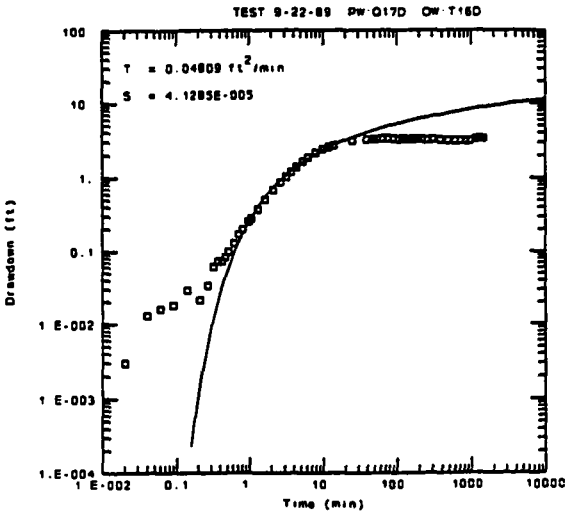
Four multiple well aquifer tests (9-22-89, 4-4-90, 4-11-90 and 6-3-90) were conducted in the E fractured basalt aquifer. Based on the above discussion, Theis, Hantush (r/B solution) and modified Hantush models are applied. Certain portions of the data are matched with alternative type curves according to the model applicability.

Aquifer Test 9-22-89

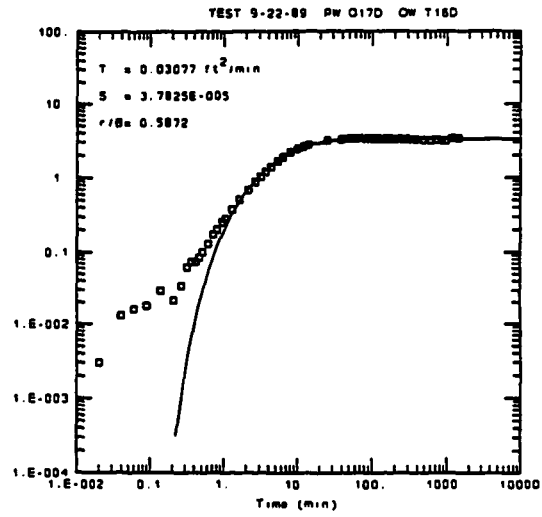
The graphical curve matches of the data from observation well T16D are shown in Figure 7-3 for Theis, Hantush (r/B) and modified Hantush (β) solutions. As shown in Figure 7-3, the very early data ($t < 0.2$ minutes) deviate from all the type curves because of heterogeneity of the aquifer. This deviation of drawdown is believed to be a typical early time response for a fractured aquifer. The large fractures respond first to the pumping; a larger T/S ratio is expected at very early times.

The late data of well T16D deviate significantly from the Theis curve. There are two possibilities for this deviation: 1) positive (recharge) boundary, or 2) leakage from unpumped aquifers. Leakage is believed to be the cause of the deviation because drawdown is observed in the unpumped alluvial aquifer. The hydraulic connection between the stream and fractured rock aquifers is via the alluvial aquifer. The Hantush leaky aquifer (r/B) solution provides a very good type curve match with the intermediate and late portions of the data.

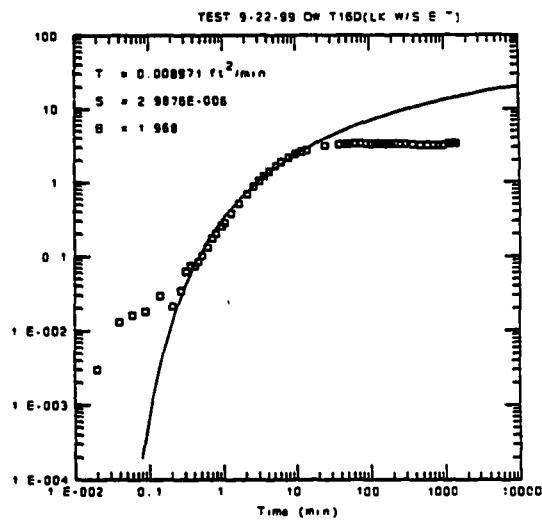
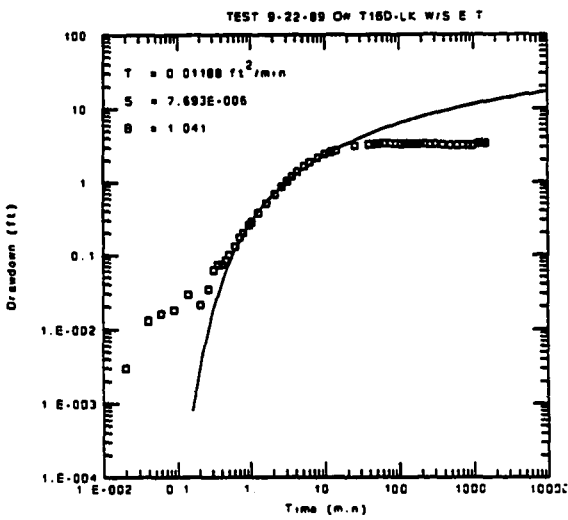
The modified Hantush (β) solution is applicable only to early time data. Drawdown data from $t=0.2$ to $t=10$ minutes are selected for the graphical curve-matching based on two criteria: 1) near well fracture flow characteristics are very significant when $t < 0.2$ minutes, and 2) strong



Theis Solution



Hantush (Leaky w/o Storage)



Modified Hantush (leaky w/ Storage)

$$R = 70 \text{ ft}$$

Figure 7-3. Graphical curve matching of observation well T16D data with alternative analytical models during test 9-22-89

leakage impact from the unpumped aquifer is shown after $t=10$ minute, when the rate of change in drawdown slows down considerably.

Two curve matches of modified Hantush solution with $\beta=1$ and $\beta=2$ are illustrated in Figure 7-3. The alternative curve matches are presented because the unique "best match" for this data set is difficult to determine.

The Neuman and Witherspoon solutions capture both the r/B and β solutions of the Hantush and modified Hantush models. However, as is discussed in the previous chapter, the application of the Neuman and Witherspoon solution is not practical because of the large number of variables; the model is not included in the computer software AQTESOLV.

The estimated parameters based on graphical curve matches of well T16D data (Figure 7-3) are presented in Table 7-1. The Theis solution gives the largest aquifer T and S values because leakage impacts from the aquitards and unpumped aquifer are ignored. The estimated T and S values by the Hantush leaky aquifer model (r/B solution) are close to the Theis solution. This is because the portion of the data curve prior to the significant leakage effects from the unpumped aquifer was used for the Theis curve match. The lowest aquifer T and S values are estimated using the modified Hantush model. As seen in Table 7-1, the S value by the modified Hantush solution is approximately one-fourth of that estimated by the Theis and Hantush solutions, whereas the T value by the modified Hantush is about one-third of the values estimated by the Theis and Hantush solutions. Generally, the aquifer parameters T and S estimated by the modified Hantush model are inversely proportional to the leakage parameter β (Table 7-1).

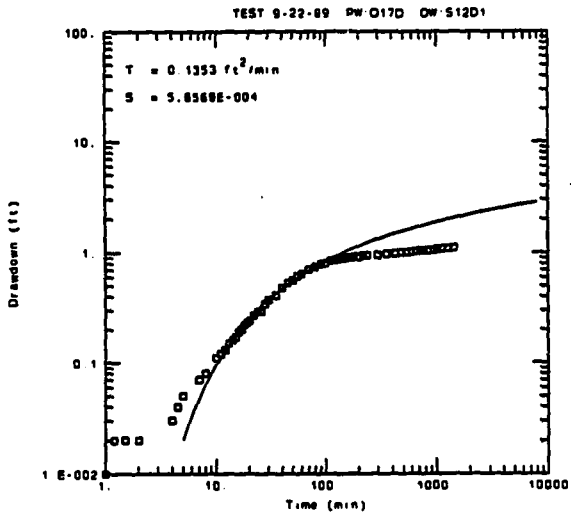
**Table 7-1. Calculated Aquifer Parameters from Well T16D Data,
Aquifer Test 9-22-89**

(Pumping Well Q17D. R=70 ft)

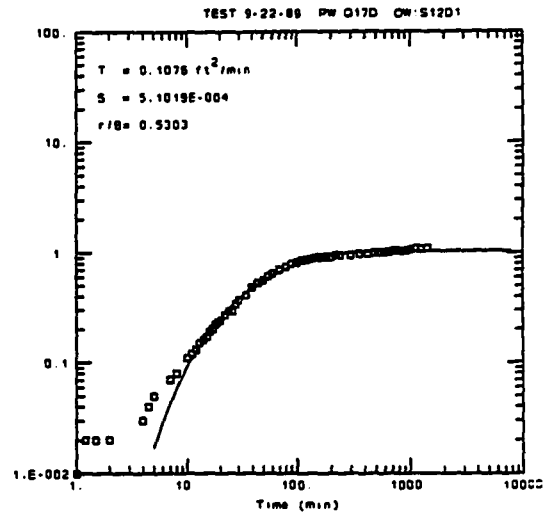
METHOD	T (ft ² /d)	S	β	r/B	$\sqrt{\frac{K'S'}{TS}}$ (1/ft)	$\sqrt{\frac{K'}{TB'}}$ (1/ft)
THEIS	69	4.1×10^{-5}	-	-	-	-
HANTUSH	43	3.2×10^{-5}		0.59		0.008
MODIFIED HANTUSH	17	7.7×10^{-6}	1		0.06	
	13	3×10^{-6}	2		0.11	

The graphical curve matches of observation well S12D1 data from aquifer test 9-22-89 are illustrated in Figure 7-4. The Theis, Hantush and modified Hantush solutions are applied. Figure 7-4 shows that the curve matching features of well S12D1 data are very similar to that of well T16D data shown in Figure 7-3. The very early data deviations caused by aquifer heterogeneity can not be matched by any type curves, and the late data deviations due to leakage from the unpumped aquifer can only be simulated by the Hantush leaky aquifer solution.

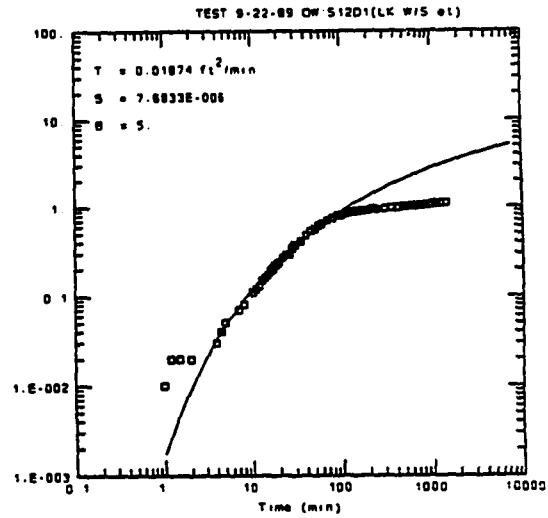
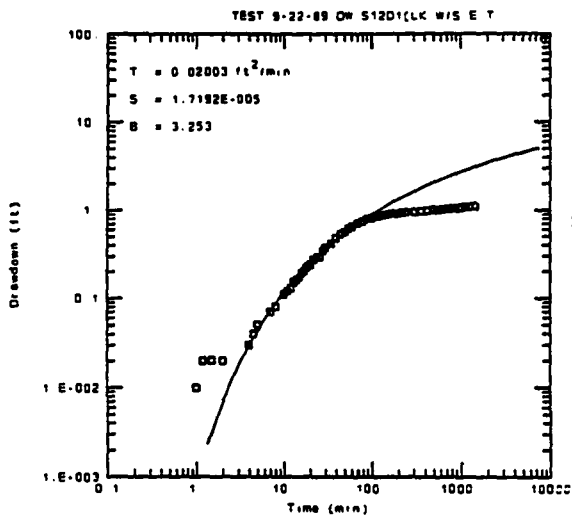
The same criteria are applied to select the matching portions of data to the alternative analytical models. The data also are matched alternatively by the modified Hantush solution with two β values. The estimated aquifer and aquitard parameters are presented in Table 7-2. As shown in Table 7-2, the T and S values estimated by the Theis and Hantush methods are approximately one order of magnitude greater than that from the modified Hantush method.



Theis Solution



Hantush (Leaky w/o Storage)



Modified Hantush (Leaky w/ Storage)

$$R = 100 \text{ ft}$$

Figure 7-4. Graphical curve matching of observation well S12D1 data with alternative analytical models during test 9-22-89

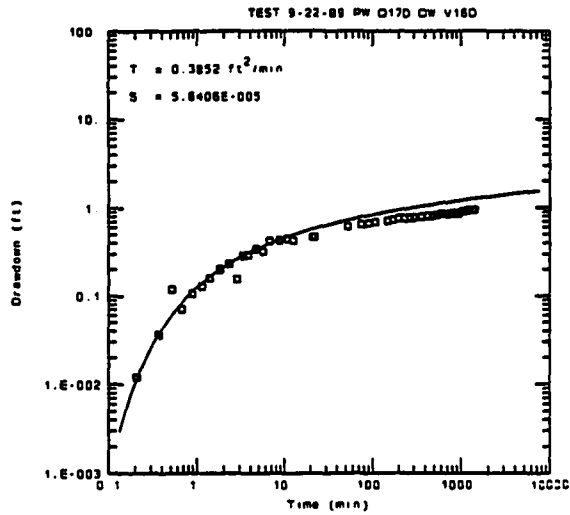
**Table 7-2. Calculated Aquifer Parameters from Well S12D1 Data,
Aquifer Test 9-22-89**

(Pumping Well Q17D. R=100 ft)

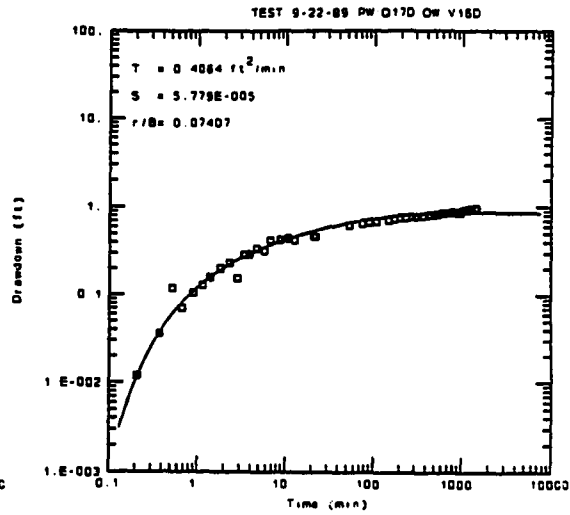
METHOD	T (ft ² /d)	S	β	r/B	$\sqrt{\frac{K'S'}{TS}}$ (1/ft)	$\sqrt{\frac{K'}{TB'}}$ (1/ft)
THEIS	200	5.7×10^{-4}	-	-	-	-
HANTUSH	155	5.1×10^{-4}		0.53		0.005
MODIFIED HANTUSH	29	1.7×10^{-5}	3.3		0.13	
	27	7.7×10^{-6}	5		0.2	

The impact of leakage derived from the aquitards on drawdown observed in well S12D1 ($\sqrt{K'S'/TS}$) is about twice that estimated for well T16D (Table 7-2). Also, the T and S values estimated with the Theis, Hantush, and modified Hantush methods from well S12D1 data are greater than the results from T16D data (Tables 7-1 and 7-2). The estimated r/B values with S12D1 and T16D data are fairly close. Because the distance from S12D1 to pumping well Q17D is greater, the actual impact of leakage derived from the unpumped alluvial aquifer on well S12D1 may be slightly smaller than that on the well T16D.

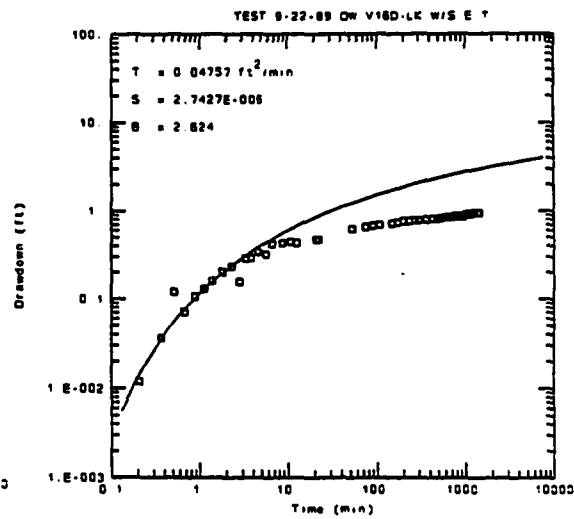
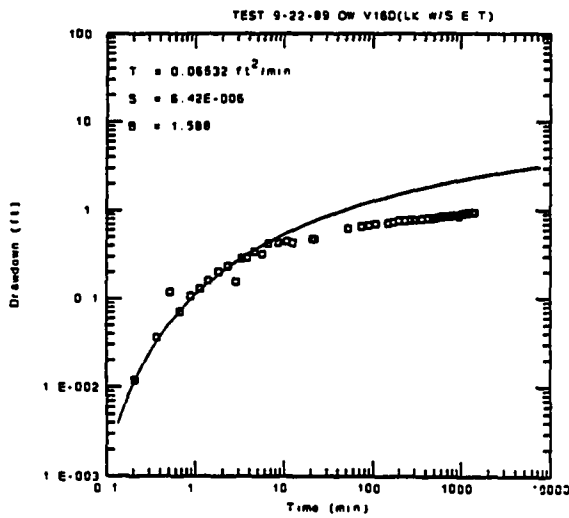
The graphical curve matches for observation well V16D data from test 9-22-89 are presented in Figure 7-5. The same analytical models (Theis, Hantush and modified Hantush) are applied for curve matches. Two significant differences are illustrated in Figure 7-5 in comparison with the curve matches of T16D and S12D1 data (Figures 7-3 and 7-4): 1) the very early data deviations from the type curves are not observed from well V16D, and 2) the log-log plot of the late-time data of well V16D are not as flat



This Solution



Hantush (Leaky w/o Storage)



Modified Hantush (leaky w/ Storage)

$R = 100 \text{ ft}$

Figure 7-5. Graphical curve matching of observation well V16D data with alternative analytical models during test 9-22-89

as that of wells T16D and S12D1.

The different drawdown response pattern from V16D is difficult to understand, probably reflecting the very complex fracture patterns in the E aquifer. The intraflow structures of the Lolo basalt flow probably are more developed in the vicinity of well V16D, as the yield of this well is the highest at the UIGRS. The hydrogeological interpretations of the drawdown responses of well V16D are: 1) the E aquifer may be more like a porous medium in the vicinity of V16D so that the early data deviations from the type curves are not evident, and 2) the E aquifer may have a more direct hydraulic connection to the unpumped alluvial aquifer in the vicinity of V16D.

The estimated aquifer and aquitard parameters from V16D data are presented in Table 7-3. The aquifer S values are consistent in comparison with the previous estimates but the T values are significantly greater. As discussed above, the estimated results suggest that the E fracture zone is more developed in the vicinity of V16D.

**Table 7-3. Calculated Aquifer Parameters from Well V16D Data,
Aquifer Test 9-22-89**

(Pumping Well Q17D. R=100 ft)

METHOD	T (ft ² /d)	S	β	r/B	$\sqrt{\frac{K's'}{TS}}$ (1/ft)	$\sqrt{\frac{K'}{Tb'}}$ (1/ft)
THEIS	550	5.6×10^{-5}	-	-	-	-
HANTUSH	576	5.7×10^{-5}		0.07		0.0007
MODIFIED HANTUSH	96	6.4×10^{-6}	1.6		0.06	
	69	2.7×10^{-6}	2.6		0.1	

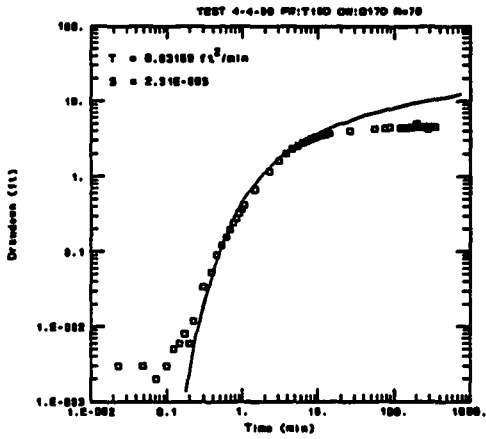
As shown in Table 7-3, the two β values estimated by alternative curve matches of the modified Hantush model are very close to the previous estimates from other data sets. These β values indicate that the impacts of leakage derived from the aquitards to the pumped E aquifer are fairly consistent on the different observation wells because the distances from the observation wells to the pumping well are similar.

Aquifer Test 4-4-90

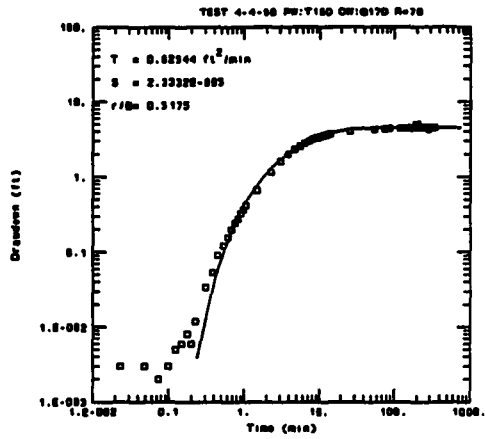
The graphical curve matches of observation well Q17D data during aquifer test 4-4-90 (pumping well: T16D) are presented in Figure 7-6. The same analytical models (Theis, Hantush and modified Hantush) and the same curve matching criteria for the alternative models are applied for parameter estimation. The curve matches illustrated in Figure 7-6 is almost identical to that of observation well T16D data during test 9-22-89 (Figure 7-3). The very early drawdown deviation from all the type curves and the impacts of leakage derived from aquitards and alluvial aquifer are clearly shown in Figure 7-6.

Alternative curve matches by the modified Hantush model are presented in Figure 7-6; two sets of estimated parameters are obtained. A summary of the parameters calculated via the type curve matches of the three analytical models (Figure 7-6) is presented in Table 7-4.

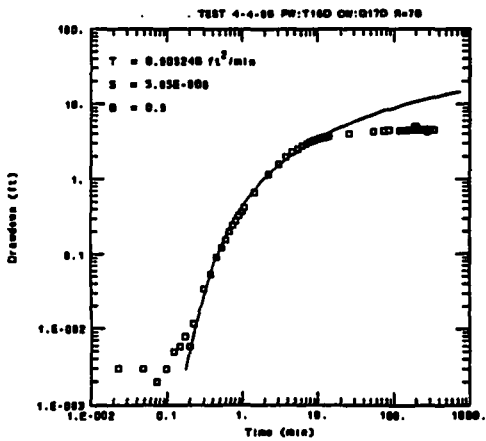
As shown in Table 7-4, the estimated aquifer T and S values with the Theis and Hantush solutions have no significant difference. The two results with the modified Hantush model also are close. The aquifer T and S values estimated via the modified Hantush are considerably smaller because early leakage from the aquitards is taken into account.



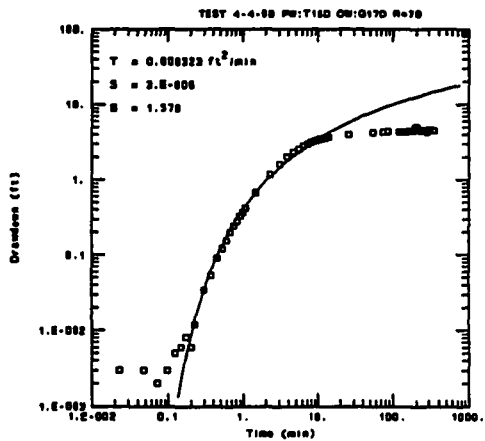
Theis Solution



Hantush (Leaky w/o Storage)



Modified Hantush (leaky w/ Storage)



R = 70 feet

Figure 7-6. Graphical curve matching of observation well Q17D data with alternative analytical models during test 4-4-90

**Table 7-4. Calculated Aquifer Parameters from Well Q17D Data,
Aquifer Test 4-4-90**

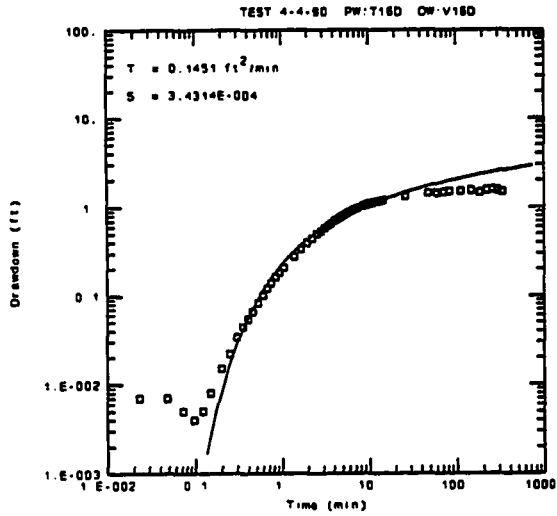
(Pumping Well T16D, R=70 ft)

METHOD	T (ft ² /d)	S	β	r/B	$\sqrt{\frac{\kappa's'}{TS}}$ (1/ft)	$\sqrt{\frac{\kappa'}{TB'}}$ (1/ft)
THEIS	46	2.5×10^{-5}	-	-	-	-
HANTUSH	36	2.4×10^{-5}		0.52		0.007
MODIFIED HANTUSH	13	5.9×10^{-6}	0.9		0.05	
	9	3×10^{-6}	1.6		0.09	

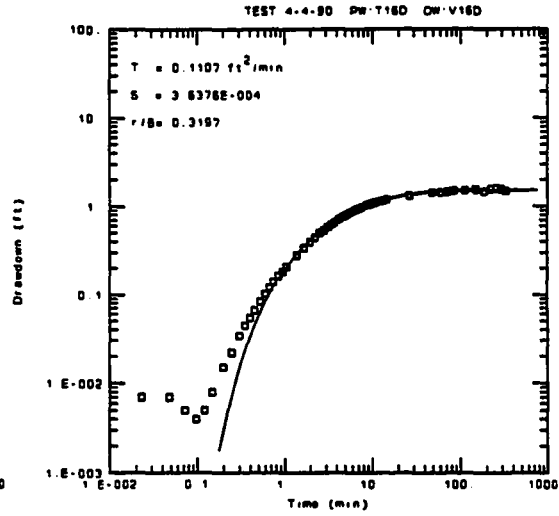
The graphical curve matches of observation well V16D data during test 4-4-90 are illustrated in Figure 7-7. The three analytical models (Theis, Hantush and modified Hantush) and the same type curve matching criteria are applied for parameter estimation. Very early data are ignored because of drawdown deviation, and the late data are matched only by the Hantush solution.

Only one "best match" of the well V16D data to the type curves of modified Hantush is obtained (Figure 7-7). The calculated parameters based on the curve matches of V16D data are tabulated in Table 7-5.

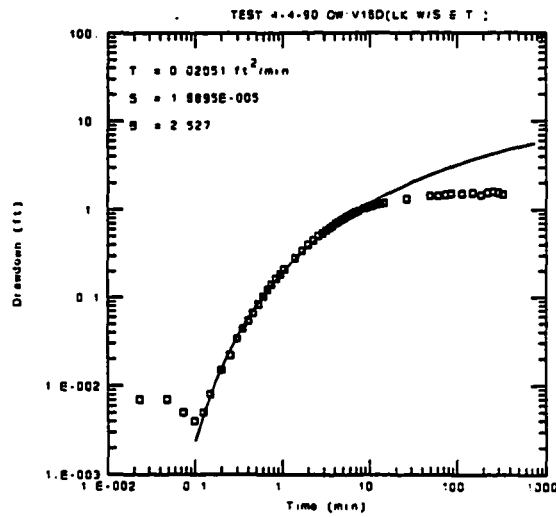
The estimated aquifer T and S values by the Theis and Hantush models are high compared with the estimates obtained from Q17D data. According to the estimated β value and the distance from V16D to the pumping well (T16D), the impact of leakage from aquitards is considerably greater in the vicinity of well V16D (Table 7-5).



Theis Solution



Hantush (Leaky w/o Storage)



Modified Hantush (leaky w/ Storage)

R = 30 feet

Figure 7-7. Graphical curve matching of observation well V16D data with alternative analytical models during test 4-4-90

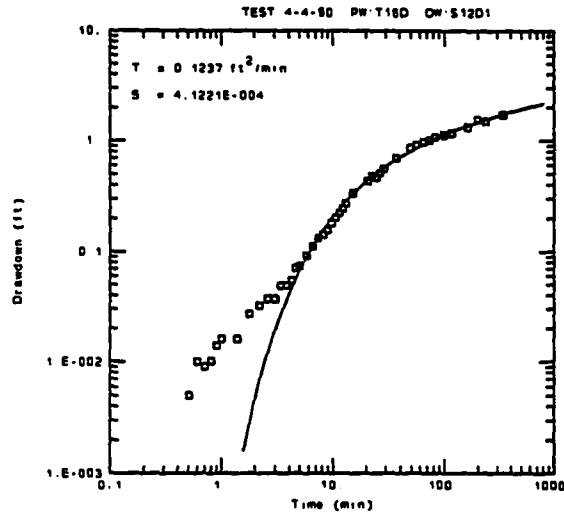
**Table 7-5. Calculated Aquifer Parameters from Well V16D Data,
Aquifer Test 4-4-90**

(Pumping Well T16D, R=30 ft)

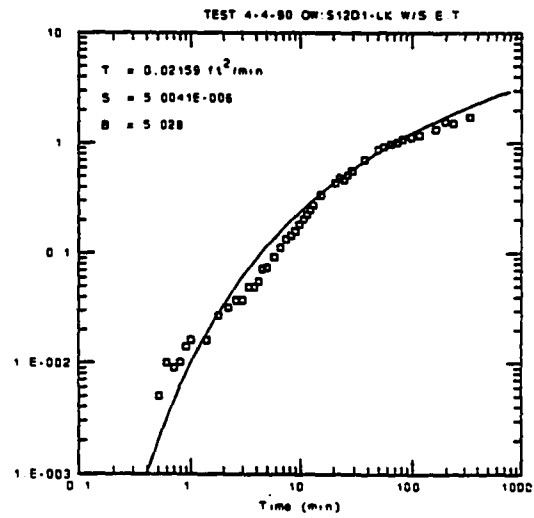
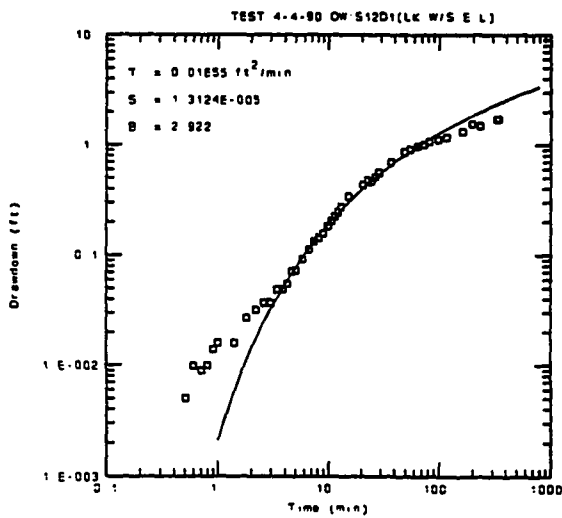
METHOD	T (ft ² /d)	S	β	r/B	$\sqrt{\frac{K's'}{TS}}$ (1/ft)	$\sqrt{\frac{K'}{Tb'}}$ (1/ft)
THEIS	209	3.4×10^{-4}	-	-	-	-
HANTUSH	158	3.6×10^{-4}		0.32		0.01
MODIFIED HANTUSH	29	1.9×10^{-5}	2.5		0.33	

The data from observation well S12D1 during test 4-4-90 are analyzed using the Theis and modified Hantush models. The Hantush leaky aquifer model (r/B solution) is not applied because the plot of log drawdown vs. log time from well S12D1 does not exhibit the impact of leakage derived from unpumped aquifers. Either the shallow alluvial aquifer is missing or the thickness and grain size of the sediments are too small to yield significant amount of water in the central portion of the UIGRS. The graphical curve matches of well S12D1 data during test 4-4-90 for Theis and modified Hantush solutions are presented in Figure 7-8.

The Theis type curve matches the intermediate and late portions of the S12D1 data well but a large portion of the early data ($t < 5$ minutes) is ignored (Figure 7-8). The early data deviate from the Theis curve probably because of two combined effects: double-porosity features of the fractured aquifer and leakage from the aquitards. The test data are matched by alternative modified Hantush type curves with two β values. The very early data ($t < 1$ min.) and some of the late data points ($t > 200$ min.) can not be matched by the type curves (Figure 7-8).



Theis Solution



Modified Hantush (leaky w/ Storage)

R = 89 feet

Figure 7-8. Graphical curve matching of observation well S12D1 data with the Theis and modified Hantush models during test 4-4-90

The estimated aquifer parameters based on the graphical curve matches of Figure 7-8 are tabulated in Table 7-6. The aquifer S value with the Theis solution is nearly two magnitudes higher than that calculated by the modified Hantush solution.

**Table 7-6. Calculated Aquifer Parameters from Well S12D1 Data,
Aquifer Test 4-4-90**

(Pumping Well T16D, R=89 ft)

METHOD	T (ft ² /d)	S	β	r/B	$\sqrt{\frac{k's'}{TS}}$ (1/ft)	$\sqrt{\frac{k'}{Tb'}}$ (1/ft)
THEIS	173	4.1×10^{-4}	-	-	-	-
MODIFIED HANTUSH	25	1.3×10^{-5}	2.9		0.13	
	29	5×10^{-6}	5		0.22	

Aquifer Test 4-11-90

Only two observation wells were monitored for drawdown responses during test 4-11-90. The data show a strong effect of leakage from the unpumped alluvial aquifer. The Theis and Hantush leaky aquifer models are applied for parameter estimation. The graphical curve matches of wells T16D and V16D data during the test 4-11-90 are illustrated in Figures 7-9 and 7-10. The calculated aquifer parameters are presented in Table 7-7.

The modified Hantush model is not applied for the curve matches of test 4-11-90 data because the early time data do not show the impact of leakage from the aquitards. As is discussed in chapter VI, the early time data of the test may have considerable measurement error from the pressure transducers. Thus, the early time data are not valid for the aquifer test analysis.

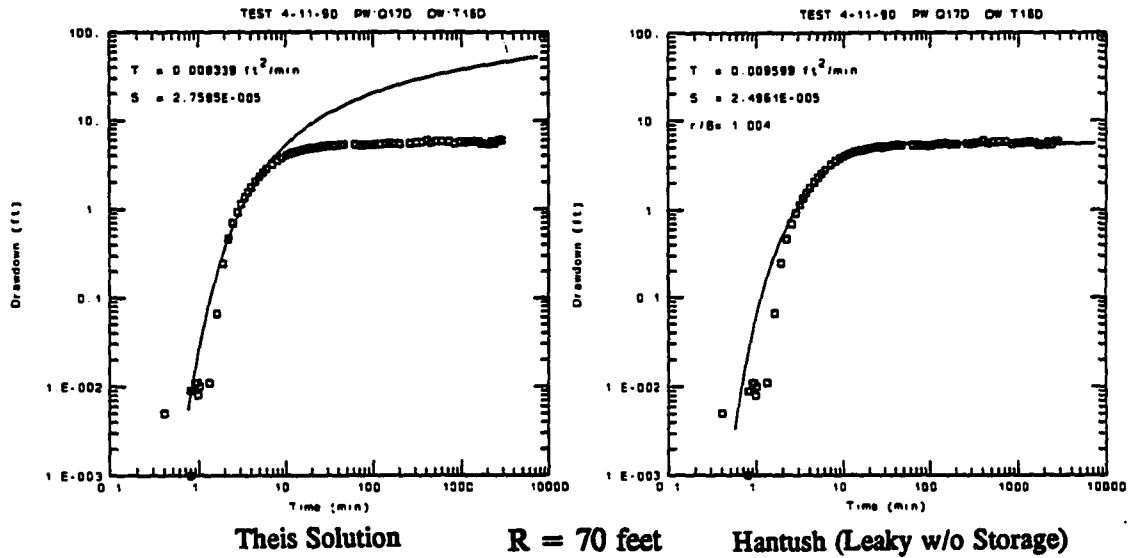


Figure 7-9. Graphical curve matching of observation well T16D data with the Theis and Hantush models during test 4-11-90

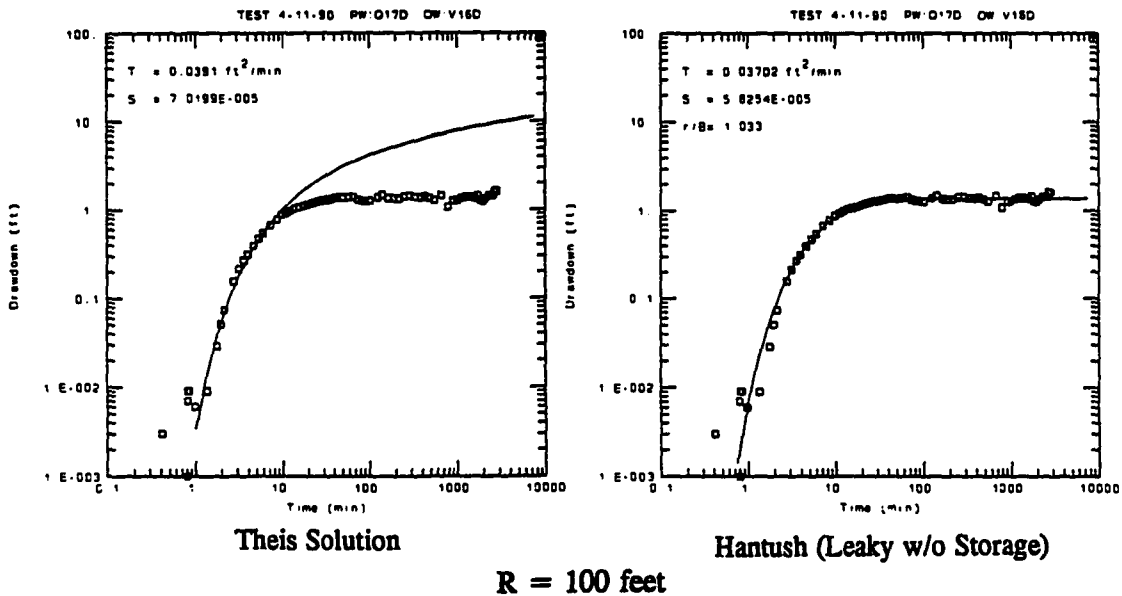


Figure 7-10. Graphical curve matching of observation well V16D data with the Theis and Hantush models during test 4-11-90

Table 7-7. Calculated Aquifer Parameters from Wells T16D and V16D Data, Aquifer Test 4-11-90

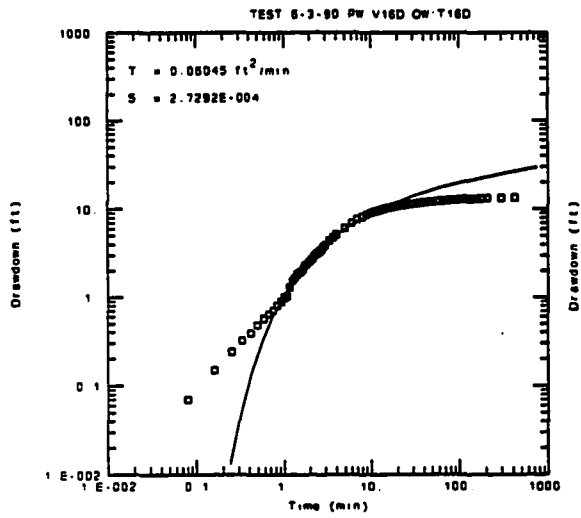
(Pumping Well Q17D, R=70 ft and 100 ft)

WELL	METHOD	T (ft ² /d)	S	r/B	$\sqrt{\frac{K'}{Tb'}}$ (1/ft)	REMARKS
T16D	THEIS	12	2.8×10^{-5}			r=70 ft
	HANTUSH	14	2.5×10^{-5}	1.0	0.014	
V16D	THEIS	56	7×10^{-5}			r=100 ft
	HANTUSH	53	5.8×10^{-5}	1.0	0.01	

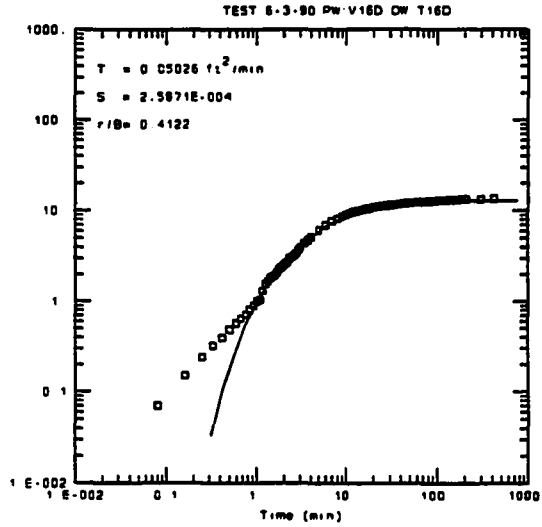
Aquifer Test 6-3-90

The data from four observation wells T16D, Q17D, S12D1 and Q16D during test 6-3-90 are also used for the aquifer parameter estimation. The graphical curve matches of well T16D data are shown in Figure 7-11 for the Theis, Hantush and modified Hantush solutions.

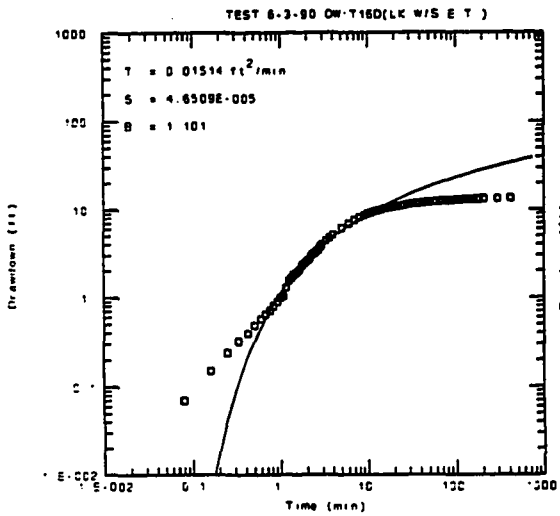
The same curve matching criteria are applied for parameter estimation. As shown in Figure 7-11, the Theis type curve can match only the middle portion of the T16D data because of three reasons: 1) the early data deviations of fractured aquifer responses from the porous medium models, 2) the impact of leakage derived from the aquitards at the early times, and 3) the impact of leakage derived from the unpumped shallow alluvial aquifer at the late stage of the test. The Hantush r/B solution, which considers leakage from the unpumped aquifer, has a good match to the intermediate and late portions of T16D data but not the early time data. Two alternative curve matches are obtained using the modified Hantush β solution. The early and intermediate portions of the data are applied



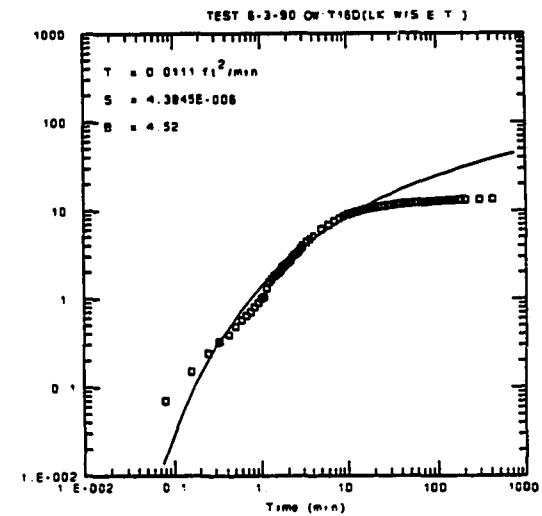
Theis Solution



Hantush (Leaky w/o Storage)



Modified Hantush (leaky w/ Storage)



$R = 30 \text{ feet}$

Figure 7-11. Graphical curve matching of observation well T16D data with alternative analytical models during test 6-3-90

because the β solution is for small time values. A few data of the earliest time reflect the early drawdown deviation and can not be used for the curve matches. The estimated aquifer parameters based on these graphical curve matches (Figure 7-11) are presented in Table 7-8.

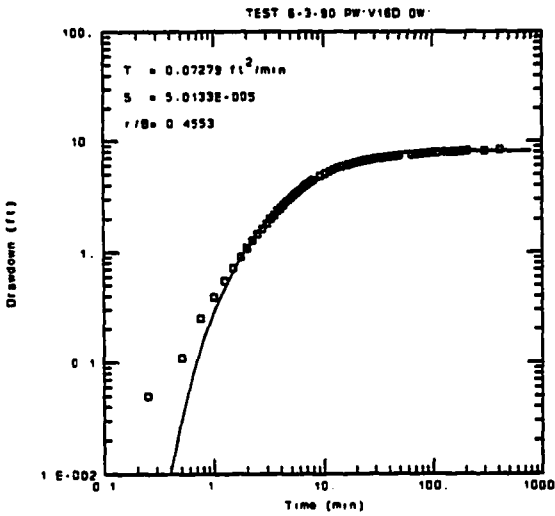
**Table 7-8. Calculated Aquifer Parameters from Well T16D Data,
Aquifer Test 6-3-90**

(Pumping Well V16D, R=30 ft)

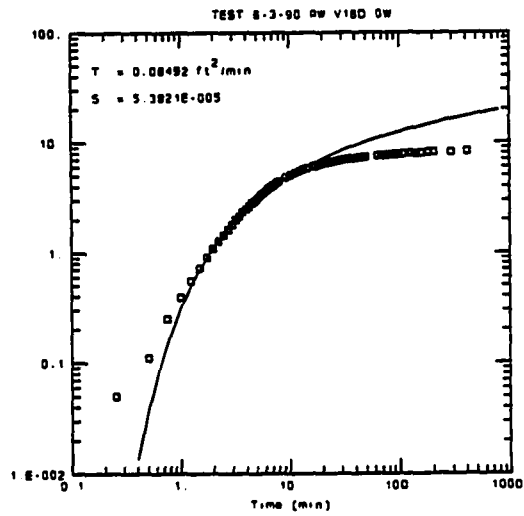
METHOD	T (ft ² /d)	S	β	r/B	$\sqrt{\frac{k's'}{TS}}$ (1/ft)	$\sqrt{\frac{K'}{Tb'}}$ (1/ft)
THEIS	86	2.7×10^{-4}				
HANTUSH	72	2.6×10^{-4}		0.4		0.01
MODIFIED HANTUSH	22	4.7×10^{-5}	1.1		0.15	
	16	4.4×10^{-6}	4.5		0.6	

The T and S values estimated from the Theis and Hantush models are similar. Lower T and S values are obtained using the modified Hantush solution. For the alternative estimates by the modified Hantush model, the T and S values are inversely proportional to the β value (Table 7-8).

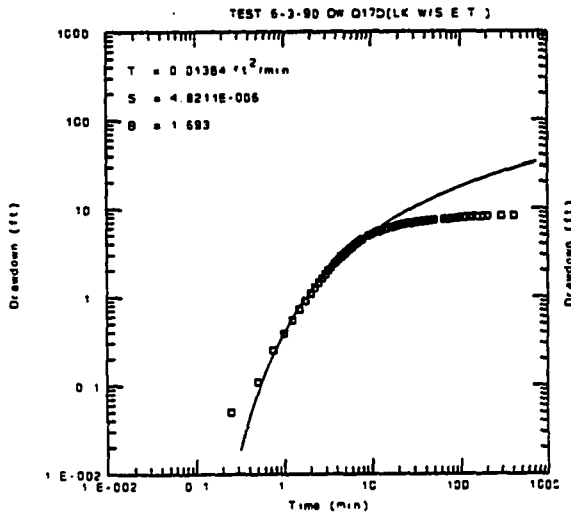
The graphical curve matches of well Q17D data during test 6-3-90 are illustrated in Figure 7-12. The same analytical models (Theis, Hantush and modified Hantush) and matching criteria are applied. The curve matching features of different analytical models to well Q17D data are very similar to that of well T16D data, as shown in Figures 7-11 and 7-12. The results of parameter estimations from the curve matches are tabulated in Table 7-9.



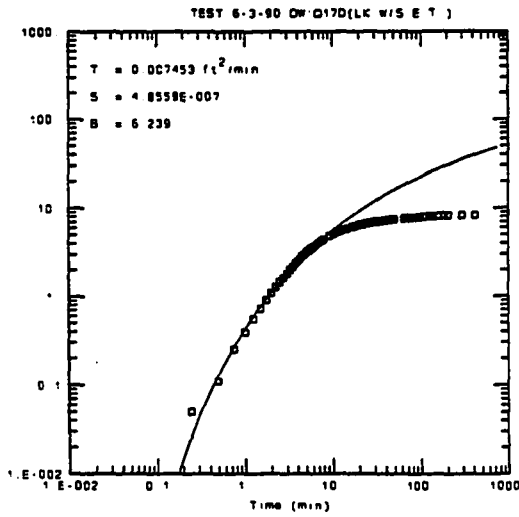
Hantush (Leaky w/o Storage)



Theis Solution



Modified Hantush (Leaky w/ Storage)



R = 100 feet

Figure 7-12. Graphical curve matching of observation well Q17D data with alternative analytical models during test 6-3-90

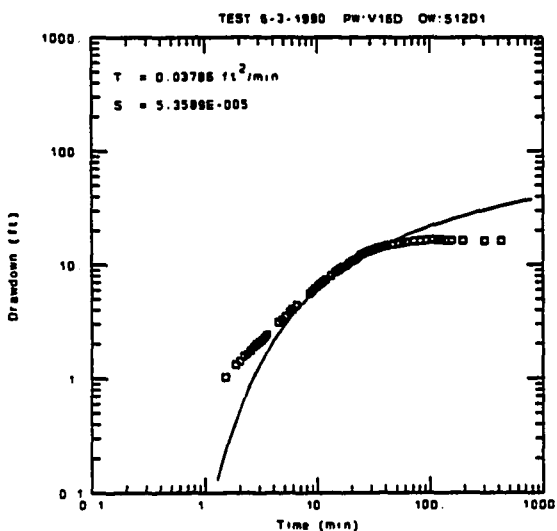
**Table 7-9. Calculated Aquifer Parameters from Well Q17D Data,
Aquifer Test 6-3-90**

(Pumping Well V16D, R=100 ft)

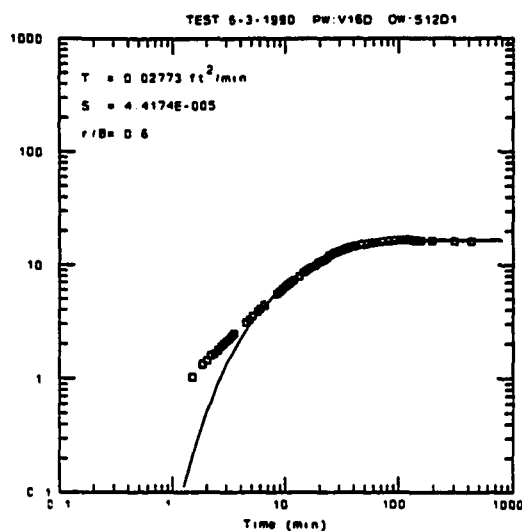
METHOD	T (ft ² /d)	S	β	r/B	$\sqrt{\frac{k's'}{TS}}$ (1/ft)	$\sqrt{\frac{k'}{Tb'}}$ (1/ft)
THEIS	122	5.4×10^{-6}				
HANTUSH	105	5×10^{-5}		0.46		0.005
MODIFIED HANTUSH	20	4.8×10^{-6}	1.7		0.07	
	11	4.9×10^{-7}	6.2		0.25	

The estimated T values from Q17D data are within a similar range as the T values from T16D data, but the S values from Q17D data are almost one order of magnitude smaller than that from T16D (Tables 7-8 and 7-9). The S values are so different probably because of two reasons: 1) heterogeneities of the fractured aquifer, particularly for the aquifer storage properties that are predominated by the primary porosity of small joints and fissures within the matrix blocks, and 2) estimation error. The range in storativity of a fractured aquifer is generally large; thus, one order of magnitude of S values could represent a error band of the estimation.

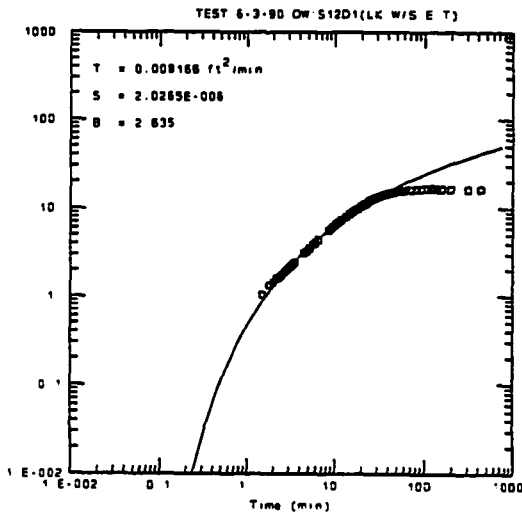
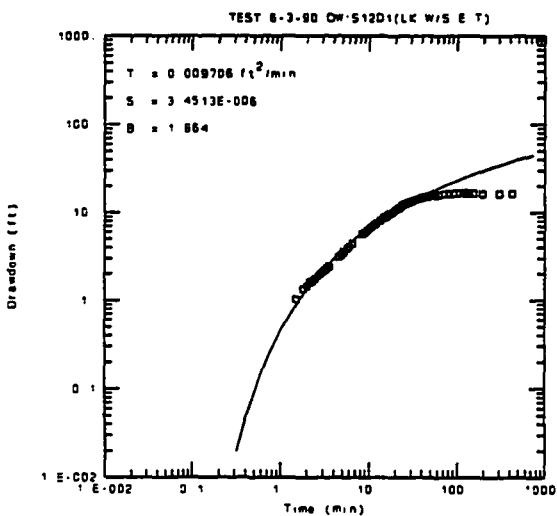
The graphical curve matches of the Theis, Hantush and modified Hantush solutions with wells S12D1 and Q16D data during test 6-3-90 are illustrated in Figures 7-13 and 7-14. The characteristics of the curve matching of S12D1 and Q16D data to the alternative type curves are nearly identical to that of T16D data (Figure 7-11); discussions of these curve matching features are presented in the previous section.



Theis Solution



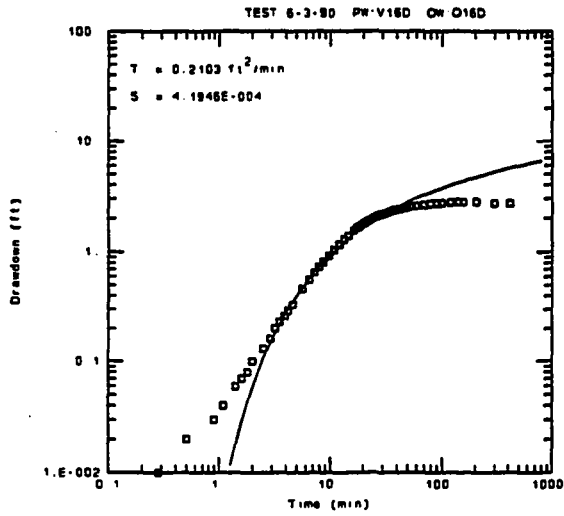
Hantush (Leaky w/o Storage)



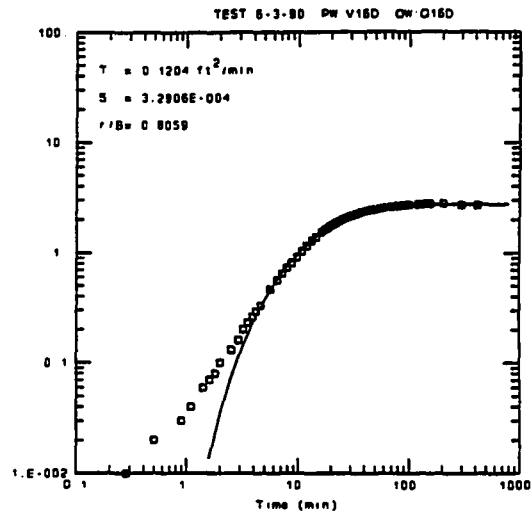
Modified Hantush (leaky w/ Storage)

$R = 100 \text{ feet}$

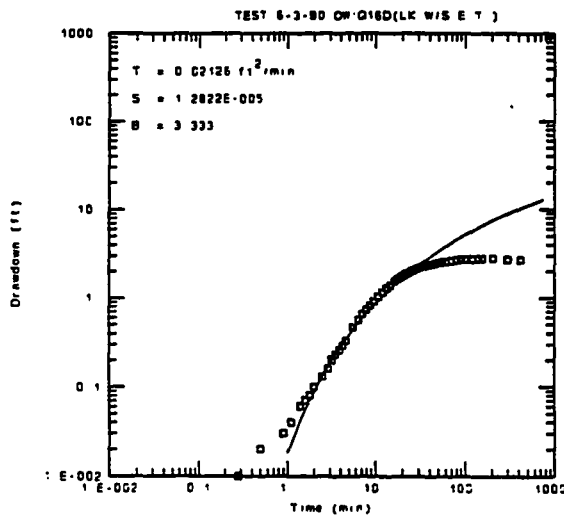
Figure 7-13. Graphical curve matching of observation well S12D1 data with alternative analytical models during test 6-3-90



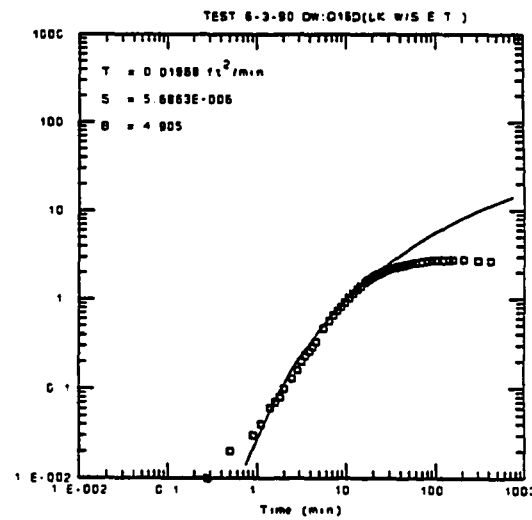
This Solution



Hantush (Leaky w/o Storage)



Modified Hantush (Leaky w/ Storage)



R = 92 feet

Figure 7-14. Graphical curve matching of observation well Q16D data with alternative analytical models during test 6-3-90

The same curve matching criteria are applied for parameter estimations from wells S12D1 and Q16D data. The estimated aquifer and aquitard parameters from wells S12D1 and Q16D data are presented in Table 7-10.

Table 7-10. Calculated Aquifer Parameters from Wells S12D1 and Q16D Data, Aquifer Test 6-3-90

(Pumping Well V16D)

OBS. WELL	METHOD	T (ft ² /d)	S	β	r/B	$\sqrt{\frac{K'S'_z}{TS}}$ (1/ft)	$\sqrt{\frac{K'}{Tb'}}$ (1/ft)
S12D1 R=100 ft	THEIS	55	5.4×10^{-5}				
	HANTUSH	40	4.4×10^{-5}		0.6		0.006
	MODIFIED HANTUSH	14	3.5×10^{-6}	1.9		0.08	
		12	2×10^{-6}	2.6		0.1	
Q16D R=92 ft	THEIS	302	4.2×10^{-4}				
	HANTUSH	172	3.3×10^{-4}		0.8		0.009
	MODIFIED HANTUSH	29	1.3×10^{-5}	3.3		0.14	
		27	5.7×10^{-6}	4.9		0.24	

The estimated aquifer T and S values as well as the leakage parameters (r/B and β) from Q16D data generally are greater than the values estimated from S12D1 data (Table 7-10). This could be caused mainly by two factors: 1) complexity of the fractured aquifer system at the UIGRS (aquifer heterogeneity and anisotropy); the estimated parameter values may represent the directional T values from different observation wells or S values at different well locations, and 2) more direct hydraulic connection

of well Q16D to the unpumped shallow aquifer through uncompleted wellbore of Q16D; significantly different final drawdowns in the two wells at the end of test 6-3-90 may reflect the impact of this connection (Figures 7-13 and 7-14).

Summary

A comparison and summary of the estimated aquifer and aquitards parameters from four multiple well aquifer tests conducted in the E aquifer are presented in Table 7-11. The tabulated parameters are calculated based on the data from different observation wells during each aquifer test. The ranges in values of each parameter are presented along with the geometric means.

The aquifer T and S values listed in Table 7-11 are representative of the average E aquifer hydraulic properties. The values (T and S) are calculated based on the Hantush (r/B) and modified Hantush (β) solutions. As discussed early in this chapter, the T and S values are generally over-estimated by the Theis model because leakage from the aquitards and unpumped aquifers is ignored. The listed aquitard parameters K^*Ss' (Table 7-11) are the lumped values that represent the combined characteristics of the aquitards overlying and underlying the E aquifer (upper and middle aquitards).

The estimated E aquifer parameters (T and S) by the Hantush r/B solution range from 14 to 576 ft^2/day and 2×10^{-5} to 5×10^{-4} , respectively. The T values estimated by the modified Hantush have a smaller range. The average T values are 22 ft^2/day by the modified Hantush method and 80 ft^2/day by the Hantush method. The storativity estimated by the Hantush

Table 7-11. Comparison and Summary of the Parameters Estimated from the E Aquifer Tests

Aquifer and Aquitard Parameters	Test 9-22-89 (PW: Q17D)			Test 4-4-90 (PW: T16D)			Test 4-11-90 (PW: Q17D)		Test 6-3-90 (PW: V16D)				Value Range	Geometric Mean
	T16D	V16D	S12D1	Q17D	V16D	S12D1	T16D	V16D	T16D	Q17D	S12D1	Q16D		
Transmissivity by Modified Hantush (ft ² /day)	17	96	29	13	29	25			22	20	14	29	9-96	22
	13	69	27	9		29			16	11	12	27		
Transmissivity by Hantush (ft ² /day)	43	576	155	36	158		14	53	72	105	40	172	14-576	80
Storativity by Modified Hantush	8x10 ⁻⁶	6x10 ⁻⁶	2x10 ⁻⁵	6x10 ⁻⁶	2x10 ⁻⁵	10 ⁻⁵			5x10 ⁻⁵	5x10 ⁻⁶	4x10 ⁻⁶	10 ⁻⁵	5x10 ⁻⁷ - 5x10 ⁻⁶	7x10 ⁻⁶
	3x10 ⁻⁶	3x10 ⁻⁶	8x10 ⁻⁶	3x10 ⁻⁶		5x10 ⁻⁶			4x10 ⁻⁵	5x10 ⁻⁷	2x10 ⁻⁶	6x10 ⁻⁶		
Storativity by Hantush	3x10 ⁻⁵	6x10 ⁻⁶	5x10 ⁻⁴	2x10 ⁻⁵	4x10 ⁻⁴		3x10 ⁻⁵	6x10 ⁻⁵	3x10 ⁻⁴	5x10 ⁻⁵	4x10 ⁻⁵	3x10 ⁻⁴	2x10 ⁻⁵ - 5x10 ⁻⁴	9x10 ⁻⁵
$\sqrt{\frac{K'}{Tb'}}$ (1/ft)	.008	.0007	.005	.007	.01		.01	.01	.01	.005	.006	.009	.0007- .01	0.008
$\sqrt{\frac{K'S'_e}{TS}}$ (1/ft)	.06	.06	.13	.05	.33	.13			.15	.07	.08	.14	.05- .6	0.13
	.11	.1	.2	.09		.22			.6	.25	.1	.24		
K'Ss' (1/day)	5x10 ⁻⁷	2x10 ⁻⁶	8x10 ⁻⁶	2x10 ⁻⁷	6x10 ⁻⁵	6x10 ⁻⁶			8x10 ⁻⁵	4x10 ⁻⁷	3x10 ⁻⁷	8x10 ⁻⁶	2x10 ⁻⁷ - 8x10 ⁻⁵	3x10 ⁻⁶

model is approximately one order of magnitude greater than that by the modified Hantush model; average storativity values are 9×10^{-5} for the Hantush solution and 7×10^{-6} for the modified Hantush solution. The average T and S values are 22 ft²/day and 7×10^{-6} . The error bands of the estimated parameters are unknown.

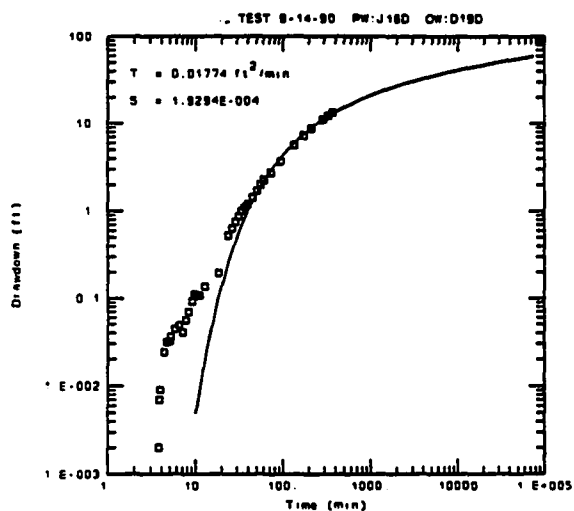
The W Fractured Aquifer

The hydraulic parameters of the W fracture zone are estimated with application of the modified Hantush leaky aquifer and Moench double-porosity with fracture skin models. These models are applicable in the W fractured aquifer as is discussed in the previous chapter. The Theis model is applied with graphical curve matching for purposes of comparison. Data from multiple well aquifer tests 8-14-90, 8-17-90 and 3-8-91 conducted in the W aquifer are utilized.

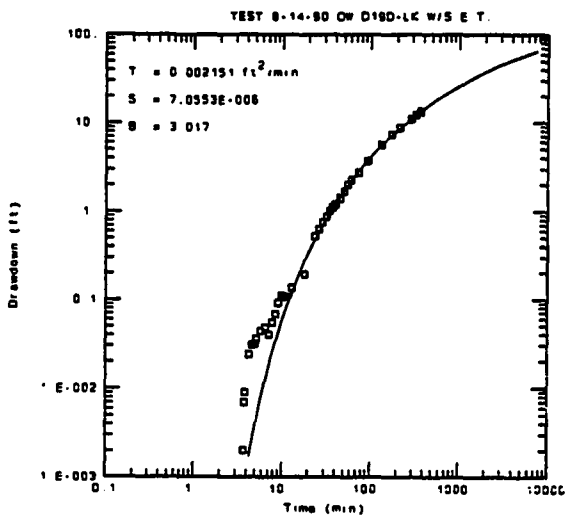
Aquifer 8-14-90

The graphical curve matches of data from observation wells D19D during test 8-14-90 are presented in Figure 7-15 for the Theis and modified Hantush solutions. Applications of the Moench model with different combinations of the parameters are illustrated in Figure 7-16.

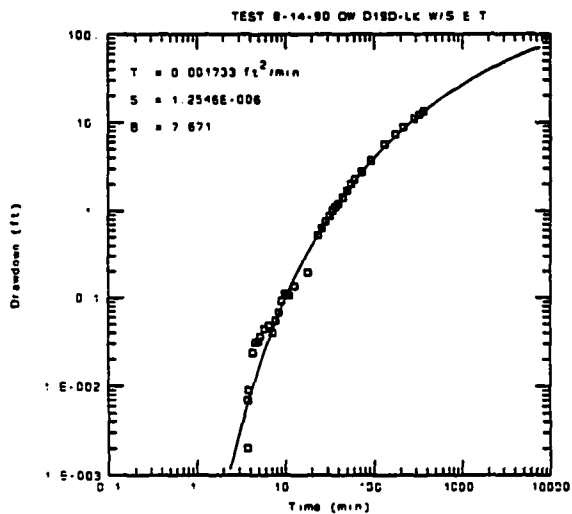
The Theis type curve only can be matched by a small portion of the data during the late period of the test ($t > 100$ minutes, Figure 7-15). This is not surprising because the W fracture zone behaves more like a double-porosity fractured medium than an equivalent porous medium. As is discussed in the previous section, the early drawdown is influenced by the larger T/S ratio of the fractures and deviates from the Theis type curve.



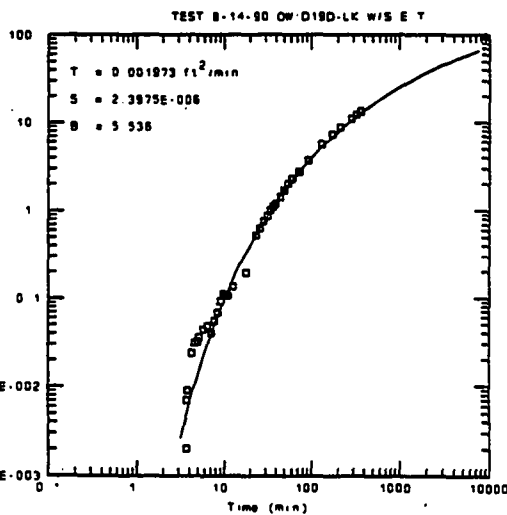
Theis Solution



Modified Hantush (leaky w/ Storage)

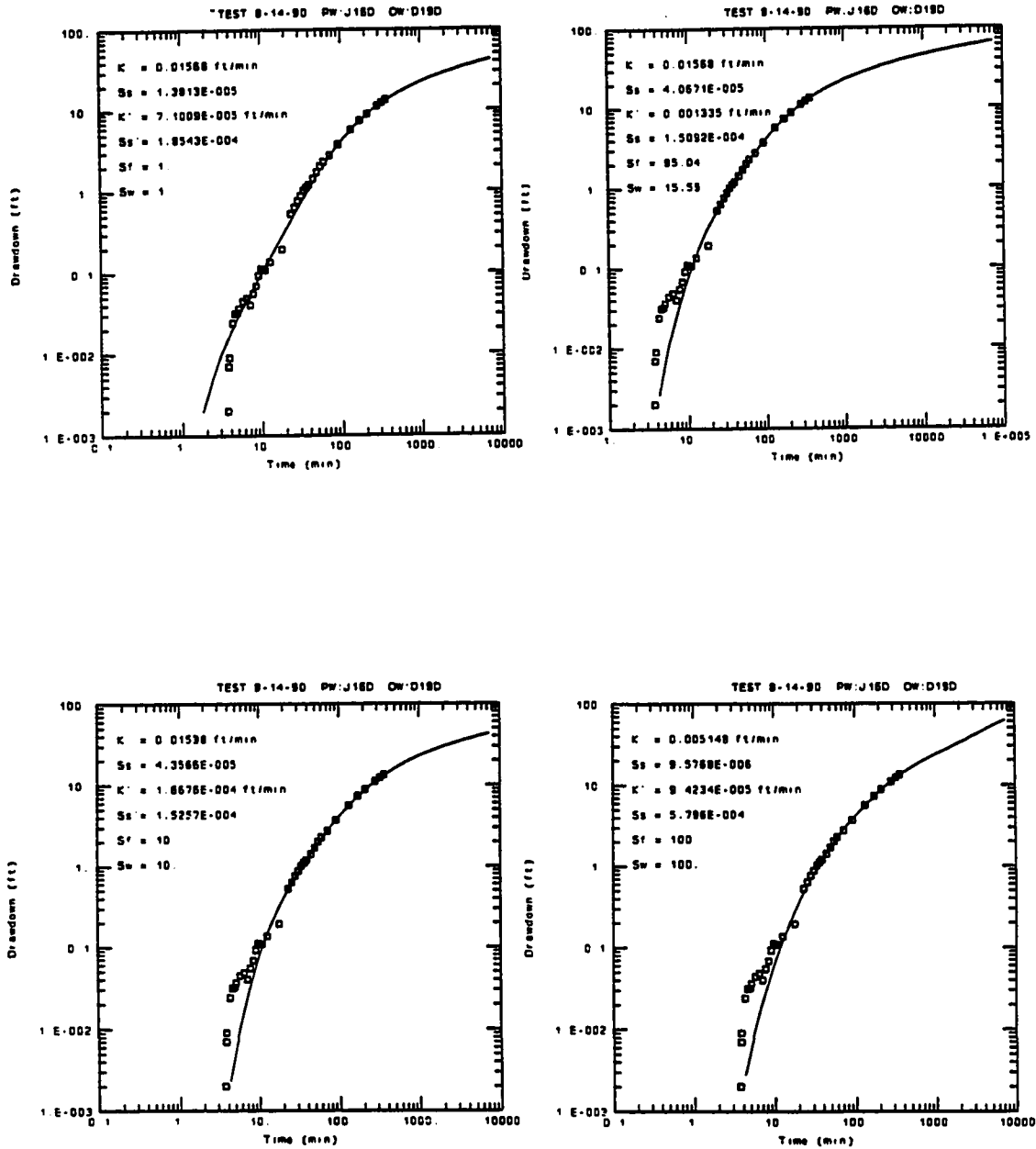


Modified Hantush (Leaky w/ Storage)



R = 144 feet

Figure 7-15. Graphical curve matching of observation well D19D data with the Theis and modified Hantush models during test 8-14-90



R = 144 feet

Figure 7-16. Graphical curve matching of observation well D19D data with the Moench model during test 8-14-90

This deviation is more significant if the fractured rock shows a strong double-porosity behavior and the REV of the aquifer is large.

Three alternative curve matches of D19D data by the modified Hantush model are presented in Figure 7-15. All three type curves defined by different combinations of the hydraulic parameters (T , S and β) match the data reasonably well. These matches can be understood by the similarity of the hydraulic behavior of two conceptual models of double-porosity and leaky aquifer with storage in the aquitard. The similarity of two conceptual models is discussed in detail in chapter IV.

The graphical curve matches of D19D data by the Moench double-porosity with fractured skin model (Figure 7-16) are accomplished by manual match with assistance of the statistical estimation approaches provided by the computer software AQTESOLV. As a major weak point, the Moench model can generate many similar type curves with different combinations of the six hydraulic parameters (K , S_s , K' , S_s' , S_f and S_w). Therefore, there is no unique solution or unique type curve match with the Moench model. The data of D19D are matched by several type curves of the Moench model; Figure 7-16 shows some examples of these matches.

The estimated hydraulic parameters using the Theis and modified Hantush models and D19D data are presented in Table 7-12. The aquifer T and S values calculated by the Theis solution are significantly higher than those from the modified Hantush solution. The Theis method generally is not valid for analysis of the W aquifer test data; the Theis solutions are presented in Table 7-12 only for purpose of comparison. Interestingly enough, the T values of the W aquifer estimated using the modified Hantush model are consistent but the S values are inversely proportional to the β values (Table 7-12).

Table 7-12. Estimated Aquifer Parameters by Theis and Modified Hantush Models with Well D19D Data, Aquifer Test 8-14-90

(Pumping Well J16D, R=144 ft)

METHOD	T (ft ² /d)	S	β	$\sqrt{\frac{K'S_0}{TS}}$ (1/ft)
THEIS	26	1.9×10^{-4}		
MODIFIED HANTUSH (Leaky w/s)	3	7×10^{-6}	3	0.08
	3	2.4×10^{-6}	5.5	0.15
	2.4	1.3×10^{-6}	7.7	0.21

Nine estimates of hydraulic parameters are obtained with the Moench model by changing the combinations of the six parameters. A summary of the results is presented in Table 7-13. The first row of the estimates is obtained by changing the values of all six parameters; the remainder of the estimates is gained by giving different combinations of dimensionless parameters S_F and S_W and alternating the remaining parameters. The combinations of two dimensionless parameters (S_F and S_W) were selected within a range of reasonable values. The purpose of these matches with selected S_F and S_W values is to illustrate significance of the two parameters on the graphical curve matches of the data. The geometric mean values of the hydraulic parameters estimated from the nine "best matches" of the Moench type curves are calculated and tabulated in the last row of Table 7-13.

Table 7-13. Estimated Aquifer Parameters by Moench Model with Application of Well D19D Data of Aquifer Test 8-14-90

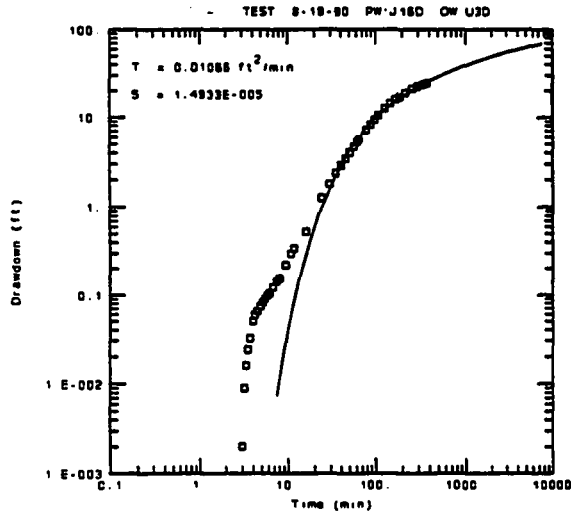
(Pumping Well J16D, R=144 ft)

Sf	Sw	K (ft/d)	Ss (1/ft)	K' (ft/d)	Ss' (1/ft)	$\sqrt{KK'}$ (ft/d)	$\sqrt{S_s S_s'}$ (1/ft)	REMARKS
95	16	23	4×10^{-5}	2	2×10^{-4}	6.6	7.8×10^{-5}	varying all six parameters
1	1	23	1×10^{-5}	0.11	2×10^{-4}	1.6	5.1×10^{-5}	giving Sf and Sw
5	5	22	5×10^{-5}	0.14	2×10^{-4}	1.7	8.5×10^{-5}	"
10	10	22	4×10^{-5}	0.24	2×10^{-4}	2.3	8.1×10^{-5}	"
100	100	7.3	1×10^{-5}	0.14	6×10^{-4}	1	7.4×10^{-5}	"
10	1	22	6×10^{-5}	0.29	2×10^{-4}	2.4	9.2×10^{-5}	"
1	10	26	10^{-9}	0.1	2×10^{-4}	1.6	1.3×10^{-9}	"
100	1	22	6×10^{-5}	2.9	2×10^{-4}	7.9	9.2×10^{-5}	"
0	0	26	1×10^{-9}	0.1	2×10^{-4}	1.6	1.4×10^{-9}	"
2.6	2.3	20	5×10^{-9}	0.27	2×10^{-4}	2.3	3.1×10^{-5}	geometric mean

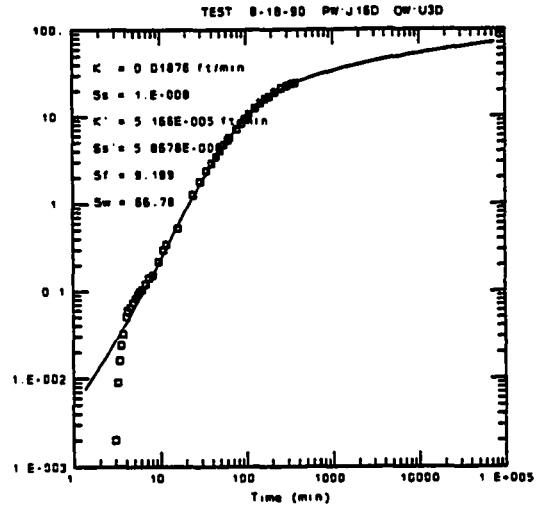
As shown in Table 7-13, the S_f and S_w have very little influence on the hydraulic conductivity values of the fissures (K) and specific storage values of the matrix blocks (S_s') except for $S_f=S_w=100$. Varying S_f and S_w values basically changes the specific storage of fissures (S_s) and hydraulic conductivity of the matrix blocks (K').

The graphical curve matches of observation well U3D data from the test 8-14-90 are presented in Figure 7-17 for the Theis, modified Hantush and Moench models. More alternative curve matches of Moench model to the U3D data are illustrated in Figure 7-18.

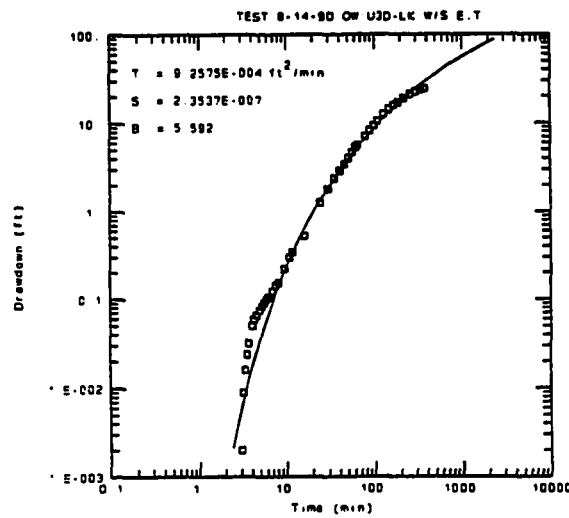
The type curve matches of U3D data by the Theis and modified Hantush solutions (Figure 7-17) are very similar to that of D19D data by the same analytical solutions (Figure 7-15). Very limited data points at the late



This Solution



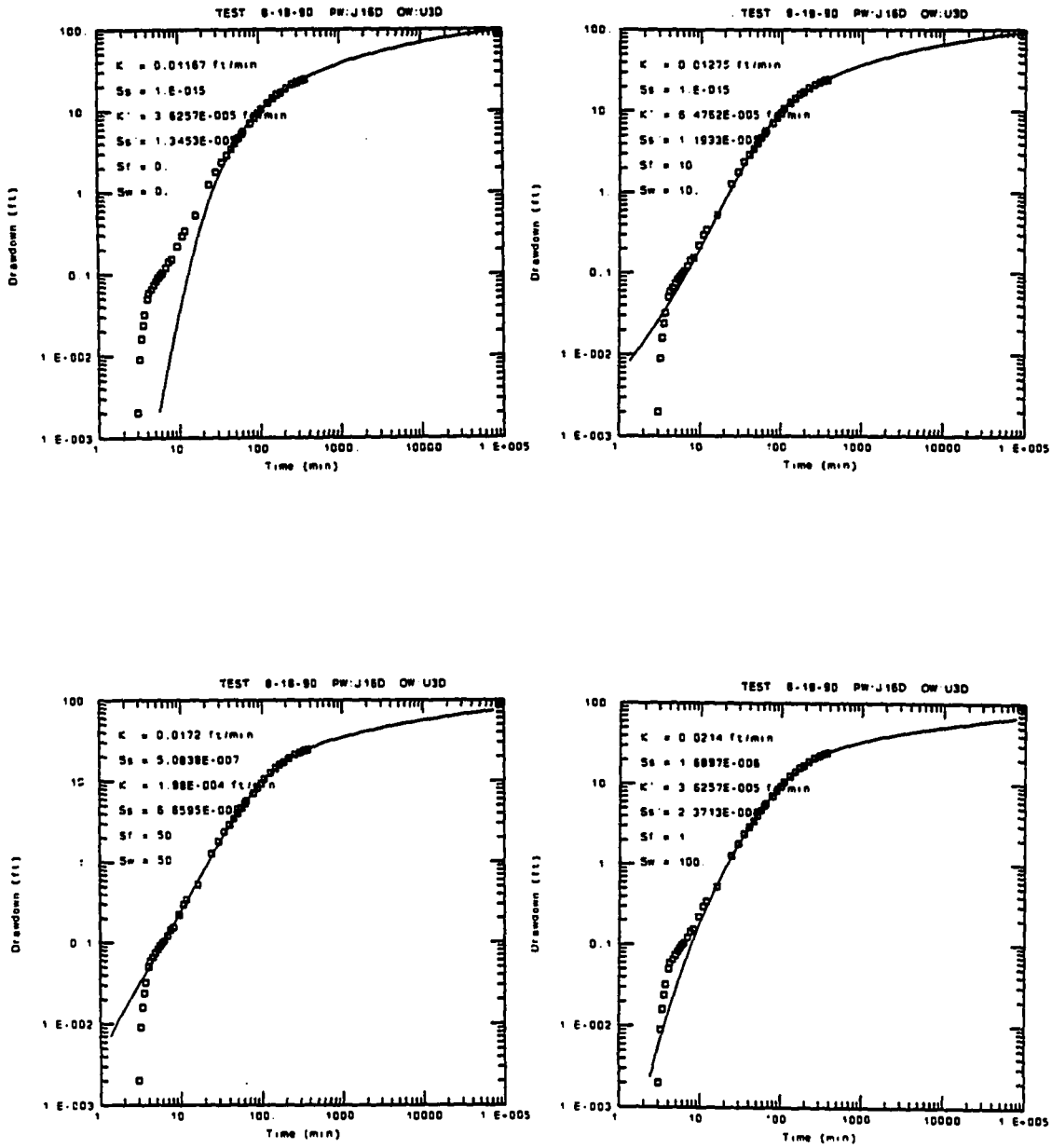
Moench Double-porosity w/ Fracture Skin



Modified Hantush (leaky w/ Storage)

R = 303 feet

Figure 7-17. Graphical curve matching of observation well U3D data with alternative analytical models during test 8-14-90



R = 303 feet

Figure 7-18. Graphical curve matching of observation well U3D data with the Moench model during test 8-14-90

time are matched by the Theis solution. The modified Hantush and Moench type curves are matched fairly well by the U3D data except for a few data points at the early time. The reason for the deviations of these data points from the modified Hantush and Moench type curves is unknown, but the heterogeneity of the fractured W aquifer may be one of the primary factors. Only one "best match" is obtained by the modified Hantush solution.

The data from well U3D during test 8-14-90 are matched by the Moench double-porosity model with different combinations of the six hydraulic parameters. Some examples of these matches are presented in Figure 7-18. Most of these matches are accomplished by using different combinations of S_f and S_w and changing the remaining parameters.

The estimated aquifer parameters by the Theis and modified Hantush models are tabulated in Table 7-14. The Theis solutions are presented only for purpose of the comparison; the T and S values estimated using the Theis model may not be meaningful because the model probably is not valid for analysis of data from the W aquifer tests.

Table 7-14. Estimated Aquifer Parameters by Theis and Modified Hantush Models with Well U3D Data, Aquifer Test 8-14-90

(Pumping Well J16D, R=303 ft)

METHOD	T (ft ² /d)	S	β	$\sqrt{\frac{k's'}{rS}}$ (1/ft)
THEIS	16	1.5×10^{-5}		
MODIFIED HANTUSH	1.3	2.4×10^{-7}	5.6	0.07

The calculated aquifer parameters using well U3D data with the Moench model are presented in Table 7-15. A total of eleven estimates of the aquifer parameters are obtained and tabulated. The first estimate (row one in Table 7-15) is obtained by changing all of the six parameters; the remainders are obtained by giving combination of S_F and S_W and changing the remaining parameters. The geometric mean of the eleven estimates is presented in the last row of Table 7-15.

Table 7-15. Estimated Aquifer Parameters by Moench Model with Application of Well U3D Data of Aquifer Test 8-14-90

(Pumping Well J16D, R=303 ft)

Sf	S _w	K (ft/d)	S _s (1/ft)	K' (ft/d)	S _s ' (1/ft)	$\sqrt{KK'}$ (ft/d)	$\sqrt{S_F S_W}$ (1/ft)	REMARKS
9	67	27	10 ⁻⁸	0.075	6x10 ⁻⁶	1.4	2.4x10 ⁻⁷	varying all six parameters
10	0	16	10 ⁻⁸	0.19	1x10 ⁻⁵	1.7	3.7x10 ⁻⁷	giving Sf and Sw
10	10	17	10 ⁻¹⁵	0.09	1x10 ⁻⁵	1.3	1.1x10 ⁻¹⁰	"
1	1	17	2x10 ⁻⁷	0.05	1x10 ⁻⁵	1	1.8x10 ⁻⁶	"
50	50	25	5x10 ⁻⁷	0.27	7x10 ⁻⁶	2.6	1.8x10 ⁻⁶	"
100	1	17	4x10 ⁻¹⁵	1.6	1x10 ⁻⁵	5.2	2.1x10 ⁻¹⁰	"
100	100	30	4x10 ⁻⁷	6.2	4x10 ⁻⁶	13.7	1.2x10 ⁻⁶	"
10	100	30	4x10 ⁻⁷	0.6	4x10 ⁻⁶	4.3	1.2x10 ⁻⁶	"
1	10	19	1x10 ⁻⁸	0.05	10 ⁻⁵	1	3.7x10 ⁻⁶	"
1	100	30	2x10 ⁻⁸	0.05	2x10 ⁻⁶	1.3	2x10 ⁻⁶	"
0	0	17	10 ⁻¹⁵	0.05	1x10 ⁻⁵	1	1.1x10 ⁻¹⁰	"
9.3	11	22	1x10 ⁻⁸	0.19	8x10 ⁻⁶	2.1	1x10 ⁻⁷	geometric mean

As shown in Table 7-15, the changes in S_F and S_W values do not have much influence on the fissure hydraulic conductivity (K) and matrix specific storage (S_s'). The significant influence of S_F on the matrix

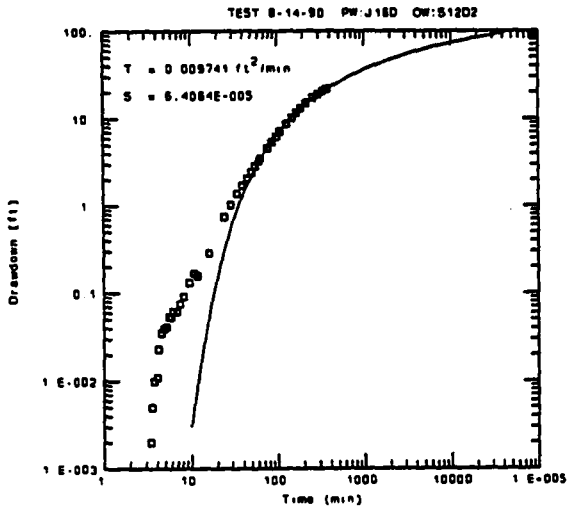
hydraulic conductivity (K') is understandable because S_F is directly proportional to K' by the definition. However, the impact on the fissure specific storage (S_s) by varying S_F and S_W is difficult to understand.

The curve matches of the same analytical models (Theis, Moench and modified Hantush) with well S12D2 data during test 8-14-90 are illustrated in Figure 7-19. Two matches by the modified Hantush model with different β values are obtained. More examples of alternative curve matches by the Moench model with assigned S_F and S_W values are presented in Figure 7-20.

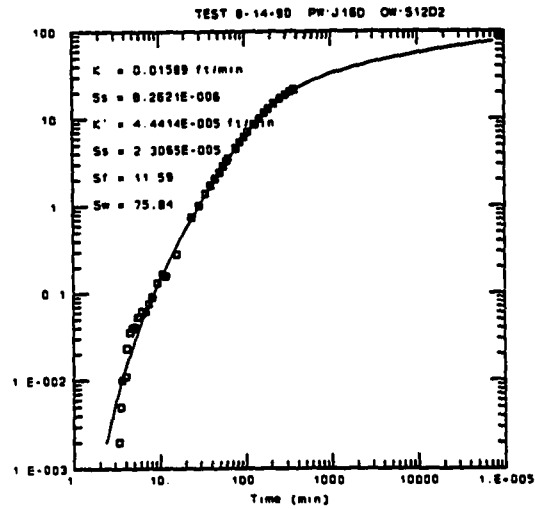
The characteristics of type curve matching of S12D2 data are almost identical to that of the graphical curve matches of D19D and U3D data. The modified Hantush and Moench type curves match the data well except for a few data at the early time. The Theis model probably is not applicable because the type curve is matched only by a small portion of the data at late times (Figure 7-19).

As shown in Figure 7-20, the normal double-porosity model ($S_F=S_W=0$) has a poor match with S12D2 data; only a few data points at the late time are matched by the type curve. This probably indicates that the fracture skin effect occurs in the fractured basalt at the UIGRS and that this fracture skin factor has some influence on the hydraulic behavior of the W aquifer. The same feature is observed from the well U3D data (Figure 7-18).

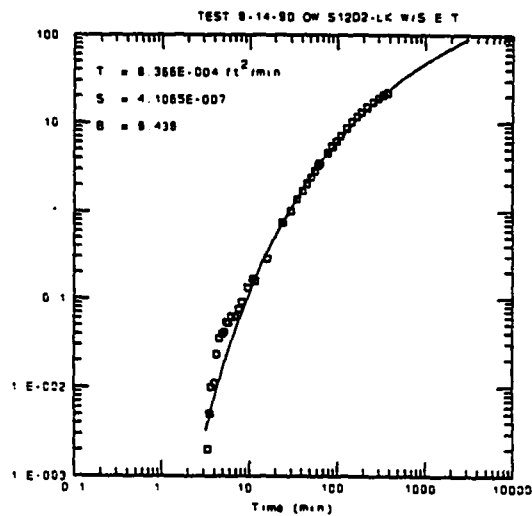
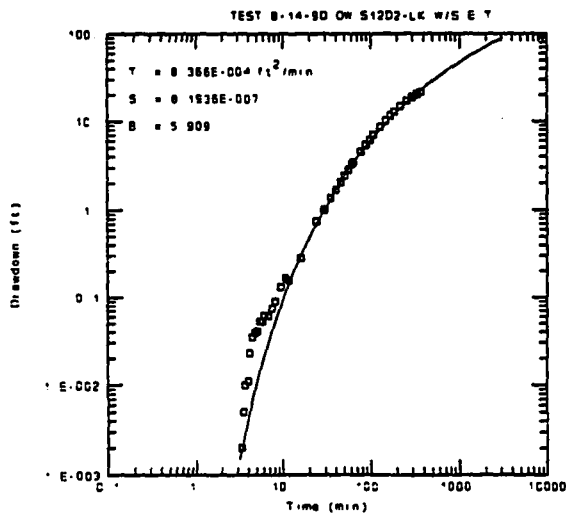
The estimated aquifer parameters by the Theis and modified Hantush models with S12D2 data are presented in Table 7-16. Again, the Theis solution probably is not valid. For the modified Hantush solutions, changing β values has no influence on the aquifer T values; the estimated S values are inversely proportional to the β values.



Theis Solution



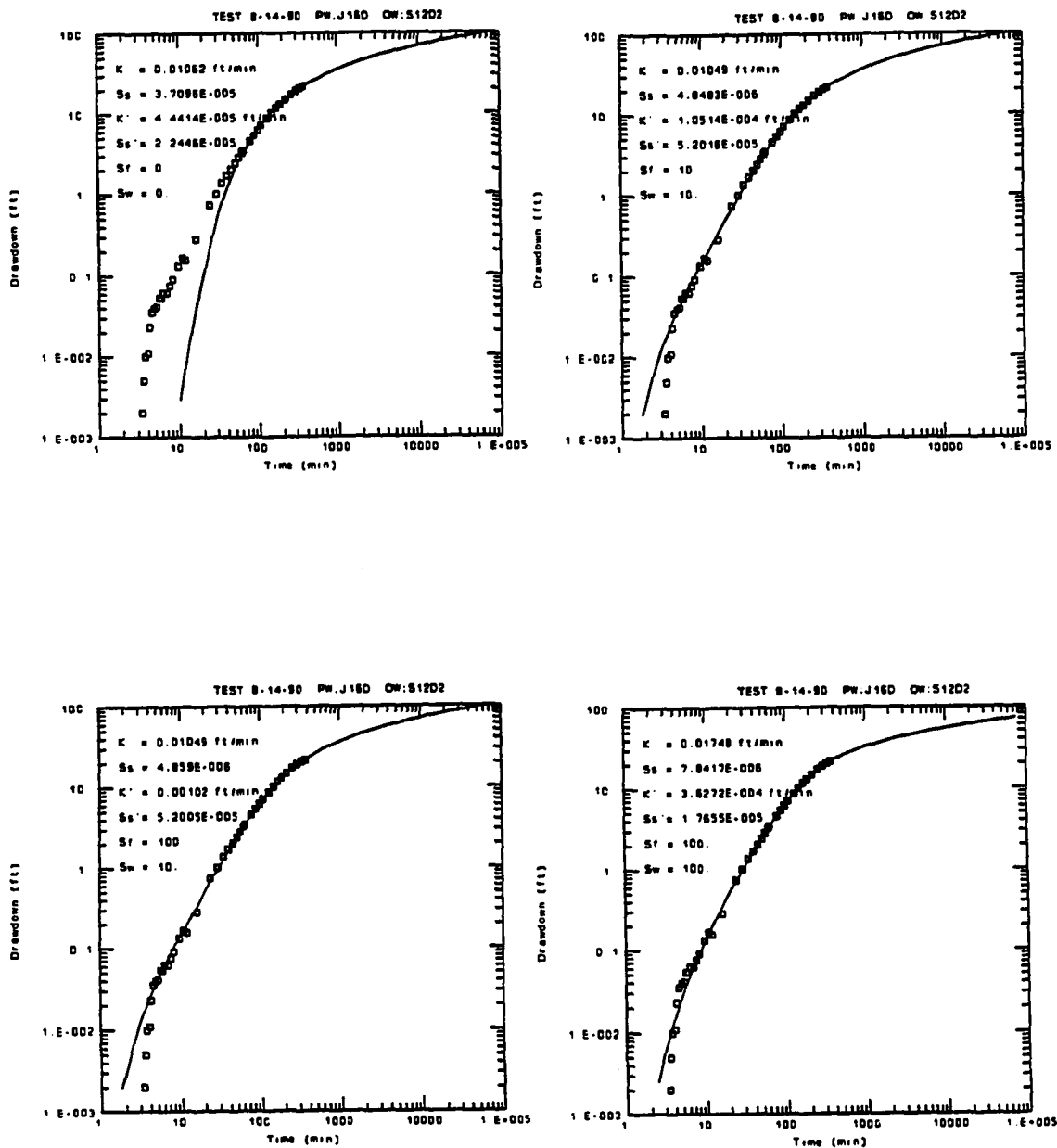
Moench Double-porosity w/ Fracture Skin



Modified Hantush (Leaky w/ Storage)

R = 181 feet

Figure 7-19. Graphical curve matching of observation well S12D2 data with alternative analytical models during test 8-14-90



R = 181 feet

Figure 7-20. Graphical curve matching of observation well S12D2 data with the Moench model during test 8-14-90

Table 7-16. Estimated Aquifer Parameters by Theis and Modified Hantush Models with Well S12D2 Data, Aquifer Test 8-14-90

(Pumping Well J16D, R=181 ft)

METHOD	T (ft ² /d)	S	β	$\sqrt{\frac{K'S_s'}{TS}}$ (1/ft)
THEIS	14	6.4×10^{-5}		
MODIFIED HANTUSH (Leaky w/s)	1.2	8.2×10^{-7}	5.9	0.13
	1.2	4×10^{-7}	8.4	0.19

Ten estimates of the hydraulic parameters from well S12D2 data by the Moench model with different combinations of S_f and S_w values are presented in Table 7-17. The same methodology is applied to obtain the alternative estimates. The geometric means of all estimates also are presented in Table 7-17.

Table 7-17. Estimated Aquifer Parameters by Moench Model with Application of Well S12D2 Data of Aquifer Test 8-14-90

(Pumping Well J16D, R=181 ft)

Sf	Sw	K (ft/d)	Ss (1/ft)	K' (ft/d)	Ss' (1/ft)	$\sqrt{KK'}$ (ft/d)	$\sqrt{S_s S_s'}$ (1/ft)	REMARKS
12	76	23	8×10^{-9}	0.06	2×10^{-5}	1.2	1.4×10^{-5}	varying all parameters
10	10	14	5×10^{-9}	0.14	5×10^{-5}	1.4	1.6×10^{-5}	giving Sf and Sw
1	1	14	3×10^{-9}	0.06	6×10^{-5}	.95	1.3×10^{-5}	"
100	100	25	8×10^{-9}	0.5	2×10^{-5}	3.6	1.2×10^{-5}	"
10	100	26	2×10^{-5}	0.06	2×10^{-9}	1.3	6×10^{-9}	"
1	10	17	5×10^{-5}	0.06	10^{-9}	1.1	7.2×10^{-9}	"
0	0	14	4×10^{-5}	0.06	2×10^{-5}	.95	2.9×10^{-5}	"
100	1	14	1×10^{-9}	2.6	6×10^{-5}	6	8.7×10^{-9}	"
100	10	14	5×10^{-9}	1.4	5×10^{-5}	4.5	1.6×10^{-5}	"
10	1	14	1×10^{-9}	0.27	6×10^{-5}	2	8.5×10^{-9}	"
10	7.7	17	7×10^{-9}	0.19	2×10^{-5}	1.8	1.2×10^{-5}	geometric mean

Aquifer Test 8-17-90

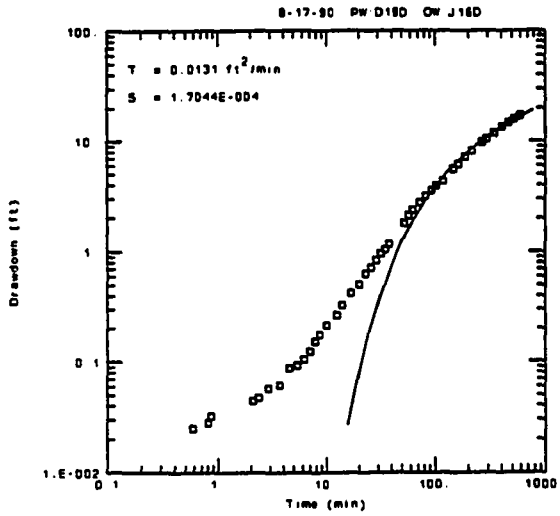
The hydraulic parameter estimates are obtained using the data of three observation wells (J16D, S12D2 and U3D) from the 8-17-90 test. The quality of the data is questionable because of significant disturbances in the drawdown responses with wells S12D2 and U3D and unavailable hand measurements.

The graphical curve matches of the Theis and modified Hantush solutions with well J16D data are illustrated in Figure 7-21. The alternative curve matches by the Moench double-porosity with fracture skin model with the same data are presented in Figure 7-22.

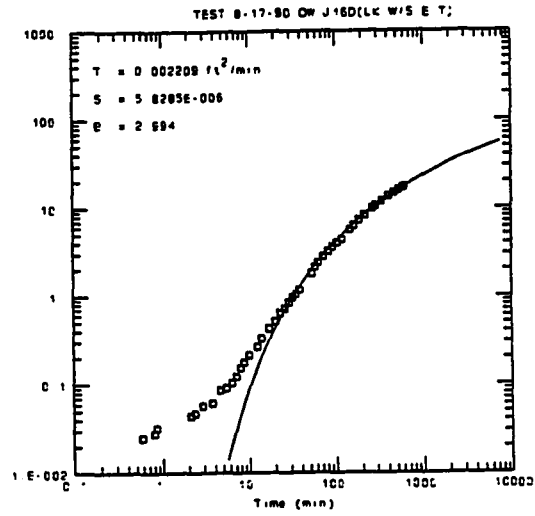
Three graphical curve matches by the modified Hantush solution are obtained with different β values (Figure 7-21). As with the previous data, the modified Hantush type curves provide better matches with the data than the Theis type curve but the early data still can not be included in the matches (Figure 7-21). The early data are not considered to be important because of two reasons: 1) the early drawdown is out of the precision limits of the pressure transducers, and 2) the aquifer heterogeneity has strong impacts on early drawdown.

The parameter calculation results with the Theis and modified Hantush models are presented in Table 7-18. The results estimated by the modified Hantush method show that leakage from the aquitards was very significant during the test. The aquifer T is not affected by varying the β values but the estimated storativity decreases with increasing of the β value. The Theis solution is not valid for the W aquifer.

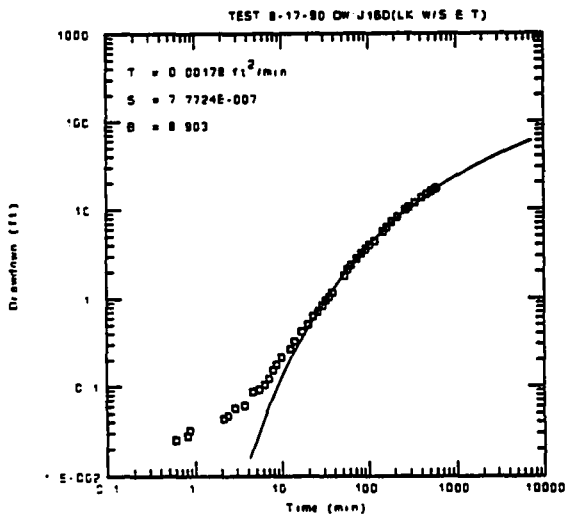
The alternative curve matches by the Moench model shown in Figure 7-22 are obtained by changing all six hydraulic parameters because giving certain S_f and S_w values can not provide good matches of type curves to the



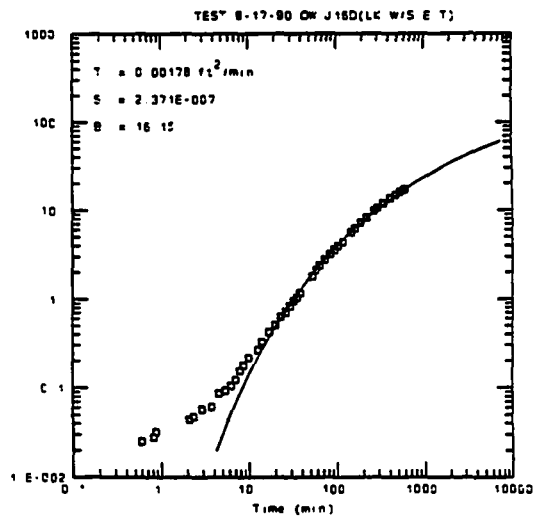
Theis Solution



Modified Hantush (leaky w/ Storage)

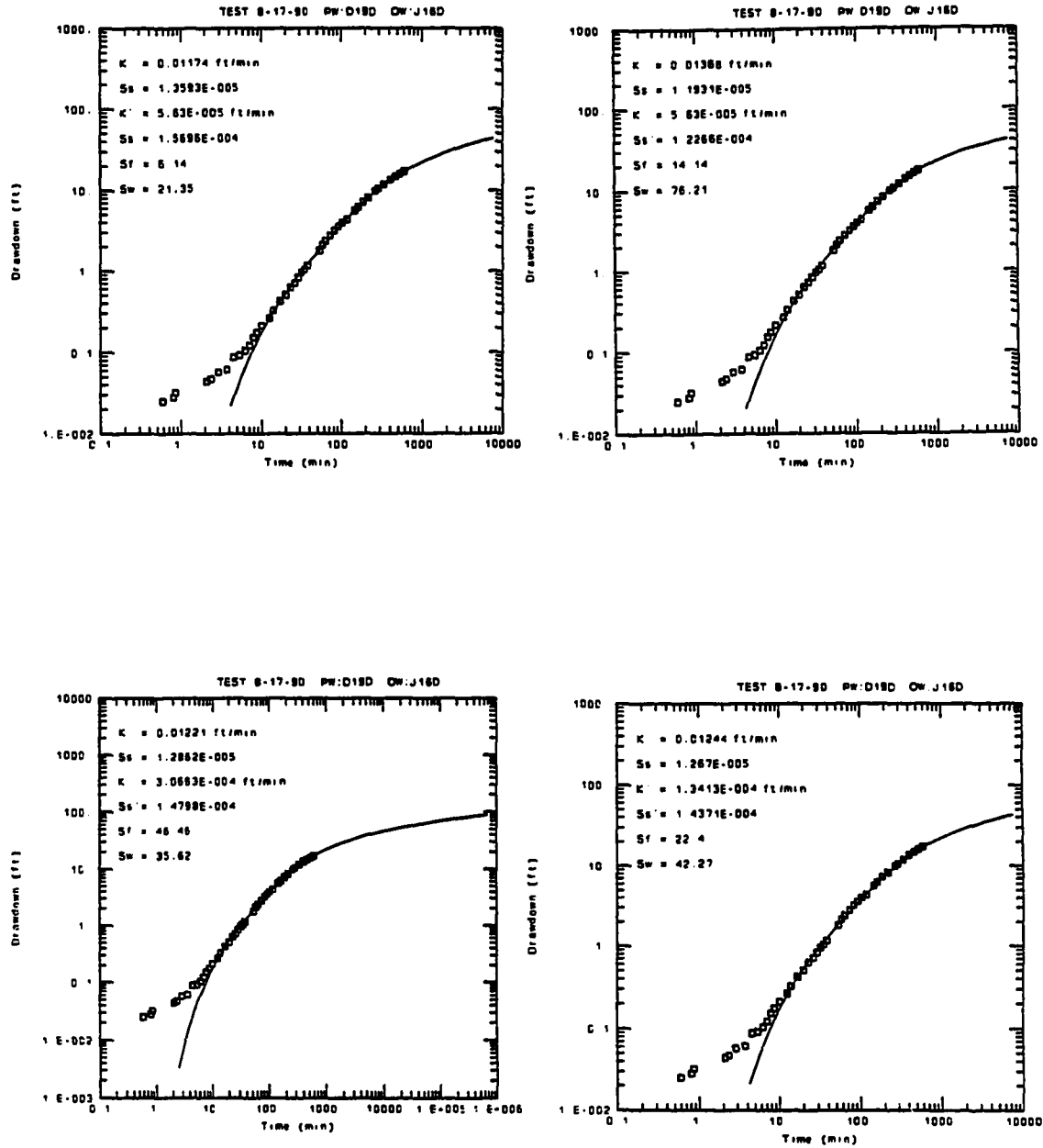


Modified Hantush (Leaky w/ Storage)



R = 144 feet

Figure 7-21. Graphical curve matching of observation well J16D data with the Theis and modified Hantush models during test 8-17-90



R = 144 feet

Figure 7-22. Graphical curve matching of observation well J16D data with the Moench model during test 8-17-90

data. The early data can not be matched by any of the type curves. The results of four matches are close and the estimated parameters are presented in Table 7-19.

Table 7-18. Estimated Aquifer Parameters by Theis and Modified Hantush Models with Well J16D Data, Aquifer Test 8-17-90

(Pumping Well D19D, R=144 ft)

METHOD	T (ft ² /d)	S	β	$\sqrt{\frac{K'S'}{TS}}$ (1/ft)
THEIS	19	1.7×10^{-4}	-	-
MODIFIED HANTUSH (Leaky w/s)	3	5.8×10^{-6}	3	0.08
	2.6	7.8×10^{-7}	8.9	0.25
	2.6	2.4×10^{-7}	16.2	0.45

Table 7-19. Estimated Aquifer Parameters by Moench Model with Application of Well J16D Data, Aquifer Test 8-17-90

(Pumping Well D19D)

Sf	Sw	K (ft/d)	Ss (1/ft)	K' (ft/d)	Ss' (1/ft)	$\sqrt{KK'}$ (ft/d)	$\sqrt{S_s S'_s}$ (1/ft)	REMARKS
14	76	20	1×10^{-5}	0.08	1×10^{-4}	1	3.8×10^{-5}	varying all six parameters
47	36	17	1×10^{-5}	0.4	2×10^{-4}	3	4.4×10^{-5}	"
22	42	17	1×10^{-5}	0.2	1×10^{-4}	2	4.3×10^{-5}	"
6	21	17	1×10^{-5}	0.08	2×10^{-4}	1	4.7×10^{-5}	"
17	40	18	1×10^{-5}	0.15	1×10^{-4}	1.7	4.3×10^{-5}	geometric mean

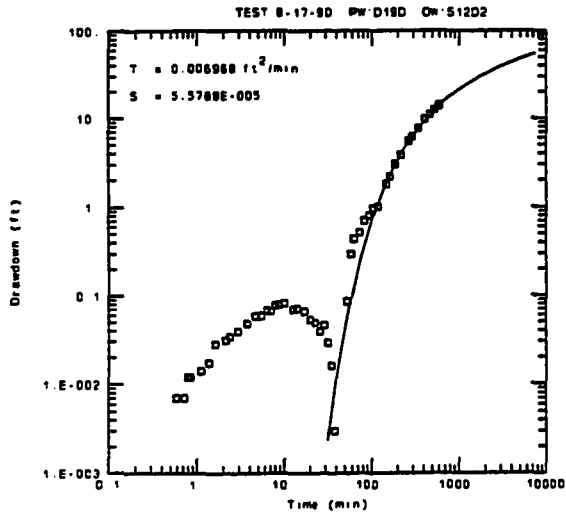
The graphical curve matches of observation wells S12D2 and U3D data during test 8-17-90 by the three analytical models (Theis, modified Hantush and Moench) are presented in Figures 7-23 and 7-24. As mentioned earlier, all the data points can not be matched because of a disturbance caused by unknown factors. The late portion of the data is used for the type curve matches and parameter calculation. However, the curve matches (Figures 7-23 and 7-24) and hydraulic parameter estimates probably are not reliable. Therefore, the analysis results from wells S12D2 and U3D data during test 8-17-90 are not presented in this study.

The early time data of S12D2 from test 8-17-90 have a disturbance pattern similar to that of transducer measurements from test 8-14-90, which are presented in Figure 5-2 in comparison with hand measurements. Thus, the observed drawdown disturbances of wells S12D2 and U3D likely resulted from the measurement error by pressure transducers.

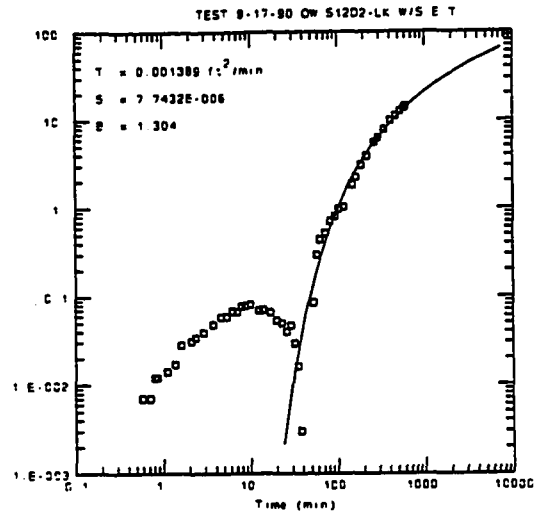
Aquifer Test 3-8-91

The graphical curve matches and parameter estimation of aquifer test 3-8-91 data are based upon the Theis, modified Hantush and Moench models. In addition to the three observation wells (J16D, D19D and S12D2), pumping well U3D data also are analyzed using the semi-log method of the Theis model (Cooper and Jacob, 1946) and the Moench pumping well solution.

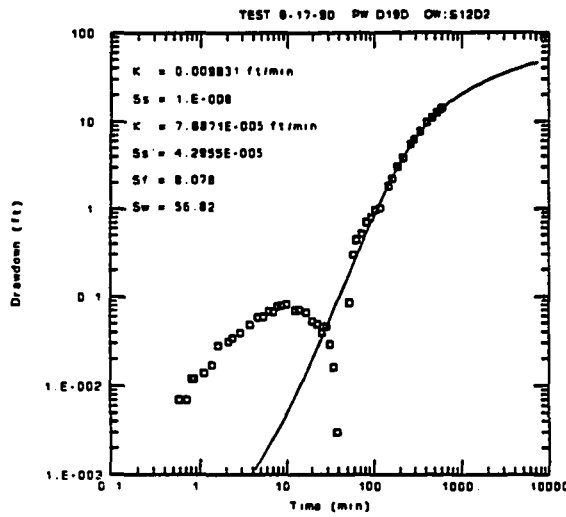
The Cooper-Jacob solution and the Moench type curve match with pumping well U3D data are presented in Figure 7-25. The late time data from the pumping well show a clearly straight line in the semi-log graph. The Moench pumping well solution also matches the late data very well but deviates remarkably from early data. Because the Moench pumping well solution considers the well bore storage but not the well loss, the early



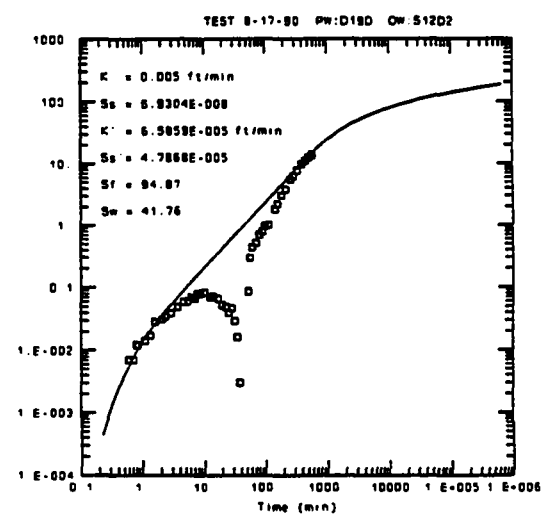
Theis Solution



Modified Hantush (Leaky w/ Storage)

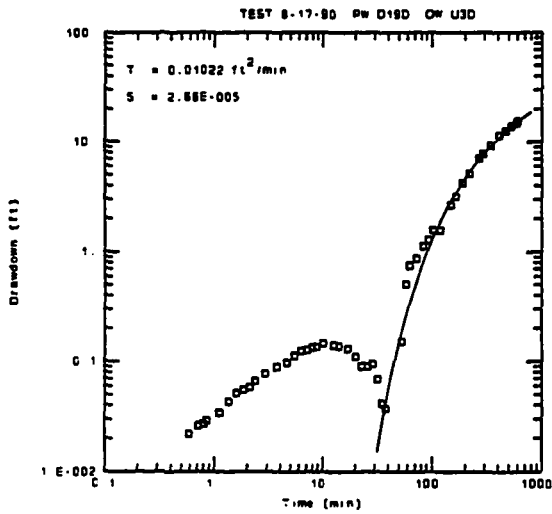


Moench Double-porosity w/ Fracture Skin

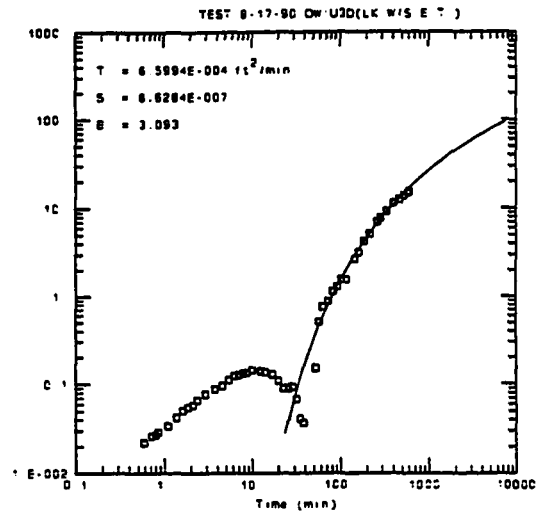


R = 325 feet

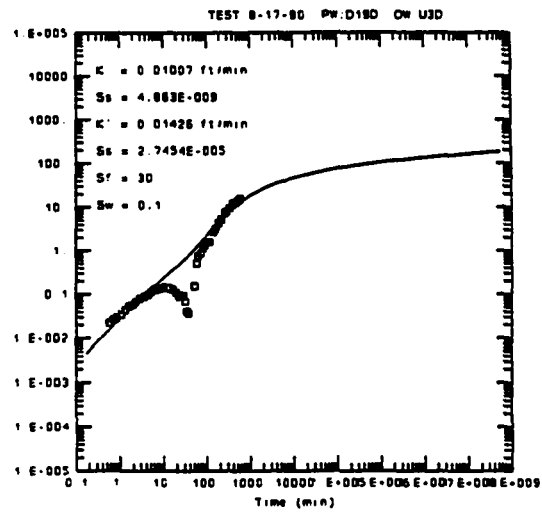
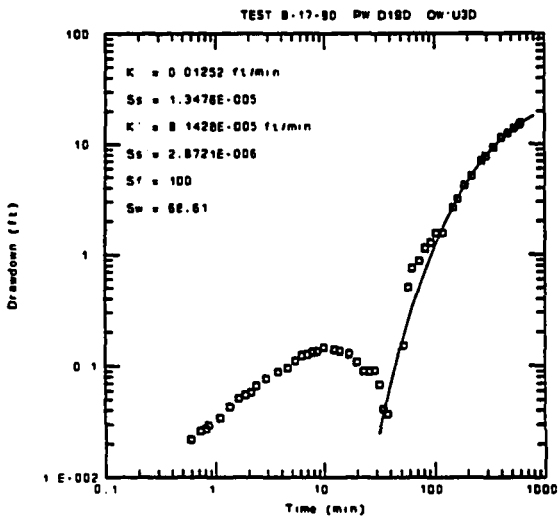
Figure 7-23. Graphical curve matching of observation well S12D2 data with alternative analytical models during test 8-17-90



Theis Solution



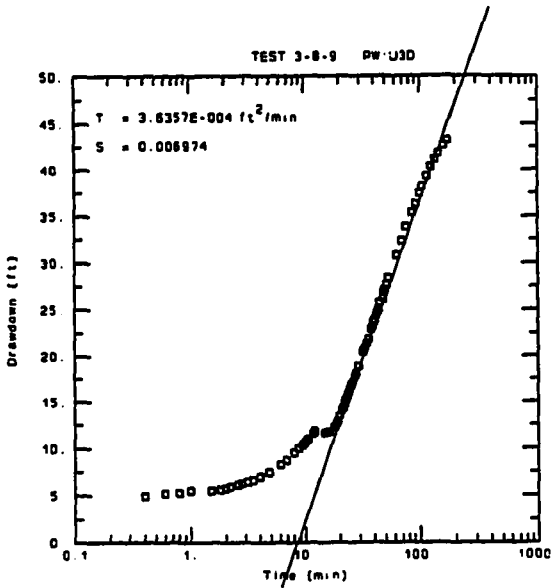
Modified Hantush (leaky w/ Storage)



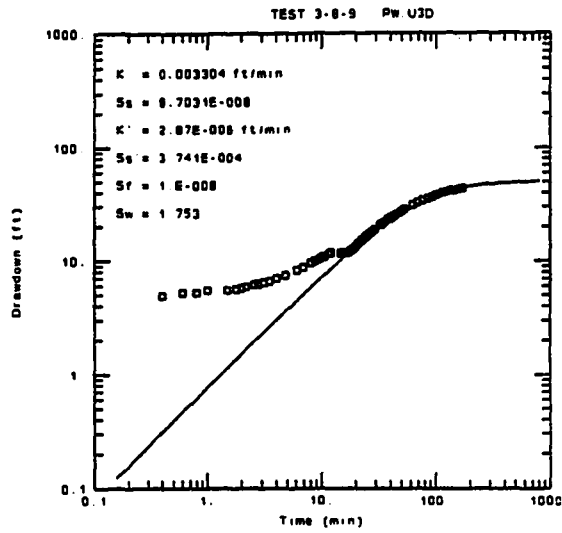
Moench Double-porosity w/ Fracture Skin

R = 441 feet

Figure 7-24. Graphical curve matching of observation well U3D data with alternative analytical models during test 8-17-90

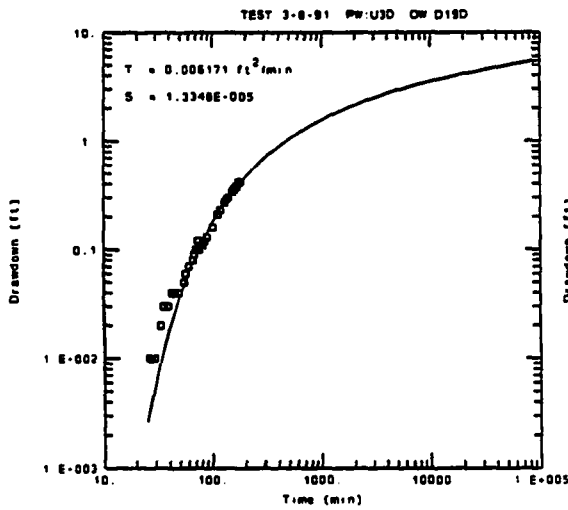


Cooper-Jacob Solution (semi-log)

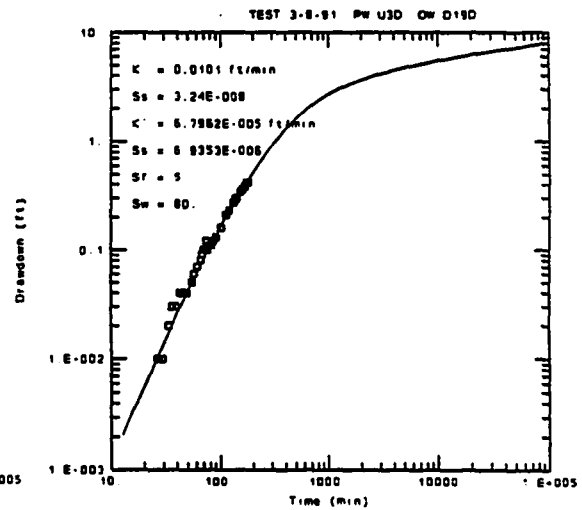


Moench Double-porosity w/ Fracture Skin

Figure 7-25. Graphical curve matching of pumping well U3D data with the Jacob straight line and Moench models during test 3-8-91



Theis Solution



Moench Double-porosity w/ Fracture Skin

R = 441 feet

Figure 7-26. Graphical curve matching of observation well D19D data with the Theis and Moench models during test 3-8-91

data deviation from the type curve may be caused markedly by the well loss.

The graphical curve matches of observation well D19D data with the Theis and Moench solutions are illustrated in Figure 7-26. The Theis type curve matches closely with the late data of well D19D but not the early data. The data are matched reasonably well by the Moench model; only one "best match" of the Moench type curves is obtained using well D19D data (Figure 7-26).

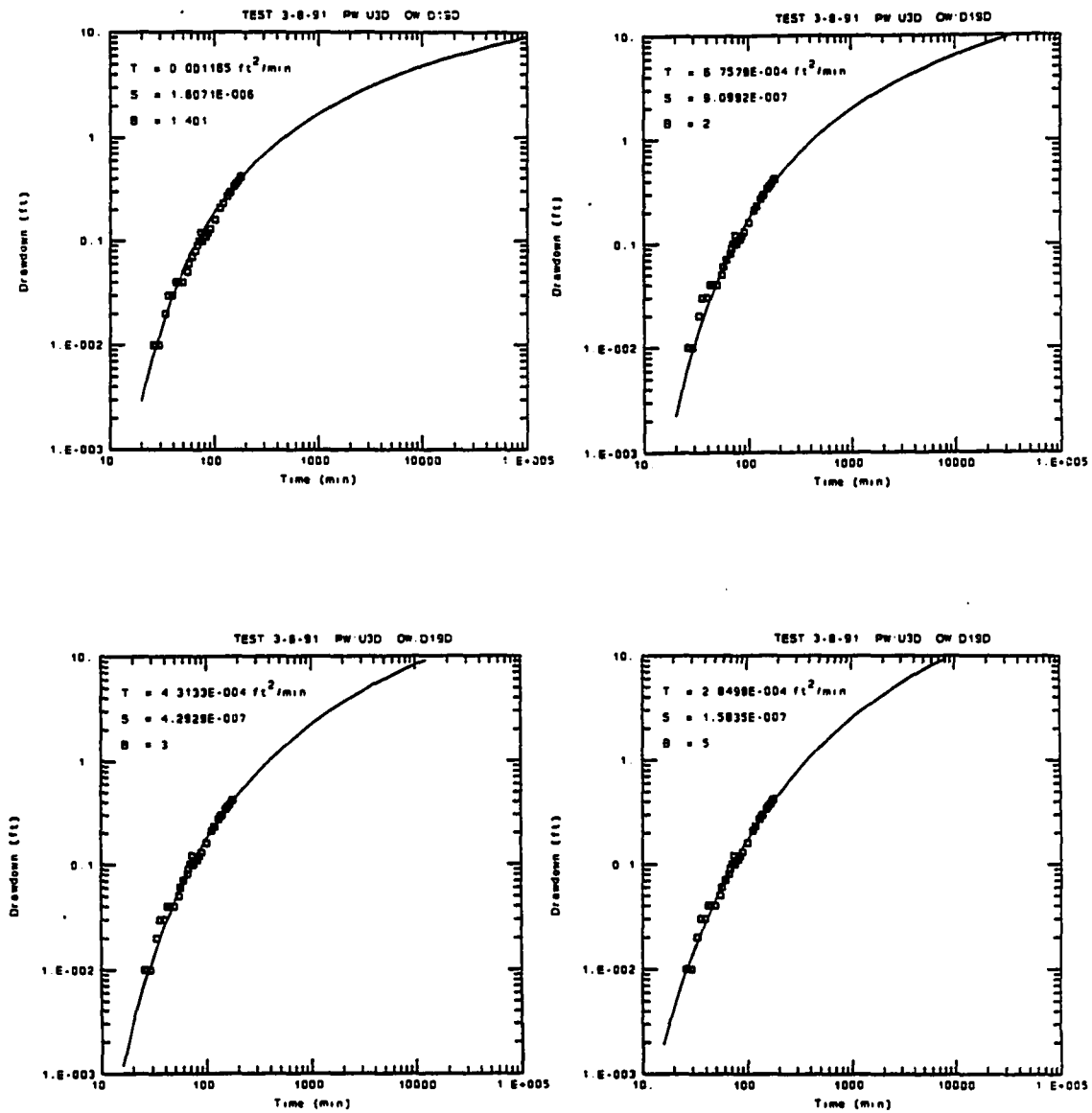
The application of the modified Hantush model to well D19D data is presented in Figure 7-27. Four different β values are selected with four sets of aquifer T and S values to obtain the "best matches" to the data. All the type curves match well with well D19D data (Figure 7-27).

The estimated aquifer parameters via the Theis and modified Hantush models with D19D data are presented in Table 7-20. The Moench results for well D19D are presented later along with the results for the pumping well U3D and the other observation wells (J16D and S12D2) in Table 7-22.

Table 7-20. Estimated Aquifer Parameters by Theis and Modified Hantush Models with Well D19D Data, Aquifer Test 3-8-91

(Pumping Well U3D, R=441 ft)

METHOD	T (ft ² /d)	S	β	$\sqrt{\frac{k's'}{TS}}$ (1/ft)
THEIS	9	1.3×10^{-5}	-	-
MODIFIED HANTUSH (Leaky w/s)	1.7	1.6×10^{-6}	1.4	0.013
	1	9.1×10^{-7}	2	0.018
	.6	4.3×10^{-7}	3	0.03
	.4	1.6×10^{-7}	5	0.05



$R = 441$ feet

Figure 7-27. Graphical curve matching of observation well D19D data with the modified Hantush model during test 3-8-91

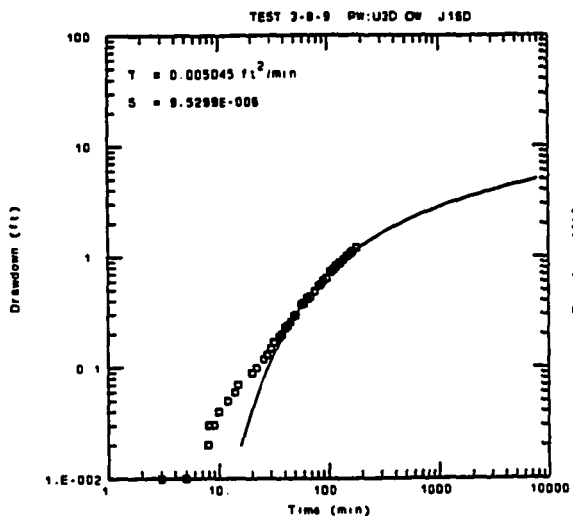
The graphical curve matches of the three analytical models (Theis, modified Hantush and Moench) with observation wells J16D and S12D2 data are demonstrated in Figures 7-28 and 7-29. The Theis type curve can only be matched with the late portions of the both data sets. The overall matches of both J16D and S12D2 data with the modified Hantush and Moench models are good. Only one "best fit" of the Moench type curve with each of J16D and S12D2 data is obtained (Figures 7-28 and 7-29).

The estimated aquifer parameters using the Theis and modified Hantush models with J16D and S12D2 data are tabulated in Table 7-21. The aquifer T values calculated using the modified Hantush model are fairly consistent. A large range of the aquifer S values is obtained.

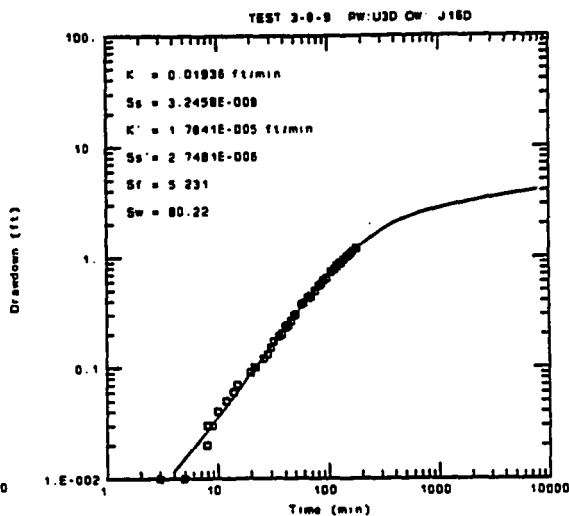
Table 7-21. Estimated Aquifer Parameters by Theis and Modified Hantush Models with Wells J16D and S12D2 Data, Aquifer Test 3-8-91

(Pumping Well U3D)

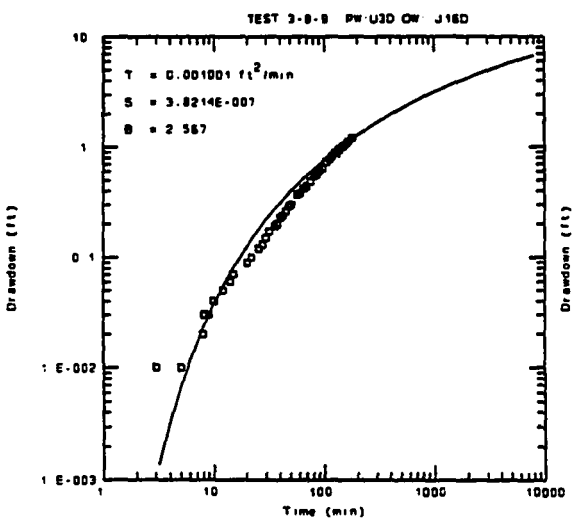
OBS. WELL	METHOD	T (ft ² /d)	S	β	$\sqrt{\frac{K'S'}{TS}}$ (1/ft)
J16D (R=303 ft)	THEIS	7	1.0×10^{-5}	-	-
	MODIFIED HANTUSH (Leaky w/s)	1.4	3.8×10^{-7}	2.6	0.034
		0.8	3.3×10^{-7}	3	0.04
		1	1.3×10^{-7}	4.8	0.06
		0.7	1.3×10^{-7}	5	0.07
		0.8	5.0×10^{-9}	26.3	0.035
S12D2 (R=155 ft)	THEIS	5	6.3×10^{-5}	-	-
	MODIFIED HANTUSH (Leaky w/s)	1	8.8×10^{-6}	1.2	0.03
		0.3	1.8×10^{-6}	3.2	0.08
		0.2	7.5×10^{-7}	5	0.13



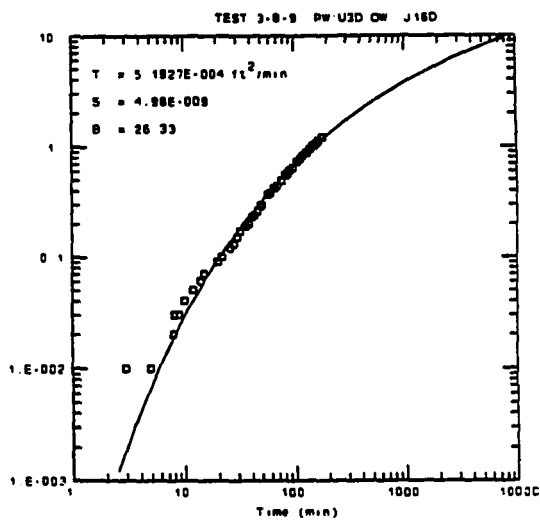
Theis Solution



Moench Double-porosity w/ Fracture Skin

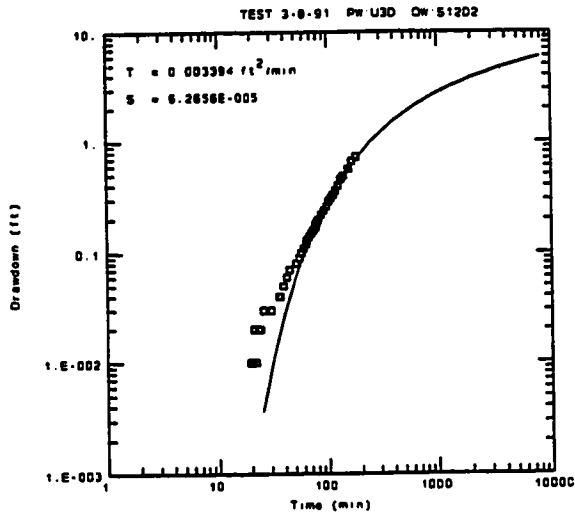


Modified Hantush (Leaky w/ Storage)

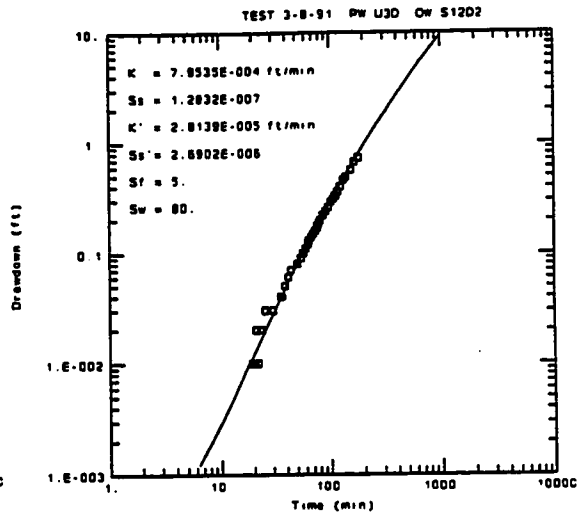


R = 303 feet

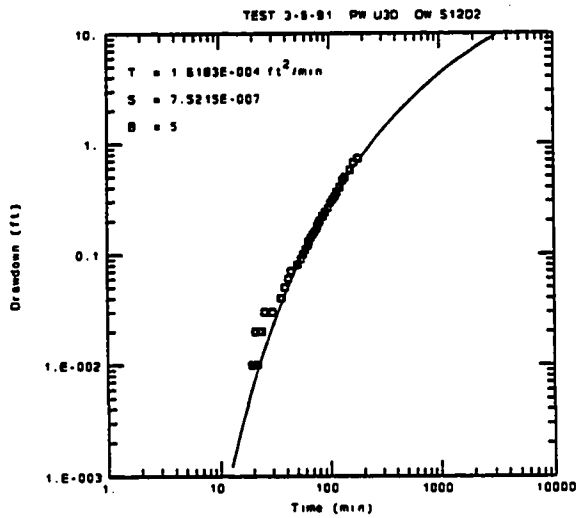
Figure 7-28. Graphical curve matching of observation well J16D data with alternative analytical models during test 3-8-91



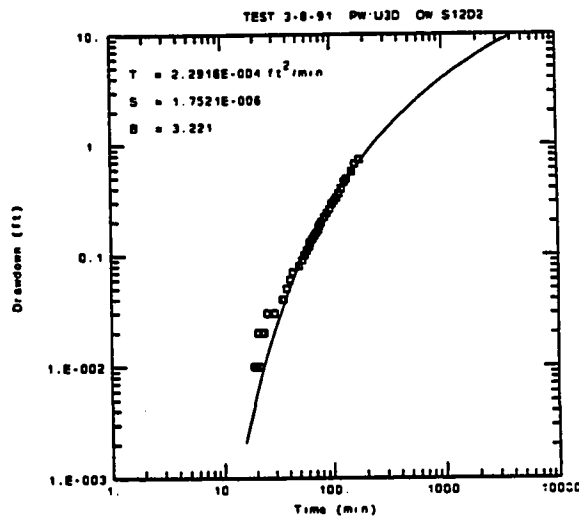
Theis Solution



Moench Double-porosity w/ Fracture Skin



Modified Hantush (leaky w/ Storage)



R = 155 feet

Figure 7-29. Graphical curve matching of observation well S12D2 data with alternative analytical models during test 3-8-91

The hydraulic parameters estimated using the Moench model with application of data from pumping well U3D and three observation wells (D19D, J16D and S12D2) during test 3-8-91 are presented in Table 7-22. The fracture skin and well bore skin (S_f and S_w) values estimated from the observation well data are significantly different with the values from the pumping well. The remaining hydraulic parameters estimated with the pumping well and the observation well data are within reasonable ranges (Table 7-22).

Table 7-22. Estimated Parameters by Moench Model with Application of the Data from All Wells during Aquifer Test 3-8-91

WELL	S_f	S_w	K (ft/d)	S_s (1/ft)	K' (ft/d)	S_s' (1/ft)	$\sqrt{KK'}$ (ft/d)	$\sqrt{S_s S_s'}$ (1/ft)
U3D(PW)	0	2	4.8	9×10^{-9}	0.004	4×10^{-4}	0.14	6×10^{-8}
D19D	5	80	14	3×10^{-9}	0.1	7×10^{-9}	1.2	5×10^{-7}
J16D	5	80	27	3×10^{-9}	0.03	3×10^{-9}	0.8	3×10^{-7}
S12D2	5	80	1.2	10^{-7}	0.04	3×10^{-9}	0.2	6×10^{-7}

Summary

The estimated aquifer and aquitard parameters for the W fracture zone using aquifer tests 8-14-90, 8-17-90 and 3-8-91 data are summarized in Table 7-23. The aquifer transmissivity and storativity as well as aquitard parameters estimated using the modified Hantush method are presented. The hydraulic conductivities and specific storages of the fissures and matrix blocks estimated by the Moench models also are presented in Table 7-23.

Table 7-23. Comparison and Summary of the Parameters Estimated from the W Aquifer Tests

Aquifer and Aquitard Parameters	Test 8-14-90 (PW: J16D)			Test 8-17-90 (PW: D19D)	Test 3-8-91 (PW: U3D)			Parameter Value Range	Geometric Mean
	D19D	U3D	S12D2	J16D	J16D	D19D	S12D2		
Transmissivity (T) (ft ² /day) by modified Hantush	2.8	1.3	1.2	2.7	0.8	0.8	0.4	0.4-2.8	1.2
Storativity (S) by modified Hantush	3x10 ⁻⁶	2.4x10 ⁻⁷	5.7x10 ⁻⁷	10 ⁻⁶	10 ⁻⁷	5.6x10 ⁻⁷	2.3x10 ⁻⁶	5x10 ⁻⁷ -5x10 ⁻⁵	9x10 ⁻⁷
$\sqrt{\frac{K'S'_e}{TS}}$ (1/ft)	0.14	0.07	0.15	0.21	0.05	0.02	0.07	0.02-0.21	0.09
K'*Ss' (1/day) by modified Hantush	2x10 ⁻⁷	1.5x10 ⁻⁹	1.5x10 ⁻⁸	10 ⁻⁷	2x10 ⁻¹⁰	2x10 ⁻¹⁰	4.5x10 ⁻⁹	2x10 ⁻¹⁰ -2x10 ⁻⁷	4x10 ⁻⁸
Fracture K (ft/day) by Moench Model	20	22	17	18	27	14	1.2	1.2-27	13
Fracture Ss (1/ft) by Moench Model	5x10 ⁻⁶	10 ⁻⁹	7x10 ⁻⁶	10 ⁻⁵	3x10 ⁻⁸	3x10 ⁻⁸	10 ⁻⁷	10 ⁻⁹ -10 ⁻⁵	2.2x10 ⁻⁷
Matrix K' (ft/day) by Moench Model	0.27	0.19	0.19	0.15	0.03	0.1	0.04	0.03-0.27	0.1
Matrix Ss' (1/ft) by Moench Model	2x10 ⁻⁴	8x10 ⁻⁶	2x10 ⁻⁵	10 ⁻⁴	3x10 ⁻⁶	7x10 ⁻⁶	3x10 ⁻⁶	3x10 ⁻⁶ -2x10 ⁻⁴	1.6x10 ⁻⁵

The hydraulic parameters listed in Table 7-23 for the individual wells in each aquifer test are calculated from the "best fit" of data with the type curves. In cases where more than one best match is presented, geometric means of the estimates from the alternative best matches of data are presented.

The average transmissivity values of the W fractured basalt aquifer at the UIGRS, estimated by the modified Hantush model, are 1.2 ft²/day. This value is approximately one magnitude smaller than the E aquifer values. The fissure hydraulic conductivity of the W fracture zone, estimated by the Moench model, ranges from 1.2 to 27 ft/day and averages 13 ft/day. The estimated fissure K values may represent only the hydraulic conductivities of the large fractures instead of the entire W fracture zone. Total thickness of these large fractures probably is smaller than the thickness of the fracture zone, and thus the aquifer T and the fissure K values are comparable.

The average value of the aquifer storativity by the modified Hantush is 9×10^{-7} . The specific storages of the fractures by the Moench model average 2×10^{-7} approximately. These values also are compatible with the aquifer S values of the E aquifer.

The hydraulic conductivity (K') and specific storage (Ss') of the matrix blocks presented in Table 7-23 are geometric means of the K' and Ss' estimated by alternative type curve matches of the Moench solution. The product of hydraulic conductivity and specific storage ($K' * Ss'$) is calculated using the modified Hantush β solution; the values represent the lumped parameters of the middle and lower aquitards.

The average value of the product of K' and Ss' presented in Table 7-

23 is approximately two magnitudes smaller than the mean value of $K' * Ss'$ from the upper and middle aquitards (Table 7-11). This indicates that the upper aquitard has significant higher values of the product of K' and Ss' than the lower aquitard. This conclusion is consistent with the results of site geological investigation; the intraflow structures of the upper portion of the Lolo basalt flow are more developed.

Graphical Curve Matching and Parameter Estimation for Slug Test Data

Graphical curve matches of the slug test data are presented in this section. As discussed in the chapter VI, the homogeneous slug test model by Cooper *et al.* (1967) is applicable to the fractured aquifers at the UIGRS to estimate the hydraulic conducting properties of the fractures. The data analysis of the nine slug tests was conducted using the computer software AQTESOLV.

The type curve matches of the Cooper slug test model with the test data from five wells completed in the E aquifer (V16D, T16D, Q17D, Q16D and S12D1) are presented in Figure 7-30. The graphical curve matches of the Cooper solution with the test data from the W aquifer wells (J16D, D19D, U3D and S12D2) are presented in Figure 7-31. Both Figures (7-30 and 7-31) illustrate that the observational data are matched well with the type curves of Cooper model. The estimated aquifer transmissivity values from the graphical curve matching are presented in Table 7-24.

The estimated transmissivity values from different wells generally correspond with well yield capacity. The T values listed in Table 7-24 probably represent the transmissivity of major fractures within a small

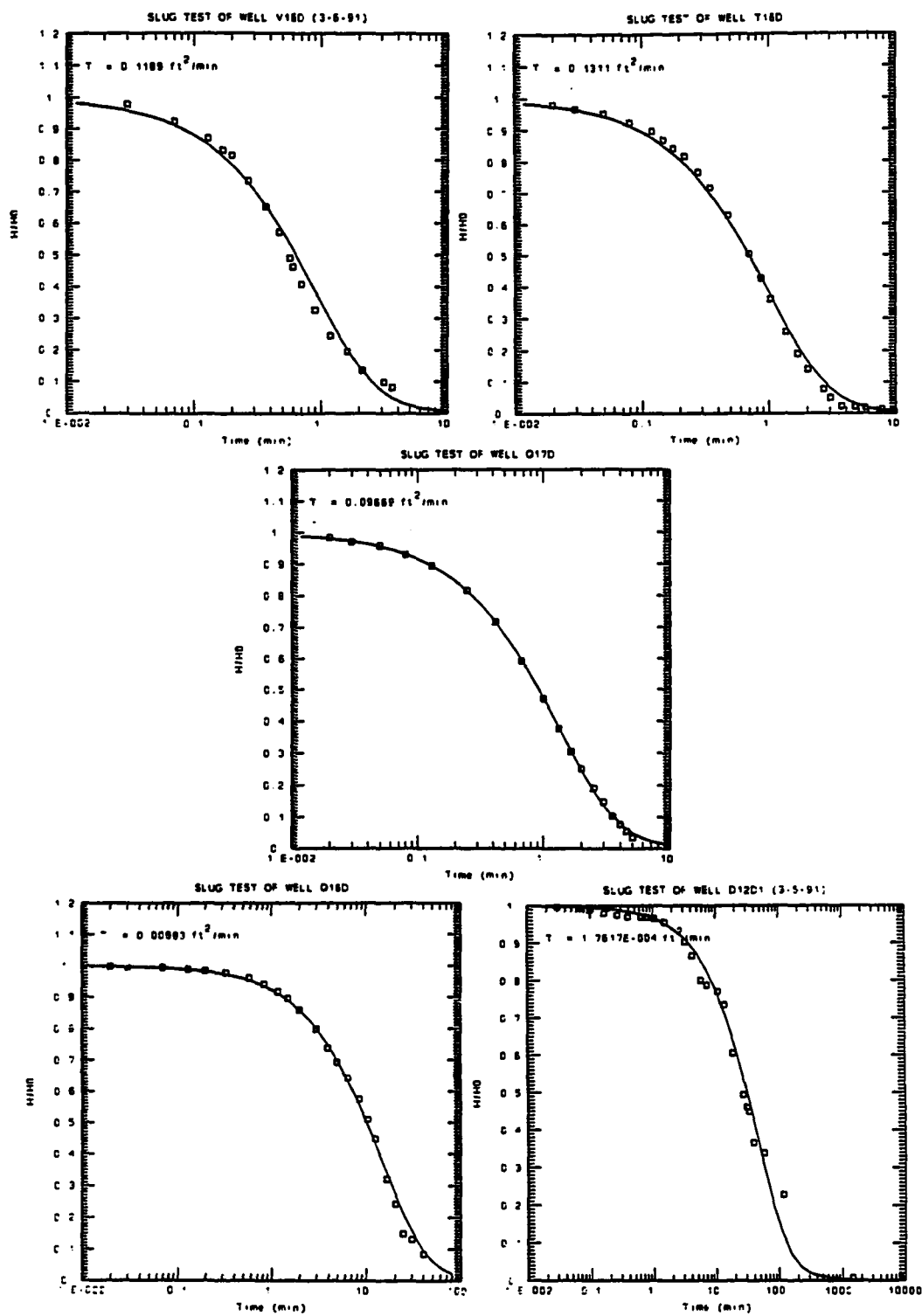


Figure 7-30. Graphical curve matching of single well slug tests conducted in the E fractured aquifer

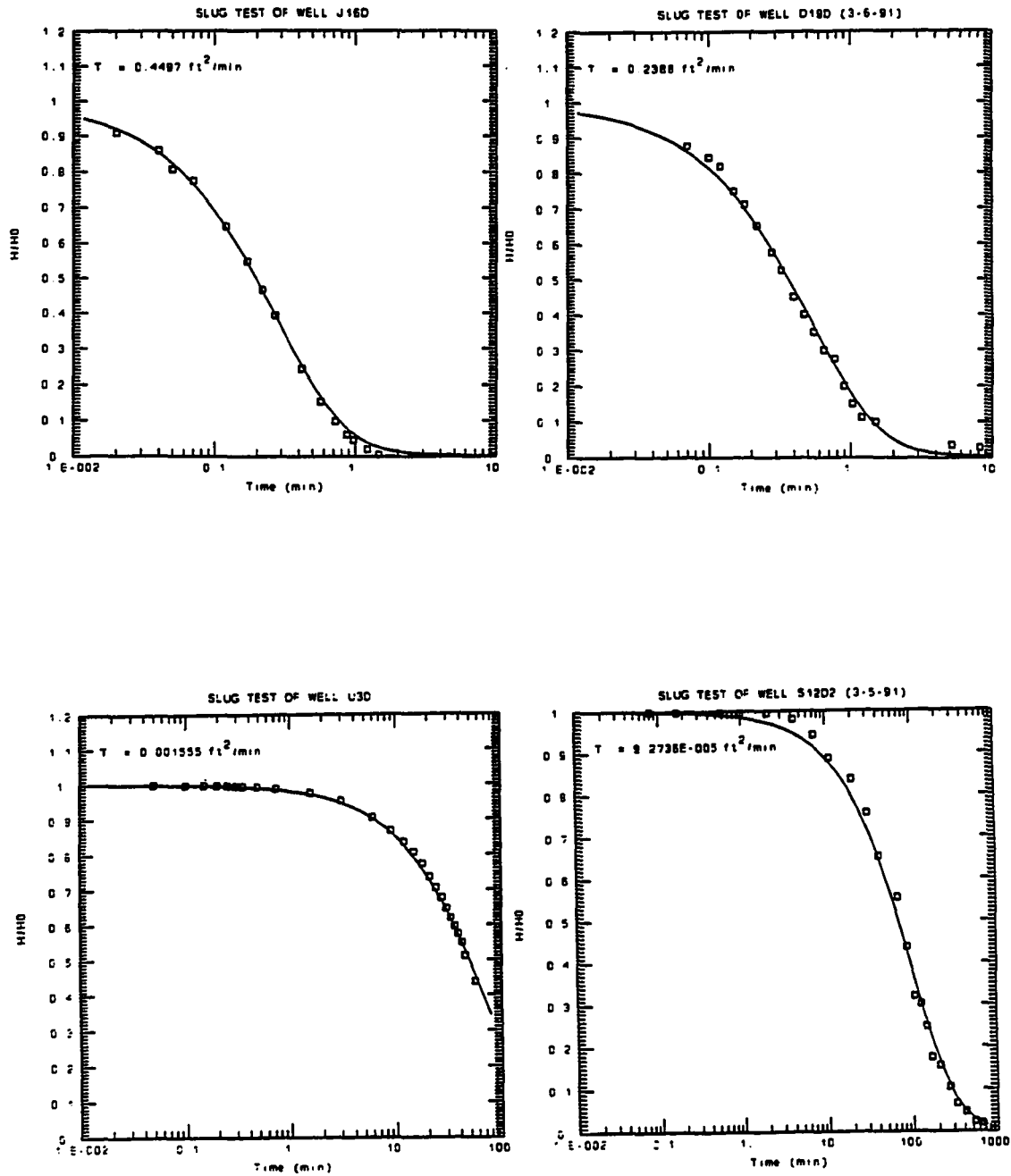


Figure 7-31. Graphical curve matching of single well slug tests conducted in the W fractured aquifer

area adjacent to the test well. These values should be considered as point estimates of transmissivity when compared with the results of the multiple well aquifer tests.

Table 7-24. Estimated Aquifer Parameters by Cooper Model with Slug Test Data

Testing Well	Transmissivity (ft ² /d)	Well Yield (gpm)	Remarks	
E ZONE	V16D	170	40-50	
	T16D	180	7-10	
	Q17D	140	7-10	
	Q16D	13	2-3(?)	well has not been tested
	S12D1	0.26	<1	well has not been tested
W ZONE	J16D	650	40-60	
	D19D	340	30-50	
	U3D	2.2	1-2	
	S12D2	0.13	<1	well has not been tested

The T value variations estimated by the slug test data are consistent with the geological observations. The Lolo basalt at the UIGRS tends to become harder and less fractured in the central portion of the site in the vicinity of wells S12D1 and S12D2 relative to the north (near wells V16D, T16D and Q17D).

CHAPTER VIII

Discussion of the Test Results and Summary of the Findings

The purpose of this chapter is to discuss the results from the hydraulic testing conducted at the UIGRS and to summarize the findings of this study. The transmissivity and storativity of the two fractured aquifers and the lumped parameters for the aquitards are summarized and discussed.

Discussion of the Aquifer Test Results

Aquifer Transmissivity

The transmissivities estimated from the multiple well aquifer tests and single well slug tests are presented in Table 8-1. The listed value of the slug tests for each well represents the transmissivity of the fractured aquifer in the immediate vicinity of that well. The T values estimated from each observation well during the multiple well aquifer tests are tabulated under the heading of that well (Table 8-1). T values are missing for some observation wells during the multiple well aquifer tests because the wells are not completed in the same aquifer as the pumping well.

The T values of the E aquifer listed in Table 8-1 for the multiple well aquifer tests are estimated using the Hantush model (r/B solution). These values likely represent the average transmissivity values of the E fractured aquifer on a larger scale than that for the slug tests. The T values listed for the W aquifer (Table 8-1) are estimated using the modified Hantush model (β solution).

**Table 8-1. Estimated Transmissivity Values for Different Observation Wells
(ft²/day)**

Aquifer Test	E Aquifer					W aquifer			
	V16D	T16D	Q17D	Q16D	S12D1	J16D	D19D	U3D	S12D2
Slug Tests	170	180	140	13	0.26	650	340	2.2	0.13
Test 9-22-89 (PW: Q17D)	576	43	-	-	155	-	-	-	-
Test 4-4-90 (PW: T16D)	158	-	36	-	27	-	-	-	-
Test 4-11-90 (PW: Q17D)	53	14	-	-	-	-	-	-	-
Test 6-3-90 (PW: V16D)	-	72	105	172	40	-	-	-	-
Test 8-14-90 (PW: J16D)	-	-	-	-	-	-	2.8	1.3	1.2
Test 8-17-90 (PW: D19D)	-	-	-	-	-	2.7	-	-	-
Test 3-8-90 (PW: U3D)	-	-	-	-	-	0.8	0.8	-	0.4

The T values of the E aquifer for wells V16D and T16D of the aquifer tests 9-22-89 and 4-11-90 are rather different (Table 8-1). These two tests were conducted with the same pumping well (Q17D). The differences of the estimates in T values may be caused by three reasons. First, the tests were conducted during different seasons; 9-22-89 was conducted during the dry season with low static water levels while 4-11-90 was conducted in the spring with high water levels in the aquifers. Second, test 4-11-90 was conducted during a three day period when extensive rainfall occurred. Recharge to the shallow alluvial aquifer was observed from the water level rising in the shallow wells during test 4-11-90. Third, the drawdown was measured and recorded only via pressure transducers and data logger during

test 4-11-90; measurement error by the transducers could contribute to the differences in estimates of the aquifer parameters.

The heterogeneity of both the E and W aquifers is exhibited by the T values from the slug tests, as shown in Figure 8-1. The E aquifer has high transmissivity in the vicinity of wells V16D, T16D and Q17D, located in the northeast side of the UIGRS. The T values decrease toward the south and reach the lowest value of 0.3 ft²/day at well S12D1. The W fractured aquifer has high T values at the northwest portion of the UIGRS. The T values of the W aquifer decrease more than two orders of magnitude from the northwest corner to the southeast side near well U3D. The lowest value of transmissivity in the W aquifer is observed in the vicinity of well S12D2 in the east central portion of the UIGRS.

The T values from the multiple well aquifer tests are mostly smaller than values from the slug tests except for wells S12D1 and Q16D in the E aquifer and S12D2 in the W aquifer (Table 8-1 and Figure 8-1). This may be caused by two factors: 1) heterogeneity of the fractured aquifers, and 2) testing scale effect. For the E aquifer, the fractures probably are more developed in the northeastern portion of the UIGRS where the wells V16D, T16D and Q17D are located (Figure 8-1). The T values estimated from the multiple well aquifer test data of these three wells generally are smaller than the point values because the less developed fractures away from the wells may contribute to the average T values. The opposite situation occurs in wells Q16D and S12D1; the wells intercept limited fractures with low T values. As the testing scale increases, more fractures are included in the test and larger average T values are obtained for these wells. The T value variations of the W fractured aquifer are more significant than those of the E aquifer; but the variations may be explained by similar

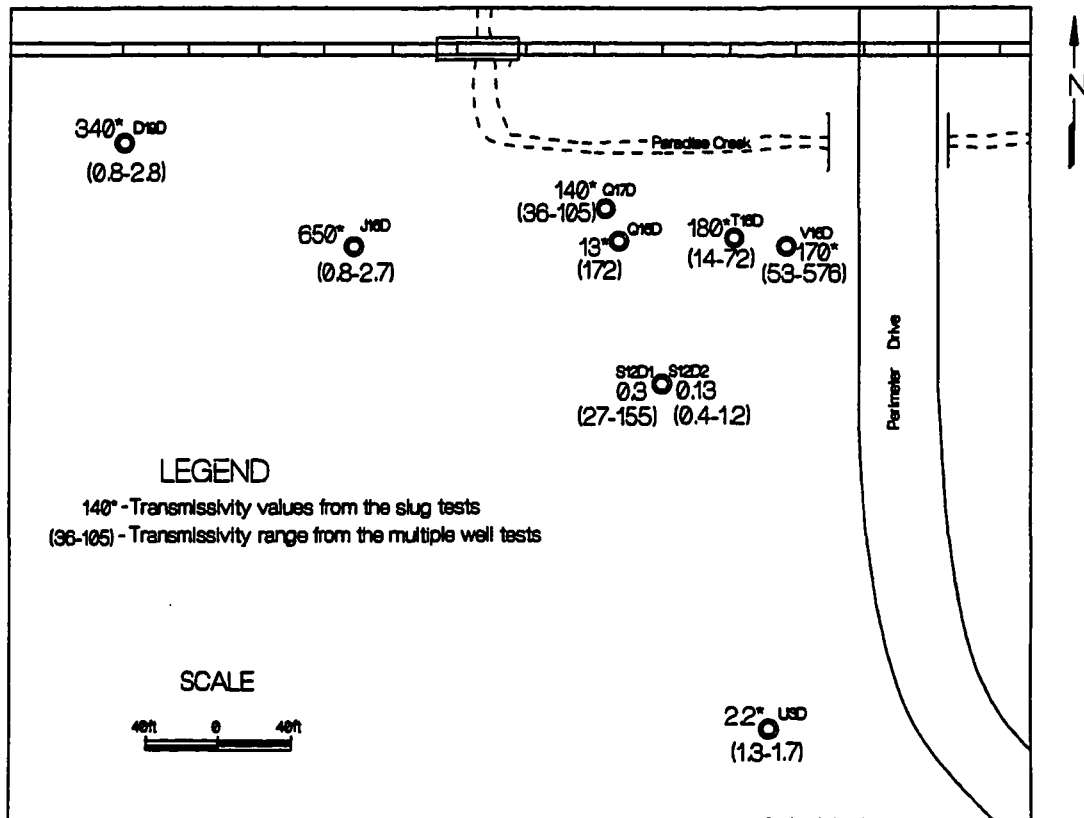


Figure 8-1. The transmissivity values (ft²/day) at the different well locations in the UIGRS

development patterns and hydraulic behavior of the fractures.

The T values estimated from the multiple well aquifer tests for a given observation well generally are different depending on the location of the pumping well (Table 8-1). This reflects aquifer anisotropy due to the complex fracture system; the different T values represent the aquifer transmissivities in the directions from the observation well to the various pumping wells. An example of the directional T values from well S12D1 is shown in Figure 8-2.

The T values from different observation wells for a given test also are different (Table 8-1). This illustrates the complex fracture patterns and probably aquifer anisotropy from another aspect; the different T values represent aquifer transmissivities in alternate directions from different observation wells to the pumping well. An example of directional T values from test 4-4-90 is presented in Figure 8-3.

The T value variations also may be caused by other factors: 1) estimation errors involved in application of the various analytical models, 2) the errors involved in drawdown measurements, and 3) the testing scope and conditions (the pumping rate, the test period, and the weather condition). Cumulative effects of all these factors are not fully understood at this time.

An error band or confidence interval for estimates of the T values or other aquifer parameters is difficult to determine because of two main reasons: 1) the number of the estimates (sample size) probably is too small, and 2) the estimates may not be a normal distribution or an arithmetic mean may not represent a true average. Therefore, the aquifer anisotropic conditions may not be identified clearly without knowing the error band associated with each of the solutions described in this report.

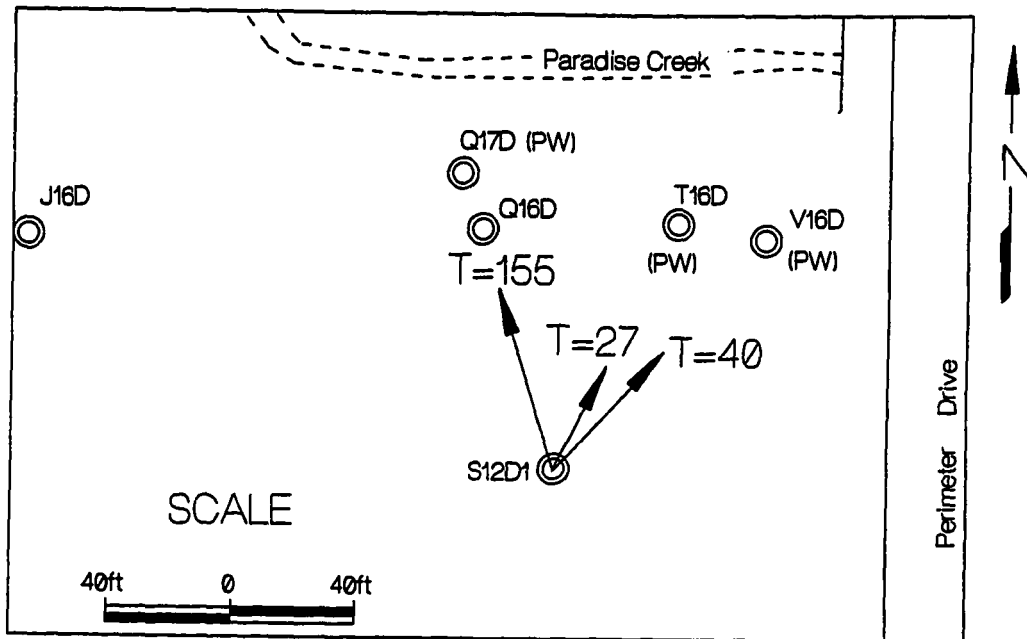


Figure 8-2. Directional T values (ft²/day) from well S12D1 to different pumping wells during the multiple well aquifer tests

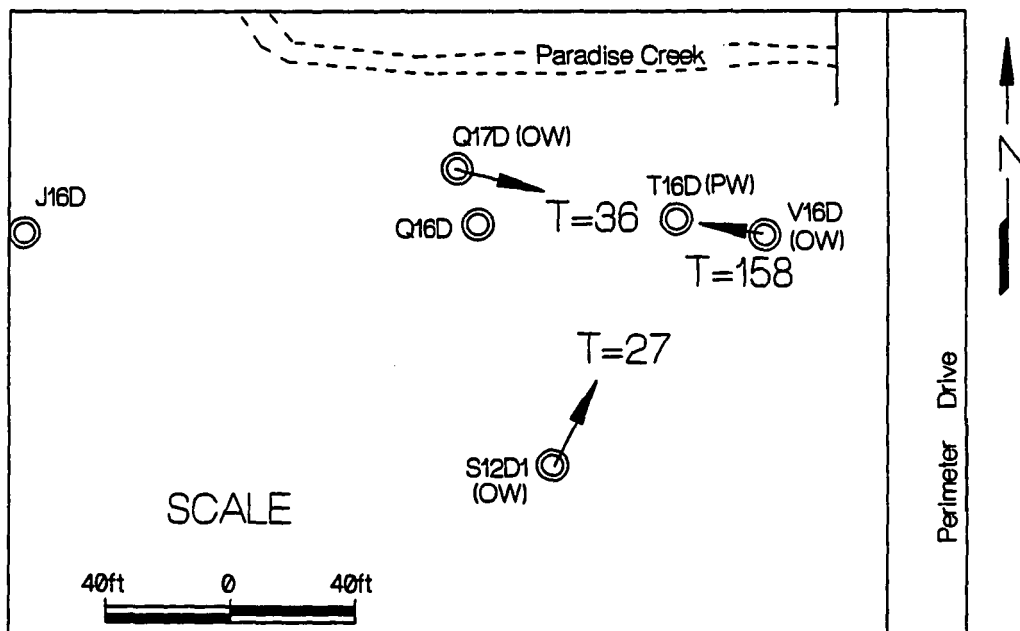


Figure 8-3. Directional T values (ft²/day) from different observation wells to the pumping well during aquifer test 4-4-90

Aquifer Storativity

The storativity values estimated from the multiple well aquifer tests are presented in Table 8-2. The S values listed in Table 8-2 are estimated using the Hantush r/B solution for the E aquifer and the modified Hantush for the W aquifer. These values probably represent the average aquifer storativities over the area that includes the pumping well and the observation wells.

**Table 8-2. Estimated Storativity Values for Different Observation Wells
($\times 10^{-6}$)**

Aquifer Test	E Aquifer					W aquifer			
	V16D	T16D	Q17D	Q16D	S12D1	J16D	D19D	U3D	S12D2
Test 9-22-89 (PW: Q17D)	6	30	-	-	500	-	-	-	-
Test 4-4-90 (PW: T16D)	400	-	20	-	7	-	-	-	-
Test 4-11-90 (PW: Q17D)	60	30	-	-	-	-	-	-	-
Test 6-3-90 (PW: V16D)	-	300	50	300	40	-	-	-	-
Test 8-14-90 (PW: J16D)	-	-	-	-	-	-	3	0.2	0.6
Test 8-17-90 (PW: D19D)	-	-	-	-	-	1	-	-	-
Test 3-8-90 (PW: U3D)	-	-	-	-	-	0.1	0.6	-	2.3
Well Yield (gpm)	40- 50	7-10	7-10	2-3	<1	40- 60	30- 50	1-2	<1

The S values of the E aquifer for a given observation well (V16D, T16D and S12D1) are different by one to two orders of magnitude depending on the pumping well. Significant differences in S values also are observed for the different observation wells in a given aquifer test except for 4-11-90 (Table 8-2). The variation pattern in the S values is more complex than the T values, and any patterns are difficult to interpret. The S values for the different observation wells generally are not consistent with well yield capacity (Table 8-2). The aquifer heterogeneity and a large error associated with application of the analytical models probably cause the great variations in S values of the E aquifer.

The S values of the W fractured aquifer are significantly smaller than the E aquifer, which is similar with the T values between the two aquifers. Reasons for the smaller T and S values in the W aquifer probably are: 1) the estimates are obtained from different analytical models, 2) the thickness of the W aquifer is less than the E aquifer, and 3) the fractures of the W aquifer may be less developed and the compressibility (α) of the W fracture zone may be lower.

Variations in the S values for the W aquifer are less significant than those for the E aquifer. Variations in the S values for different observation wells during the W aquifer tests generally are less than one order of magnitude (Table 8-2). These variations could be mostly due to estimation errors.

Lumped Aquitard Parameter $K' * Ss'$

The estimated lumped aquitard parameters ($K' * Ss'$) for the upper and middle aquitards from the E aquifer tests as well as the middle and lower aquitards from the W aquifer tests are presented in Table 8-3. The

aquitard parameters are estimated using the modified Hantush model. As discussed in the previous chapters, the modified Hantush solution is applicable for analysis of early time data from the tests conducted in both E and W aquifers. The results for aquifer test 4-11-90 are not available because the leakage from the aquitards at the early times was not observed during the test.

Table 8-3. Estimated Lumped Aquitard Parameter $K'Ss'$ Values for Different Observation Wells
($\times 10^{-8}$ 1/day)

Aquifer Test	Upper and Middle Aquitards					Middle and Lower Aquitards			
	V16D	T16D	Q17D	Q16D	S12D1	J16D	D19D	U3D	S12D2
9-22-89 (PW: Q17D)	200	50	-	-	800	-	-	-	-
4-4-90 (PW: T16D)	6000	-	20	-	600	-	-	-	-
6-3-90 (PW: V16D)	-	8000	40	800	30	-	-	-	-
8-14-90 (PW: J16D)	-	-	-	-	-	-	20	0.2	1.5
8-17-90 (PW: D19D)	-	-	-	-	-	10	-	-	-
3-8-90 (PW: U3D)	-	-	-	-	-	0.02	0.02	-	0.5

The $K'Ss'$ values of the upper and middle aquitards generally are greater than the values of the middle and lower aquitards (Table 8-3). This is consistent with the previous discussions on site geology and hydraulic behavior of the aquitards; the upper aquitard contains more small fissures and joints and has a relatively large vertical hydraulic

conductivity. Much smaller K' values are expected in the lower aquitard because the lower portion of the Lolo flow probably is less fractured. The lumped aquitard parameters reflect this characteristic of the Lolo basalt flow.

The variation of lumped aquitard parameter ($K'*Ss'$) values for a given observation well or a given aquifer test ranges from one to three orders of magnitude, which is similar to the estimated aquifer storativity values. The great variation of the estimates may be caused by: 1) the great heterogeneity of the aquitards because of the complex fracture patterns, and 2) the accumulated estimation errors for two parameters (K' and Ss'). Any spatial patterns in the $K'*Ss'$ values cannot be identified readily.

Summary of the Findings

Geology, Stratigraphy and Basalt Intraflow Structures

The UIGRS is underlain by the Lolo flow of the Priest Rapids basalt within the Wanapum Formation of the Yakima Subgroup of the Columbia River Basalt Group. Black loess soil, clay and silt of the Palouse Formation, as well as a limited distribution of alluvial sand and gravel overlie the basalt flow. The basalt is underlain by the Vantage Formation of interbedded sediments and the Grande Ronde Basalt Formation.

Total thickness of the Lolo flow is approximately 150 to 200 feet (46 to 61 meters). The surface layer of loess soil and clay are about 9 to 12 feet (2.7 to 3.6 meters) in thickness. The alluvial gravel and sand unit, with a spatial distribution very likely controlled by the ancient Paradise Creek channel, has various thicknesses from zero up to 10 feet (3 meters).

The basalt intraflow fractures form the primary structural system at the UIGRS. All the deep wells at the UIGRS were drilled within the Lolo flow and no flow contact zone was explored. Two major fracture zones, the E and W fracture zones, are identified along with the eroded top of the flow. Several minor fissure and joint zones are recognized at different depths within the eastern portion of the UIGRS.

The E fracture zone is located in the northeast portion of the site and lies at depths of 63 to 75 feet (19 to 23 meters). The W fracture zone was detected in much of the site with a much larger range of depth (65 to 137 feet, 20 to 42 meters). A Z-shape in cross-section is proposed for the W fracture zone in this study.

Vertical structures at the UIGRS have not been studied adequately because all of the drill holes used in this study were drilled vertically. However, information was obtained from examination of outcrops of the same basalt flow along contiguous Paradise Creek Valley. The columnar fracture zones formed by aggregation of vertical or nearly vertical joints occurs in both entablature and colonnade portions of the flow. The vertical structures that connect the major or minor horizontal fracture zones make the ground water flow system at the UIGRS very complex.

Ground Water Hydrology and Conceptual Model

Three aquifers have been identified at the UIGRS: 1) a shallow alluvial aquifer composed of sand, gravel, basalt rubble and broken basalt, 2) the E fractured basalt aquifer, and 3) the W fractured basalt aquifer. The aquifers are separated by less fractured basalt flow interior blocks that behave as aquitards. An upper aquitard that separates the alluvial and E aquifers and a middle aquitard between the E and W aquifers are

detected. A lower aquitard is present below the W aquifer but was not investigated.

The E fractured aquifer and the shallow alluvial aquifer at UIGRS are horizontal or nearly horizontal. The W fractured aquifer may comprise more than one horizontal fracture zone at different depths connected by vertical fractures. Thicknesses of the E and W fractured aquifers are approximately 1 to 3 feet (0.3 to 0.9 meters) and 0.5 to 1 foot (0.1 to 0.3 meters), respectively. The total saturated thickness of the shallow alluvial aquifer is about 3 to 10 feet (1 to 3 meters).

The fractured basalt aquifers are confined with the static water levels average of 2537 feet AMSL in the E aquifer and 2518 feet AMSL in the W aquifer. The shallow alluvial aquifer is unconfined with a static water level close to that of the E aquifer. The yield of wells completed in the E and W aquifers varies from 0.5 to 50 gpm.

Static water levels of the shallow alluvial aquifer, the E fractured aquifer, and Paradise Creek correspond with each other very closely. The recharge to the shallow and the E aquifers occurs mainly from infiltration through the soil profile; discharge occurs laterally to the creek and downward to the lower fractured basalt aquifers. The recharge-discharge relationship between Paradise Creek and the shallow aquifers can be reversed when high flow occurs in the creek.

The W fractured aquifer has no direct hydraulic connection with the shallow alluvial aquifer and Paradise Creek. Annual ground water level fluctuations of the W aquifer are fairly small in comparison with those of other aquifers. The daily change of the water level appears to be affected mainly by barometric pressure. The static water level in the W aquifer is about 10 to 15 feet (3 to 4.5 meters) below creek level. A limited

hydraulic connection between the E and W fractured aquifers through the aquitard is recognized.

Hydraulic Behavior of the Fractured Aquifer System

The E fractured basalt aquifer behaves like an equivalent porous medium during the multiple well aquifer testing. Alternative analytical approaches including the Theis, Hantush leaky aquifer, modified Hantush leaky aquifer and Neuman and Witherspoon leaky aquifer models are applicable to the test data analysis. Drawdown data from the early period of the aquifer tests deviate from the type curves because of fractured aquifer characteristics.

The W fractured basalt aquifer behaves like a double-porosity fractured medium during the multiple well aquifer tests. The Moench double-porosity with fracture skin model is applicable to the test data analysis. The modified Hantush leaky aquifer model also may be applicable. The analysis results provided by the two approaches are reasonably consistent.

Data analysis of the W aquifer shows that satisfactory results can be obtained using the Moench double-porosity with fracture skin model when the model is applied with care. However, a unique solution may not be obtained in most cases. Many combinations of the dimensionless parameters (S_f and S_w) have been utilized for the trial-and-error analyses. The results indicate that the estimated fracture hydraulic conductivities and matrix block specific storages are closely consistent. The fracture and well bore skin effects are shown in some of the test data. However, the significance of the fractured skin effect may vary over a large range.

A typical feature of the drawdown data from the multiple well aquifer

tests is early drawdown deviation from the type curves of the alternative analytical models. The drawdown deviation is believed to be a characteristic feature of a fractured aquifer with double-porosity behavior. The responses may be described by a conceptual model similar to the delayed yield responses in an unconfined aquifer.

Transmissivity (T) and storativity of the E fractured aquifer range from 14 to 580 ft²/day and 2×10^{-5} to 5×10^{-4} respectively; these values are estimated using the Hantush r/B solution. Averages of T and S values are approximately 80 ft²/day and 9×10^{-5} in the E aquifer. Smaller T and S values for the E aquifer are obtained using the modified Hantush β solution. The transmissivity and storativity of the W aquifer estimated by the modified Hantush range from 0.4 to 3 ft²/day and 5×10^{-7} to 5×10^{-5} respectively. The hydraulic conductivity (K) of the fractures in the W aquifer ranges from 1.2 to 27 ft/day, as estimated by the Moench model.

The lumped parameter values for the upper and middle aquitards, as well as the middle and lower aquitards, are estimated using the modified Hantush model with the multiple well aquifer test data. The product of hydraulic conductivity and specific storage of the upper and middle aquitards ($K' * Ss'$) ranges from 2×10^{-7} to 8×10^{-5} 1/day with an average value of $K' * Ss'$ at approximately 3×10^{-6} 1/day. The lumped parameter of the middle and lower aquitards ($K'' * Ss''$) ranges from 2×10^{-10} to 2×10^{-7} 1/day with an average of 4×10^{-8} 1/day. These values for the middle and lower aquitards are consistent with the product of hydraulic conductivity and specific storage of the matrix rock as estimated by the Moench solution.

The homogeneous and isotropic slug test model is applicable in both of the E and W aquifers for estimation of aquifer transmissivity. Small

scale heterogeneity of the fractured basalt aquifers is significant.

Analysis of the slug test data indicates that transmissivity values vary from less than one to several hundred ft²/day at different locations in the UIGRS.

CHAPTER IX

Conclusions and Recommendations

Conclusions

The two fractured aquifers, identified within the Lolo basalt flow at the UIGRS, have different hydraulic characteristics. The E fractured aquifer behaves like a porous medium and the W fractured aquifer has a double-porosity behavior characteristic of fractured rocks. Porous media analytical models are applicable for analyzing the hydraulic test data from the E aquifer, whereas the double-porosity model is optimal for characterizing the W aquifer. The specific conclusions of this study are as follows:

- 1) A multiple aquifer system with three aquifers is identified within the upper 160 feet (49 meters) of the subsurface at the UIGRS: a) a shallow alluvial aquifer composed of sand, gravel, and broken basalt of the eroded flow top, b) the E fractured aquifer, and c) the W fractured aquifer. At least two aquitards are recognized: a) the upper aquitard that separates the alluvial aquifer and the E aquifer, and b) the middle aquitard between the E and W aquifers. A lower aquitard below the W aquifer is present but not investigated in this study.
- 2) The E aquifer behaves like a porous medium during multiple well aquifer testing. The analytical models applicable to analyze the test data from the E aquifer include the Hantush (r/B solution) and modified Hantush (β solution) leaky aquifer models. The Hantush model may be the optimum approach for analyzing the E aquifer data

because significant leakage occurs from the alluvial aquifer. The modified Hantush β solution is applicable for analysis of the early time data.

- 3) The W aquifer exhibits double-porosity behavior during multiple well aquifer testing. The Moench double-porosity with fracture skin model probably is the optimum analytical approach to analyze the test data from the W aquifer. An alternative model for analysis of the data at small and intermediate times is the modified Hantush β solution. The Hantush r/B solution is not applicable because the W aquifer has no hydraulic connection with the alluvial aquifer and leakage from the unpumped E aquifer is small.
- 4) Early drawdown deviations from type curves of the analytical models are recognized as a common feature in all the observation wells during each of the multiple well aquifer tests. The drawdown deviations may be described by a conceptual model of fractured rock with double-porosity behavior, which is similar to the delayed yield responses of an unconfined aquifer.
- 5) Transmissivity (T) of the E aquifer ranges from 14 to 580 ft²/day and averages approximately 80 ft²/day. Storativity (S) of the E aquifer ranges from 2×10^{-5} to 5×10^{-4} and averages 9×10^{-5} . The average transmissivity and storativity of the W aquifer range from 0.5 to 3 ft²/day and 5×10^{-7} to 5×10^{-5} respectively. The hydraulic conductivity (K) of the fractures in the W aquifer ranges from 1.2 to 27 ft/day. The lumped values of the product of hydraulic conductivity and specific storage of the upper and middle aquitards ($K' * Ss'$) are estimated from 2×10^{-7} to 8×10^{-5} 1/day. The product of these same

parameters of the middle and lower aquitards (K^*S_s) ranges from 2×10^{-10} to 2×10^{-7} 1/day.

- 6) The heterogeneity of the two fractured aquifers at the UIGRS is well illustrated by aquifer test results. The transmissivities of both the E and W aquifers vary from less than one to several hundred ft^2/day at different well locations. Anisotropy of the fractured aquifers probably occurs primarily between the horizontal and vertical directions. In terms of anisotropy in the horizontal directions, directional T values are obtained from a given observation well to various pumping wells and from different observation wells to the pumping well for a given aquifer test.

Recommendations

Based on the results of this study, the following recommendations can be made:

- 1) Drill cores should be collected to allow for a more complete fracture analysis. Laboratory permeability measurements should be conducted on cores collected from the Lolo basalt flow.
- 2) Quantitative evaluation of ground water hydrograph data with emphasis on the interrelationship of surface and ground water should be conducted. The long term static ground water level monitoring program should be continued and correlated with pumpage data (pumping time and discharge) of the water supply well of the University of Idaho Aquaculture Laboratory located southwest of the UIGRS.
- 3) More extensive multiple well hydraulic testing should be conducted in

the W fractured aquifers. Aquifer tests should be designed with a smaller discharge rate and longer test period for wells D19D and J16D; a pumping rate of 6 gpm and a duration of 36 to 48 hours is recommended. Injection tests should be conducted in wells U3D, S12D1 and S12D2 because of low yield capacity of these wells and small diameters of S12D1 and S12D2. The injection rates should be controlled within 0.3 gpm in well U3D and less than 0.1 gpm in wells S12D1 and S12D2. Durations of the injection tests should be from several days to several weeks.

- 4) A geostatistical analysis of the distribution of aquifer parameters should be conducted as more wells drilled and more aquifer test data collected at the UIGRS. The predicted parameters can be either the calculated aquifer or aquitard hydraulic properties or statistical coefficients developed to describe drawdown responses at particular locations. Estimation based on the Kriging method should be used to interpolate the static water level data for a more detailed ground water hydrograph.
- 5) The borehole seismic refraction tomography techniques should be utilized to map the vertical and horizontal fractures at the UIGRS. Other borehole geophysical techniques such as borehole television or cross-hole electromagnetic survey also may be used to study the fracture system. These techniques should be applied to allow more detailed understanding of the fracture system at the UIGRS.
- 6) Tracer tests should be conducted at the UIGRS for solute transport characterization of the fractured basalt aquifers at the UIGRS. Well pairs D19D/J16D, and V16D/T16D are recommended for two well tracer tests.

REFERENCES

- Barker, J. A. and Black, J. H., 1983, Slug test in fissured aquifer, *Water Resources Research*, Vol. 19, No. 6, pp. 1558-1564.
- Barenblatt, G. I., Zheltov, I. P. and Kocina, I. N., 1960, Basic concepts in the theory of seepage of homogeneous liquids in fissured rocks, *Journal of Applied Mathematics and Mechanics (USSR)*, Vol. 24, No. 5, pp. 1286-1303.
- Barker, R. A., 1979, Computer simulation and geohydrology of a basalt aquifer system in the Pullman-Moscow basin, Washington and Idaho, *Washington Department of Ecology Water-Supply Bulletin* 48, 119p.
- Beauheim, R. L., 1988, Scale effects in well testing in fractured media, *The Fourth Canadian/American Conference on Hydrogeology: Fluid flow, Heat Transfer and Mass Transport in Fractured Rocks*, pp. 152-159.
- Boulton, N. S., 1970, Analysis of data from pumping tests in unconfined anisotropic aquifers, *Journal of hydrology*, Vol. 10, pp. 369-378.
- Boulton, N. S. and Pintin J. M. A., 1971, An extended theory of delayed yield from storage applied to pumping tests in unconfined anisotropic aquifers, *Journal of Hydrology*, Vol. 14, No. 1, pp. 53-65.
- Boulton, N. S. and Streltsova, T. D., 1977, Unsteady flow to a pumped well in a fissured water-bearing formation, *Journal of Hydrology*, Vol. 35, pp. 257-270.
- Boulton, N. S. and Streltsova, T. D., 1978, Unsteady flow to a pumped well in a fissured aquifer with a free surface level maintained constant, *Water Resources Research*, Vol. 14, No. 3, pp. 527-532.
- Bouwer, H. and Rice, R. C., 1976, A slug test for determining hydraulic conductivity of unconfined aquifers with completely or partially penetrating wells, *Water Resources Research*, Vol. 12, No. 3, pp. 423-428.
- Brown, J. C., 1976, Well construction and stratigraphic information: Pullman test and observation well, Pullman, Washington, College of Engineering Research Report 76/15-6, Washington State University, Pullman, Washington, 35p.
- Cooper, H. H., Bredehoeft, J. D. and Papadopoulos, I. S., 1967, Response of a finite-diameter well to an instantaneous charge of water, *Water Resources Research*, Vol. 3, No. 1, pp. 263-269.
- Cooper, H. H. and Jacob, C. E., 1946, A generalized graphical method for evaluating formation constants and summarizing well field history, *American Geophysical Union Transactions*, Vol. 27, pp. 526-534.
- deSwaan, A. O., 1976, Analytic solutions for determining naturally fractured reservoir properties by well testing, *Transactions of Society*

- of Petroleum Engineers of AIME, Vol. 261, pp. 117-122.
- DOE (Department of Energy), 1981, Site Characterization Report for Basalt Waste Isolation Project, Vol. I, Rockwell Hanford operations, Richland, Washington, 2200p.
- Duffield, G. M. and Rumbaugh III, J. O., 1989, AQTESOLV, Aquifer test solver Version 1.00 documentation, Geraghty & Miller Modeling Group, 1895 Preston White Drive, Suite 301, Reston, VA 22091, 135p.
- Freeze, R. A. and Cherry, J. A., 1979, Groundwater, Prentice-Hall, Inc., Englewood Cliffs, N. J., 604p.
- Gale, J. E., 1982, Assessing the permeability characteristics of fractured rock, Geological Society of America, Special Paper 189, pp. 163-181.
- Gringarten, A. C., 1982, Flow-test evaluation of fractured reservoirs, Geological Society of America, Special Paper 189, pp. 237-263.
- Gringarten, A. C., 1984, Interpretation of tests in fissured and multilayered reservoirs with double-porosity behavior: theory and practice, Journal of Petroleum technology, April, pp. 549-564.
- Gringarten, A. C. and Ramey, H. J. Jr., 1974, Unsteady-state pressure distributions created by a well with a single horizontal fracture, partial penetration, or restricted entry, Society of Petroleum Engineers Journal, Vol. 14, No. 4, pp. 413.
- Gringarten, A. C., and Ramey, H. J. Jr. and Raghavan, R., 1974, Unsteady-state pressure distributions created by a single infinite conductivity vertical fracture, Society of Petroleum Engineers Journal, Vol. 14, No. 4., pp. 347.
- Gringarten, A. C., and Witherspoon, P. A. 1972, A method of analyzing pump test data from fractured aquifers, Proceedings, Symposium on Percolation through Fissured Rock: Stuttgart, International Society of Rock Mechanics, Vol. 3, pp. b1-b9.
- Hantush, M. S., 1960, Modification of the theory of leaky aquifers, Journal of Geophysical Research, Vol. 65, No. 11, pp. 3713-3725.
- Hantush, M. S., 1962a, Drawdown around a partially penetrating well, Transactions, American Society of Civil Engineers, Vol. 127, Part I, pp. 268-283.
- Hantush, M. S., 1962b, Aquifer tests on partially penetrating wells, Transactions, American Society of Civil Engineers, Vol. 127, Part I, pp. 284-308.
- Hantush, M. S., 1966a, Wells in homogeneous anisotropic aquifers, Water Resources Research, Vol. 2, No. 2, pp. 273-279.

- Hantush, M. S., 1966b, Analysis of data from pumping tests in anisotropic aquifers, *Journal of Geophysical Research*, Vol. 71, No. 2, pp. 421-426.
- Hantush, M. S. and Jacob, C. E., 1955, Nonsteady radial flow in an infinite leaky aquifer, *Transactions of the American Geophysical Union*, Vol. 36, pp. 95-100.
- Hantush, M. S. and Thomas, R. G., 1966, A method for analyzing a drawdown test in anisotropic aquifers, *Water Resources Research*, Vol. 2, No. 2, pp. 281-285.
- Harenberg, W. A., Jones, M. L., O'Dell, I. and Cordes, S. C., 1990, *Water Resources Data, Idaho, Water Year 1989*, U.S. Geological Survey Water-Data Report ID-89-1, 681p.
- Harenberg, W. A., Jones, M. L., O'Dell, I., Brennan, T. S. and Lehmann, A. K., 1991, *Water Resources Data, Idaho, Water Year 1990*, U.S. Geological Survey Water-Data Report ID-90-1, 641p.
- Hearn, P. P., Steinkampf, W. C., Bortleson, G. C. and Drost, B. W., 1984, Geochemical controls on dissolved sodium in basalt aquifers of the Columbia plateau, Washington, U.S. Geological Survey Water-Resources Investigations Report 84-4304, 38p.
- Hooper, P. R. and Webster, G. D., 1982, *Geology of the Pullman, Moscow West, Colton, and Uniontown 7 1/2 minute quadrangles, Washington and Idaho*, Geologic Map GM-26, Washington State Department of Natural Resources, Division of Geology and Earth Resources, Scale 1:62,500.
- Hooper, P. R. and Camp, V. E., 1981, Deformation of the southeast part of the Columbia Plateau, *Geology*, Vol. 9, July, pp. 323-328.
- Hsieh, P. A., and Neuman, S. P., 1985, Field determination of the three-dimensional hydraulic conductivity tensor of anisotropic media: 1. theory, *Water Resources Research*, Vol. 21, No.11, pp. 1655-1665.
- Hsieh, P. A., Neuman, S. P., Stiles, G. K. and Simpson, E. S., 1985, Field determination of the three-dimensional hydraulic conductivity tensor of anisotropic media: 2. methodology and application to fractured rocks, *Water Resources Research*, Vol. 21, No. 11, pp. 1667-1676.
- Javandel, I. and Witherspoon, P. A., 1969, A method of analyzing transient fluid flow in multilayered aquifers, *Water Resources Research*, Vol. 5, No. 4, pp. 856-869.
- Javandel, I. and Witherspoon, P. A., 1983, Analytical solution of a partially penetrating well in a two-layer aquifer, *Water Resources Research*, Vol. 19, No. 2. pp567-578.
- Jenkins, D. N. and Prentice, J. K., 1982, Theory for aquifer test analysis in fractured rocks under linear (nonradial) flow conditions, *Ground Water*, Vol. 20, No. 1, pp. 12-21.

- Kabala, Z. L., Pinder, G. F. and Milly, C. D., 1985, Analysis of well-aquifer response to a slug test, *Water Resources Research*, Vol. 21, No.9, pp. 1433-1436.
- Kazemi, H., 1969, Pressure transient analysis of naturally fractured reservoirs with uniform fracture distribution, *Transactions, Society of Petroleum Engineers of AIME*, Vol. 246, pp. 451-462.
- Kazemi, H., Seth, M. S. and Thomas, G. W., 1969, The interpretation of interference tests in naturally fractured reservoirs with uniform fracture distribution, *Transactions, Society of Petroleum Engineers of AIME*, Vol. 246, pp. 463-472.
- Keys, W. S., 1986, Analysis of geophysical logs of water wells with a microcomputer, *Ground Water*, Vol. 24, No. 6, pp. 750-760.
- Keys, W. S., 1989, *Borehole Geophysics Applied to Groundwater Investigations*, National Water Well Association, Dublin, Ohio, 313p.
- Klein, D. P., Sneddon, R. A. and Smoot, J. L., 1987, A magnetotelluric study of thickness of volcanic and sedimentary rock in the Pullman-Moscow Basin of eastern Washington, U.S. Geological Survey Open-File Report 87-140, 30p.
- Kruseman, G. P. and de Ridder, N. A., 1983, *Analysis and Evaluation of Pumping Test Data*, Bulletin II, International Institute for Land Reclamation and Improvement, Wageningen, The Netherlands, Third Edition, 200p.
- Kunkel, J. R., Way, S. C. and McKee C. R., 1988, Comparative evaluation of selected continuum and discrete-fracture models: Emphasis on dispersivity calculations for application to fractured geologic media, Creston Study Area, Eastern Washington, Prepared for U.S. Nuclear Regulatory Commission, In-Situ, Inc., Laramie, WY., 61p.
- Lavenue, A. M. and Domenico, P. A. 1986, A preliminary assessment of the regional dispersivity of selected basalt flows at the Hanford site, Washington, U.S.A., *Journal of Hydrology*, Vol. 85, pp. 151-167.
- Lee, J. 1982, *Well Testing*, Society of Petroleum Engineers of AIME, New York and Dallas.
- Levens, R. L., 1990, Analysis of the hydrogeologic role of geologic structures with application to acid mine drainage abatement, M. S. Thesis, University of Idaho, Moscow, Idaho, 193pp.
- Long, J. C. S., Remer, J. S., Wilson, C. R. and Witherspoon, P. A., 1982, Porous media equivalents for networks of discontinuous fractures, *Water Resources Research*, Vol. 18, No. 3, pp. 645-658.
- Long, J. C. S. and Witherspoon, P. A., 1985, The relationship of the degree of interconnection to permeability in fracture networks, *Journal of Geophysical Research*, Vol. 90, No. B4, pp. 3087-3098.

- Long, P. E., 1978, Characterization and Recognition of intraflow structures, Grande Ronde basalt, RHO-BWI-LD-10, Rockwell Hanford Operations, Richland, Washington.
- Long, P. E. and Davidson, N. J., 1981, Lithology of the Grande Ronde basalt with emphasis on Umtanum and McCoy Canyon Flows, Subsurface Geology of the Cold Creek Syncline, RHO-BWI-ST-14, Rockwell Hanford Operations, Richland, Washington.
- Lum II, W. E., Smoot, J. L. and Ralston, D. R. 1990, Geohydrology and numerical model analysis of ground-water flow in the Pullman-Moscow area, Washington and Idaho, U.S. Geological Survey Water-Resources Investigations Report 89-4103, 73p.
- Moench, A. F., 1984, Double-porosity models for a fissured groundwater reservoir with fracture skin, Water Resources Research, Vol. 20, No. 7, pp. 831-846.
- Najurieta, H. L., 1980, A theory for pressure transient analysis in naturally fractured reservoirs, Transactions of Society of Petroleum Engineers AIME, Vol. 269, pp. 1241-1250.
- Neuman, S. P., 1972, Theory of flow in unconfined aquifers considering delayed response of the water table, Water Resources Research, Vol. 8, No. 4, pp. 1031-1045.
- Neuman, S. P., 1973, Supplementary comments on "Theory of flow in unconfined aquifers considering delayed response of water table", Water Resources Research, Vol. 9, No. 4, pp. 1102-1103.
- Neuman, S. P., 1974, Effect of partial penetration on flow in unconfined aquifer considering delayed gravity response, Water Resources Research, Vol. 10 No. 3, pp. 303-312.
- Neuman, S. P., 1975, Analysis of pumping test data from anisotropic unconfined aquifers considering delayed gravity response, Water Resources Research, Vol. 11, No. 2, pp. 329-342.
- Neuman, S. P. and Witherspoon, P. A., 1969a, Theory of flow in a confined two aquifer system, Water Resources Research, Vol. 5, No. 4, pp. 803-816.
- Neuman, S. P. and Witherspoon, P. A., 1969b, Applicability of current theories of flow in leaky aquifers, Water Resources Research, Vol. 5, No. 4, pp. 817-829.
- Neuman, S. P. and Witherspoon, P. A., 1972, Field determination of hydraulic properties of leaky multiple aquifer systems, Water Resources Research, Vol. 8, No. 5, pp. 1284-1298.
- Neuman, S. P., Walter, G. R., Bentley, H. W., Ward, J. J. and Gonzalez, D. D., 1984, Determination of horizontal aquifer anisotropy with three wells, Ground Water, Vol. 22, No. 1, pp. 66-72.

- Pandit, N. S. and Miner, R. F. 1986, Interpretation of slug test data, *Ground Water*, Vol. 24, No. 6, pp. 743-749.
- Papadopoulos, I. S., 1966, Nonsteady flow to multiaquifer wells, *Journal of Geophysical Research*, Vol. 71, No. 20, pp. 4791-4797.
- Papadopoulos, I. S. and Cooper, H. H. Jr. 1967, Drawdown in a well of large diameter, *Water Resources Research*, Vol. 3, No. 1, pp. 241-244.
- Patrick, J. A., 1990, Relation between Paradise Creek and groundwater levels at the University of Idaho Groundwater Research Site, A non-thesis project report, University of Idaho, Moscow, Idaho, 45p.
- Pirson, S. J., 1953, Performance of fractured oil reservoirs, *Bulletin of American Association of Petroleum Geologists*, Vol. 31, No. 2, pp. 232-244.
- Prudic, D. E., 1982, Hydraulic conductivity of a fine-grained till, Cattaraugus County, New York, *Ground Water*, Vol. 20, No. 2, pp. 194-204.
- Ralston, D. R. and Li, T. 1989, Analysis of ground water recharge from Paradise Creek at the University of Idaho Ground Water Research Site: part I, Idaho Water Resources Research Institute, University of Idaho, Moscow, Idaho, 17p.
- Ramey, H. J. Jr., 1982, Well-loss function and the skin effect: a review, *Geological Society of America, Special Paper 189*, pp. 265-271.
- Sauveplane, C. 1981, Pumping test analysis in fractured aquifer formations: state of art and some perspectives, AGU Spring meeting 1981, John Ferris Symposium on "Groundwater Hydraulics", 33p.
- Sen, Z., 1986a, Aquifer test analysis in fractured rocks with linear flow pattern, *Ground Water*, Vol. 24, No. 1, pp. 72-78.
- Sen, Z., 1986b, Determination of aquifer parameters by the slope-matching method, *Ground Water*, Vol. 24, No. 2, pp. 217-223.
- Snow, D. T., 1968, Rock fracture spacings, openings and porosities, *Journal of the Soil Mechanics and Foundations Division, Proceedings of the American Society of Civil Engineers, SM1, January*, pp. 73-91.
- Snow, D. T., 1969, Anisotropic permeability of fractured media, *Water Resources Research*, Vol. 5, No. 6, pp. 1273-1289.
- Streltsova, T. D., 1976a, Hydrodynamics of groundwater flow in a fractured formation, *Water Resources Research*, Vol. 12, No. 3, pp. 405-414.
- Streltsova, T. D., 1976b, Analysis of aquifer-aquitard flow, *Water Resources Research*, Vol. 12, No. 3, pp. 415-422.

- Streltsova, T. D., 1983, Well pressure behavior of a naturally fractured reservoir, Society of Petroleum Engineers Journal, October, pp. 769-780.
- Streltsova, T. D., 1988, Well Testing in Heterogeneous Formations, An Exxon Monograph, John Wiley & Sons, Inc., New York, 413p.
- Swanson, D. A., 1967, Yakima basalt of the Tieton River area, south-central Washington, Geological Society of America Bulletin, Vol. 78, pp. 1077-1110.
- Swanson, D. A., Wright, T. L., Camp, V. E., Gardner, J. N., Helz, R. T., Price, S. A. and Ross, M. E., 1977, Reconnaissance geological map of the Columbia River Basalt Group, Pullman and Walla Walla quadrangles, southeast Washington and adjacent Idaho, U.S. Geological Survey Open-File Report 77-100, Scale 1:250,000.
- Swanson, D. A., Wright, T. L., Hooper, P. R. and Bentley, R. D., 1979, Revisions in stratigraphic nomenclature of the Columbia River Basalt Group, USGS. Bulletin 1457-G, 59p.
- Swanson, D. A., Wright, T. L., Camp, V. E., Gardner, J. N., Helz, R. T., Price, S. A. and Ross, M. E., 1980, Reconnaissance geological map of the Columbia River Basalt Group, Pullman and Walla Walla quadrangles, southeast Washington and adjacent Idaho, U.S. Geological Survey Miscellaneous Geological Investigations Map I-1139, Scale 1:250,000.
- Theis, C. V., 1935, The relation between the lowering of the piezometric surface and the rate and duration of discharge of a well using groundwater storage, Transactions of the American Geophysical Union, Vol. 16, pp. 519-524.
- Tolan, T. L., Reidel, S. P., Beeson, M. H., Anderson, J. L., Fecht, K. R. and Swanson D. A., 1989, Revisions to the estimates of the areal extent and volume of the Columbia River Basalt Group, Geological Society of America, Special Paper 239, pp. 1-20.
- Uhl, V. W. Jr. and Joshi, V. G., 1986, Results of pumping tests in the Deccan Trp basalts of central India, Journal of Hydrology, Vol. 86, pp. 147-168.
- Warren, J. E. and Root, P. J., 1963, The behavior of naturally fractured reservoirs, Transactions of Society of Petroleum Engineers AIME, Vol. 228, No. 3(3), pp. 245-255.
- Way, S. C. and McKee, C. R., 1982, In-situ determination of three-dimensional aquifer permeabilities, Ground Water, Vol. 20, No. 5, pp. 594-603.
- Weeks, E. P., 1969, Determining the ratio of horizontal to vertical permeability by aquifer-test analysis, Water Resources Research, Vol. 5, No. 1, pp. 196-214.

- Williams, R. E. 1985, Comment on "Double-porosity models for a fissured groundwater reservoir with fracture skin" by Allen F. Moench, Water Resources Research, Vol. 21, No. 6, pp. 889-891.
- Wood, T. R., 1987, The hydrogeology of the Wanapum basalt, Creston study area, Lincoln County, Washington, M.S. Thesis, Washington State University, Pullman, Washington, 166p.
- Wright, T. L., Grolier, M. J. and Swanson, D. A., 1973, Chemical variation related to the stratigraphy of the Columbia River basalt, Geological Society of America Bulletin, Vol. 84, No. 2, pp. 371-385.

APPENDIX A
Well Construction and Geological Logs
at UIGRS

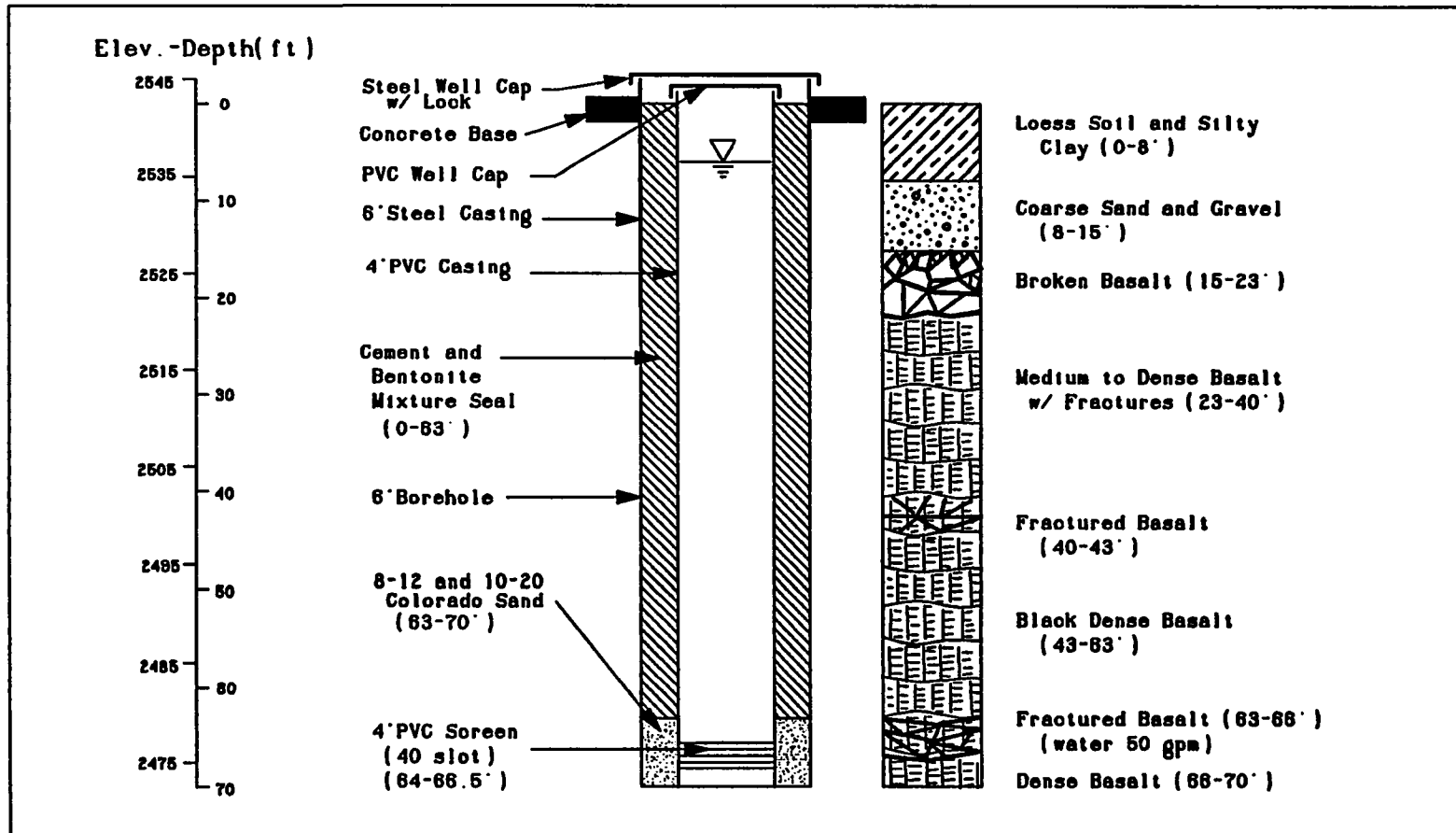


Figure A-1. Construction and geology logs of well V16D

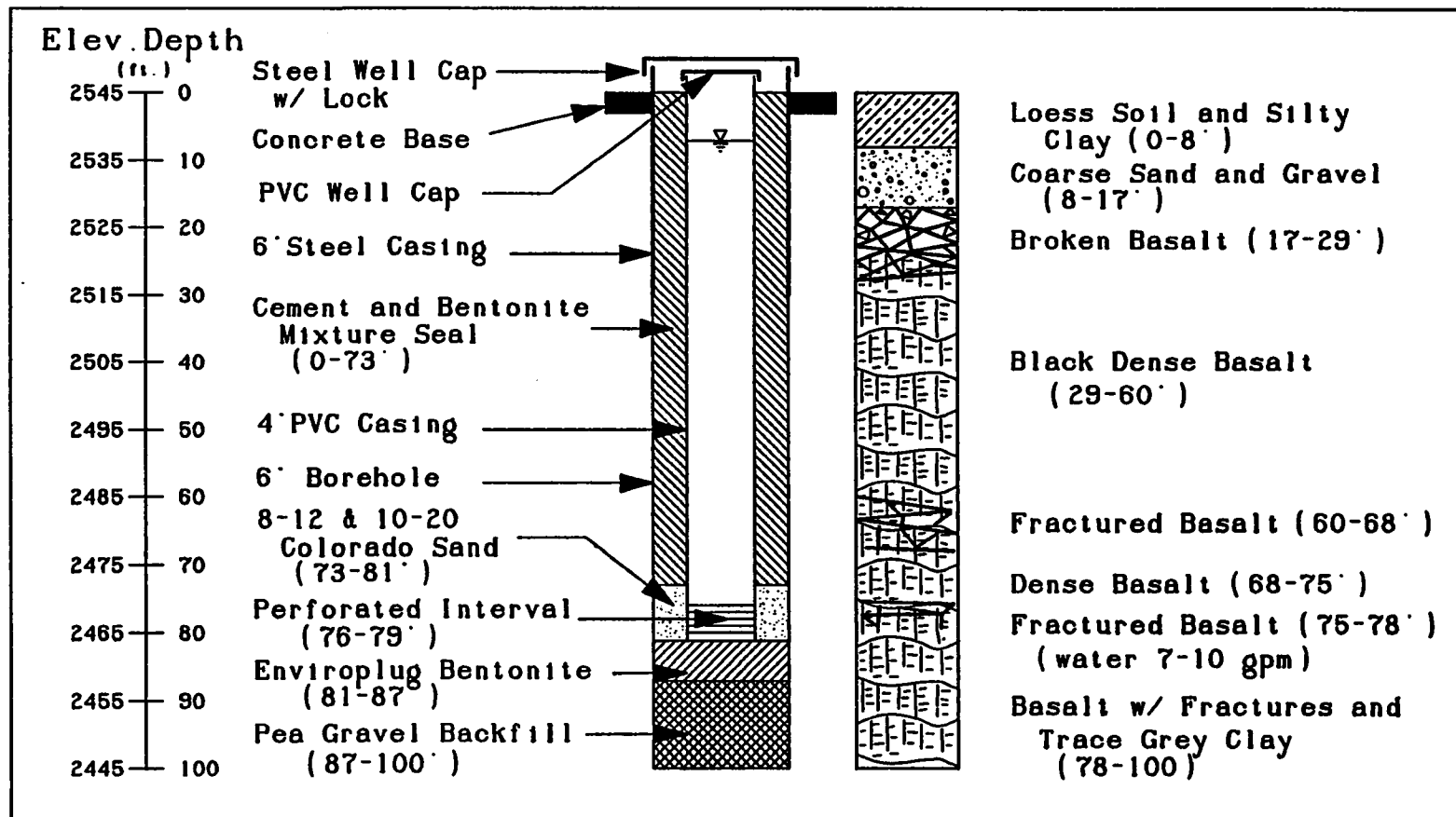


Figure A-2. Construction and geology logs of well Q17D

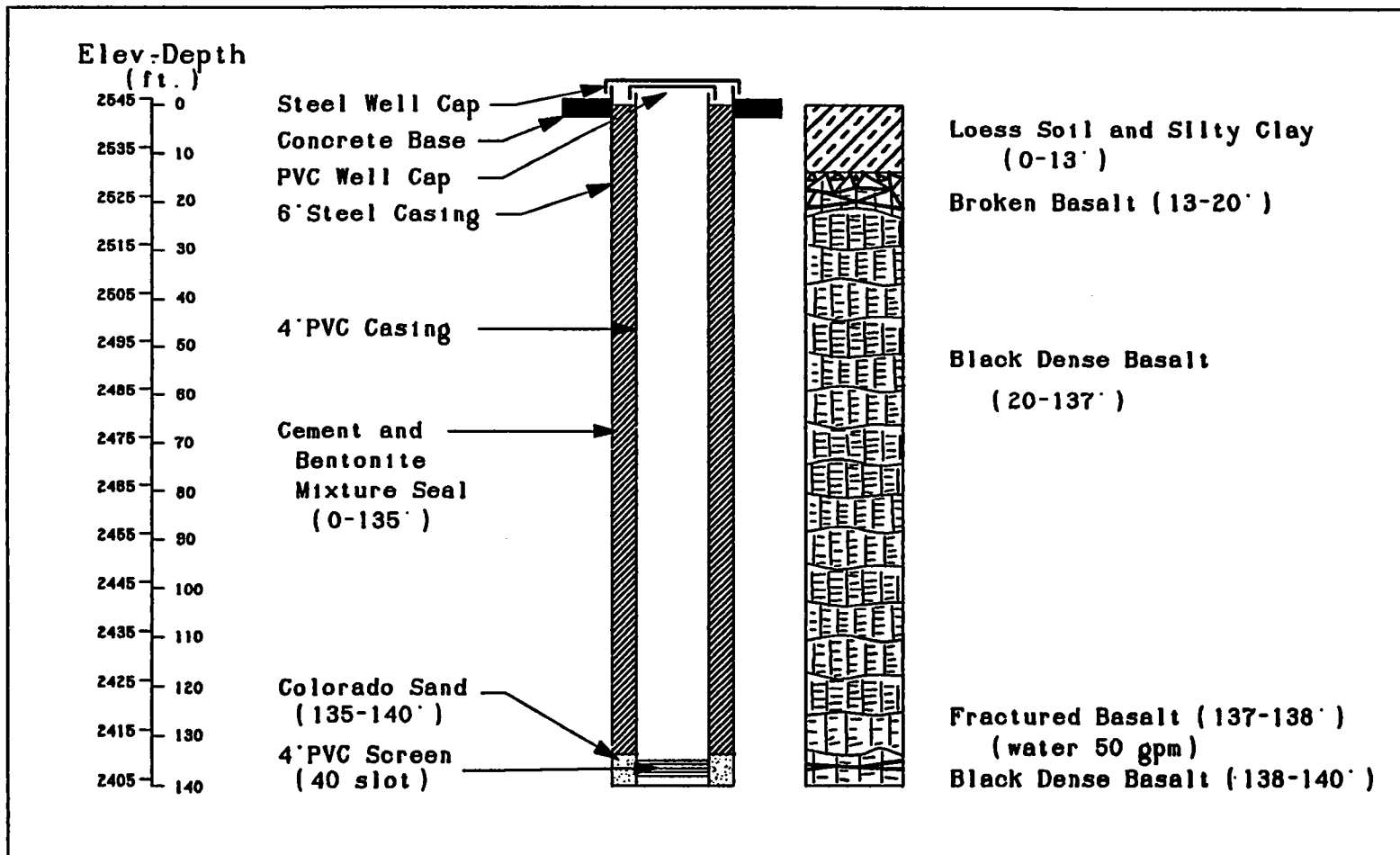


Figure A-3. Construction and geology logs of well D19D

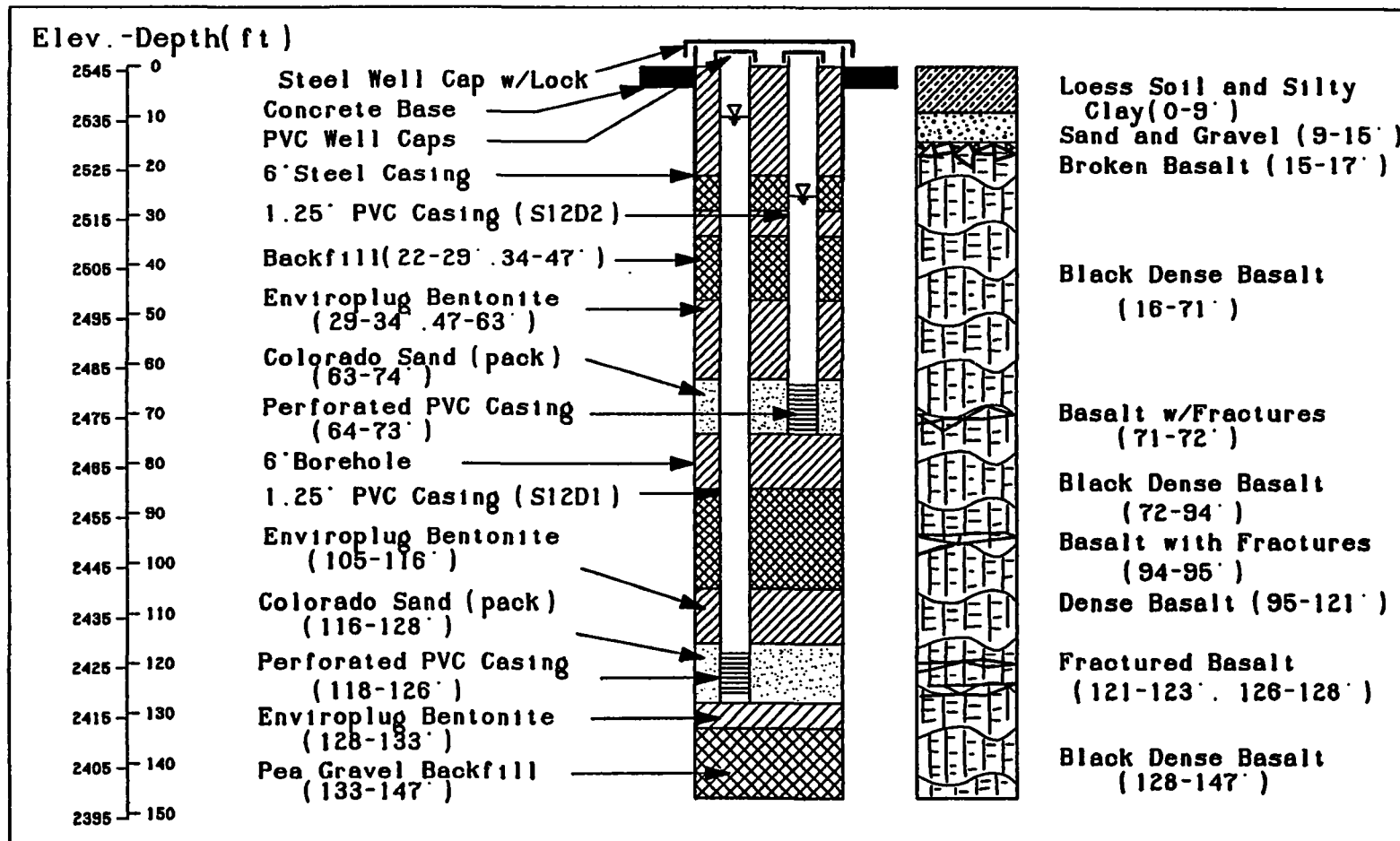


Figure A-4. Construction and geology logs of wells S12D1 and S12D2

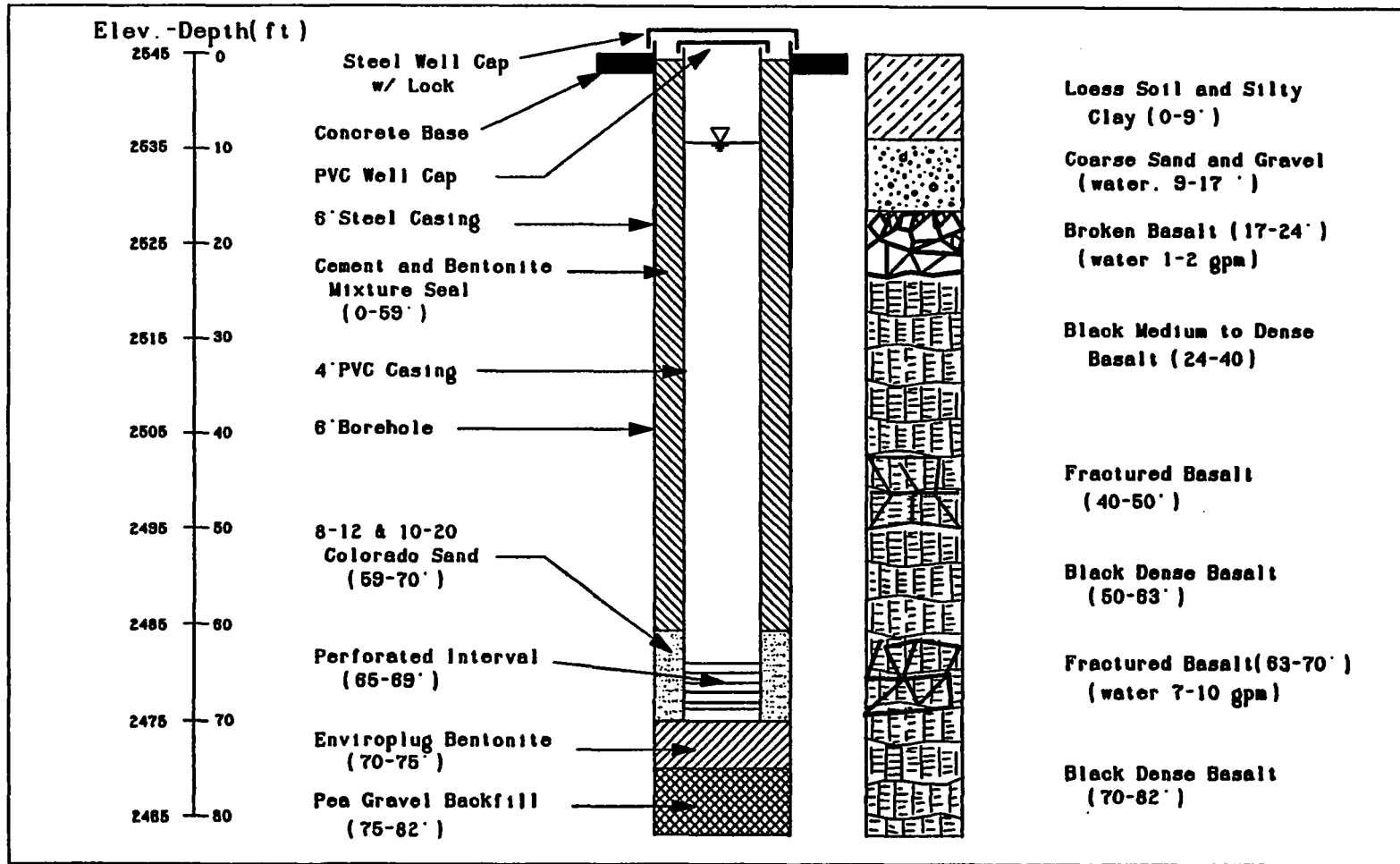


Figure A-5. Construction and geology logs of well T16D

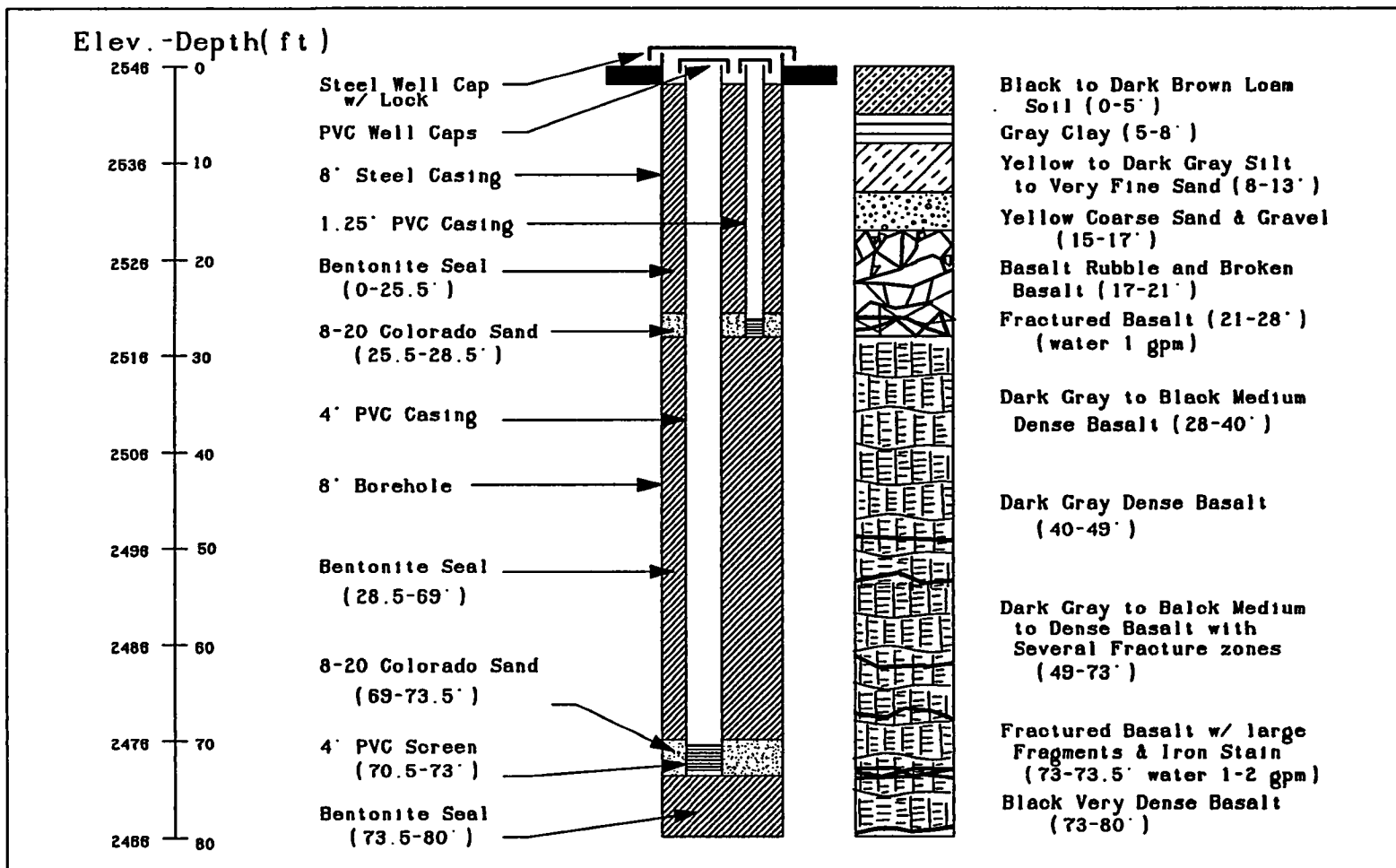


Figure A-6. Construction and geology logs of wells Q16D and Q16S

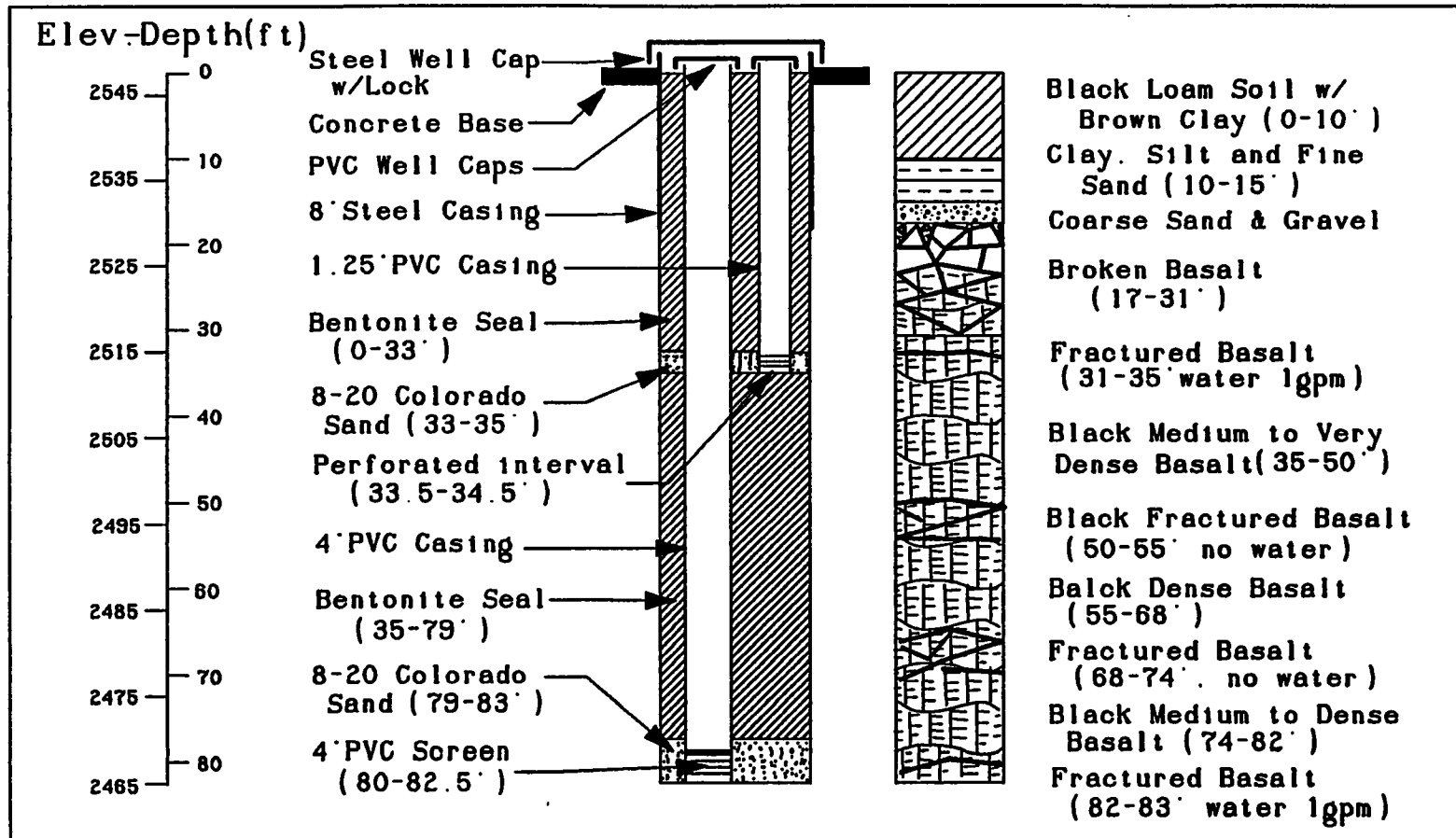


Figure A-7. Construction and geology logs of wells U3D and U3S

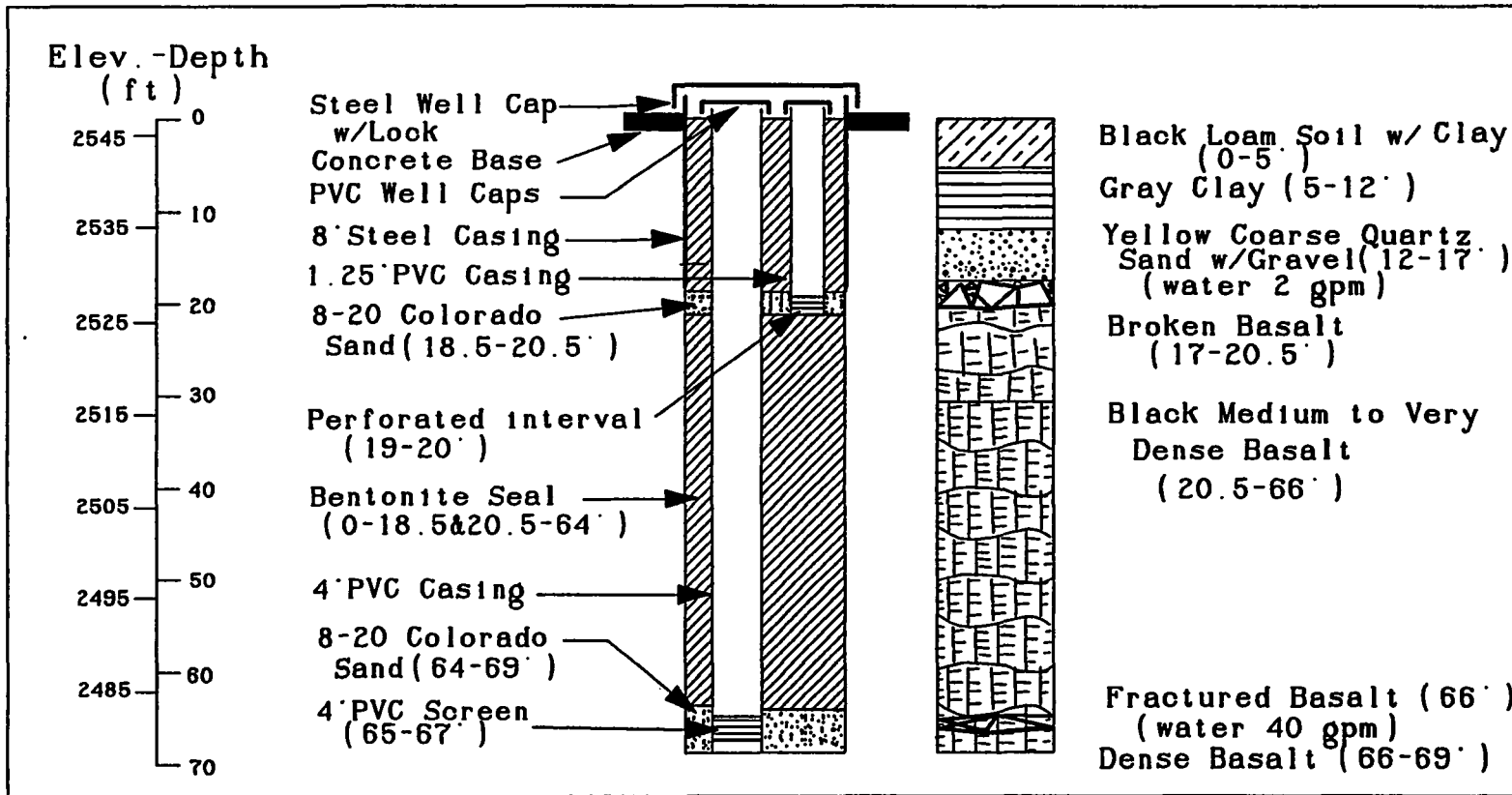


Figure A-8. Construction and geology logs of wells J16D and J16S

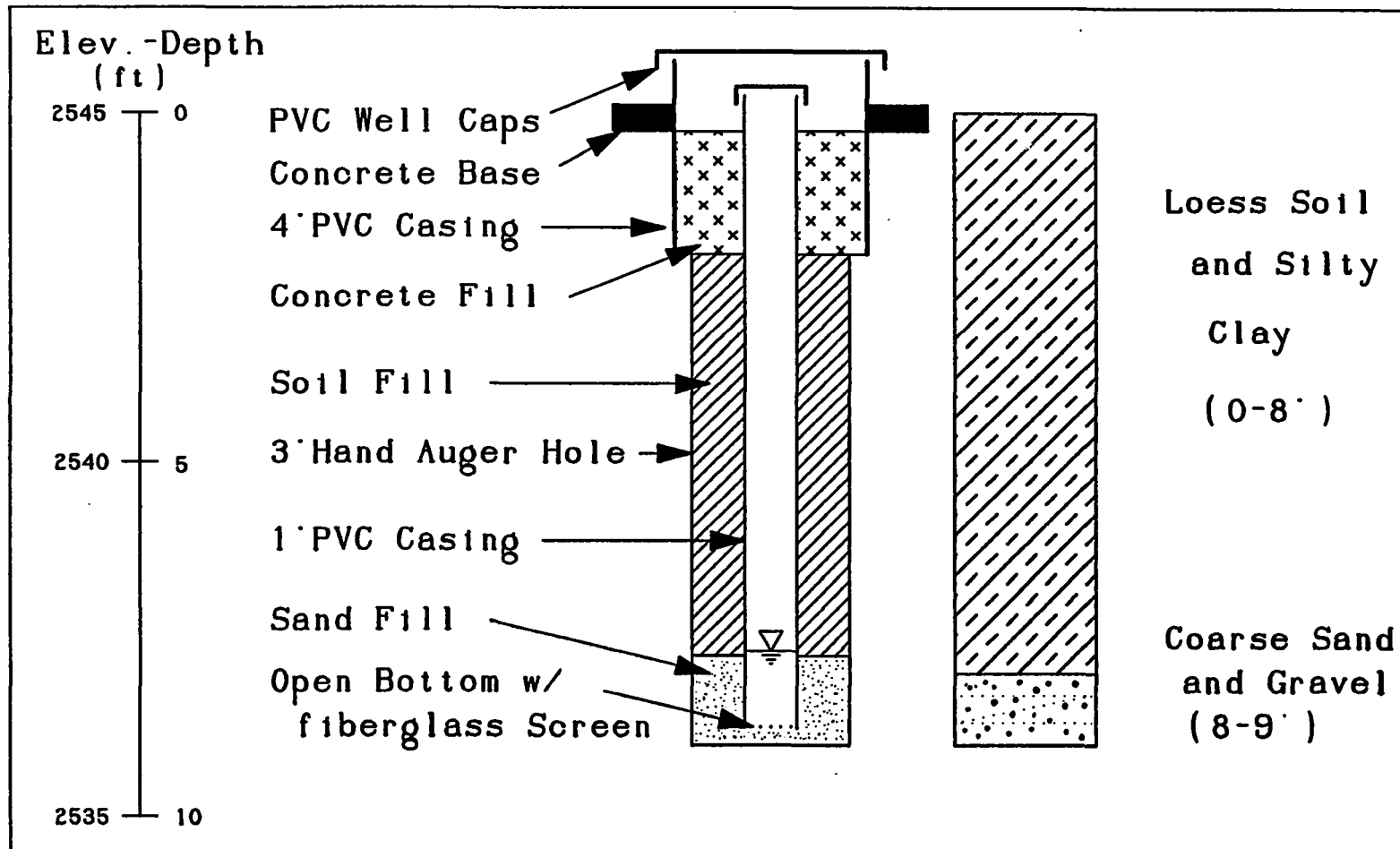


Figure A-9. Construction and geology logs of well P17S

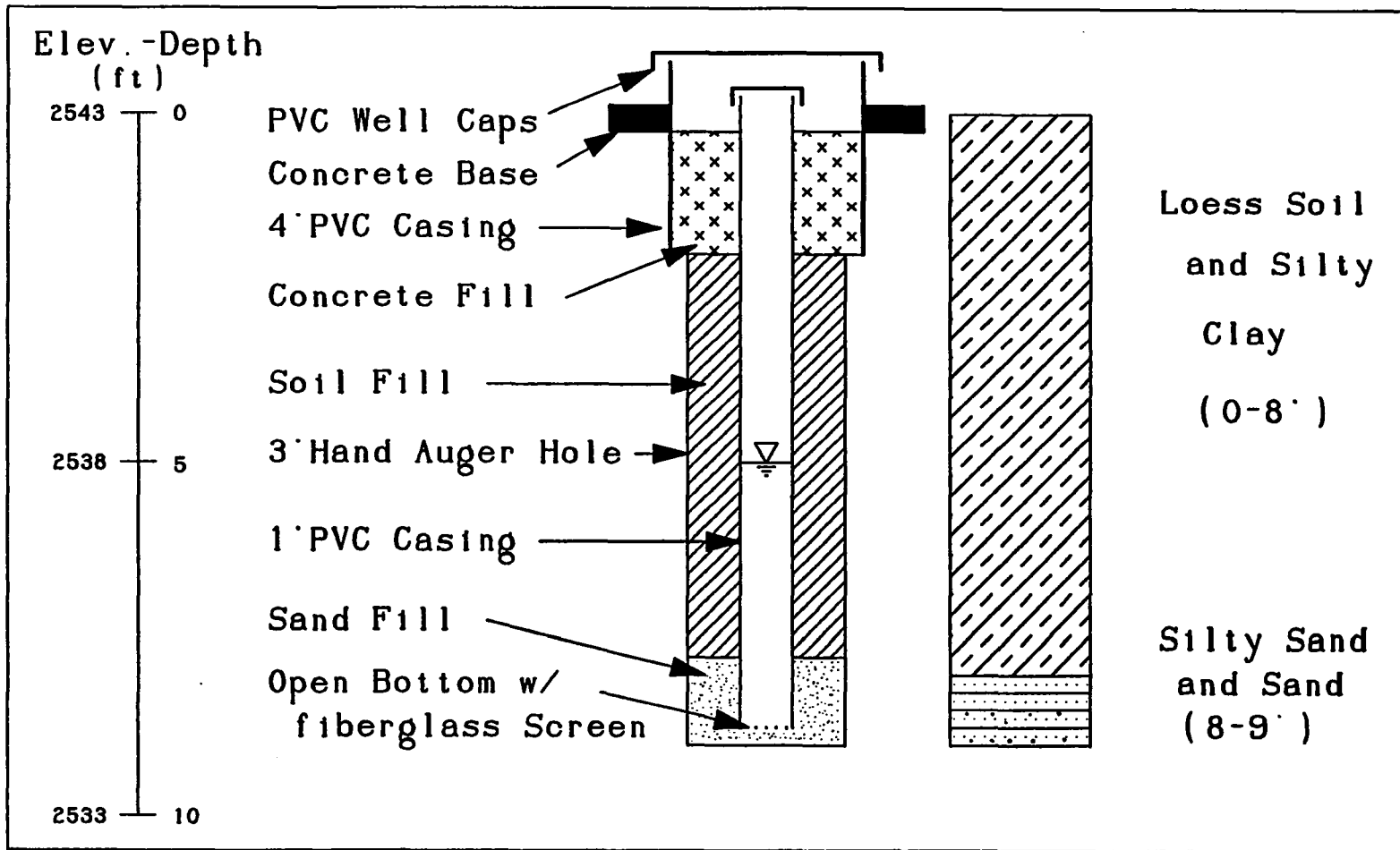


Figure A-10. Construction and geology logs of well V16S

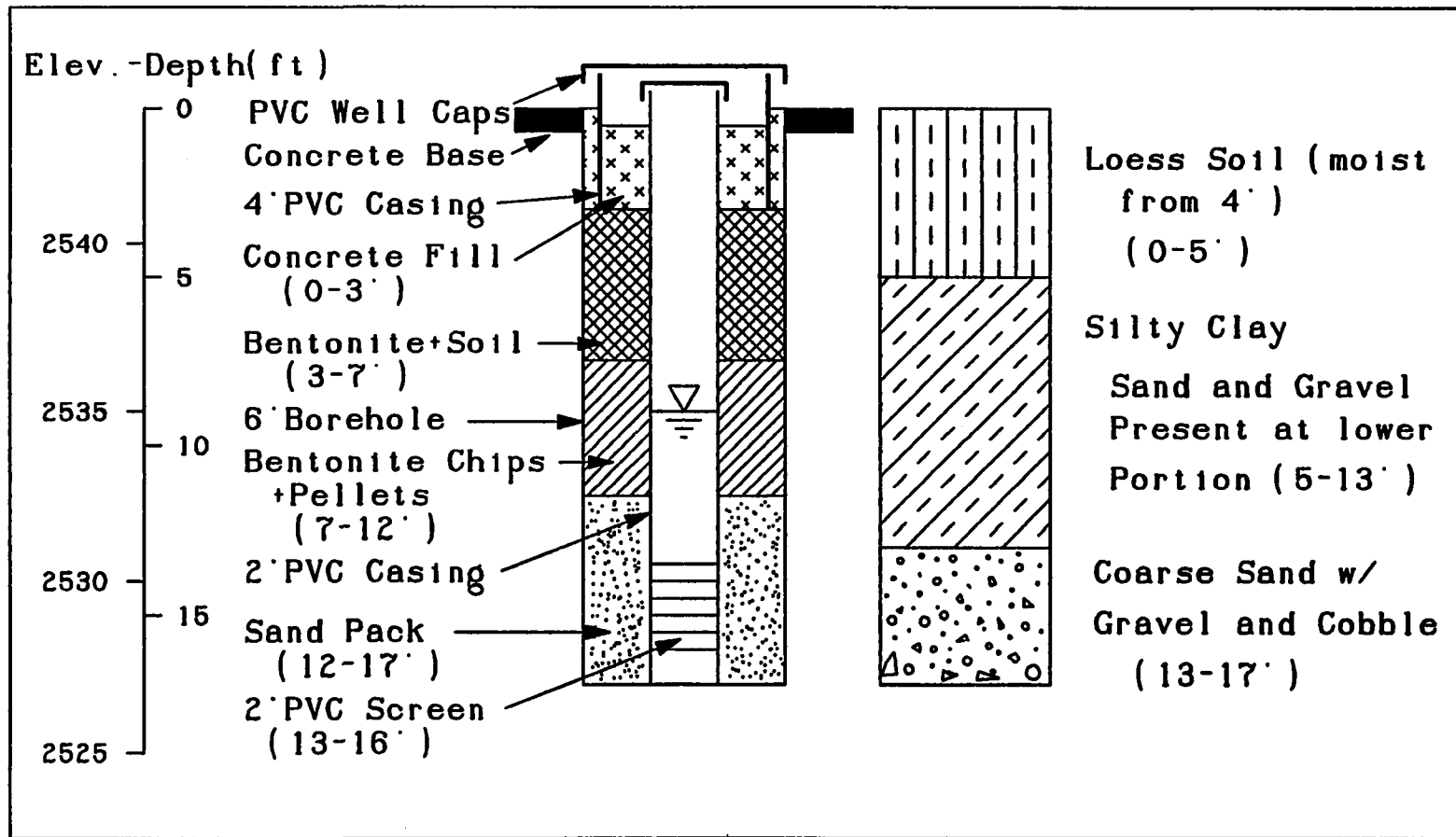


Figure A-11. Construction and geology logs of well N18S

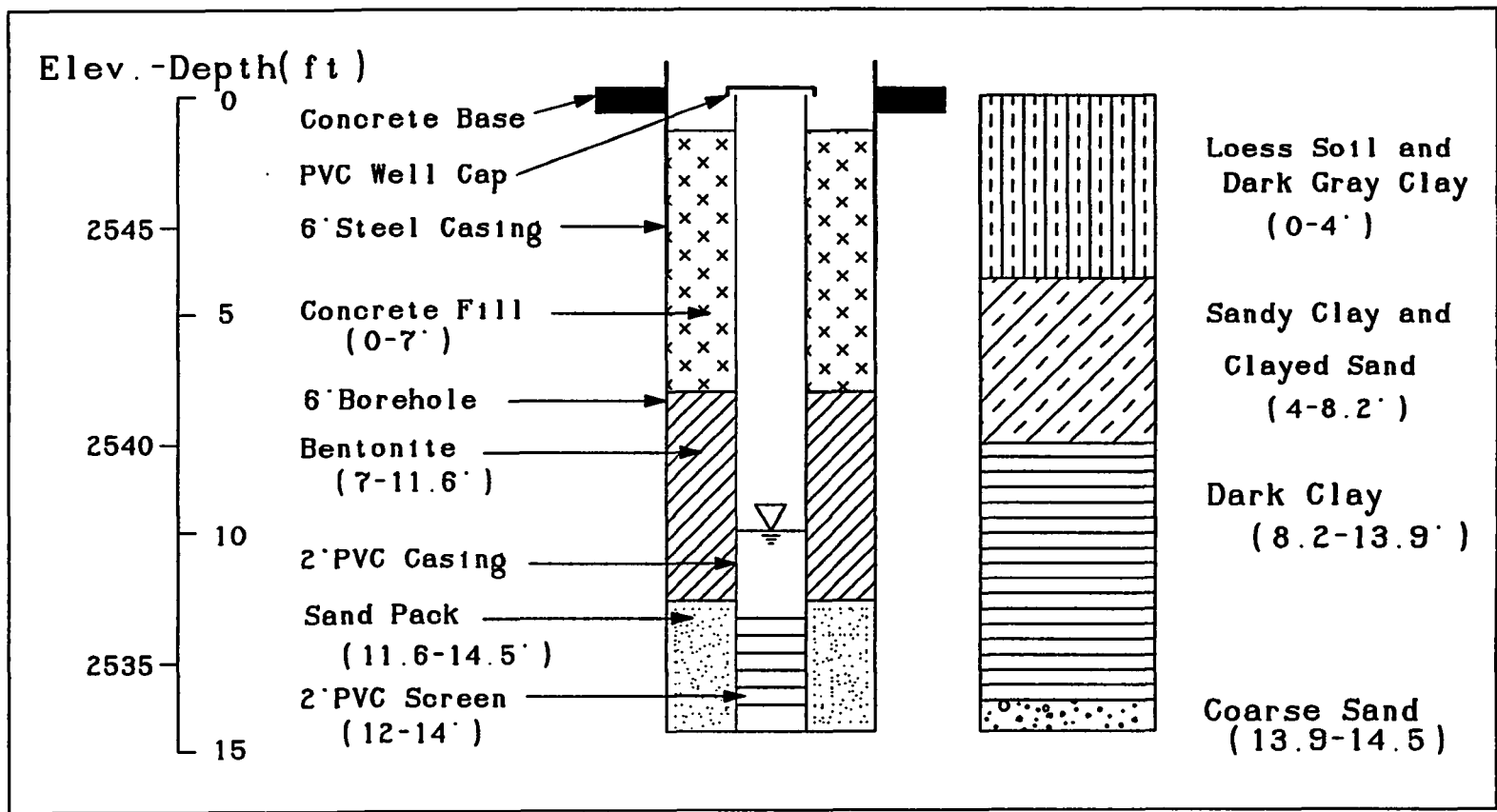


Figure A-12. Construction and geology logs of well T8S

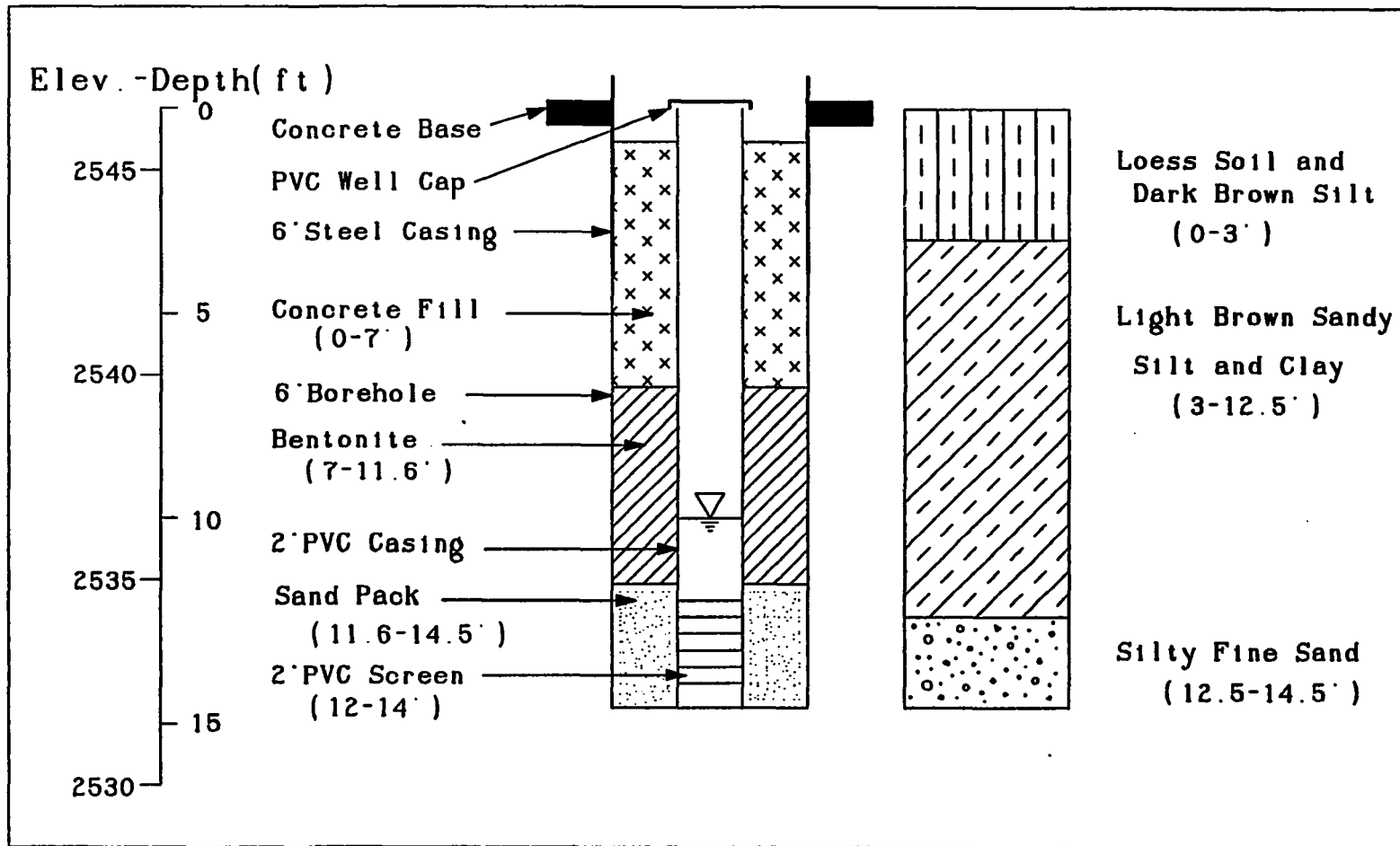


Figure A-13. Construction and geology logs of well H12S

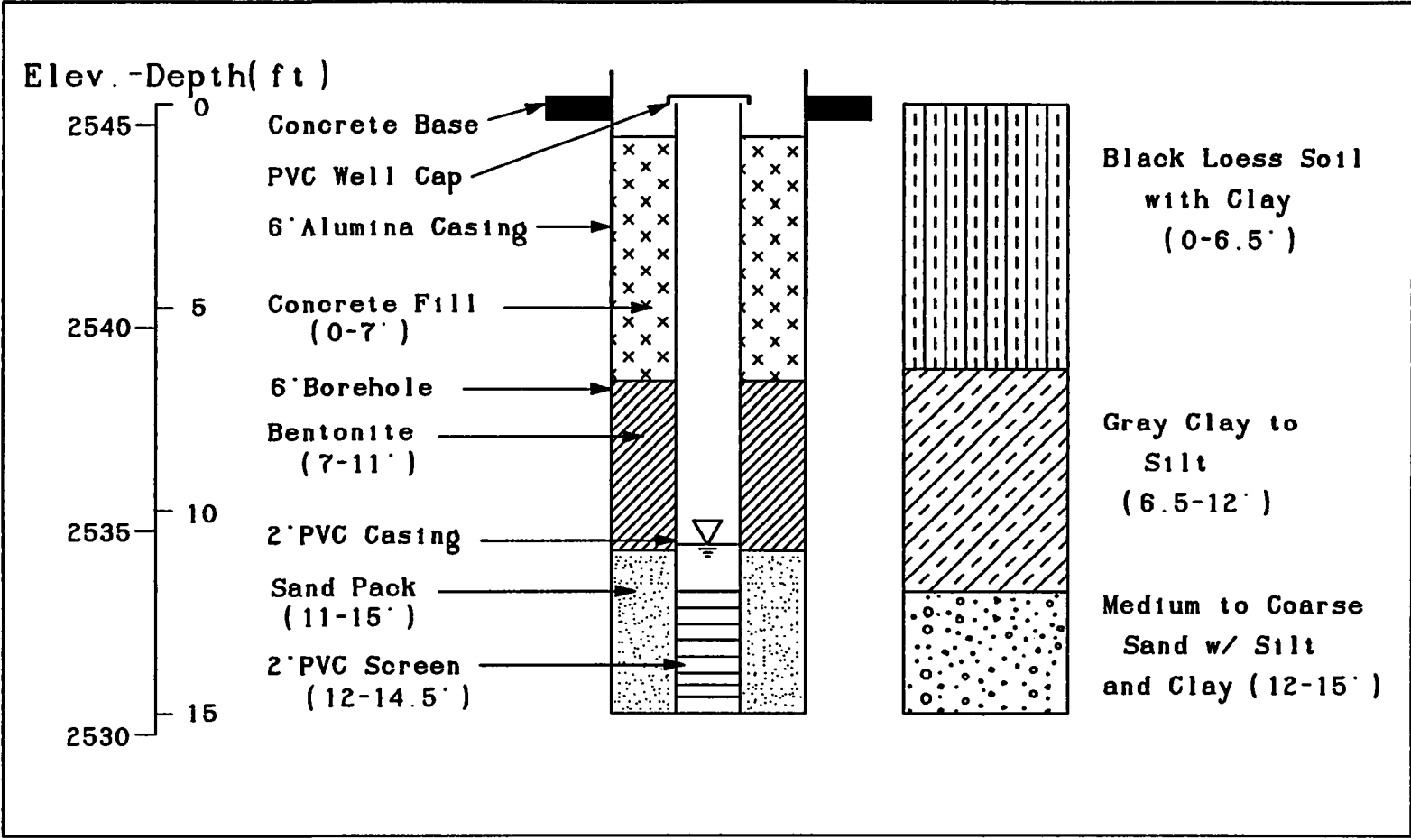


Figure A-14. Construction and geology logs of well J17S

APPENDIX B
Aquifer Hydraulic Test Data

Table B-1. AQUIFER TEST 9-22-89 DATA**PUMPING WELL Q17D (DATA LOGGER MEASUREMENTS)**

Elapse Time (min)	Drawdown (feet)	Elapse Time (min)	Drawdown (feet)
0.01	0.72	22	22.97
0.04	1.94	34	23.21
0.07	2.25	49	21.81
0.09	2.21	65	24.17
0.11	2.43	80	24.06
0.14	2.80	95	23.75
0.17	2.87	110	23.62
0.21	3.30	125	23.49
0.27	3.71	140	23.18
0.32	4.02	160	23.49
0.52	5.42	185	23.45
0.67	6.25	200	23.69
0.89	7.47	230	23.54
1.14	8.63	280	23.25
1.39	9.72	340	23.22
1.81	11.28	440	23.19
2.31	12.82	570	22.99
3.14	14.90	720	23.59
3.97	16.46	870	23.66
4.97	17.86	1020	23.75
6.64	19.47	1110	24.52
8.67	20.72	1200	24.42
10.67	21.46	1380	24.47
12.67	22.05	1440	24.59
14.67	22.40		

OBSERVATION WELL S12D2**DATA LOGGER MEASUREMENTS**

Elapse Time (min)	Drawdown (feet)
750	0.09
780	0.02
810	0.06
840	0.02
870	0.04
900	0.02
930	0.02
960	0.01
990	0.01
1020	0.05
1050	0.13
1080	0.14
1110	0.14
1140	0.22
1170	0.28
1200	0.31
1230	0.33
1260	0.27
1290	0.30
1320	0.31
1350	0.29
1380	0.31
1410	0.27
1440	0.19

HAND MEASUREMENTS

Elapse Time (min)	Drawdown (feet)
109	0.01
153	0.02
202	0.02
237	0.03
298	0.04
359	0.05
421	0.04
480	0.04
536	0.07
595	0.08
653	0.09
719	0.1
775	0.11
840	0.11
896	0.13
955	0.13
1019	0.16
1098	0.19
1143	0.19
1203	0.19
1263	0.21
1315	0.21
1378	0.22

OBSERVATION WELL V16D

DATA LOGGER MEASUREMENTS

Elapse Time (min)	Drawdown (feet)
0.21	0.01
0.37	0.04
0.52	0.12
0.67	0.07
0.89	0.11
1.14	0.13
1.39	0.16
1.81	0.20
2.31	0.23
2.81	0.16
3.31	0.29
3.81	0.29
4.64	0.34
5.64	0.32
6.64	0.42
8.67	0.43
10.67	0.45
12.67	0.43
21	0.47
22	0.47
53	0.62
75	0.65
90	0.67
107	0.69
149	0.71
171	0.73
199	0.76
234	0.76
272	0.77
301	0.78
363	0.79
429	0.81
485	0.81
540	0.82
599	0.84
657	0.85
724	0.85
780	0.86
842	0.87
899	0.87
958	0.85
1028	0.90
1101	0.92
1149	0.91
1210	0.93
1264	0.94
1377	0.94
1434	0.94

HAND MEASUREMENTS

Elapse Time (min)	Drawdown (feet)
3	0.13
4	0.16
5	0.18
6	0.2
21	0.47
22	0.47
53	0.62
107	0.69
149	0.71
171	0.73
199	0.76
234	0.76
272	0.77
301	0.78
363	0.79
429	0.81
485	0.81
540	0.82
599	0.84
657	0.85
724	0.85
780	0.86
842	0.87
899	0.87
958	0.85
1028	0.9
1101	0.92
1149	0.91
1210	0.93
1264	0.94
1377	0.94
1434	0.94

OBSERVATION WELL D19D (HAND MEASUREMENTS)

Elapse Time (min)	Drawdown (feet)	Elapse Time (min)	Drawdown (feet)
445	0.01	854	0.15
500	0.04	898	0.2
556	0.04	966	0.17
611	0.05	1046	0.22
667	0.06	1111	0.22
735	0.1	1283	0.15
788	0.12	1382	0.16

OBSERVATION WELL T16D

DATA LOGGER MEASUREMENTS

Elapse Time (min)	Drawdown (feet)	Elapse Time (min)	Drawdown (feet)
0.02	0.003	14	2.72
0.04	0.01	25	3.13
0.06	0.02	39	3.26
0.09	0.02	49	3.31
0.14	0.03	54	3.32
0.21	0.02	65	3.34
0.27	0.03	75	3.34
0.32	0.06	90	3.34
0.37	0.07	105	3.30
0.42	0.07	120	3.32
0.47	0.08	135	3.31
0.52	0.10	155	3.30
0.62	0.13	175	3.29
0.72	0.17	195	3.31
0.81	0.20	220	3.32
0.97	0.25	260	3.24
1.06	0.28	300	3.27
1.31	0.38	380	3.23
1.64	0.51	480	3.17
2.14	0.68	600	3.16
2.64	0.87	720	3.18
3.14	1.03	840	3.13
3.64	1.19	960	3.12
4.31	1.39	1140	3.32
5.31	1.66	1230	3.34
6.31	1.87	1320	3.36
8.01	2.15	1410	3.35
10	2.41	1440	3.39
12	2.58		

HAND MEASUREMENTS

Elapse Time (min)	Drawdown (feet)	Elapse Time (min)	Drawdown (feet)
0.1	0.05	546	3.2
1	0.28	604	3.21
2	0.77	660	3.24
18	2.71	728	3.25
19	2.75	784	3.27
20	2.76	846	3.26
21	2.78	903	3.29
43	3.05	961	3.24
44	3.06	1036	3.31
94	3.15	1105	3.4
168	3.15	1215	3.4
211	3.21	1320	3.41
366	3.21	1440	3.41
491	3.21		

OBSERVATION WELL S12D1 (HAND MEASUREMENTS)

Elapse Time (min)	Drawdown (feet)	Elapse Time (min)	Drawdown (feet)
1	0.01	70	0.7
1.2	0.02	80	0.74
1.5	0.02	90	0.79
2	0.02	100	0.8
4	0.03	110	0.84
4.5	0.04	120	0.85
5	0.05	130	0.87
7	0.07	140	0.88
8	0.08	150	0.89
10	0.11	160	0.9
11	0.12	170	0.9
12	0.13	180	0.91
13	0.15	201	0.91
14	0.16	220	0.94
15	0.17	240	0.94
16	0.19	300	0.95
17	0.2	361	0.97
18	0.22	425	0.98
19	0.23	486	1
20	0.24	538	1
22	0.27	597	1.01
24	0.29	654	1.02
26	0.29	721	1.04
28	0.34	777	1.04
30	0.37	838	1.04
35	0.41	953	1.05
40	0.48	1020	1.07
45	0.53	1145	1.09
50	0.56	1265	1.09
55	0.61	1440	1.1
60	0.64		

PIEZOMETER P17S (HAND MEASUREMENTS)

Elapse Time (min)	Drawdown (feet)	Elapse Time (min)	Drawdown (feet)
15	0.01	150	0.24
17	0.02	180	0.26
19	0.02	200	0.27
20	0.03	220	0.28
22	0.04	240	0.29
28	0.04	305	0.31
34	0.06	436	0.32
40	0.08	494	0.33
45	0.1	549	0.36
55	0.12	662	0.37
60	0.14	785	0.38
70	0.16	903	0.4
80	0.17	1031	0.43
90	0.2	1154	0.44
110	0.22	1278	0.46
140	0.23	1418	0.46

PIEZOMETER V16S (HAND MEASUREMENTS)

Elapse Time (min)	Drawdown (feet)	Elapse Time (min)	Drawdown (feet)
1	0.01	160	0.31
2	0.02	170	0.33
6	0.03	180	0.35
35	0.04	200	0.36
45	0.04	240	0.39
50	0.06	302	0.44
55	0.07	365	0.46
60	0.09	430	0.48
70	0.11	543	0.51
80	0.14	658	0.52
90	0.16	782	0.54
100	0.2	901	0.56
110	0.22	1033	0.58
120	0.24	1212	0.6
130	0.27	1320	0.62
140	0.29	1379	0.62
150	0.31		

PIEZOMETER N18S (HAND MEASUREMENTS)

Elapse Time (min)	Drawdown (feet)	Elapse Time (min)	Drawdown (feet)
5	0.01	90	0.31
6	0.03	100	0.3
7	0.04	110	0.33
8	0.04	120	0.33
9	0.05	130	0.34
10	0.06	140	0.34
11	0.07	150	0.34
12	0.08	160	0.34
13	0.09	170	0.34
14	0.1	180	0.35
15	0.11	200	0.36
16	0.12	220	0.37
17	0.13	240	0.38
18	0.13	307	0.38
19	0.14	371	0.39
20	0.14	442	0.4
22	0.16	498	0.4
24	0.17	552	0.42
26	0.18	608	0.42
28	0.19	664	0.44
30	0.2	731	0.44
35	0.22	787	0.44
40	0.24	851	0.44
45	0.25	901	0.45
50	0.26	964	0.45
55	0.26	1044	0.47
60	0.26	1280	0.48
70	0.29	1440	0.51
80	0.3		

Table B-2. AQUIFER TEST 4-4-90 DATA**PUMPING WELL T16D (HAND MEASUREMENTS)**

Elapse Time (min)	Drawdown (feet)	Elapse Time (min)	Drawdown (feet)
0.3	2.6	15.3	21.5
0.5	3.55	16.5	21.7
0.7	5.1	18	21.9
0.9	6.6	19	22
1	7.4	20	22.1
1.2	8	21	22.2
1.4	8.7	22	22.3
1.5	9.2	25	22.45
1.6	9.6	27	22.6
1.8	10.5	29	22.75
2	10.8	33	23
2.2	11.3	35	23.15
2.4	11.8	41	23.4
2.5	12.2	45	23.65
2.8	12.95	50	23.8
3	13.35	62	24.3
3.2	13.8	70	24.65
3.5	14.35	78	24.85
3.7	14.7	82	24.9
4	15.35	93	25.25
4.3	15.7	100	25.45
4.5	16	109	25.6
5.1	16.7	124	25.76
5.9	17.6	134	25.98
7	18.55	144	26.25
7.9	19.1	162	26.5
9	19.65	175	26.6
10	20.05	229	27.35
11	20.4	254	27.53
12	20.75	288	27.67
13	21.05	303	27.9
14.3	21.3		

OBSERVATION WELL S12D2 (HAND MEASUREMENTS)

Elapse Time (min)	Drawdown (feet)	Elapse Time (min)	Drawdown (feet)
41	0.01	84	0.01
44	0.01	108	0.01
46	0.01	122	0.02
49	0.015	143	0.03
52	0.02	171	0.05
54	0.01	217	0.08
56	0.02	290	0.12
58	0.01	316	0.12
66	0.01	326	0.18
69	0.02		

OBSERVATION WELL V16D

DATA LOGGER MEASUREMENTS

Elapse Time (min)	Drawdown (feet)
0.02	0.01
0.05	0.01
0.07	0.01
0.10	0.00
0.12	0.01
0.15	0.01
0.20	0.02
0.25	0.02
0.30	0.03
0.35	0.04
0.40	0.05
0.45	0.07
0.52	0.08
0.60	0.10
0.67	0.12
0.75	0.14
0.85	0.16
0.95	0.18
1.05	0.21
1.37	0.28
1.67	0.34
1.97	0.40
2.27	0.44
2.57	0.50
2.87	0.54
3.17	0.58
3.47	0.62
3.77	0.65
4.07	0.70
4.37	0.73
4.67	0.76
4.97	0.79
5.27	0.81
5.57	0.84
5.87	0.87
6.17	0.89
6.47	0.91
6.77	0.93
7.17	0.95
7.57	0.98
8.57	1.03
8.97	1.04
9.37	1.06
9.77	1.07
10.17	1.08
10.57	1.10
10.97	1.12
12.17	1.14
13.37	1.17
14.57	1.19
26.57	1.32
48.41	1.44
60.41	1.43
72.41	1.46
84.41	1.50
113.41	1.51
149.41	1.54
185.41	1.46
221.41	1.56
257.41	1.59
293.41	1.56
329.41	1.49

HAND MEASUREMENTS

Elapse Time (min)	Drawdown (feet)
0.5	0.03
1	0.22
1.5	0.32
2.9	0.49
3.5	0.6
4	0.68
4.7	0.73
5	0.79
5.5	0.83
5.9	0.86
6.75	0.91
7.5	0.94
8.3	1.01
9.2	1.04
9.75	1.08
10.5	1.09
11.2	1.1
11.9	1.14
12.5	1.15
13.5	1.16
15.5	1.21
16.2	1.22
16.7	1.23
17.2	1.24
17.9	1.26
18.5	1.26
19.5	1.27
20	1.28
21	1.29
22	1.3
23	1.3
24	1.31
25	1.33
26	1.34
27	1.34
29	1.35
33	1.36
35	1.37
37	1.38
39	1.39
41	1.4
43	1.41
47	1.42
50	1.45
58	1.46
62	1.46
69	1.47
74	1.49
79	1.49
84	1.51
89	1.51
94	1.51
112	1.53
127	1.55
149	1.56
172	1.57
181	1.58
226	1.62
237	1.63
318	1.64

OBSERVATION WELL Q17D

DATA LOGGER MEASUREMENTS

Elapse Time (min)	Drawdown (feet)
0.023	0.003
0.048	0.003
0.073	0.002
0.098	0.003
0.123	0.005
0.15	0.01
0.17	0.01
0.20	0.01
0.22	0.01
0.30	0.03
0.37	0.05
0.45	0.09
0.52	0.12
0.60	0.16
0.67	0.20
0.75	0.24
0.82	0.28
0.90	0.33
0.97	0.37
1.05	0.41
1.45	0.67
2.25	1.17
3.05	1.61
3.85	1.99
4.65	2.31
5.45	2.57
6.25	2.79
7.05	2.97
7.85	3.13
8.65	3.24
9.45	3.34
10.25	3.42
11.05	3.49
11.92	3.56
12.72	3.61
13.92	3.69
25.57	4.00
54.41	4.25
75.41	4.33
87.41	4.36
122	4.40
131	4.42
149	4.43
167	4.45
185	4.45
194	4.89
203	4.96
212	4.59
221	4.54
230	4.46
248	4.50
266	4.52
284	4.25
302	4.53
347	4.50

HAND MEASUREMENTS

Elapse Time (min)	Drawdown (feet)
0.2	0.17
0.5	0.22
0.7	0.42
1	0.47
1.5	0.92
2	1.12
2.5	1.37
3	1.67
3.5	1.87
4	2.17
5	2.47
6	2.67
7	2.97
8	3.17
9	3.32
10	3.42
11	3.52
12	3.57
14	3.67
16	3.77
19	3.87
21	3.92
25	3.97
30	4.02
35	4.07
41	4.12
49	4.17
61	4.22
70	4.26
80	4.3
91	4.33
114	4.37
131	4.41
152	4.45
173	4.47
219	4.57
242	4.55
250	4.54
282	4.55
288	4.57
306	4.55

OBSERVATION WELL S12D1

DATA LOGGER MEASUREMENTS

Elapse Time (min)	Drawdown (feet)
0.5	0.005
0.6	0.01
0.7	0.009
0.8	0.01
0.9	0.014
1.0	0.02
1.4	0.02
1.8	0.03
2.2	0.03
2.6	0.04
3.0	0.04
3.4	0.05
3.8	0.05
4.2	0.06
4.6	0.07
5.0	0.07
5.8	0.09
6.6	0.11
7.4	0.13
8.2	0.14
9.0	0.16
9.8	0.18
10.6	0.20
11.4	0.23
12.2	0.25
13.0	0.27
15.2	0.34
20.7	0.44
22.7	0.48
24.7	0.47
26.7	0.51
28.7	0.56
37.4	0.70
49.4	0.86
55.4	0.91
64.4	0.98
73.4	1.01
82.4	1.08
98.4	1.13
116.4	1.17
161.4	1.33
197.4	1.56
233.4	1.50
332.4	1.72
341.4	1.71

HAND MEASUREMENTS

Elapse Time (min)	Drawdown (feet)
2	0.02
4.5	0.02
7	0.09
9	0.16
13	0.24
16.5	0.33
19	0.39
22	0.45
24	0.52
28	0.58
31.5	0.66
34	0.7
37	0.73
40	0.78
42	0.82
45	0.85
48	0.88
50	0.91
53	0.93
56	0.97
58	0.99
61	1.01
68	1.07
82	1.15
105	1.25
124	1.32
141	1.36
169	1.44
215	1.74

PIEZOMETER P17S (HAND MEASUREMENTS)

Elapse Time (min)	Drawdown (feet)	Elapse Time (min)	Drawdown (feet)
17	0.01	99	0.115
29	0.015	113	0.12
33	0.03	132	0.135
51	0.05	142	0.14
60	0.07	152	0.15
68	0.08	169	0.16
82	0.1	209	0.18
90	0.105	249	0.2

PIEZOMETER V16S (HAND MEASUREMENTS)

Elapse Time (min)	Drawdown (feet)	Elapse Time (min)	Drawdown (feet)
22	0.04	117	0.24
27	0.06	127	0.24
44	0.09	134	0.26
53	0.11	158	0.27
60	0.16	198	0.29
75	0.19	248	0.32
85	0.2	356	0.33
93	0.21		

PIEZOMETER N18S (HAND MEASUREMENTS)

Elapse Time (min)	Drawdown (feet)	Elapse Time (min)	Drawdown (feet)
3	0.01	82	0.2
10	0.035	89	0.19
16	0.07	103	0.2
18	0.1	122	0.2
26	0.11	132	0.2
41	0.155	141	0.2
49	0.165	150	0.2
58	0.175	201	0.25
72	0.19	250	0.24

Table B-3. AQUIFER TEST 4-11-90 DATA**OBSERVATION WELL V16D (DATA LOGGER MEASUREMENTS)**

Elapse Time (min)	Drawdown (feet)	Elapse Time (min)	Drawdown (feet)
0.41	0.003	40	1.38
0.80	0.001	43	1.39
0.81	0.01	50	1.38
0.82	0.01	58	1.39
0.82	0.01	66	1.42
0.83	0.01	74	1.34
0.84	0.01	82	1.29
0.85	0.01	90	1.26
0.98	0.01	102	1.27
1.35	0.01	126	1.40
1.75	0.03	142	1.48
1.95	0.05	166	1.36
2.15	0.07	190	1.35
2.75	0.16	218	1.34
3.15	0.21	250	1.41
3.55	0.27	290	1.44
3.95	0.32	330	1.40
4.58	0.39	390	1.38
5.25	0.47	430	1.42
5.92	0.54	482	1.36
7.17	0.67	550	1.28
8.50	0.77	670	1.47
9.83	0.88	790	1.08
10.8	0.93	910	1.26
11.5	0.95	1000	1.28
12.3	0.99	1120	1.35
13.7	1.04	1240	1.41
15.4	1.07	1360	1.39
17.4	1.11	1480	1.39
19.4	1.15	1620	1.35
21	1.19	1740	1.45
23	1.21	1860	1.28
25	1.25	1980	1.26
27	1.26	2100	1.35
29	1.28	2340	1.43
31	1.30	2580	1.45
33	1.32	2700	1.63
35	1.33	2820	1.60
37	1.35		

OBSERVATION WELL T16D (DATA LOGGER MEASUREMENTS)

Elapse Time (min)	Drawdown (feet)	Elapse Time (min)	Drawdown (feet)
0.407	0.005	32	5.17
0.798	0.001	36	5.24
0.807	0.01	40	5.31
0.815	0.01	44	5.34
0.823	0.01	46	5.35
0.832	0.01	62	5.37
0.84	0.01	70	5.32
0.91	0.01	78	5.27
0.96	0.01	86	5.25
0.98	0.01	94	5.26
1.0	0.01	102	5.29
1.3	0.01	122	5.43
1.6	0.07	138	5.52
1.9	0.25	154	5.53
2.2	0.47	170	5.43
2.5	0.70	202	5.45
2.8	0.92	266	5.52
3.1	1.15	314	5.57
3.4	1.36	362	5.68
3.7	1.56	410	5.99
4.0	1.76	458	5.57
4.5	2.05	518	5.79
5.0	2.31	610	5.80
5.5	2.56	730	5.79
6.1	2.81	850	5.45
7.1	3.20	970	5.63
8.1	3.52	1090	5.62
9.1	3.79	1210	5.73
10	4.02	1330	5.76
11	4.19	1450	5.69
12	4.32	1590	5.68
13	4.43	1710	5.35
14	4.55	1830	5.39
16	4.65	1950	5.36
18	4.76	2070	5.37
20	4.85	2190	5.71
22	4.93	2430	5.41
24	5.00	2670	5.91
26	5.06	2790	5.95
28	5.10	2910	5.85
30	5.13		

Table B-4. AQUIFER TEST 6-3-90 DATA

OBSERVATION WELL T16D (HAND MEASUREMENTS)

Elapse Time (min)	Drawdown (feet)	Elapse Time (min)	Drawdown (feet)
0.08	0.07	10	8.97
0.16	0.15	11	9.28
0.25	0.24	12	9.58
0.33	0.32	13	9.77
0.42	0.39	14.3	10.02
0.5	0.48	15.5	10.25
0.59	0.57	16	10.35
0.67	0.64	17	10.45
0.75	0.71	18	10.58
0.83	0.8	19	10.69
0.92	0.89	20	10.79
1	0.99	22	10.98
1.08	1.04	24	11.11
1.16	1.3	26	11.25
1.25	1.55	28	11.39
1.33	1.66	30	11.49
1.42	1.8	33	11.62
1.5	1.88	36	11.75
1.59	1.95	39	11.84
1.67	2.08	42	11.93
1.75	2.26	45	12.01
1.83	2.35	48	12.09
1.92	2.45	51	12.14
2	2.54	57	12.24
2.08	2.64	60	12.27
2.16	2.73	65	12.35
2.25	2.96	70	12.44
2.33	3.05	75	12.52
2.42	3.13	80	12.59
2.5	3.2	85	12.64
2.59	3.29	90	12.7
2.67	3.38	95	12.75
2.75	3.48	100	12.8
2.83	3.7	110	12.89
2.92	3.78	120	12.92
3	3.95	130	12.98
3.33	4.38	140	13.03
3.67	4.73	145	13.09
4	5.12	158.5	13.1
5	6.12	182	13.2
6	6.89	204	13.3
7	7.6	296	13.32
8	8.12	414	13.51
9	8.58		

OBSERVATION WELL D19D (HAND MEASUREMENTS)

Elapse Time (min)	Drawdown (feet)	Elapse Time (min)	Drawdown (feet)
5	0.04	115	0.08
37	0.05	135	0.09
60	0.03	192	0.09
75	0.05	311	0.18
90	0.06	420	0.33
100	0.07		

OBSERVATION WELL Q16D

DATA LOGGER MEASUREMENTS

Elapse Time (min)	Drawdown (feet)
0.69	0.025
0.71	0.025
0.72	0.025
0.74	0.029
0.76	0.026
0.77	0.029
0.79	0.029
0.81	0.029
0.87	0.03
0.94	0.04
1.01	0.04
1.07	0.04
1.14	0.05
1.26	0.06
1.32	0.06
1.56	0.07
1.89	0.09
2.0	0.10
2.7	0.16
4.0	0.25
5.3	0.38
6.7	0.53
8.9	0.79
11.1	1.03
11.8	1.10
13.8	1.29
14.3	1.34
15.3	1.42
16.8	1.54
18.3	1.65
20	1.78
22	1.88
24	1.97
26	2.03
28	2.09
30	2.15
32	2.20
34	2.25
36	2.33
38	2.40
40	2.45
42	2.48
44	2.48
46	2.48
48	2.52
50	2.55
54	2.63
58	2.70
62	2.67
67	2.66
72	2.69
77	2.71
82	2.75
87	2.89
92	2.74
102	2.76
112	2.66
122	2.62
132	2.65
142	2.63
152	2.66
162	2.66
172	2.70
192	2.75
212	2.72

HAND MEASUREMENTS

Elapse Time (min)	Drawdown (feet)
0.3	0.01
0.5	0.02
0.9	0.03
1.1	0.04
1.4	0.06
1.6	0.07
1.8	0.08
2.0	0.1
2.5	0.13
2.9	0.16
3.2	0.2
3.5	0.23
3.9	0.26
4.2	0.29
4.6	0.33
5.6	0.46
6.5	0.56
7.3	0.65
8.0	0.73
8.8	0.81
9.7	0.91
10.8	1.03
12.0	1.15
13.4	1.28
14.6	1.38
16.4	1.53
17.4	1.61
18.4	1.65
19.4	1.71
20	1.77
21	1.82
22	1.87
24	1.93
25	2
27	2.06
29	2.13
31	2.17
33	2.23
35	2.27
37	2.32
39	2.35
41	2.38
43	2.4
45	2.43
47	2.45
49	2.47
54	2.52
59	2.55
69	2.61
79	2.67
89	2.7
99	2.71
119	2.75
139	2.77
154	2.78
204	2.8
297	2.71
414	2.71

232	2.78
252	2.68
272	2.74
292	2.64
312	2.64

(CONTINUE FROM LEFT)----

OBSERVATION WELL Q17D (HAND MEASUREMENTS)

Elapse Time (min)	Drawdown (feet)	Elapse Time (min)	Drawdown (feet)
0.3	0.05	18	6.21
0.5	0.11	19	6.31
0.8	0.25	20	6.39
1.0	0.39	21	6.46
1.3	0.55	22	6.51
1.5	0.72	23	6.6
1.8	0.9	24	6.65
2.0	1.09	25	6.7
2.3	1.27	26	6.74
2.5	1.45	27	6.8
2.8	1.62	28	6.84
3.0	1.8	29	6.88
3.3	2	30	6.91
3.5	2.15	32	6.97
3.8	2.36	34	7.05
4.0	2.5	36	7.1
4.3	2.65	38	7.14
4.5	2.84	40	7.2
4.8	2.96	42	7.23
5.0	3.1	44	7.27
5.3	3.25	46	7.31
5.5	3.38	48	7.35
5.8	3.5	50	7.37
6.0	3.61	65	7.53
6.3	3.75	70	7.58
6.5	3.87	75	7.65
6.8	3.97	80	7.69
7.0	4.08	85	7.72
7.3	4.17	90	7.77
7.5	4.28	95	7.8
7.8	4.37	100	7.84
8.0	4.46	110	7.89
9.3	4.85	130	7.97
10.3	5.08	140	7.99
11.3	5.33	160	8.04
12.3	5.5	184	8.13
13.3	5.69	206	8.2
14.5	5.85	299	8.21
16.5	6.09	416	8.36
17.0	6.12		

OBSERVATION WELL S12D2 (HAND MEASUREMENTS)

Elapse Time (min)	Drawdown (feet)	Elapse Time (min)	Drawdown (feet)
3	0.02	81	0.16
18	0.02	115	0.21
27	0.06	134	0.22
38	0.08	143	0.25
60	0.11	160	0.28
68	0.12	426	0.48

OBSERVATION WELL S12D1 (HAND MEASUREMENTS)

Elapse Time (min)	Drawdown (feet)	Elapse Time (min)	Drawdown (feet)
1.5	1.03	20	10.63
1.8	1.33	21	10.96
2.0	1.43	22	11.18
2.2	1.58	23	11.58
2.3	1.64	24	12.13
2.5	1.75	25	12.33
2.7	1.88	26	12.58
2.8	1.98	27	12.83
3.0	2.08	28	12.96
3.2	2.17	29	13.15
3.3	2.29	30	13.33
3.5	2.42	32	13.63
4.5	3.08	34	13.96
4.8	3.25	36	14.18
5.2	3.5	38	14.42
5.7	3.83	40	14.63
6.0	4.05	42	14.8
6.5	4.38	47	15.17
8.5	5.58	52	15.47
9.0	5.85	57	15.71
9.5	6.13	62	15.83
10.0	6.42	72	16.17
10.5	6.69	82	16.33
11.0	6.93	92	16.5
11.5	7.19	107	16.63
12.0	7.44	117	16.67
13.3	8	127	16.71
14.5	8.6	137	16.5
15.2	8.86	155	16.42
16	9.21	195	16.33
17	9.58	303	16.27
18	9.83	425	16.28
19	10.29		

OBSERVATION WELL J16D (HAND MEASUREMENTS)

Elapse Time (min)	Drawdown (feet)	Elapse Time (min)	Drawdown (feet)
32	0.06	115	0.21
39	0.08	125	0.21
50	0.08	134	0.22
60	0.11	143	0.25
69	0.12	160	0.28
77	0.13	191	0.29
84	0.12	310	0.42
96	0.12	631	0.5
105	0.14		

OBSERVATION WELL U3D (HAND MEASUREMENTS)

Elapse Time (min)	Drawdown (feet)	Elapse Time (min)	Drawdown (feet)
99	0.01	159	0.05
109	0.02	306	0.09
139	0.03	639	0.1

PIEZOMETER P17S (HAND MEASUREMENTS)

Elapse Time (min)	Drawdown (feet)	Elapse Time (min)	Drawdown (feet)
1	0.01	37	0.27
2	0.01	39	0.28
4	0.02	41	0.28
6	0.03	45	0.3
8	0.04	48	0.32
10	0.07	52	0.37
12	0.06	60	0.47
14	0.08	65	0.5
16	0.08	75	0.6
18	0.13	90	0.67
20	0.13	112	0.72
22	0.14	127	0.75
24	0.15	142	0.77
26	0.16	155	0.77
28	0.22	187	0.64
30	0.22	300	0.57
33	0.25	417	0.57
35	0.25		

PIEZOMETER V16S (HAND MEASUREMENTS)

Elapse Time (min)	Drawdown (feet)	Elapse Time (min)	Drawdown (feet)
25	0.3	96	1.14
27	0.34	103	1.18
29	0.37	110	1.22
33	0.44	117	1.25
42	0.6	131	1.3
59	0.84	140	1.33
66	0.92	181	1.35
71	0.96	203	1.38
76	1.01	295	1.41
81	1.05	413	1.45
87	1.09		

PIEZOMETER T8S (HAND MEASUREMENTS)

Elapse Time (min)	Drawdown (feet)	Elapse Time (min)	Drawdown (feet)
29	0.01	127	0.07
60	0.02	137	0.07
87	0.03	160	0.08
97	0.04	200	0.09
107	0.05	305	0.11
117	0.06	428	0.12

PIEZOMETER N18S (HAND MEASUREMENTS)

Elapse Time (min)	Drawdown (feet)	Elapse Time (min)	Drawdown (feet)
2	0.05	36	0.62
3	0.08	38	0.64
5	0.11	42	0.66
7	0.15	44	0.68
9	0.14	50	0.74
11	0.28	58	0.79
13	0.34	65	0.79
17	0.35	75	0.79
19	0.37	90	0.87
21	0.38	112	0.88
23	0.39	127	0.92
25	0.47	142	0.93
29	0.48	155	0.93
30	0.49	188	0.65
32	0.54	302	0.65
34	0.59	419	0.65

PIEZOMETER H12S (HAND MEASUREMENTS)

Elapse Time (min)	Drawdown (feet)	Elapse Time (min)	Drawdown (feet)
21	0.01	115	0.12
36	0.02	125	0.13
52	0.03	135	0.14
58	0.04	161	0.17
68	0.05	198	0.19
75	0.06	308	0.21
85	0.08	427	0.21
105	0.11		

Table B-5. AQUIFER TEST 8-14-90 DATA

**PUMPING WELL J16D
(DATA LOGGER MEASUREMENTS)**

Elapse Time (min)	Drawdown (feet)	Elapse Time (min)	Drawdown (feet)
0.01	0.32	13	14.44
0.02	1.08	16	15.30
0.04	1.91	19	16.11
0.06	2.70	23	16.89
0.07	3.42	26	17.60
0.09	4.11	29	18.27
0.11	4.72	33	18.90
0.12	5.01	36	19.49
0.14	5.19	43	20.61
0.19	5.66	49	21.69
0.27	6.33	56	22.68
0.37	6.94	63	23.54
0.49	7.51	73	24.62
0.64	8.11	83	25.62
0.81	8.61	93	26.63
1.0	9.03	103	27.59
1.4	9.66	128	27.96
1.8	10.10	153	28.36
3.0	10.85	178	29.25
5.1	11.89	203	29.08
6.8	12.54	238	29.21
8.0	12.95	288	28.99
9.3	13.37	338	29.01
10.1	13.66	373	29.05
11.4	14.02		

OBSERVATION WELL Q16D (DATA LOGGER MEASUREMENTS)

Elapse Time (min)	Drawdown (feet)	Elapse Time (min)	Drawdown (feet)
3.0	0.001	48	0.07
3.2	0.007	54	0.11
3.5	0.014	60	0.15
3.8	0.017	73	0.02
4.0	0.019	88	0.10
4.5	0.02	103	0.15
5.4	0.01	118	0.13
6.0	0.01	133	0.13
6.5	0.00	148	0.12
9.0	0.02	163	0.15
9.8	0.04	178	0.21
10.5	0.03	193	0.16
11.3	0.01	208	0.08
21	0.01	228	0.24
24	0.05	258	0.25
27	0.07	288	0.09
30	0.02	318	0.22
36	0.07	348	0.18
42	0.08	373	0.27

OBSERVATION WELL D19D

DATA LOGGER MEASUREMENTS

Elapse Time (min)	Drawdown (feet)
3.7	0.002
3.8	0.007
3.9	0.009
4.3	0.024
4.6	0.031
4.9	0.032
5.1	0.036
5.8	0.044
6.4	0.048
7.1	0.04
7.8	0.06
8.4	0.07
9.1	0.09
9.8	0.11
10	0.11
11	0.11
13	0.14
18	0.19
23	0.53
26	0.63
29	0.76
31	0.87
34	1.01
37	1.11
39	1.19
45	1.42
50	1.69
55	2.01
61	2.27
73	2.75
93	3.71
133	5.65
173	7.31
213	8.81
288	11.06
328	12.26
368	13.33

HAND MEASUREMENTS

Elapse Time (min)	Drawdown (feet)
5.3	0.02
7.3	0.04
8.5	0.07
9.5	0.08
10	0.1
11	0.12
12	0.14
13	0.17
14	0.19
15	0.26
16	0.3
17	0.32
18	0.33
19	0.37
20	0.4
22	0.47
24	0.55
26	0.62
28	0.72
30	0.82
35	1.02
40	1.21
45	1.47
50	1.64
59	2.06
69	2.58
87	3.42
105	4.32
125	5.22
138	6.09
195	8.11
240	9.67
276	10.92
361	14.17

OBSERVATION WELL Q17D (DATA LOGGER MEASUREMENTS)

Elapse Time (min)	Drawdown (feet)	Elapse Time (min)	Drawdown (feet)
5	0.01	133	0.10
10	0.02	148	0.09
24	0.02	163	0.11
27	0.04	178	0.17
36	0.04	193	0.14
42	0.04	208	0.05
48	0.05	228	0.21
54	0.09	258	0.25
60	0.11	288	0.08
88	0.08	318	0.19
103	0.13	348	0.16
118	0.11	373	0.26

OBSERVATION WELL S12D2

DATA LOGGER MEASUREMENTS

Elapse Time (min)	Drawdown (feet)
3.4	0.002
3.5	0.005
3.7	0.01
4.0	0.011
4.2	0.023
4.5	0.035
4.9	0.039
5.2	0.041
5.5	0.05
5.9	0.05
6.2	0.06
6.9	0.06
7.5	0.08
8.2	0.09
9.5	0.13
11	0.17
12	0.16
16	0.28
24	0.74
29	1.01
35	1.37
40	1.69
45	2.04
51	2.41
56	2.83
61	3.26
64	3.47
78	4.55
88	5.38
98	6.16
108	7.10
128	8.64
148	10.17
168	11.67
188	12.96
218	14.80
258	17.06
298	18.82
338	20.43
372	21.56

HAND MEASUREMENTS

Elapse Time (min)	Drawdown (feet)
3.2	0.01
4.9	0.03
6.5	0.07
8.2	0.09
9.5	0.16
11	0.19
12.2	0.23
14	0.29
16	0.36
17	0.44
20	0.56
21	0.65
23	0.7
24.5	0.79
26	0.87
27.5	0.95
29	1.04
30.5	1.16
32	1.26
34	1.34
35.5	1.45
37	1.55
38	1.65
40	1.74
41	1.82
43.5	1.99
45	2.09
48	2.24
49.5	2.39
51.5	2.53
53.5	2.67
55	2.79
57	2.92
59	3.03
60	3.18
62	3.34
64	3.48
66	3.62
68	3.76
70	3.9
72	4.11
76	4.4
89	5.47
115	7.47
175	12.24
250	16.62

OBSERVATION WELL V16D (DATA LOGGER MEASUREMENTS)

Elapse Time (min)	Drawdown (feet)	Elapse Time (min)	Drawdown (feet)
30	0.01	210	0.07
52	0.02	247	0.09
57	0.01	283	0.1
117	0.02	315	0.12
185	0.06	351	0.12

OBSERVATION WELL U3D

DATA LOGGER MEASUREMENTS

Elapse Time (min)	Drawdown (feet)	Elapse Time (min)	Drawdown (feet)
3.0	0.002	29	1.79
3.2	0.009	35	2.37
3.4	0.016	40	2.89
3.5	0.02	45	3.43
3.7	0.03	51	4.04
4.0	0.05	56	4.70
4.2	0.06	61	5.33
4.5	0.07	64	5.65
4.9	0.07	78	7.13
5.2	0.08	88	8.27
5.5	0.09	98	9.36
5.9	0.10	108	10.59
6.2	0.10	128	12.57
6.9	0.12	148	14.34
7.5	0.14	168	15.97
8.2	0.15	188	16.93
9.5	0.22	218	19.00
11	0.30	258	21.08
12	0.34	298	22.49
16	0.53	338	23.63
24	1.26	372	24.39

HAND MEASUREMENTS

Elapse Time (min)	Drawdown (feet)	Elapse Time (min)	Drawdown (feet)
7	0.16	29	1.69
8	0.19	34	2.24
8.7	0.21	37	2.49
9.2	0.24	42	3.09
10.3	0.29	46	3.49
12	0.39	50	3.94
13.7	0.49	60	5.09
15.3	0.59	72	6.49
16.5	0.69	80	7.39
19.2	0.89	91	8.64
20.5	0.99	136	13.38
22	1.14	185	17.04
23	1.19	200	18.12
25	1.39	260	19.87

OBSERVATION WELL S12D1

DATA LOGGER MEASUREMENTS

Elapse Time (min)	Drawdown (feet)	Elapse Time (min)	Drawdown (feet)
2.8	0.003	30	0.32
2.9	0.007	36	0.47
3.0	0.009	42	0.58
3.2	0.019	48	0.65
3.5	0.021	54	0.72
3.8	0.03	60	0.82
4.0	0.04	73	0.84
4.5	0.05	88	1.00
5.4	0.05	103	1.14
6.0	0.05	118	1.20
6.5	0.04	133	1.24
7.0	0.04	148	1.23
7.5	0.04	163	1.24
8.3	0.04	178	1.24
9.0	0.06	193	1.17
9.8	0.08	208	1.10
10.5	0.07	228	1.26
11.3	0.06	258	1.30
18	0.09	288	1.15
21	0.19	318	1.29
24	0.25	348	1.34
27	0.29	373	1.41

HAND MEASUREMENTS

Elapse Time (min)	Drawdown (feet)	Elapse Time (min)	Drawdown (feet)
6	0.01	38	0.41
7.5	0.03	42	0.48
9	0.04	46	0.53
10	0.06	52	0.63
13	0.08	56	0.64
15	0.1	63	0.71
18	0.13	71	0.78
22	0.19	90	0.95
25	0.22	115	1.09
29	0.28	175	1.18
33	0.34	251	1.24

OBSERVATION WELL T16D (DATA LOGGER MEASUREMENTS)

Elapse Time (min)	Drawdown (feet)	Elapse Time (min)	Drawdown (feet)
24	0.04	133	0.22
27	0.05	148	0.23
30	0.01	163	0.27
36	0.06	178	0.38
42	0.06	193	0.37
48	0.06	208	0.28
54	0.13	228	0.49
60	0.14	258	0.57
73	0.02	288	0.42
88	0.13	318	0.54
103	0.22	348	0.53
118	0.21	373	0.60

Table B-6. AQUIFER TEST 8-17-90 DATA**PUMPING WELL D19D (DATA LOGGER MEASUREMENTS)**

Elapse Time (min)	Drawdown (feet)	Elapse Time (min)	Drawdown (feet)
0.59	11.59	26	22.63
0.72	11.97	29	23.36
0.81	12.16	32	24.05
0.86	12.26	35	24.68
0.94	12.44	38	25.28
1.0	12.53	53	28.40
1.1	12.65	58	29.32
1.4	12.95	63	30.14
1.6	13.17	73	31.60
1.9	13.35	83	32.92
2.1	13.50	93	34.07
2.4	13.65	103	35.20
2.9	14.09	118	36.56
3.8	14.61	148	39.46
4.6	14.99	163	40.62
5.4	15.45	188	42.43
6.3	15.81	218	44.13
7.1	16.15	268	45.71
7.9	16.59	293	46.61
8.8	17.02	343	46.99
10.1	17.58	408	47.11
12.6	18.48	468	47.03
14	19.04	528	47.05
17	20.00	588	46.91
20	20.96	607	47.03
23	21.85		

OBSERVATION WELL J16D (DATA LOGGER MEASUREMENTS)

Elapse Time (min)	Drawdown (feet)	Elapse Time (min)	Drawdown (feet)
0.6	0.025	35	1.04
0.8	0.028	38	1.16
0.9	0.032	53	1.79
2.1	0.044	58	2.10
2.4	0.047	63	2.36
2.9	0.057	73	2.76
3.8	0.061	83	3.17
4.6	0.087	93	3.55
5.4	0.092	103	3.95
6.3	0.10	118	4.35
7.1	0.12	148	5.59
7.9	0.15	163	6.17
8.8	0.18	188	7.17
10	0.21	218	8.14
13	0.26	268	9.78
14	0.32	293	10.45
17	0.42	343	11.80
20	0.50	408	13.47
23	0.63	468	14.68
26	0.71	528	15.85
29	0.83	588	16.82
32	0.95	607	17.23

OBSERVATION WELL S12D2 (DATA LOGGER MEASUREMENTS)

Elapse Time (min)	Drawdown (feet)	Elapse Time (min)	Drawdown (feet)
0.6	0.007	29	0.05
0.7	0.007	32	0.03
0.8	0.012	35	0.02
0.9	0.012	38	0.00
1.1	0.014	53	0.09
1.4	0.02	58	0.30
1.6	0.03	63	0.44
2.1	0.03	73	0.52
2.4	0.03	83	0.70
2.9	0.04	93	0.79
3.8	0.05	103	0.96
4.6	0.06	118	1.01
5.4	0.06	148	1.81
6.3	0.07	163	2.20
7.1	0.07	188	3.02
7.9	0.08	218	3.82
8.8	0.08	268	5.50
10	0.08	293	6.22
13	0.07	343	7.73
14	0.07	408	9.79
17	0.07	468	11.09
20	0.05	528	12.47
23	0.05	588	13.63
26	0.04	607	14.21

OBSERVATION WELL U3D (DATA LOGGER MEASUREMENTS)

Elapse Time (min)	Drawdown (feet)	Elapse Time (min)	Drawdown (feet)
0.6	0.022	29	0.09
0.7	0.026	32	0.07
0.8	0.027	35	0.04
0.9	0.03	38	0.04
1.1	0.03	53	0.15
1.4	0.04	58	0.51
1.6	0.05	63	0.75
1.9	0.06	73	0.87
2.1	0.06	83	1.13
2.4	0.07	93	1.28
2.9	0.08	103	1.56
3.8	0.09	118	1.57
4.6	0.10	148	2.66
5.4	0.11	163	3.16
6.3	0.12	188	4.22
7.1	0.13	218	5.13
7.9	0.13	268	7.03
8.8	0.13	293	7.73
10	0.14	343	9.28
13	0.14	408	11.40
14	0.14	468	12.52
17	0.13	528	13.80
20	0.11	588	14.81
23	0.09	607	15.43
26	0.09		

OBSERVATION WELL S12D1 (DATA LOGGER MEASUREMENTS)

Elapse Time (min)	Drawdown (feet)	Elapse Time (min)	Drawdown (feet)
1.9	0.001	98	0.18
2.0	0.003	128	0.18
2.0	0.01	138	0.15
2.7	0.02	148	0.06
3.2	0.02	158	0.11
3.7	0.03	168	0.17
4.5	0.04	188	0.33
6	0.06	208	0.21
9	0.06	228	0.39
10	0.06	258	0.53
11	0.07	288	0.55
13	0.05	318	0.69
14	0.05	348	0.85
15	0.04	378	0.90
18	0.04	408	1.08
21	0.01	468	1.00
58	0.14	528	1.03
68	0.20	588	1.00
78	0.19	607	1.20
88	0.09		

OBSERVATION WELL Q16D (DATA LOGGER MEASUREMENTS)

Elapse Time (min)	Drawdown (feet)	Elapse Time (min)	Drawdown (feet)
1.9	0.01	11	0.08
2.0	0.02	12	0.08
2.0	0.02	13	0.07
2.2	0.02	14	0.07
2.7	0.03	15	0.07
3.2	0.03	18	0.04
3.7	0.04	21	0.03
4.5	0.05	58	0.06
6	0.07	68	0.09
9	0.07	78	0.05
10	0.08		

OBSERVATION WELL Q17D (DATA LOGGER MEASUREMENTS)

Elapse Time (min)	Drawdown (feet)	Elapse Time (min)	Drawdown (feet)
1.9	0.004	11	0.07
2.0	0.01	12	0.06
2.0	0.01	13	0.06
2.7	0.02	14	0.06
3.2	0.02	15	0.06
3.7	0.03	18	0.03
4.5	0.04	21	0.02
6	0.06	58	0.05
9	0.08	68	0.07
10	0.08	78	0.04

OBSERVATION WELL T16D (DATA LOGGER MEASUREMENTS)

Elapse Time (min)	Drawdown (feet)	Elapse Time (min)	Drawdown (feet)
1.9	0.001	11	0.08
2.0	0.003	12	0.08
2.0	0.004	13	0.07
2.7	0.01	14	0.07
3.2	0.02	15	0.06
3.7	0.02	18	0.05
4.5	0.04	21	0.03
6	0.05	58	0.02
9	0.07	68	0.09
10	0.07	78	0.07

Table B-7. AQUIFER TEST 3-8-91 DATA

PUMPING WELL U3D

DATA LOGGER MEASUREMENTS

Elapse Time (min)	Drawdown (feet)
0.02	1.31
0.05	1.85
0.07	2.68
0.08	3.55
0.1	4.36
0.15	4.38
0.2	4.51
0.27	4.63
0.32	4.80
0.35	4.84
0.38	4.93
0.4	4.97
0.62	5.26
0.65	5.19
0.68	5.29
0.7	5.26
0.72	5.28
0.75	5.21
0.78	5.23
0.88	5.25
0.92	5.33
0.95	5.32
1	5.23
1.03	5.33
1.05	5.29
1.07	5.20
1.08	5.22
1.1	5.38
1.12	5.35
1.13	5.37
1.15	5.38
1.17	5.39
1.18	5.43
1.2	5.37
1.22	5.34
1.27	5.41
1.37	5.49
1.42	5.49
1.45	5.50
1.48	5.66
1.7	5.68
2.0	5.75
2.1	5.88
2.5	6.15
2.9	6.32
3.2	6.55
3.5	6.76
3.8	6.83
4.1	7.11
4.4	7.28
4.7	7.42
5.1	7.69
5.5	7.98
6.4	8.62
6.8	8.85
7.3	9.14
7.8	9.43
8.1	9.58
8.4	9.85
9.0	10.15
9.7	10.46

HAND MEASUREMENTS

Elapse Time (min)	Drawdown (feet)
0.4	4.92
0.6	5.22
0.8	5.27
1	5.52
1.5	5.52
1.8	5.62
2	5.77
2.2	5.91
2.6	6.14
2.8	6.27
3.1	6.42
3.5	6.62
4.1	6.97
4.8	7.42
6.1	8.26
6.9	8.74
8.1	9.52
8.8	9.94
9.6	10.27
10.0	10.52
10.3	10.77
10.6	10.92
11.7	11.49
12.1	11.77
14.9	11.59
15.8	11.66
16.4	11.68
17.3	11.72
18.0	12.18
18.4	12.29
18.9	12.61
19.5	12.92
20.2	13.48
20.9	13.98
21.4	14.32
22.2	14.8
22.4	15.07
22.9	15.33
23.6	15.7
24.2	16.05
24.6	16.27
25.2	16.62
25.7	16.85
26.2	17.14
27.0	17.54
27.5	17.81
28.0	18.11
29.5	18.84
32.5	20.41
33	20.69
34	20.99
35	21.39
36	21.81
38	22.86
39	23.14
40	23.61
41	23.84
42	24.38
43	24.65
44	25.02
45	25.72

PUMPING WELL U3D (Continued)

DATA LOGGER MEASUREMENTS

Elapse Time (min)	Drawdown (feet)
10.0	10.72
10.7	11.12
11.3	11.48
14	11.70
15	11.73
16	11.84
17	12.04
18	12.37
19	12.96
20	13.59
21	14.26
22	15.05
23	15.63
24	16.21
25	16.71
27	17.88
29	18.85
31	19.91
33	20.82
35	21.74
37	22.56
39	23.53
41	24.33
43	25.04
45	25.80
47	26.41
49	27.13
55	28.92
65	31.63
75	33.76
85	35.67
95	37.10
105	38.41
115	39.46
125	40.54
135	41.38
145	41.97

HAND MEASUREMENTS

Elapse Time (min)	Drawdown (feet)
48	26.12
49	26.86
50	27.15
51.5	27.68
53	28.4
62.5	30.82
69	32.34
76	33.84
85	35.4
92	36.34
100	37.47
105	38.22
115	39.32
125	40.33
135	41.16
145	41.84
160	42.69
172	43.22

OBSERVATION WELL S12D2

DATA LOGGER MEASUREMENTS

Elapse Time (min)	Drawdown (feet)
6.2	0.03
6.8	0.08
7.5	0.09
8.2	0.10
8.8	0.10
11	0.12
13	0.09
17	0.13
19	0.14
21	0.12
23	0.15
25	0.16
30	0.12
36	0.14
42	0.19
48	0.14
55	0.21
65	0.22
75	0.22
85	0.35
95	0.34
105	0.36
115	0.45
125	0.44
135	0.48
145	0.44
155	0.51
165	0.71
175	0.84
181	0.89

HAND MEASUREMENTS

Elapse Time (min)	Drawdown (feet)
19.5	0.01
20.5	0.01
21	0.02
22	0.01
23	0.02
24	0.02
25.5	0.03
30	0.03
35.5	0.04
36.5	0.04
39	0.05
42	0.06
44.5	0.07
51	0.08
55	0.09
57	0.1
58	0.1
61	0.11
64	0.12
65	0.13
68	0.14
71	0.15
74	0.16
77	0.17
78	0.18
80	0.19
82	0.2
87	0.22
92	0.24
97	0.26
102	0.29
107	0.31
112	0.33
117	0.36
124	0.4
132	0.46
139	0.49
154	0.57
165	0.67
180	0.73

OBSERVATION WELL D19D

DATA LOGGER MEASUREMENTS

Elapse Time (min)	Drawdown (feet)
0.13	0.001
0.2	0.001
0.27	0.003
0.33	0.004
0.4	0.006
0.47	0.008
0.53	0.01
0.6	0.02
0.67	0.02
0.73	0.01
0.8	0.01
0.87	0.02
0.93	0.02
1.0	0.02
1.3	0.02
1.5	0.02
1.8	0.03
2.1	0.03
2.7	0.03
3.1	0.05
3.7	0.06
4.3	0.07
4.5	0.07
4.8	0.07
5.1	0.08
6.2	0.07
6.8	0.07
7.5	0.08
8.2	0.09
8.8	0.09
11	0.10
13	0.11
17	0.14
19	0.16
21	0.15
23	0.16
25	0.13
30	0.09
36	0.11
42	0.17
48	0.16
55	0.12
65	0.19
75	0.23
85	0.37
95	0.26
105	0.31
115	0.26
125	0.43
135	0.46
145	0.35
155	0.33
165	0.48
175	0.51
181	0.64

HAND MEASUREMENTS

Elapse Time (min)	Drawdown (feet)
26.3	0.01
27	0.01
29	0.01
33.5	0.02
36	0.03
39	0.03
42.5	0.04
45	0.04
49	0.04
55	0.05
57	0.06
61	0.07
66	0.08
68	0.09
71	0.1
74	0.12
75	0.1
76	0.1
79	0.11
82	0.11
86	0.12
90	0.13
101	0.16
113	0.21
120	0.23
131	0.27
137	0.29
141	0.3
153	0.34
160	0.36
168	0.38
176	0.41
180	0.42

OBSERVATION WELL J16D

DATA LOGGER MEASUREMENTS

Elapse Time (min)	Drawdown (feet)
0.13	0.003
0.2	0.005
0.27	0.006
0.33	0.008
0.4	0.008
0.47	0.01
0.53	0.01
0.6	0.01
0.67	0.01
0.73	0.01
0.8	0.01
0.87	0.01
0.93	0.01
1.0	0.02
1.3	0.02
1.5	0.02
1.8	0.02
2.1	0.03
2.7	0.04
3.1	0.04
3.7	0.06
4.3	0.07
4.5	0.07
4.8	0.07
5.1	0.06
6.2	0.07
6.8	0.09
7.5	0.09
8.2	0.09
8.8	0.09
11	0.10
13	0.14
17	0.19
19	0.22
21	0.21
23	0.25
25	0.24
30	0.23
36	0.29
42	0.37
48	0.40
55	0.42
65	0.55
75	0.57
85	0.75
95	0.72
105	0.82
115	0.84
125	1.00
135	1.07
145	1.02
155	1.06
165	1.18
175	1.31
181	1.39

HAND MEASUREMENTS

Elapse Time (min)	Drawdown (feet)
3	0.01
5	0.01
7.9	0.02
8.1	0.03
9	0.03
10	0.04
12	0.05
14	0.06
15	0.07
20	0.09
22	0.1
26	0.12
28	0.13
30	0.15
32	0.17
36	0.19
38	0.2
41	0.23
43	0.24
46	0.26
49	0.29
51	0.3
58	0.37
61	0.38
66	0.42
70	0.44
76	0.49
83	0.55
87	0.57
91	0.61
97	0.64
106	0.73
113	0.77
119	0.82
127	0.87
131	0.88
138	0.94
147	1
152	1.02
159	1.07
166	1.12
180	1.2

Table B-8. SLUG TEST DATA

TEST ONE -- WELL V16D ($H_0=0.184$ ft)		TEST TWO -- WELL Q17D ($H_0=1.97$ ft)	
Time (min)	H (ft)	Time (min)	H (ft)
0	0.184	0	1.97
0.03	0.18	0.02	1.936
0.07	0.17	0.03	1.91
0.13	0.16	0.05	1.886
0.17	0.153	0.08	1.832
0.2	0.15	0.13	1.762
0.27	0.135	0.25	1.609
0.37	0.12	0.42	1.412
0.47	0.105	0.67	1.167
0.57	0.09	1	0.928
0.6	0.085	1.33	0.741
0.7	0.075	1.67	0.6
0.9	0.06	2	0.496
1.2	0.045	2.5	0.377
1.63	0.036	3	0.291
2.13	0.025	3.5	0.204
3.13	0.018	4	0.152
3.63	0.015	4.5	0.109
		5	0.07

TEST THREE -- WELL T16D ($H_0=3.12$ ft)		TEST FOUR -- WELL Q16D ($H_0=3.50$ ft)	
Time (min)	H (ft)	Time (min)	H (ft)
0	3.12	0	3.5
0.02	3.059	0.02	3.461
0.03	3.015	0.03	3.456
0.05	2.969	0.07	3.448
0.08	2.881	0.13	3.432
0.12	2.794	0.2	3.417
0.15	2.708	0.33	3.39
0.18	2.624	0.58	3.333
0.22	2.545	0.83	3.266
0.28	2.387	1.17	3.181
0.35	2.238	1.5	3.106
0.48	1.964	2	2.983
0.7	1.579	3	2.771
0.87	1.334	4	2.563
1.03	1.127	5	2.408
1.37	0.808	6.5	2.233
1.7	0.594	8.5	1.996
2.03	0.441	10.5	1.769
2.7	0.239	12.5	1.557
3.03	0.156	16.5	1.114
3.7	0.071	20.5	0.842
4.7	0.066	24.5	0.517
5.7	0.055	30.5	0.456
7.7	0.041	40.5	0.295
9.7	0.02		

TEST FIVE -- WELL S12D1
($H_0=2.014$ ft)

Time (min)	H (ft)
0	2.014
0.03	2.007
0.07	1.999
0.1	1.99
0.17	1.973
0.27	1.963
0.4	1.954
0.65	1.953
0.82	1.951
1.07	1.946
1.57	1.924
3.23	1.819
4.23	1.744
5.73	1.612
7.23	1.587
10.73	1.553
13.73	1.48
18.73	1.22
26.73	0.996
30.73	0.928
32.73	0.906
38.73	0.739
56.73	0.683
116.73	0.459
1466.73	0.016

TEST SIX -- WELL S12D2
($H_0=3.54$ ft)

Time (min)	H (ft)
0	3.54
0.08	3.536
0.17	3.531
0.58	3.526
1	3.521
2.08	3.518
4.25	3.471
7.25	3.338
11.25	3.138
20.25	2.963
30.83	2.679
41.92	2.31
67.92	1.964
87.92	1.545
107.92	1.131
127.92	1.068
147.92	0.873
167.92	0.619
207.92	0.55
267.92	0.371
327.92	0.232
417.92	0.164
537.92	0.083
657.92	0.068

TEST SEVEN -- WELL J16D
($H_0=3.20$ ft)

Time (min)	H (ft)
0	3.2
0.02	2.908
0.04	2.752
0.05	2.585
0.07	2.48
0.12	2.073
0.17	1.754
0.22	1.494
0.27	1.26
0.42	0.782
0.57	0.491
0.72	0.312
0.87	0.197
0.97	0.146
1.22	0.063
1.47	0.016

TEST EIGHT -- WELL D19D
($H_0=.4$ ft)

Time (min)	H (ft)
0	0.399
0.07	0.36
0.1	0.337
0.12	0.327
0.15	0.299
0.18	0.284
0.22	0.274
0.28	0.258
0.33	0.246
0.4	0.23
0.47	0.217
0.55	0.203
0.65	0.188
0.77	0.165
0.87	0.15
1.03	0.137
1.2	0.135
5.18	0.014
8.18	0.011

TEST NINE -- WELL U3D
(H₀=3.53 ft)

Time (min)	H (ft)
0	3.53
0.05	3.53
0.1	3.52
0.15	3.52
0.2	3.52
0.25	3.52
0.3	3.52
0.35	3.51
0.49	3.51
0.74	3.49
1.57	3.45
3.07	3.36
6.07	3.20
9.07	3.06
12.07	2.95
15.07	2.84
18.07	2.73
21.07	2.60
24.07	2.49
27.07	2.39
30.07	2.28
33.07	2.19
36.07	2.10
39.07	2.02
42.07	1.94
45.07	1.81
56.57	1.54

APPENDIX C

Static Water Level Data at UIGRS

**Table C-1. Static Water Level of Five Deep Wells
(Elevation in feet AMSL)**

DATE	V16D	Q17D	D19D	S12D	T16D
12-28-87	2536.21	2533.96	2525.89	2533.58	
1-1-88	2536.10	2533.77	2525.35	2533.40	
1-4-88	2536.11	2533.85	2525.45	2533.48	
1-8-88	2536.07	2533.81	2525.25	2533.33	
1-12-88	2536.71	2534.45	2525.19	2533.73	
1-15-88	2538.51	2535.97	2525.90	2535.16	
1-18-88	2537.89	2535.47	2525.77	2535.17	
1-22-88	2537.29	2534.95	2525.21	2534.62	2536.74
1-25-88	2536.96	2534.74	2524.90	2534.56	2536.47
1-29-88	2537.83	2535.66	2524.87	2534.80	2537.30
2-1-88	2537.45	2535.28	2524.53	2534.69	2536.93
2-5-88	2536.98	2534.8	2523.94	2534.29	2536.47
2-9-88	2538.34	2536.03	2524.78	2535.23	2537.81
2-12-88	2538.01	2535.78	2524.93	2535.24	2537.44
2-15-88	2538.10	2535.86	2525.00	2535.59	2537.54
2-19-88	2537.65	2535.45	2524.64	2535.17	2537.09
2-22-88	2537.40	2535.25	2524.64	2535.02	2536.93
2-26-88	2537.14	2535.04	2524.54	2534.68	2536.61
2-29-88	2537.00	2534.91	2524.55	2534.54	2536.48
3-4-88	2536.86	2534.82	2524.23	2534.30	2536.34
3-7-88	2537.24	2535.18	2524.27	2534.61	2536.73
3-11-88	2537.10	2535	2524.39	2534.50	2536.58
3-18-88	2536.83	0	2524.19	2534.33	2536.32
3-22-88	2536.81	0	2524.18	2534.32	2536.30
3-25-88	2536.90	2535.04	2523.93	2534.36	2536.41
3-28-88	2538.02	2536.17	2524.72	2535.33	2537.49
4-1-88	2538.49	0	2524.49	2535.60	2537.96
4-5-88	2538.43	0	2524.42	2535.94	2537.90
4-8-88	2538.12	0	2524.03	2535.74	2537.59
4-11-88	2537.84	0	2524.37	2535.48	2537.32
4-14-88	2537.62	2535.88	2524.38	2535.27	2537.11
4-18-88	2537.35	2534.97	2526.14	2535.34	2536.83
4-22-88	2537.70	2535.4	0	2535.68	2537.20
4-29-88	2538.07	2535.72	0	2535.99	2537.60
5-2-88	2537.55	2535.3	0	2535.76	2537.05
5-6-88	2537.39	2535.2	0	2535.56	2536.91
5-9-88	2537.21	2535.02	0	2535.25	2536.72
5-12-88	2537.19	2535.11	2526.29	2535.28	2536.73
5-20-88	2537.03	2534.89	2525.87	2534.94	2536.54
5-26-88	2536.93	2534.88	2525.94	2534.93	2536.44
6-1-88	2537.27	2534.92	2526.69	2536.87	2536.82
6-9-88	2537.20	2535.45	2526.68	2535.84	2536.74
6-16-88	2536.98	2535.27	2526.56	2535.74	2536.51
6-24-88	2536.78	2535.07	2526.41	2535.48	2536.35
6-27-88	2537.16	2535.47	2526.50	2535.93	2536.72
7-2-88	2536.92	2535.25	2526.38	2535.69	2536.49
7-7-88	2536.95	2535.31	2526.41	2535.87	2536.51
7-8-88	2536.89	2535.25	2526.31	2535.71	2536.47
7-15-88	2537.23	2535.55	2526.67	2536.21	2536.86
7-20-88	2536.99	2535.33	2526.76	2536.11	2536.56
7-23-88	2536.91	2535.16	2526.73	2536.03	2536.44
7-29-88	2536.83	2535.17	2526.78	2536.08	2536.34
7-30-88	2536.83	2535.17	2526.84	2536.15	2536.43
8-3-88	2536.81	2535.12	2526.79	2536.11	2536.39
8-6-88	2536.74	2535.08	2526.88	2536.39	2536.28
8-12-88	2536.74	2535.07	2527.26	2536.12	2536.32
8-15-88	2536.76	2535.14	2527.30	2536.18	2536.35
8-19-88	2536.73	2535.14	2527.52	2536.14	2536.31
8-26-88	2536.63	2535.01	2527.33	2536.09	2536.23
8-30-88	2536.62	2535	2527.53	2536.09	2536.22
9-2-88	2536.62	2535	2527.56	2536.10	2536.23
9-5-88	2536.63	2535	2527.71	2536.12	2536.24
9-9-88	2536.62	2535.12	2527.72	2536.11	2536.24
9-12-88	2536.69	2535.13	2527.38	2536.15	2536.28
9-16-88	2536.77	2535.18	2527.52	2536.24	2536.37
9-19-88	2536.97	2535.41	2527.81	2536.50	2536.58
9-27-88	2536.86	2535.26	2527.74	2536.36	2536.47
9-30-88	2536.68	2535.12	2527.86	2536.21	2536.31

10-5-88	2536.56	2535	2527.78	2536.08	2536.18
10-7-88	2536.47	2534.9	2527.60	2536.00	2536.10
10-10-88	2536.42	2534.88	2527.70	2535.96	2536.06
10-13-88	2536.40	2534.84	2527.74	2535.96	2536.04
10-17-88	2536.49	2534.94	2527.71	2536.01	2536.14
10-21-88	2536.62	2536.1	2527.49	2536.00	2536.46
10-25-88	2536.51	2536.15	2520.24	2534.93	2536.31
10-26-88	2536.45	2536.06	2519.98	2534.74	2536.20
10-28-88	2536.42	2536.04	2519.92	2534.70	2536.19
11-1-88	2536.40	2536.01	2519.85	2534.85	2536.18
11-4-88	2536.58	2536.24	2519.66	2534.53	2536.35
11-7-88	2536.75	2536.44	2519.97	2534.83	2536.53
11-11-88	2536.74	2536.45	2520.17	2534.90	2536.54
11-15-88	2536.88	2536.48	2520.11	2535.17	2536.68
11-18-88	2536.86	2536.56	2520.11	2535.19	2536.65
11-25-88	2537.63	2537.26	2520.82	2536.05	2537.39
12-1-88	2537.67	2537.25	2520.61	2536.03	2537.41
12-8-88	2537.42	2537.02	2520.45	2536.03	2537.16
12-14-88	2537.17	2536.8	2520.16	2535.78	2536.93
12-20-88	2536.99	2536.63	2520.75	2535.66	2536.75
12-23-88	2536.86	2536.55	2520.52	2535.52	2536.64
12-27-88	2536.77	2536.47	2520.40	2535.49	2536.56
1-3-89	2536.99	2536.68	2520.35	2535.59	2536.79
1-6-89	2537.29	2536.97	2520.68	2535.93	2537.07
1-11-89	2537.40	2537.1	2520.26	2536.02	2537.18
1-16-89	2538.14	2537.78	2520.68	2536.54	2537.92
1-20-89	2539.30	2538.88	2521.25	2537.53	2539.00
1-23-89	2538.96	2538.56	2521.29	2537.54	2538.68
1-26-89	2538.60	2538.36	2521.00	2537.36	2538.32
1-30-89	2538.35	2538	2521.13	2537.18	2538.10
2-6-89	2538.21	2537.87	2520.72	2537.17	2537.97
2-10-89	2537.80	2537.47	2520.59	2536.81	2537.58
2-13-89	2537.69	2537.37	2520.82	2536.70	2537.47
2-17-89	2537.62	2537.34	2520.58	2536.55	2537.43
2-20-89	2537.97	2537.65	2520.60	2536.99	2537.75
2-26-89	2539.66	2539.23	2521.11	2538.64	2539.40
3-2-89	2539.12	2538.72	2521.63	2538.41	2538.89
3-5-89	2538.77	2538.43	2521.09	2538.07	2538.55
3-8-89	2540.15	2539.71	2521.25	2539.17	2539.91
3-11-89	2540.92	2540.5	2521.42	2539.73	2540.69
3-16-89	2539.92	2539.55	2521.74	2539.33	2539.68
3-19-89	2539.98	2539.55	2521.26	2539.42	2539.72
3-23-89	2539.80	2539.39	2521.38	2539.37	2539.55
3-26-89	2540.05	2539.62	2521.43	2539.61	2539.81
3-29-89	2539.74	2539.39	2521.15	2539.37	2539.52
4-2-89	2539.37	2539.05	2521.30	2539.04	2539.14
4-5-89	2539.28	2538.93	2521.09	2538.77	2539.09
4-12-89	2538.61	2538.24	2521.14	2538.18	2538.43
4-16-89	2538.37	2538.07	2521.13	2537.91	2538.20
4-19-89	2538.17	2537.89	2520.97	2537.71	2538.01
4-23-89	2538.25	2537.98	2520.99	2537.75	2538.09
4-27-89	2538.22	2537.88	2520.73	2537.53	2537.98
4-30-89	2537.92	2537.64	2521.10	2537.43	2537.77
5-4-89	2537.79	2537.51	2520.63	2537.27	2537.60
5-7-89	2537.71	2537.45	2520.80	2537.20	2537.56
5-11-89	2537.76	2537.49	2520.86	2537.16	2537.55
5-16-89	2537.75	2537.45	2520.70	2537.23	2537.58
5-19-89	2537.74	2537.4	2520.34	2537.21	2537.57
5-22-89	2537.77	2537.46	2520.64	2537.28	2537.61
5-26-89	2537.84	2537.54	2520.56	2537.29	2537.66
5-30-89	2538.14	2537.9	2520.22		2537.99
6-4-89	2538.07	2537.76	2520.51		2537.88
6-8-89	2537.92	2537.58	2520.61		2537.73
6-12-89	2537.81	2537.46	2520.46		2537.63
6-16-89	2537.92	2537.7	2520.05		2537.72
6-21-89	2537.87	2537.44	2520.11		2537.56
6-23-89	2537.61	2537.37	2520.23		2537.45
6-26-89	2537.44	2537.22	2520.3		2537.28
7-4-89	2537.32	2537.06	2519.88		2537.13
7-11-89	2537.18	2536.88	2518.73		2536.83
7-14-89	2537.23	2536.96	2520.73		2536.95
7-26-89	2537.09	2536.77	2521.08		2536.82
7-31-89	2537.14	2536.8	2521.12		2536.85
8-3-89	2537.09	2536.76	2520.94		2536.81
8-10-89	2537.12	2536.79	2520.79		2536.84

8-14-89	2537.11	2536.77	2520.66	2536.84
8-17-89	2537.14	2536.78	2520.72	2536.87
8-25-89	2538.21	2537.86	2521.09	2537.92
8-29-89	2537.69	2537.36	2521.16	2537.43
9-5-89	2537.47	2537.17	2520.97	2537.23
9-11-89	2537.31	2537	2521.51	2537.07
9-15-89	2537.27	2536.93	2520.69	2537.02
9-18-89	2537.38	2537.06	2520.16	2537.14
9-19-89	2537.29	2536.98	2519.99	2537.06
9-22-89	2537.23	2536.94	2519.7	2537
9-29-89	2537.14	2536.83	2519.78	2536.93
10-2-89	2537.03	2536.73	2519.61	2536.84
10-6-89	2536.96	2536.64	2519.44	2536.76
10-10-89	2536.97	2536.65	2519.6	2536.77
10-15-89	2536.88	2536.51	2519.32	2536.69
10-17-89	2536.84	2536.51	2519.18	2536.65
10-23-89	2537.27	2537.02	2519.56	2537.09
10-26-89	2537.4	2537.13	2519.43	2537.2
10-30-89	2537.13	2536.93	2519.27	2536.95
11-3-89	2537.04	2536.72	2519.21	2536.86
11-7-89	2537.18	2536.81	2519.27	2536.99
11-10-89	2537.3	2537	2519.32	2537.13
11-14-89	2537.58	2537.3	2519.14	2537.41
11-18-89	2537.51	2537.22	2519.21	2537.35
11-28-89	2537.53	2537.2	2518.87	2537.37
12-1-89	2537.32	2537.07	2518.77	2537.14
12-5-89	2538.41	2538.08	2519.06	2538.25
12-8-89	2538.09	2537.85	2519.29	2537.86
12-14-89	2537.5	2537.12	2519.04	2537.32
12-22-89	2537.17	2536.91	2518.69	2536.99
12-26-89	2537.17	2537.06	2518.81	2536.99
12-29-89	2537.06	2536.79	2518.78	2536.89
1-9-90	2539.34	2538.93	2519.32	2539.11
1-11-90	2538.98	2538.62	2519.08	2538.77
1-17-90	2538.52	2538.34	2519.12	2538.35
1-25-90	2538.32	2537.96	2519.27	2538.13
1-30-90	2538.52	0	2519.62	2538.32
1-31-90	2538.47	0	2519.66	2538.28
2-1-90	2538.43	2538.09	2519.37	2538.22
2-2-90	2538.31	2537.98	2519.01	2538.11
2-3-90	2538.53	2538.09	2519.13	2538.19
2-4-90	2538.56	2538.11	2519.03	2538.21
2-5-90	2538.61	2538.11	2519.03	2538.26
2-6-90	2538.56	2538.1	2519.04	2538.21
2-7-90	2538.5	2538	2518.87	2538.16
2-8-90	2538.5	2537.99	2519.25	2538.16
2-9-90	2538.49	2538.03	2519.2	2538.18
2-10-90	2540.26	2539.87	2519.24	2539.93
2-11-90	2540.54	2540.05	2519.49	2540.19
2-12-90	2539.94	2539.43	2519.7	2539.58
2-13-90	2539.66	2539.16	2519.84	2539.32
2-14-90	2539.34	2538.85	2519.59	2538.99
2-15-90	2539.27	2538.78	2519.78	2538.93
2-16-90	2539.11	2538.59	2520.07	2538.75
2-17-90	2538.98	2538.51	2519.84	2538.66
2-18-90	2538.8	2538.33	2519.47	2538.47
2-19-90	2538.69	2538.23	2519.37	2538.37
2-20-90	2538.65	2538.18	2519.53	2538.32
2-21-90	2538.65	2538.2	2519.48	2538.32
2-21-90	2538.86	2538.42	2519.42	2538.53
2-22-90	2539.1	2538.59	2519.37	2538.75
2-22-90	2539.2	2538.71	2519.39	2538.85
2-23-90	2539.42	2538.91	2519.46	2539.06
2-24-90	2539.59	2539.03	2519.52	2539.18
2-25-90	2539.46	2538.97	2519.59	2539.11
2-26-90	2539.31	2538.82	2519.54	2538.96
2-27-90	2539.11	2538.62	2519.46	2538.76
2-28-90	2539.01	2538.54	2519.5	2538.67
3-1-90	2538.93	2538.44	2519.58	2538.59
3-2-90	2538.86	2538.38	2519.6	2538.54
3-3-90	2538.81	2538.34	2519.75	2538.49
3-4-90	2538.73	2538.26	2519.72	2538.42
3-5-90	2538.63	2538.18	2519.66	2538.42
3-6-90	2538.52	2538.08	2519.42	2538.21
3-7-90	2538.53	2538.08	2519.62	2538.22

3-8 -90	2538.64	2538.2	2519.61	2538.33
3-9 -90	2538.57	2538.12	2519.55	2538.26
3-10-90	2538.7	2538.26	2519.8	2538.39
3-11-90	2538.89	2538.46	2519.7	2538.59
3-12-90	2538.69	2538.27	2519.47	2538.39
3-13-90	2538.63	2538.2	2519.41	2538.33
3-14-90	2538.58	2538.14	2519.47	2538.28
3-15-90	2538.6	2538.17	2519.27	2538.31
3-16-90	2538.53	2538.09	2519.27	2538.22
3-17-90	2538.49	2538.03	2519.35	2538.17
3-18-90	2538.42	2537.99	2519.27	2538.11
3-19-90	2538.4	2537.96	2519.38	2538.1
3-20-90	2538.32	2537.88	2519.17	2538.02
3-21-90	2538.31	2537.86	2519.23	2538
3-22-90	2538.29	2537.84	2519.26	2537.99
3-23-90	2538.44	2538.02	2519.21	2538.14
3-24-90	2538.37	0	2519.08	2538.07
3-25-90	2538.32	2537.9	2519.11	2538.03
3-26-90	2538.26	2537.82	2519.1	2537.96
3-27-90	2538.22	2537.79	2519.13	2537.92
3-28-90	2538.18	2537.73	2519.15	2537.88
3-29-90	2538.15	2537.7	2519.14	2537.85
3-30-90	2538.12	2537.66	2519.12	2537.83
3-31-90	2538.09	2537.55	2519.12	2537.79
4-1 -90	2538.06	2537.62	2519.08	2537.76
4-2 -90	2538	2537.55	2518.99	2537.71
4-3 -90	2537.97	2537.52	2518.85	2537.67
4-4 -90	2537.96	2537.52	2518.86	2537.66
4-5 -90	2537.93	2537.44	2518.62	2537.66
4-6 -90	2537.91	2537.41	2518.74	2537.63
4-7 -90	2537.9	2537.46	2518.84	2537.63
4-8 -90	2537.86	2537.43	2518.93	2537.6
4-9 -90	2537.77	2537.44	2518.67	2537.52
4-10-90	2537.75	2537.34	2518.6	2537.5
4-11-90	2537.76	2537.33	2518.75	2537.5
4-12-90	2536.3	0	2518.53	2531.7
4-13-90	2536.15	0	2518.3	2531.42
4-14-90	2538.17	2537.81	2518.31	2537.92
4-15-90	2538.09	2537.68	2518.57	2537.83
4-16-90	2538.02	2537.62	2518.81	2537.76
4-17-90	2537.96	2537.54	2518.91	2537.69
4-18-90	2537.88	2537.45	2518.81	2537.61
4-19-90	2537.85	2537.43	2518.77	2537.58
4-20-90	2537.81	2537.4	2518.67	2537.55
4-21-90	2537.84	2537.4	2518.72	2537.57
4-22-90	2537.86	2537.44	2518.83	2537.58
4-23-90	2537.98	2537.57	2518.97	2537.72
4-24-90	2537.85	2537.43	2518.71	2537.6
4-25-90	2537.8	2537.39	2518.65	2537.54
4-26-90	2537.92	2537.52	2518.63	2537.67
4-27-90	2538.04	2537.63	2518.72	2537.82
4-28-90	2539.31	2538.92	2519	2539.05
4-29-90	2538.97	2538.56	2518.79	2538.71
4-30-90	2538.71	2538.32	2518.62	2538.45
5-3 -90	2538.43	2538.03	2518.59	2538.15
5-6 -90	2538.21	2537.82	2518.7	2537.95
5-9 -90	2538.1	2537.69	2518.72	2537.84
5-13-90	2538	2537.58	2518.61	2537.74
5-17-90	2537.94	2537.53	2518.61	2537.68
5-21-90	2537.87	2537.33	2526.24	2537.61
5-22-90	2537.84	2537.3	2526.94	2537.59
5-23-90	2538.04	2537.51	2528.17	2537.79
5-26-90	2538.39	2537.92	2528.84	2538.17
5-30-90	2538.56	2538.11	2527.3	2538.33
6-2 -90	2539.33	2538.87	2526.91	2539.1
6-7 -90	2538.86	2538.38	2526.18	2538.62
6-12-90	2538.09	2537.6	2525.64	2538
6-18-90	2537.84	2537.36	2525.28	2537.61
6-24-90	2537.81	2537.34	2525.24	2537.56
7-2 -90	2537.78	2537.29	2525.21	2537.54
7-6 -90	2537.42	2536.98	2525.08	2537.4
7-9 -90	2537.68	2537.17	2525.11	2537.44
7-15-90	2537.63	2537.14	2525.27	2537.42
7-19-90	2537.66	2537.16	2525.19	2537.44
7-23-90	2537.57	2537.07	2525.28	2537.35

7-27-90	2537.77	2537.26	2525.04	2537.54
7-30-90	2537.79	2537.25	2521.98	2537.55
8-7-90	2537.68	2537.22	2516.59	2537.4
8-11-90	2537.59	2537.16	2516.51	2537.32
8-14-90	2537.51	2537.24	2514.19	2537.15
8-23-90	2537.78	2537.25	2517.11	2537.23
8-28-90	2537.52	2537.03	2518.85	2536.92
9-4-90	2537.47	2536.98	2518.84	2536.9
9-8-90	2537.4	2536.93	2518.91	2536.88
9-13-90	2537.33	2536.89	2518.94	2536.87
9-17-90	2537.29	2536.85	2518.95	2536.84
9-21-90	2537.23	2536.79	2519.01	2536.79
9-26-90	2537.16	2536.71	2519.06	2536.72
10-2-90	2537.14	2536.69	2519.11	2536.69
10-10-90	2537.15	2536.72	2519.16	2536.74
10-17-90	2537.17	2536.76	2519.21	2536.78
10-24-90	2537.41	2537	2519.21	2536.97
10-31-90	2537.7	2537.2	2519.14	2537.22
11-6-90	2537.75	2537.32	2519.11	2537.33
11-15-90	2537.32	2536.9	2519	2536.91
11-23-90	2537.42	2537.02	2519.31	2537
11-30-90	2537.5	2537.08	2519.26	2537.07
12-5-90	2538.01	2537.54	2519.03	2537.58
12-11-90	2538.58	2538.13	2519.34	2538.16
12-13-90	2538.27	2537.79	2519.35	2538.06
12-14-90	2538.18	2537.73	2519.34	2537.77
1-5-91	2537.17	2545.95	0	2536.92
1-7-91	2537.2	2536.71	0	2536.78
1-8-91	2537.15	2536.72	2518.8	2536.77
1-9-91	2537.15	2536.7	2518.88	2536.76
1-10-91	2537.12	2536.7	2518.71	2536.76
1-11-91	2537.48	2537.13	2518.77	2537.15
1-12-91	2538.93	2538.52	2518.93	2538.55
1-13-91	2539.57	2539.13	2519	2539.17
1-14-91	2539.95	2539.49	2519.18	2539.55
1-15-91	2540.92	2540.43	2519.24	2540.5
1-16-91	2540.21	2539.69	2519.11	2539.76
1-18-91	2539.9	2539.42	2519.38	2539.47
1-19-91	2539.52	2539.06	2519.03	2539.12
1-21-91	2539.11	2538.65	2518.96	2538.71
1-23-91	2538.82	2538.36	2517.43	2538.43
1-25-91	2538.52	2538.09	2517.82	2538.12
1-27-91	2538.34	2537.89	2520.69	2537.97
1-29-91	2538.12	2545.95	2521.49	0
1-31-91	2537.92	2537.49	2515.62	2537.52
2-2-91	2537.97	2537.52	2517.03	2537.56
2-3-91	2538.22	2537.8	2518.85	2537.85
2-4-91	2538.27	2537.85	2520.19	2537.91
2-5-91	2538.56	2538.19	2520.88	2538.24
2-6-91	2538.41	2538.02	2520.13	2538.06
2-8-91	2538.29	2537.88	2521.31	2537.95
2-10-91	2538.21	2537.78	2521.73	2537.88
2-12-91	2538.2	2537.79	2519.79	2537.79
2-13-91	2538.1	2537.7	0	0
2-14-91	2538.48	2538.06	2519.01	2538.13
2-15-91	2538.46	2538.03	2520.71	2538.11
2-17-91	2538.32	2537.9	2521.99	2537.99
2-19-91	2538.44	2538.03	2522.33	2538.12
2-20-91	2538.58	2538.18	2522.33	2538.25
2-21-91	2538.5	2538.08	2522.42	2538.16
2-23-91	2538.3	2537.89	2522.41	2537.98
2-25-91	2538.18	2537.77	2522.37	2537.86
2-27-91	2538.16	2537.71	2519.31	2537.82
3-1-91	2538.43	2538.02	2521.84	2538.09
3-2-91	2538.57	2538.16	2522.11	2538.26
3-3-91	2539.02	2538.6	2522.36	2538.71
3-4-91	2540.12	2539.68	2522.9	2539.79
3-5-91	2539.81	2539.37	2522.4	2539.48
3-6-91	2539.68	2539.23	2522.56	2539.35

**Table C-2. Static Water Level of Three Shallow Wells
and Wells S12D1 and S12D2
(Elevation in feet AMSL)**

DATE	P17S	V16S	S12D1	S12D2	N18S
4-18-88	2536.78	2537.26			
4-22-88	2536.98	2537.84			
4-29-88	2537.33	2538.43			
5-2 -88	2536.83	2537.55			
5-6 -88	2536.72	2537.34			
5-9 -88	2536.56	2537.13			
5-12-88	2536.48	2537.07			
5-20-88	2536.30	2536.87			
5-26-88	2536.49	2536.79			
6-1 -88	2536.26	2536.85			
6-9 -88	2536.52	2537.08			
6-16-88	2536.33	2536.87			
6-24-88	2536.26	2536.71			
6-27-88	2536.53	2537.08			
7-2 -88	2536.27	2536.83			
7-7 -88	2536.30	2536.85			
7-8 -88	2536.27	2536.81			
7-15-88	2536.55	2537.16			
7-20-88	2536.36	2536.90			
7-23-88	2536.27	2536.82			
7-29-88	2536.23	2536.71			
7-30-88	2536.24	2536.76			
8-3 -88	2536.19	2536.71			
8-6 -88	2536.17	2536.66			
8-12-88	2536.14	2536.62			
8-15-88	2536.15	2536.69			
8-19-88	2536.13	2536.66			
8-26-88	2536.04	2536.53			
8-30-88	2536.02	2536.55			
9-2 -88	2536.02	2536.54			
9-5 -88	2536.03	2536.52			
9-9 -88	2536.02	2536.50			
9-12-88	2536.08	2536.58			
9-16-88	2536.08	2536.67			
9-19-88	2536.35	2536.88			
9-27-88	2536.31	2536.72			
9-30-88	2536.09	2536.58			
10-5-88	2535.98	2536.46			
10-7-88	2535.92	2536.35			
10-10-88	2535.88	2536.34			
10-13-88	2535.85	2536.33			
10-17-88	2535.97	2536.41			
10-21-88	2536.02	2536.51			
10-25-88	2535.97	2536.43			
10-26-88	2535.89	2536.32			
10-28-88	2535.89	2536.32			
11-1 -88	2535.87	2536.31			
11-4 -88	2536.05	2536.49			
11-7 -88	2536.17	2536.67			
11-11-88	2536.17	2536.66			
11-15-88	2536.31	2536.84			
11-18-88	2536.28	2536.81			
11-25-88	2536.84	2537.67			
12-1 -88	2536.85	2537.72			
12-8 -88	2536.69	2537.37			
12-14-88	2536.50	2537.11			
12-20-88	2536.34	2536.96			
12-23-88	2536.26	2536.81			
12-27-88	2536.19	2536.74			
1-3-89	2536.39	2537.32			
1-6-89	2536.55	2537.28			
1-11-89	2536.63	2537.39			
1-16-89	2537.22	2538.38			
1-20-89	2538.00	2539.81			
1-23-89	2537.90	2539.11			

1-26-89	2537.67	2538.68			
1-30-89	2537.47	2538.44			
2-6-89	2537.32	2538.45			
2-10-89	2537.07	2538.09			
2-13-89	2536.93	2537.85			
2-17-89	2536.86	2537.68			
2-20-89	2537.14	2538.17			
2-26-89	2539.03	2540.29			
3-2-89	2538.46	2539.54			
3-5-89	2538.10	2539.10			
3-8-89	2539.46	2540.64			
3-11-89	2540.10	2541.18			
3-16-89	2539.22	2540.30			
3-19-89	2539.31	2540.41			
3-23-89	2539.09	2540.13			
3-26-89	2539.31	2540.35			
3-29-89	2539.02	2540.06			
4-2-89	2538.65	2539.49			
4-5-89	2538.51	2539.70			
4-12-89	2537.90	2538.66			
4-16-89	2537.67	2538.43			
4-19-89	2537.54	2538.22			
4-23-89	2537.47	2538.37			
4-27-89	2537.39	2538.06			
4-30-89	2537.16	2537.99			
5-4-89	2537.04	2537.82			
5-7-89	2536.98	2537.75			
5-11-89	2537.02	2537.66			
5-16-89	2537.00	2537.66			
5-19-89	2536.98	2537.65			
5-22-89	2536.99	2537.68			
5-26-89	2537.06	2537.75			
5-30-89	2537.36	2538.19			
6-4-89	2537.22	2538.08			
6-8-89	2537.11	2537.93			
6-12-89	2536.95	2537.76			
6-16-89	2537.13	2537.88			
6-21-89	2537	2537.67			
6-23-89	2536.94	2537.61			
6-26-89	2536.8	2537.42			
7-4-89	2536.62	2537.2			
7-11-89	2536.43	2537.01			
7-14-89	2536.49	2537.11			
7-26-89	2536.38	2536.97			
7-31-89	2536.4	2536.99			
8-3-89	2536.39	2536.95			
8-10-89	2536.41	2536.98			
8-14-89	2536.4	2536.97			
8-17-89	2536.41	2537			
8-25-89	2537.28	2538.32			
8-29-89	2536.86	2537.84			
9-5-89	2536.68	2537.41			
9-11-89	2536.55	2537.2			
9-15-89	2536.5	2537.11			
9-18-89	2536.67	2537.23			
9-19-89	2536.56	2537.15			
9-22-89	2536.48	2537.08			
9-29-89	2536.43	2537.01			
10-2-89	2536.36	2536.9			
10-6-89	2536.3	2536.81			
10-10-89	2536.31	2536.84			
10-15-89	2536.23	2536.74			
10-17-89	2536.22	2536.7			
10-23-89	2536.59	2537.37			
10-26-89	2536.65	2537.54			
10-30-89	2536.45	2537.19			
11-3-89	2536.41	2536.95			
11-7-89	2536.53	2537			
11-10-89	2536.64	2537.63			
11-14-89	2536.89	2538.03			
11-18-89	2536.8	2537.96			
11-28-89	2536.79	2537.71			
12-1-89	2536.63	2537.4			
12-5-89	2537.5	2539.06			
			<u>S12D1</u>	<u>S12D2</u>	<u>N18S</u>
					2536.41
					2536.57
			2537.05	2521.84	2536.45
			2537.15	2520.64	2536.4
			2537.1	2519.92	2536.34
			2536.99	2519.86	2536.28
			2536.88	2519.73	2536.23
			2536.9	2519.78	2536.22
			2536.74	2519.54	2536.14
			2536.78	2519.39	2536.13
			2537.2	2519.7	2536.49
			2537.3	2519.58	2536.55
			2537.05	2519.42	2546.16
			2536.95	2519.39	2536.33
			2537.1	2519.45	2536.45
			2537.24	2519.49	2536.64
			2537.5	2519.45	2536.81
			2537.44	2519.38	2536.71
			2537.46	2519.07	2536.72
			2537.24	2518.97	2536.52
			2538.41	2519.36	2537.64

12-8 -89	2537.25	2538.38	2538	2519.51	2537.16
12-14-89	2536.78	2537.54	2537.48	2517.32	2536.65
12-22-89	2536.51	2537.19	2537.1	2518.99	2536.41
12-26-89	2536.52	2537.14	2537.1	2519.05	2536.41
12-29-89	2536.45	2537.02	2537.02	2519.04	2536.34
1-9 -90	2538.37	2539.88	2539.23	2519.58	2538.39
1-11-90	2538.24	2539.36	2538.99	2519.41	2538.04
1-17-90	2537.85	2538.63	2538.5	2519.5	2537.64
1-25-90	2538.03	2538.49	2538.25	2519.49	2537.4
1-30-90	2537.74	2538.7	2538.46	2519.84	2538
1-31-90	2537.7	2538.68	2538.43	2519.83	2538.06
2-1 -90	2537.64	2538.54	2538.37	2519.65	2537.43
2-2 -90	2537.55	2538.39	2538.26	2519.58	2537.33
2-3 -90	2537.57	2538.43	2538.43	2519.38	2537.37
2-4 -90	2537.97	2538.76	2538.46	2519.44	2537.41
2-5 -90	2537.59	2538.71	2538.51	2519.28	2537.41
2-6 -90	2537.58	2538.53	2538.48	2519.36	2537.41
2-7 -90	2537.48	2538.95	2530.44	2519.25	2537.31
2-8 -90	2537.47	2538.67	2538.45	2519.59	2537.27
2-9 -90	2537.49	2538.48	2538.45	2519.54	2537.37
2-10-90	2539.41	2540.85	2540.11	2519.62	2539.52
2-11-90	2539.91	2540.84	2540.44	2519.81	2539.66
2-12-90	2539.42	2540.21	2539.86	2520.07	2538.89
2-13-90	2539.03	2539.73	2539.62	2520.24	2538.61
2-14-90	2538.67	2539.33	2539.29	2520	2538.28
2-15-90	2538.54	2539.18	2539.24	2520.18	2538.18
2-16-90	2538.33	2538.94	2539.07	2520.46	2537.98
2-17-90	2538.23	2538.81	2538.95	2520.32	2537.94
2-18-90	2538.07	2538.65	2538.79	2519.95	2537.77
2-19-90	2537.94	2538.52	2538.74	2519.76	2537.66
2-20-90	2537.86	2538.46	2538.63	2519.88	2537.59
2-21-90	2537.83	2538.43	2538.63	2519.87	2537.6
2-21-90	2538.45	2539.5	2538.79	2519.83	2537.87
2-22-90	2538.23	2539.77	2539.12	2519.77	2538
2-22-90	2538.28	2540	2539.12	2519.78	2538.14
2-23-90	2538.52	2539.86	2539.36	2519.85	2538.35
2-24-90	2538.7	2539.88	2539.48	2519.91	2538.54
2-25-90	2538.67	2539.57	2539.41	2519.97	2538.46
2-26-90	2538.54	2539.33	2539.27	2519.98	2538.32
2-27-90	2538.32	2539.06	2539.06	2519.88	2538.1
2-28-90	2538.22	2538.93	2538.98	2519.9	2537.99
3-1 -90	2538.14	2538.81	2538.9	2519.98	2537.9
3-2 -90	2538.07	2538.72	2538.86	2520.03	2537.82
3-3 -90	2537.96	2538.62	2538.79	2520.14	2537.76
3-4 -90	2537.87	2538.54	2538.71	2520.1	2537.68
3-5 -90	2537.8	2538.47	2538.62	2520.11	2537.6
3-6 -90	2537.73	2538.42	2538.5	2519.86	2537.51
3-7 -90	2537.68	2538.38	2538.52	2519.91	2537.49
3-8 -90	2537.77	2538.43	2538.61	2520.09	2537.68
3-9 -90	2537.76	2538.37	2538.56	2519.96	2537.53
3-10-90	2537.8	2538.45	2538.66	2520.18	2537.71
3-11-90	2537.95	2538.91	2538.88	2520.23	2537.87
3-12-90	2537.82	2538.62	2538.69	2520.07	2537.64
3-13-90	2537.74	2538.53	2538.62	2519.86	2537.58
3-14-90	2537.67	2538.43	2538.57	2519.9	2537.52
3-15-90	2537.73	2538.48	2538.58	2519.79	2537.57
3-16-90	2537.63	2538.36	2538.51	2519.71	2537.47
3-17-90	2537.57	2538.28	2538.47	2519.82	2537.41
3-18-90	2537.5	2538.39	2538.39	2519.75	2537.36
3-19-90	2537.48	2538.18	2538.4	2519.81	2537.34
3-20-90	2537.42	2538.05	2538.4	2519.67	2537.28
3-21-90	2537.4	2538.02	2538.4	2519.68	2537.25
3-22-90	2537.36	2537.98	2538.27	2519.72	2537.23
3-23-90	2537.94	2538.32	2538.4	2519.67	2537.47
3-24-90	2537.46	2538.22	2538.35	2519.63	2537.31
3-25-90	2537.39	2538.09	2538.31	2519.57	2537.24
3-26-90	2537.32	2537.94	2538.25	2519.59	2537.18
3-27-90	2537.29	2537.88	2538.22	2519.6	2537.14
3-28-90	2537.23	2537.83	2538.16	2519.59	2537.09
3-29-90	2537.2	2537.79	2538.15	2519.63	2537.07
3-30-90	2537.18	2537.76	2538.12	2519.59	2537.04
3-31-90	2537.14	2537.73	2538.08	2519.6	2537.01
4-1 -90	2537.11	2537.69	2538.04	2519.56	2536.97
4-2 -90	2537.05	2537.64	2537.99	2519.53	2536.93
4-3 -90	2537.01	2537.6	2537.94	2519.48	2536.88

4-4 -90	2537.02	2537.59	2537.93	2519.29	2536.89
4-5 -90	2537.01	2537.62	2537.94	2519.04	2536.88
4-6 -90	2536.96	2537.53	2537.9	2519.22	2536.84
4-7 -90	2537.33	2537.53	2537.9	2519.33	2536.85
4-8 -90	2537.13	2537.48	2537.89	2519.48	2536.81
4-9 -90	2536.98	2537.41	2537.78	2519.23	2536.74
4-10-90	2536.93	2537.41	2537.78	2519.12	2536.73
4-11-90	2536.9	2537.41	2537.78	2519.27	2536.73
4-12-90	2536.72	2537.16	2536.25	2519.01	2536.51
4-13-90	2536.62	2536.91	2536.1	2518.69	2536.33
4-14-90	2537.37	2538.27	2537.81	2518.71	2537.28
4-15-90	2537.2	2538.02	2538.13	2519.1	2537.04
4-16-90	2537.1	2537.76	2538.07	2519.31	2536.92
4-17-90	2537	2537.59	2537.99	2519.44	2536.86
4-18-90	2536.94	2537.51	2537.93	2519.33	2536.79
4-19-90	2536.9	2537.48	2537.9	2519.29	2536.76
4-20-90	2536.86	2537.43	2537.87	2519.2	2536.72
4-21-90	2536.86	2537.44	2537.9	2519.25	2536.75
4-22-90	2536.84	2537.42	2537.92	2519.39	2536.76
4-23-90	2536.97	2537.55	2538.03	2519.51	2536.91
4-24-90	2536.8	2537.41	2537.9	2519.27	2536.79
4-25-90	2536.78	2537.37	2537.87	2519.2	2536.7
4-26-90	2536.92	2537.72	2537.99	2519.11	2536.86
4-27-90	2536.99	2537.61	2538.09	2519.24	2536.91
4-28-90	2538.29	2539.75	2539.33	2519.54	2538.38
4-29-90	2537.9	2539.29	2539	2519.35	2537.9
4-30-90	2537.71	2538.67	2538.76	2519.18	2537.62
5-3 -90	2537.47	2538.17	2538.49	2519.15	2537.34
5-6 -90	2537.22	2537.88	2538.27	2519.27	2537.09
5-9 -90	2537.08	2537.72	2538.16	2519.22	2536.96
5-13-90	2536.93	2537.55	2538.06	2519.19	2536.83
5-17-90	2536.89	2537.49	2538.01	2519.17	2536.77
5-21-90	2536.8	2537.44	2538	2527.46	2536.72
5-22-90	2536.75	2537.39	2537.93	2529.04	2536.66
5-23-90	2536.88	2537.82	2538.13	2529.48	2536.77
5-26-90	2537.25	2538.17	2538.47	2529.74	2537.13
5-30-90	2537.48	2538.34	2538.64	2528.24	2537.35
6-2 -90	2538.23	2539.5	2539.35	2528.13	2538.22
6-7 -90	2537.85	2538.6	2538.11	2527.4	2537.66
6-12-90	2536.86	2537.62	2537.04	2526.79	2536.79
6-18-90	2536.75	2537.38	2536.62	2526.58	2536.6
6-24-90	2536.7	2537.3	2536.53	2526.56	2536.59
7-2 -90	2536.65	2537.28	2536.49	2526.57	2536.56
7-6 -90	2536.6	2537.22	2536.08	2526.45	2536.48
7-9 -90	2536.55	2537.16	2536.15	2526.51	2536.44
7-15-90	2536.53	2537.14	2536.15	2526.74	2536.41
7-19-90	2536.6	2537.22	2536.01	2526.66	2536.43
7-23-90	2536.48	2537.08	2535.78	2526.84	2536.36
7-27-90	2536.69	2537.33	2535.86	2526.72	2536.56
7-30-90	2536.66	2537.37	2535.38	2522.91	2536.52
8-7 -90	2536.64	2537.3	2534.73	2517.08	2536.5
8-11-90	2536.46	2537.15	2534.55	2517.02	2536.44
8-14-90	2536.55	2537.14	2534.48	2514.55	2536.42
8-23-90	2536.79	2537.47	2535.11	2517.72	2536.66
8-28-90	2536.58	2537.16	2534.79	2519.32	2536.42
9-4 -90	2536.54	2537.12	2534.82	2519.33	2536.41
9-8 -90	2536.48	2537.06	2534.79	2519.42	2536.37
9-13-90	2536.45	2536.98	2534.85	2519.45	2536.35
9-17-90	2536.41	2536.9	2534.88	2519.46	2536.31
9-21-90	2536.38	2536.85	2534.6	2519.51	2536.27
9-26-90	2536.34	2536.79	2534.15	2519.55	2536.22
10-2 -90	2536.33	2536.78	2534.13	2519.58	2536.21
10-10-90	2536.35	2536.81	2534.33	2519.63	2536.22
10-17-90	2536.36	2536.87	2534.53	2519.69	2536.24
10-24-90	2536.56	2537.15	2534.77	2519.67	2536.43
10-31-90	2536.67	2537.5	2535.22	2519.63	2536.54
11-6 -90	2536.86	2537.61	2535.42	2519.62	2536.7
11-15-90	2536.53	2537.11	2534.85	2519.48	2536.38
11-23-90	2536.96	2537.76	2535.38	2519.78	2536.81
11-30-90	2536.97	2537.8	2535.43	2519.76	2536.84
12-5 -90	2537.07	2538.01	2535.82	2519.51	2536.89
12-11-90	2537.5	2538.91	2536.12	2519.75	2537.49
12-13-90	0	2538.22	2536.08	2519.79	2537.17
12-14-90	2537.17	2538.07	2536.02	2519.77	2537.05
1-5 -91	2536.3	2536.86	2536.07	2519.24	0

1-7 -91	2536.29	2536.86	2534.69	2519.27	0
1-8 -91	2536.29	2536.87	2534.63	2519.2	0
1-9 -91	2536.28	2536.84	2534.58	2519.17	0
1-10-91	2536.29	2536.83	2534.61	2519.14	0
1-11-91	2536.6	2537.11	2534.85	2519.14	0
1-12-91	2537.9	2539.71	2536.13	2519.35	0
1-13-91	2538.74	2540.41	2536.42	2519.46	0
1-14-91	2539.22	2540.33	2537.21	2519.58	0
1-15-91	2540.01	2541.02	2538.01	2519.71	0
1-16-91	2539.72	2540.29	2537.91	2519.57	0
1-18-91	2539.3	2539.9	2537.51	2519.8	0
1-19-91	2538.93	2539.51	2536.75	2519.45	0
1-21-91	2538.5	2539.01	2536.36	2519.4	0
1-23-91	2538.15	2538.62	2536.2	2518.56	2537.79
1-25-91	2537.83	2538.31	2536.04	2518.25	2537.5
1-27-91	2537.56	2538.1	2535.69	2520.34	2537.25
1-29-91	2537.32	2537.86	2535.49	2521.07	2537.03
1-31-91	2537.1	2537.64	2534.86	2517.59	2536.87
2-2 -91	2537.09	2537.65	2534.96	2517.35	2536.93
2-3 -91	2537.4	2537.93	2535.33	2518.67	2537.3
2-4 -91	2537.43	2537.97	2535.45	2519.8	2537.32
2-5 -91	2537.78	2538.29	2535.74	2520.45	2537.74
2-6 -91	2537.57	2538.13	2535.56	2519.99	2537.48
2-8 -91	2537.44	2538.02	2535.48	2520.86	2537.28
2-10-91	2537.34	2537.92	2535.5	2521.21	2537.18
2-12-91	2537.34	2537.92	2535.38	2521.08	2537.2
2-13-91	2537.28	2537.86	0	0	2537.11
2-14-91	2537.6	2538.35	2535.64	2518.86	2537.52
2-15-91	2537.54	2538.26	2535.73	2520.15	2537.4
2-17-91	2537.4	2538.07	2535.66	2521.31	2537.26
2-19-91	2537.52	2538.3	2535.78	2521.62	2537.43
2-20-91	2537.64	2538.34	2535.91	2521.66	2537.56
2-21-91	2537.52	2538.34	2535.8	2521.7	2537.36
2-23-91	2537.36	2538.06	2535.83	2521.66	2537.17
2-25-91	2537.24	2537.93	2535.61	2521.62	2537.05
2-27-91	2537.19	2537.9	2535.23	2519.53	2537.03
3-1 -91	2537.48	2538.42	2535.61	2521.19	2537.39
3-2 -91	2537.58	2538.41	2535.84	2521.39	2537.48
3-3 -91	2537.98	2539.1	2536.2	2521.68	2537.93
3-4 -91	2538.94	2540.33	2536.85	2523.19	2539.18
3-5 -91	2538.76	2539.97	2536.84	2521.73	2538.76
3-6 -91	2538.76	2539.82	2536.75	2521.87	2538.61

**Table C-3. Static Water Level of Three Deep Wells Q16D, U3D, and J16D
Shallow Well T8S, and Paradise Creek
(Elevation in feet AMSL)**

DATE	Q16D	U3D	J16D	T8S	CREEK
5-21-90	2535.67			2538.87	2537.01
5-22-90	2535.89	2535.95		2538.82	2536.91
5-23-90	2536.07	0	2529.75	2538.75	2536.99
5-26-90	2537.33	2536.58	2529.83	2539.2	2537.03
5-30-90	2537.7	2537.04	2528.46	2539.35	2537.25
6-2-90	2538.51	2538.15	2528.24	2539.91	2537.71
6-7-90	2538.02	2538.85	2527.67	2539.88	2537.41
6-12-90	2537.21	2539.04	2527.06	2539.07	2536.89
6-18-90	2536.95	2539.08	2526.85	2538.86	2536.87
6-24-90	2536.9	2539.07	2526.84	2538.79	2536.87
7-2-90	2536.88	2539.03	2526.83	2538.72	2536.87
7-6-90	2536.81	2539.03	2526.73	2538.58	2536.84
7-9-90	2536.78	2538.99	2526.79	2538.51	2536.83
7-15-90	2536.74	2539.09	2526.99	2538.38	2536.79
7-19-90	2536.77	2539	2526.93	2538.48	2536.84
7-23-90	2536.69	2539.07	2527.07	2538.2	2536.81
7-27-90	2536.87	2538.95	2526.95	2538.21	2536.89
7-30-90	2536.88	2537.63	2522.85	2538.27	2536.81
8-7-90	2537.35	2517.09	2517.09	2538.26	2536.83
8-11-90	2537.28	2517.04	2517.06	2538.16	2536.83
8-14-90	2537.19	2514.64	2514.98	2538.14	2533.21
8-23-90	2537.4	2517.74	2517.79	2538.22	2536.81
8-28-90	2537.16	2519.3	2519.3	2538.09	2536.79
9-4-90	2537.11	2519.3	2519.3	2538.04	2536.81
9-8-90	2537.05	2519.41	2519.44	2537.97	2536.83
9-13-90	2537.02	2519.42	2519.46	2537.88	2536.85
9-17-90	2536.97	2519.47	2519.46	2537.78	2536.87
9-21-90	2536.91	2519.51	2519.5	2537.74	2536.83
9-26-90	2536.85	2519.54	2519.54	2537.7	2536.81
10-2-90	2536.83	2519.61	2519.61	2537.68	2536.81
10-10-90	2536.86	2519.65	2519.67	2537.61	2536.71
10-17-90	2536.89	2519.7	2519.69	2537.56	2536.77
10-24-90	2537.15	2519.67	2519.64	2537.75	2536.81
10-31-90	2537.5	2519.61	2519.58	2537.89	2536.86
11-6-90	2537.65	2519.57	2519.56	2538.1	2536.88
11-15-90	2537.09	2519.42	2519.43	2537.82	2536.79
11-23-90	2537.01	2519.72	2519.75	2538.05	2536.96
11-30-90	2537.09	2519.66	2519.71	2538.1	2536.95
12-5-90	2537.69	2519.45	2519.57	2538.63	2536.97
12-11-90	2538.26	2519.75	2519.88	2538.85	2537.37
12-13-90	2537.93	2520.29	2519.79	2539.02	2537.07
12-14-90	2537.83	2519.76	2519.78	2539.02	2537.05
1-5-91	2537.16	2519.17	2519.17	2538.18	
1-7-91	2536.83	2519.27	2519.24	2538.11	
1-8-91	2536.8	2519.22	2519.2	2538.11	
1-9-91	2536.79	2519.27	2519.25	2538.07	
1-10-91	2536.81	2519.13	2519.1	2538.05	2536.87
1-11-91	2537.22	2519.14	2519.15	2538.04	2537.28
1-12-91	2538.64	2519.31	2519.35	2538.38	2538.04
1-13-91	2539.22	2519.45	2519.41	2539.43	2538.66
1-14-91	2539.62	2519.57	2519.58	2539.69	2538.71
1-15-91	2540.57	2519.7	2519.66	2540.1	2540.93
1-16-91	2539.8	2519.54	2519.54	2540.35	2538.25
1-18-91	2539.52	2519.79	2519.8	2540.88	2538
1-19-91	2539.16	2519.43	2519.42	2540.95	2537.71
1-21-91	2538.84	2519.38	2519.37	2541.05	
1-23-91	2538.54	2518.64	2518.47	2540.87	2537.31
1-25-91	2538.32	2518.21	2518.25	2540.48	2537.21
1-27-91	2538.02	2520.34	2520.36	2540.3	2537.11
1-29-91	2537.8	2521.07	2521.07	2540.02	0
1-31-91	2537.61	2517.49	2517.4	2539.74	2537.21
2-2-91	2537.65	2517.37	2517.39	2539.59	2537.31
2-3-91	2537.91	2518.64	2518.68	2539.53	2537.47
2-4-91	2537.98	2519.81	2519.84	2539.6	2537.48
2-5-91	2538.3	2520.41	2520.41	2539.61	2537.81
2-6-91	2538.11	2519.96	2519.98	2539.72	2537.51

2-8 -91	2537.99	2520.85	2520.89	2539.78	2537.3
2-10-91	2537.9	2521.21	2521.24	2539.72	2537.23
2-12-91	2537.91	2520.95	2520.78	2539.67	2537.34
2-13-91	2537.88	0	0		2537.27
2-14-91	2538.18	2518.88	2518.91	2539.68	2537.62
2-15-91	2538.15	2520.17	2520.2	2539.93	2537.4
2-17-91	2538.02	2521.3	2521.29	2540	2537.25
2-19-91	2538.1	2521.63	2521.66	2539.85	2537.45
2-20-91	2538.29	2521.64	2521.65	2539.96	2537.6
2-21-91	2538.19	2521.71	2521.72	2540.15	2537.28
2-23-91	2538.01	2521.65	2521.68	2540.25	2537.16
2-25-91	2537.87	2521.55	2521.62	2540.08	2537.11
2-27-91	2537.86	2519.53	2519.53	2540.11	2537.1
3-1 -91	2538.13	2521.23	2521.21	2539.98	2537.57
3-2 -91	2538.19	2521.39	2521.4	2539.97	2537.46
3-3 -91	2538.7	2521.64	2521.71	2540.3	2537.72
3-4 -91	2539.8	2522.17	2522.23	2541.13	2539.31
3-5 -91	2539.48		2521.73	2541.5	2538.1
3-6 -91	2539.36		2521.83	2541.83	2537.84

**Table C-4. Static Water Level of Five Shallow Wells
(Elevation in feet AMSL)**

DATE	Q16S	U3S	J16S	J17S	H12S
5-9 -90					2539.04
5-13-90					2538.79
5-17-90					2538.67
5-21-90					2538.53
5-22-90					2538.46
5-23-90					2538.35
5-26-90					2539.09
5-30-90					2539.16
6-2 -90					2539.64
6-7 -90					2539.49
6-12-90					2538.66
6-18-90					2538.28
6-24-90					2538.24
7-2 -90					2538.16
7-6 -90					2538.04
7-9 -90				2536.25	2537.95
7-15-90				2536.18	2537.88
7-19-90				2536.15	2537.82
7-23-90				2536.1	2537.77
7-27-90				2536.14	2537.76
7-30-90	2537.11			2536.5	2537.91
8-7 -90	2536.88	2541.39		2536.54	2537.88
8-11-90	2536.79	2542.07	2536.68	2536.52	2537.85
8-14-90	2536.81	2542.12	2536.68	2536.49	2537.83
8-23-90	2537.44	2542.12	2537.26	2536.7	2537.95
8-28-90	2537.2	2541.94	2536.66	2536.5	2537.76
9-4 -90	2537.15	2541.92	2536.6	2536.44	2537.72
9-8 -90	2537.06	2541.81	2536.54	2536.37	2537.68
9-13-90	2536.94	2541.74	2536.49	2536.33	2537.64
9-17-90	2536.86	2541.62	2536.5	2536.3	2537.56
9-21-90	2536.84	2541.54	2536.47	2536.27	2537.53
9-26-90	2536.78	2541.47	2536.42	2536.23	2537.46
10-2 -90	2536.76	2541.42	2536.38	2536.22	2537.44
10-10-90	2536.61	2541.32	2536.4	2536.27	2537.45
10-17-90	2536.57	2541.2	2536.4	2536.26	2537.37
10-24-90	2536.75	2541.31	2536.58	2536.43	2537.56
10-31-90	2537.04	2541.42	2536.71	2536.63	2537.74
11-6 -90	2537.08	2541.49	2536.77	2536.69	2537.89
11-15-90	2536.86	2541.57	2536.5	2536.38	2537.52
11-23-90	2537.01	2541.77	2536.92	2536.69	2537.87
11-30-90	2537.06	2541.96	2536.96	2536.74	2537.94
12-5 -90	2537.36	2542.11	2537	2536.84	2538.13
12-11-90	2537.92	2542.48	2537.53	2536.98	2538.56
12-13-90	2537.54	2542.56	2537.26	2537.11	2538.51
12-14-90	2537.46	2542.53	2537.21	2537.06	2538.45
1-5 -91	2536.61	2541.94	2536.45	2536.28	2537.55
1-7 -91	2536.55	2541.97	2536.45	2536.27	2537.55
1-8 -91	2536.53	2541.91	2536.44	2536.25	2537.54
1-9 -91	2536.53	2541.93	2536.43	2536.25	2537.52
1-10-91	2536.51	2541.85	2536.43	2536.23	2537.49
1-11-91	2536.87	2541.87	2536.76	2536.27	2537.6
1-12-91	2538.36	2542.49	2538.13	2537.59	2538.51
1-13-91	2539.06	2543.27	2539.19	2539.22	2539.45
1-14-91	2539.4	2543.65	2539.78	2539.75	2539.91
1-15-91	2540.48	2543.93	2540.49	2539.99	2540.45
1-16-91	2539.66	2543.82	2539.95	2539.89	2540.47
1-18-91	2539.34	2544.13	2539.92	2539.99	2540.51
1-19-91	2538.99	2543.77	2539.57	2539.74	2540.29
1-21-91	2538.55	2543.68	2539.14	2539.45	0
1-23-91	2538.23	2543.6	2538.84	2539.15	2539.9
1-25-91	2537.92	2543.35	2538.5	2538.79	2539.61
1-27-91	2537.7	2543.41	2538.25	2538.52	2539.44
1-29-91	2537.46	2543.2	2537.96	2538.16	2539.15
1-31-91	2537.27	2543.02	2537.72	2537.87	2538.89
2-2 -91	2537.31	2543.07	2537.71	2537.72	2538.82
2-3 -91	2537.64	2542.89	2537.9	2537.78	2538.87
2-4 -91	2537.66	2542.97	2537.92	2537.84	2539.02
2-5 -91	2538.05	2542.94	2538.22	2537.9	2539.17

2-6 -91	2537.81	2542.99	2538.06	2537.91	2539.16
2-8 -91	2537.64	2543.05	2537.91	2537.82	2539.07
2-10-91	2537.56	2543.06	2537.79	2537.71	2538.95
2-12-91	2537.57	2543.13	2537.78	2537.67	2538.9
2-13-91	2537.5	0	0	0	0
2-14-91	2537.86	2543.14	2537.97	2537.58	2538.81
2-15-91	2537.79	2543.41	2537.93	2537.76	2539.05
2-17-91	2537.63	2543.35	2537.79	2537.66	2538.9
2-19-91	2537.77	2543.34	2537.9	2537.67	2538.77
2-20-91	2537.91	2543.33	2538.01	2537.72	2538.94
2-21-91	2537.77	2543.38	2537.93	2537.76	2538.9
2-23-91	2537.59	2543.28	2537.78	2537.69	2538.85
2-25-91	2537.46	2543.21	2537.68	2537.61	2538.77
2-27-91	2537.44	2543.45	2537.69	2537.62	2538.77
3-1 -91	2537.74	2543.65	2537.9	2537.65	2538.91
3-2 -91	2537.85	2543.54	2538.02	2537.69	2539.14
3-3 -91	2538.33	2543.82	2538.7	2538.05	2539.52
3-4 -91	2539.5	2544.33	2540.12	2539.25	2540.05
3-5 -91	2539.18	2543.99	2539.96	2539.83	2540.27
3-6 -91	2539.06	2543.97	2539.93	2540.14	2540.39